Max-Planck-Institut
für Meteorologie

EXAMENSARBEIT Nr. 60

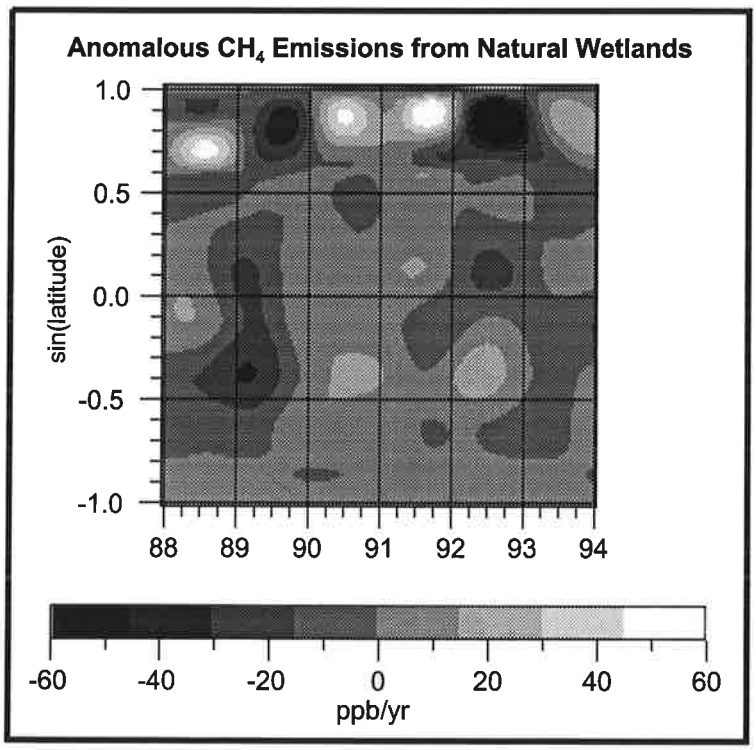

DEVELOPMENT OF A PROCESS-BASED MODEL TO DERIVE METHANE EMISSIONS FROM NATURAL WETLANDS FOR CLIMATE STUDIES

von

Bernadette Walter

HAMBURG, August 1998

Dissertation zur Erlangung des Doktorgrades

Autor:

Bernadette Walter

Max-Planck-Institut
für Meteorologie

MAX-PLANCK-INSTITUT
FÜR METEOROLOGIE
BUNDESSTRASSE 55
D - 20146 HAMBURG
GERMANY

Tel.: +49-(0)40-4 11 73-0
Telefax: +49-(0)40-4 11 73-298
E-Mail: <name> @ dkrz.de

Development of a Process-Based Model to Derive Methane Emissions from Natural Wetlands for Climate Studies

Dissertation
zur Erlangung des Doktorgrades
der Naturwissenschaften
im Fachbereich Geowissenschaften
der Universität Hamburg

vorgelegt von

Bernadette Walter

aus München

Hamburg
1998

ISSN 0938-5177

Als Dissertation angenommen vom Fachbereich Geowissenschaften der Universität Hamburg

auf Grund von Gutachten von Dr. Martin Heimann
und Prof. Dr. Klaus Hasselmann
und Dr. Peter Bergamaschi

Hamburg, den 10. Juli 1998

Prof. Dr. G. Miehlich
Dekan
des Fachbereichs Geowissenschaften

Abstract

Methane is an important greenhouse gas contributing about 22% to the greenhouse effect at present. Methane emissions from natural wetlands, which constitute the biggest methane source at present and the major non-anthropogenic one, depend highly on the climate. In order to investigate the response of methane emissions from natural wetlands to climate variations, a 1-dimensional process-based climate-sensitive model to derive methane emissions from natural wetlands is developed. In the model the processes leading to methane emission are simulated within a 1-dimensional soil column and the three different transport mechanisms diffusion, plant-mediated transport and ebullition are modeled explicitly. The model forcing consists of daily values of the soil temperature, the water table and the Net Primary Productivity. Tests of the methane model using observed data obtained at 15 field stations within 6 wetlands, representing a large variety of environmental conditions, show good agreement.

For the use of the 1-dimensional methane model on the global scale, global data sets for all model parameters are generated, derived from the output of a biosphere model and existing data sets of vegetation and soil properties. Furthermore, a simple hydrological model is developed in order to simulate the position of the water table in wetlands. Tests of the 1-dimensional hydrological model, forced by ECMWF re-analyses with observed water table levels from different wetlands, show a good agreement between model results and observations in general.

A global run of the methane model is performed using high-frequency atmospheric forcing fields from the ECMWF re-analyses of the period from 1988 to 1993. The comparison of the simulated global methane emissions from natural wetlands agree surprisingly well with results obtained by an inverse modeling approach, considering the uncertainties of both methods. The modeled methane emissions show high regional, seasonal and interannual variability. The seasonal cycle of simulated global methane emissions is dominated by the seasonal cycle of methane emissions from the higher northern latitudes. The anomalies of the simulated methane emissions are compared to the observed anomalous methane growth rate. This comparison is limited, because we do not take atmospheric transport and the other methane sources and sinks into account and because the observational data do not reflect the true zonal average. The agreement is particulary good in 1992 and 1993 and the results suggest that reduced methane emissions from northern wetlands in 1992, caused by decreased temperatures due to the eruption of Mt. Pinatubo in June 1991, contribute considerably to the observed growth rate minimum in 1992.

Table of Contents

1. Introduction

The Global Methane Cycle

Methane is one of the important greenhouse gases, contributing about 22% to the greenhouse effect at present [*Lelieveld et al.*, 1998]. Its atmospheric concentration has increased by a factor of 2.5 since the beginning of the industrialisation and is now 1720 ppbv. Since methane has a large radiative effect - one unit mass of CH_4 has 21 times the radiative effect of one unit mass of CO_2 - changes in the atmospheric methane concentration affect the temperature on earth [IPCC, 1996].

Ice core records [e.g. *Jouzel et al.*, 1993] show that the atmospheric methane concentration varied between 350 ppbv and 700 ppbv during the last 220,000 years (see Fig. 1) until the beginning of industrialisation. Those numbers show on the one hand that human activities in the last 200 years have led to a dramatic increase in the atmospheric methane concentration that has never been observed before. On the other hand, they prove that, on longer time scales, there have always been big changes in the atmospheric methane concentration. The ice core records also show, that the changes in methane concentration parallel changes in the atmospheric temperature which are inferred from variations in the $\delta^{18}O$ value (see Fig. 1).

The recent (1983-present) changes in the global atmospheric methane concentration are observed by the National Oceanic and Atmospheric Administration (NOAA) Climate Monitoring and Diagnostics Laboratory (CMDL). The global atmospheric methane concentrations obtained from this sampling network is plotted in Fig. 2 (a). It can be seen, that the atmospheric methane concentration has increased until now, but in the 1990s the slope in Fig. 2 (a) has decreased. This behaviour is also reflected by the methane growth rate shown in Fig. 2 (b): During the period from 1984-1996 the growth rate has decreased, but erratically. There is significant interannual variability and a pronounced peak in 1991 followed by a strong decrease in 1992.

The first step in understanding the variations of the global atmospheric methane concentration is to establish, what the sources and sinks of atmospheric methane and their sizes are. In Tab. 1 estimates of the different methane sources and sinks at present are listed as obtained by an inverse modeling approach by *Hein et al.* [1997]. *Hein et al.* used atmospheric methane measurements from the NOAA/CMDL and some a priori information about the different methane sources and sinks. The uncertainties of the various source strengths could be reduced by more than a third, but they are still considerable.

The sources other than wetlands are mainly of anthropogenic nature and hence were relatively low during preindustrial times. The strength of the main methane sink, reaction with OH

radicals, varies with time, because the atmospheric OH concentration is not constant over time. While OH is the major sink for methane, reaction with methane (and CO) is in turn the major sink for OH. That means that the atmospheric concentration of OH and methane are interconnected. In general, it is believed that the atmospheric OH concentration changes on glacial-interglacial time scales following changes in the methane concentration due to changed methane emissions [*Brook et al.*, 1996; *Thompson et al.*, 1993]. E.g. *Thompson et al.* calculated the OH concentration for the Last Glacial Maximum, when the global methane source was only 100-130 Tg/yr, to be 32% higher than at present. On the other hand, it is assumed that during the last 15 years the OH concentration has not changed significantly [*Prinn et al.*, 1995].

Table 1: Methane Sources and Sinks

Sources	Tg/yr	Sinks	Tg/yr
animals	90 ± 20	tropospheric OH	469 ± 30
rice	69 ± 23	stratosphere	44 ± 8
wetlands	232 ± 27	soil uptake	28 ± 14
landfills	40 ± 15		
biomass burning	41 ± 11		
fossil sources	103 ± 15		
Total Source	575	Total Sink	541

Tab. 1: Methane sources and sinks obtained from an inverse modeling approach by *Hein et al.* [1997]

The Role of Wetlands in the Global Methane Cycle

Looking at the various methane sources one sees, that the natural wetlands are the biggest methane source at present, contributing about 40% to the total methane emissions. Since most other sources listed in Tab.1 are of anthropogenic nature, it is clear that the natural wetlands form the major non-anthropogenic methane source. Furthermore, unlike most other methane sources, methane emissions from natural wetlands depend highly on the climate being influenced by temperature as well as by wetness. The present global distribution of natural wetlands has been assessed by *Matthews and Fung* [1987] (see Fig. 3.). Here the fraction of each $1^{o}*1^{o}$ grid cell covered by natural wetlands is plotted.

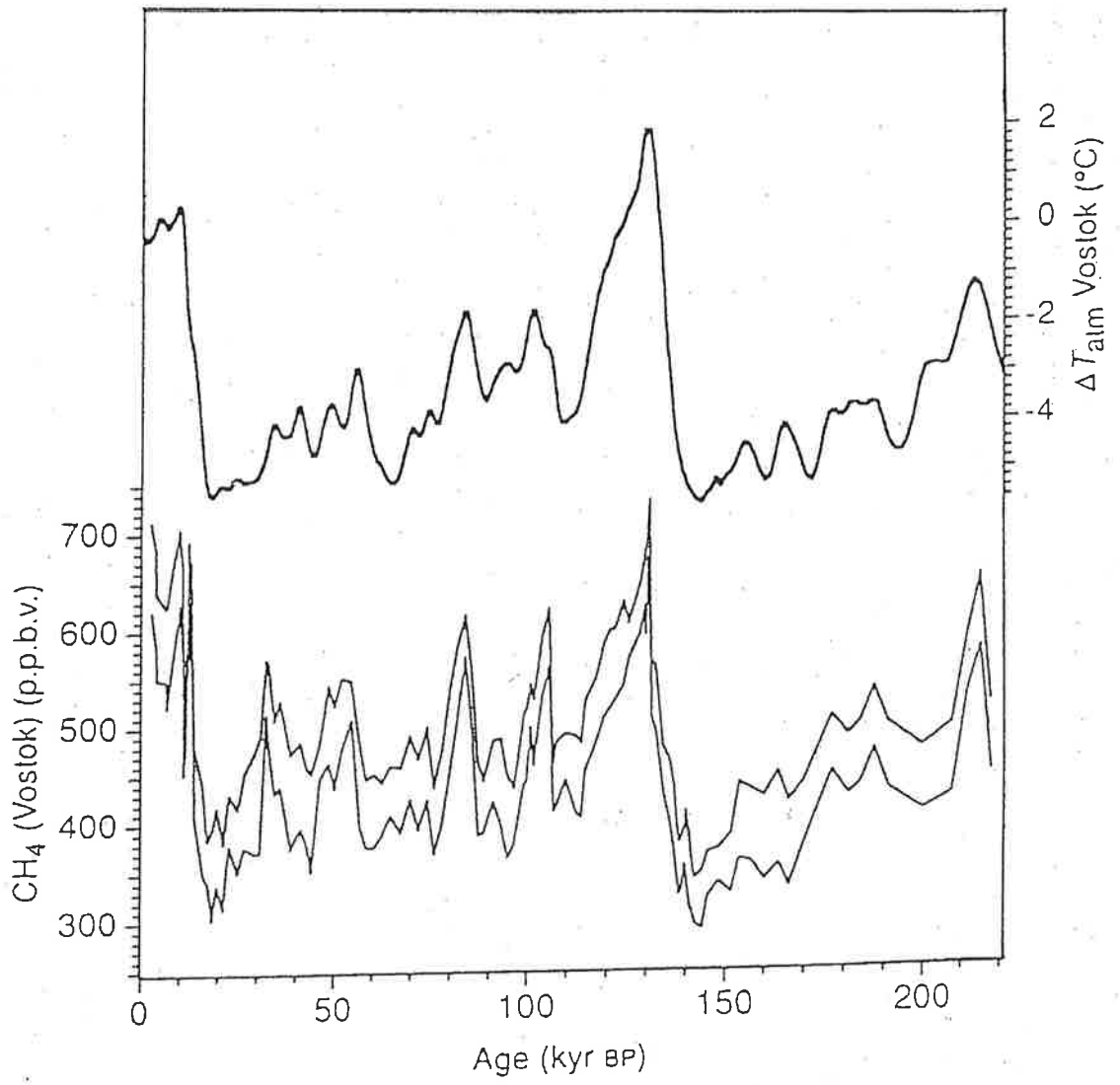

Fig. 1: Results from the Vostock ice core record: Methane concentration (the envelope corresponds to the measurement accuracy) and atmospheric temperature (change from the present day temperature derived from $\delta^{18}O$ values) [*Jouzel et al.*, 1993]

Processes in a Wetland Soil: Present Understanding

The emission of methane from natural wetlands is a result of biological and physical processes taking place in the soil: Methane production by methanogenic bacteria under anaerobic conditions, methane oxidation by methanotrophic bacteria under aerobic conditions and transport of methane to the atmosphere [e.g. *Conrad*, 1989]. Numerous studies have been carried out to investigate which factors control these processes. It has been shown that the most dominant determinants are:

1. The position of the water table, because it determines the extent of the anoxic soil zone,

where methane is produced, and the oxic soil zone, where methane is oxidized.

2. The soil temperature, since it influences the rates at which microbiological processes such as degradation of organic matter (i.e. the production of substrate for methanogenesis), methane production and methane oxidation occur.

3. The availability and quality of suitable substrate for methane production. Several authors observed a correlation between factors indicating substrate availability, such as the Net Primary Productivity (NPP), the Net Ecosystem Production (NEP) or the amount of biomass and methane production. Others observed enhanced methane emission after addition of substrate to the soil or from sites with a higher substrate quality.

Tab. 2 gives examples of studies investigating the controlling factors of methane emissions from wetlands. It demonstrates that different factors are determining at different sites.

Table 2: Factors Controlling Methane Emissions from Several Study Sites

Reference	Soil Temperature	Water Table	Substrate
Baker-Blocker et al., 1977	x		
Bartlett et al., 1992	x		
Bartlett and Harriss, 1993	x	x	
Bridgham and Richardson, 1992			x
Bubier, 1995		x	
Bubier et al., 1995	x	x	
Christensen et al., 1995	x		
Crill et al., 1988	x		
Dise et al., 1993	x	x	
Fowler et al., 1995	x	x	
Frolking and Crill, 1994	x		
Funk et al., 1994		x	
Granberg et al., 1997	x	x	
Happell et al., 1993		x	x
Harriss et al., 1982		x	
Kettunen and Kaitala, 1996	x		
Klinger et al., 1994			x
Moore and Roulet, 1993		x	

Table 2: Factors Controlling Methane Emissions from Several Study Sites

Reference	Soil Temperature	Water Table	Substrate
Moosavi et al., 1996	x	x	
Morrissey and Livingston, 1992	x	x	x
Roulet et al., 1992		x	
Sebacher et al., 1986		x	
Shurpali et al., 1993	x	x	
Torn and Chapin, III, 1993	x		
Valentine et al., 1994			x
Waddington et al., 1996			x
Whalen and Reeburgh, 1992	x		
Whiting et al., 1991			x
Whiting and Chanton, 1992			x
Whiting and Chanton, 1993			x

4. The pathways by which methane is transported to the atmosphere can be crucial for determining the fraction of produced methane that is emitted into the atmosphere. Transport can proceed by molecular diffusion, ebullition and transport through the stems of vascular plants [*Conrad*, 1989]. Depending on the prevailing soil conditions the occurrence of one or more of those mechanisms can significantly alter the amount of emitted methane:

- Ebullition can bring methane much faster to the water table than diffusion and thus increase methane emission [*Bartlett et al.*, 1990; *Boon and Sorrell*, 1995; *Devol et al.*, 1990; *Wassmann et al.*, 1992].
- Plant-mediated transport can enhance methane emission through bypassing the often existing oxic top soil layer and thereby avoiding methane oxidation there [*Bartlett et al.*, 1992; *Boon and Sorrell*, 1995; *Bubier et al.*, 1995; *Chanton et al.*, 1992a; *Chanton and Dacey*, 1991; *Dacey and Klug*, 1979; *Happell et al.*, 1993; *Holzapfel-Pschorn et al.*, 1986; *Morrissey and Livingston*, 1992; *Schimel*, 1995; *Shannon et al.*, 1996; *Shannon and White*, 1994; *Torn and Chapin, III*, 1993; *Waddington et al.*, 1996; *Whiting and Chanton*, 1992; *Yavitt and Knapp*, 1995]. On the other hand, atmospheric oxygen can be conducted by vascular plants down to the rooting zone. Therefore, in water saturated soils covered by vascular plants a small oxic zone establishes around the root tips leading to methane consumption there [*Gerard and Chanton*, 1993; *Holzapfel-Pschorn et al.*, 1986; *Schipper and Reddy*, 1996; *Schütz et al.*, 1989].

Those controlling factors are not independent of each other, e.g. higher temperatures can lead

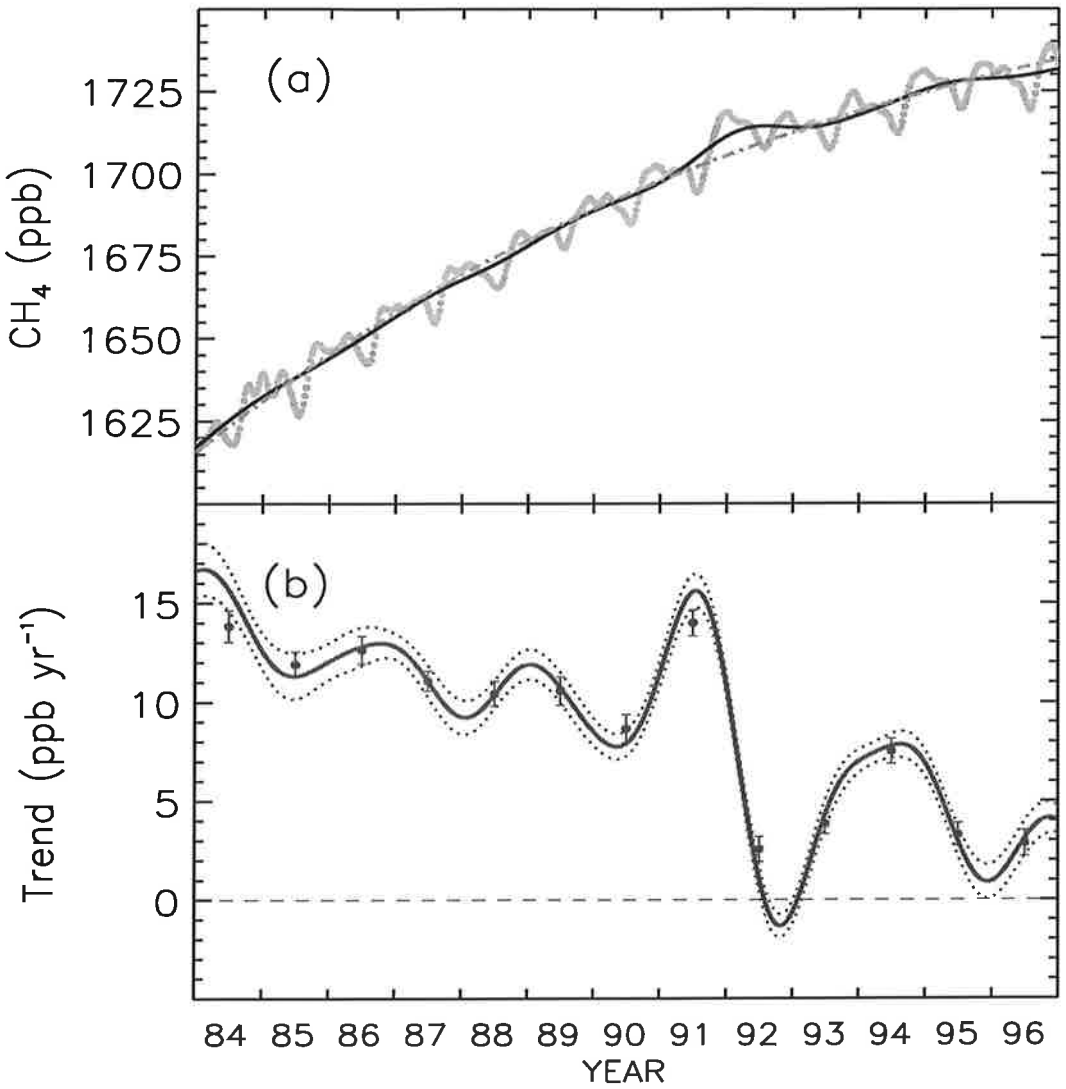

Fig. 2: (a): Globally averaged methane concentrations (grey dots) and deseasonalized trend curve fitted to the data (black solid line); (b): Atmospheric methane growth rate (thick solid line), its uncertainties (dotted lines) and annual increases in methane (symbols) [*Dlugokencky et al.*, 1998]

to lower water table levels due to enhanced evapotranspiration. Thus, higher temperatures will lead only to higher methane emissions, if the soil stays water saturated. For example *Roulet et al.* [1992] found that temperature explained the variances in methane emissions as long as the soil was water saturated, but as soon as the water table decreased below the soil surface methane emissions were determined by the position of the water table. *Valentine et al.* [1994] observed that the temperature dependence of methane production increased with increasing amount and quality of substrate at sites that were substrate limited.

In summary, the results from the huge amount of studies investigating the processes leading to methane emission from natural wetlands and the factors controlling them, one can say that:

1. The environmental factors controlling the involved processes are not independent of each other.

2. Their relative importance in influencing methane emissions depends on the conditions present which determine the processes that operate, their respective rates, and thus ultimately the rate of methane emission.

Therefore, the results of those studies are site-specific and depend on the situations prevailing during the measurements.

State-of-the-Art of Modeling Methane Emissions from Natural Wetlands

Some of the authors named above who have investigated the processes leading to methane emission and the environmental parameters influencing them have developed simple models to predict methane emissions from a wetland site. Those models are based on observed empirical relationships between the factors controlling methane emissions and methane fluxes. As discussed above those models are not capable of simulating methane emissions from other wetlands sites and under conditions different from those prevailing when the data the models are based on were obtained.

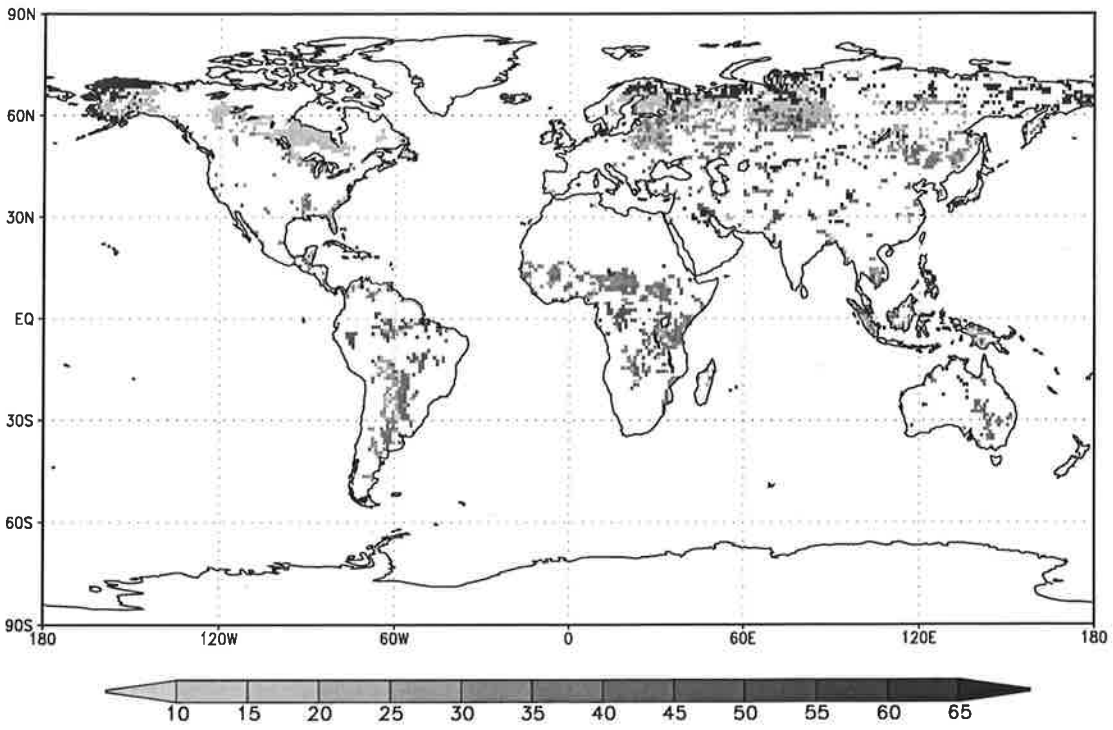

Fig. 3: Global distribution of natural wetlands at present: Fractions [%] of each $1^{o}*1^{o}$ grid cell covered by natural wetlands [*Matthews and Fung*, 1987]

Besides the model described and used here [*Walter et al.*, 1996] there are two models in the literature using a more process-based approach:

1. The model by *Cao et al.* [1996] simulates the soil carbon dynamics in the soil and derives the methane production rate as a function of the amount of decomposed organic carbon, the position of the water table and the temperature. The methane emission rate is calculated as the difference between the methane production rate and the methane oxidation rate. This model was designed for application on the global scale and its outcome has been compared to previous global estimates of methane emissions from natural wetlands which are relatively uncertain. It has not been tested against data from any wetland site.

2. The model by *Potter* [1997] is based on an ecosystem carbon cycling model and simulates methane production rates from a microbial production ratio of CO_2-to-CH_4 that changes as a function of the water table depth. The three different transport mechanisms diffusion, ebullition and plant-mediated transport are modelled as simple functions of methane production, water table and ecosystem type. However, this model when tested against data from one field site does not reproduce observations very well.

Those two models focus on deriving the amount of carbon available for methane production, but the processes leading to methane emission are parameterized in a relatively simple way. The model presented here uses the outcome of an already existing biosphere model to derive the availability of carbon. However, the soil processes involved in methane emission are resolved in more detail.

Objective of this work

The aim of this work is to investigate the origin of observed changes in the atmospheric methane concentration. Inverse models of the atmospheric transport provide one approach to this question: Using models of the atmospheric transport the spatio-temporal distribution of the sources of methane is inferred from spatial gradients in atmospheric observations at global networks [*Brown,* 1993; *Brown*, 1995; *Hein and Heimann*, 1994; *Hein et al.*, 1997]. There are a number of problems involved with the inverse approach. In particular, due to the diffusivity of atmospheric transport, the present observational network is still too sparse (globally about 30 stations) to tightly constrain source estimates exclusively by atmospheric measurements. Instead, within bayesian inversion concepts [*Tarantola*, 1987; *Enting*, 1995], the information from atmospheric observations is used to improve our prior knowledge of the source and sink distribution [*Hein and Heimann*, 1994; *Hein et al.*, 1997]. In this context, one goal of the present study is to provide a prior estimate of the spatio-temporal distribution of the source magnitude of natural wetlands, which constitute the biggest methane source at present and the major non-anthropogenic one.

In this work we also investigate the interannual variation of the methane emissions from natural wetlands of the period between 1988 and 1993. There is one problem which is discussed widely, but has not been solved so far, namely what the possible causes for the dramatically decreased growth rate of methane in 1992 are. There are different speculations about the factors which the 1992 anomaly could be attributable to: Decreased emissions from fossil fuels in the former Soviet Union [*Dlugokencky et al.*, 1994] or decreased biomass burning in the tropics are suggested [IPCC, 1996]. Others put forward enhanced tropospheric-stratospheric exchange due to the Mt. Pinatubo eruption in June 1991 [*Schauffler and Daniel*, 1994] or increased troposheric OH concentrations, which result in an enlarged sink, due to reduced stratospheric ozone levels following the Mt. Pinatubo eruption [*Bekki et al.*, 1994]. Furthermore, it is presumed that decreased methane emissions from natural wetlands due to lower temperatures in 1992 associated with the eruption of Mt. Pinatubo might be the reason for the decreased methane growth rate in 1992 [*Hogan and Harriss*, 1994]. In this context it is worth noting that the growth rate of CO_2 concentrations has been observed to be low in 1992 too. One of the reasons cited for this behaviour is the response of the biosphere to the lower temperatures in 1992 [*Keeling et al.*, 1995]. Therefore, the response of methane emissions from natural wetlands to the lower temperatures in 1992 is investigated.

In order to address the questions concerning the spatio-temporal distribution of methane emissions from natural wetlands our task is to provide a model to simulate methane emissions from natural wetlands on a global scale. To achieve this aim we need a model that:

1. Can calculate methane emissions from various wetland types.

2. Simulates methane fluxes from natural wetlands as a function of the prevailing climate.

To meet the first point we choose a process-based approach which makes it possible to derive methane emissions from natural wetlands under various conditions. The involved processes are modelled as a function of the soil temperature and the soil moisture (position of the water table). The 1-dimensional, process-based, climate-sensitive model developed in this study makes it possible to test the model against observed methane fluxes and methane concentration profiles in the soil. The applicability to various sites under different conditions allows us to extrapolate the 1-dimensional model to the global scale.

Structure of the Work

In Sect. 2, we describe the development of the methane model. In the first part we explain the processes leading to methane emission and in the second part we represent and discuss the parameterization of each of those processes in the model.

In Sect. 3 we first show and discuss some of the results obtained from tests of the methane

model against data from several field sites. Secondly, we present the results of sensitivity tests to changes in the model parameters and the input data.

In Sect. 4 we explain the steps from 1-dimension to the global scale: the generation of several global data sets needed and the extrapolation of the tuning parameter of the model to the global scale.

In Sect. 5 we describe the development of a hydrological model necessary to derive the position of the water table in wetlands globally and the comparison between results of this model and observations and some sensitivity tests.

In Sect. 6 we first show and discuss the results of a global run of the methane model using ECMWF re-analysis data of the period from 1988 to 1993 as model forcing. Second, we present the results of sensitivity tests.

In Sect. 7 we close with a discussion of the results obtained in this work and with some aspects how this model can be applied in the future.

2. Model Development

In the following the processes leading to methane emission from natural wetlands are depicted. Based on this knowledge we describe how these processes are represented in the model and discuss the assumptions of the model parameterizations. A list of all model parameters can be found in App. A.

2.1. Processes in a Wetland Soil

Wetlands

Wetlands are areas where the water table is usually at or near the soil surface or the land is covered by shallow water [*Mitsch and Gosselink*, 1993]. The reasons for the high water table are generally high precipitation and/or high inflow of water and/or impeded outflow of water because of the topography. This has some implications on many properties of those lands amongst them are (1) vegetation and (2) decomposition:

1. Wetland vegetation has adapted to the wet conditions and has often an aerenchymatic system, which is a mains system through which atmospheric oxygen can be transported down to the roots that are located in the water saturated region.

2. In water saturated soils anoxic conditions prevail. The consequence of that is, that processes demanding oxygen cannot occur and decomposition rates are generally lower than under oxic conditions. Therefore, a high amount of organic matter accumulates in the soil leading to an organic content which is at least 30%, but can be much higher [*Scheffer and Schachtschabel*, 1982]. Thus, about 24% of the global soil organic matter is stored in the water saturated soils of tundra and boreal forest regions [*Schlesinger*, 1991].

Fig. 4 illustrates the dominant processes in wetlands leading to methane emission. They are explained in more detail in the following.

Methane Production

Methane is produced by methanogenic bacteria under strictly anoxic conditions, i.e. in the absence of oxygen. This is the case in saturated soils, because the diffusion of O_2 through water is very slow. Methane production depends on the availability of suitable substrate which originates mainly from root exudates, dead fine roots and the input of plant litter. The substrate used by methanogenic bacteria mainly consists of simple organic compounds, such as CO_2+H_2 and acetate, formed by different microbial species from more complex organic material

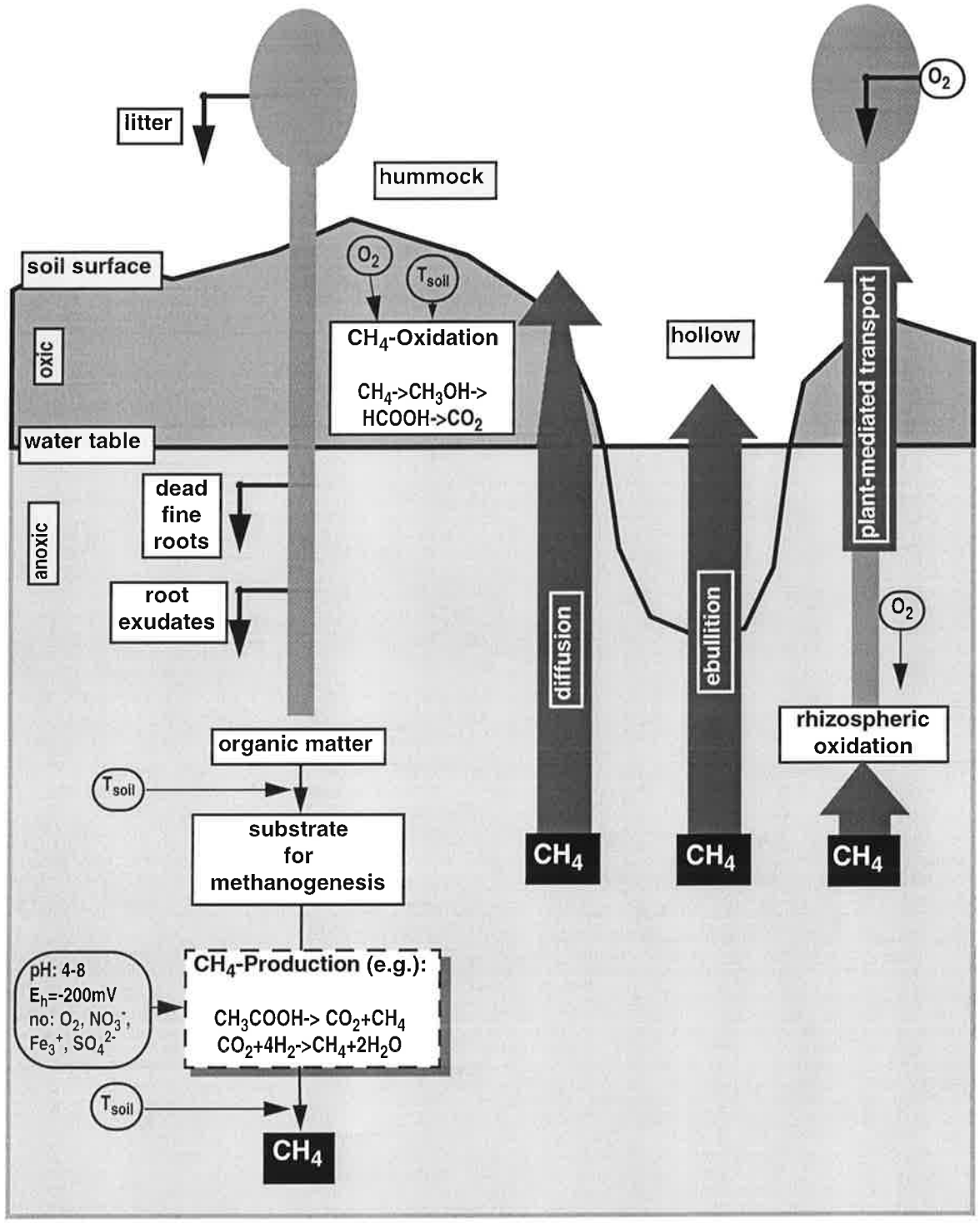

Fig. 4: Processes in a wetland soil: the water table divides the soil into the anoxic and the oxic zones; the soil surface can be either above or below the water table; wetland microtopography: hummocks are raised by several decimeters above the wetland surface, hollows are (generally water-filled) depressions; organic matter is incorporated into the soil as litter, dead fine roots and root exudates by plants; substrate for methanogenesis is obtained by degradation of organic matter (temperature (T_{soil}) dependent processes); CH_4 is produced from this substrate by methanogenic bacteria (the conditions for this process to occur are: pH=4-8, the redox potential $E_h \leq -200mV$, the absence of electron acceptors like O_2, NO_3^-, Fe_3^+, SO_4^{2-}; a temperature dependent process); CH_4 is transported up to the atmosphere by diffusion, ebullition and plant-mediated transport; CH_4 diffusing through the oxic soil zone is consumed by CH_4 oxidation (a temperature dependent process); ebullition is the formation of gas bubbles in the water saturated soil zone and their ascent to the water table; many wetland plants are conduits for gases: O_2 is conducted from the atmosphere down to the rooting zone, CH_4 is transported up to the atmosphere; the occurrence of O_2 in the rooting zone leads to rhizospheric CH_4 oxidation

[*Conrad*, 1989; *Heyer*, 1990]. It is known that it is mainly the labile, fresh organic fraction which provides the substrate for methane formation [*Chanton et al.*, 1995]. For example *Bridgham and Richardson* [1992] observed low methane production rates in a peat containing 95% organic matter, because the peat was highly decomposed and thus contained little fresh organic matter. This suggests, that methane production is related to the productivity of a site which is also confirmed by the observed correlations between NPP, NEP or biomass and methane emission (see Sect. 1). Most methanogenic bacteria seem to grow best under neutral pH conditions. However, methane emissions have been observed from soils with pH values ranging from 4 to 8 [*Conrad*, 1989; *Shannon and White*, 1994]. Moreover, methanogenesis requires the absence of competing electron acceptors like sulfate (SO_4^{2-}), nitrate (NO_3^-) or ironIII (Fe^{3+}) and a redox potential below -200 mV. Furthermore, the availability of nutrients can enhance the productivity [*Schlesinger*, 1991]. The production of suitable substrate from organic material for methanogenesis as well as the methane production rate itself are affected by temperature. Q_{10} values which describe the temperature dependence of methane production rates, lie in the range from 1.7 to 16 [*Dunfield et al.*, 1993; *Valentine et al.*, 1994; *Westermann*, 1993].

Methane Oxidation

While methane formation is confined to the anoxic soil zone below the water table, methane consumption by methanotrophic bacteria requires oxygen. The methane oxidation can be described by Michaelis-Menten kinetics [*Bender and Conrad*, 1992], that is, that the methane consumption rate increases with increasing methane concentration and approaches a maximum saturation rate at high methane concentrations. Furthermore, methane oxidation rates are affected by temperature. However, the temperature dependence of methane oxidation is much lower than that of methane production. Observed Q_{10} values for methane oxidation lie in the range between 1.4 and 2.1 [*Dunfield et al.*, 1993; *Knoblauch*, 1994].

Transport

Transport is an important factor controlling the fraction of methane, formed in the anoxic soil zone, that is emitted into the atmosphere. There are three transport mechanisms contributing to the transport of methane from the soil to the atmosphere: molecular diffusion, ebullition and plant-mediated transport [e.g. *Crill et al.*, 1991]. The occurrence of the different transport mechanisms can alter methane emissions significantly. For example ebullition through the water saturated soil proceeds much faster than diffusion. If the top soil is oxic plant-mediated transport can enhance methane emission, because the oxic soil layer is bypassed.

Diffusion: Driven by the methane concentration gradient methane diffuses through the soil pores up to the atmosphere. In the water saturated soil region, diffusion proceeds through the

water-filled pores while in the unsaturated soil zone it proceeds mostly through the air-filled fraction of the pores [*Hillel*, 1982]. Since the diffusion coefficient of methane in water is by four orders of magnitude lower than in air [*Scheffer and Schachtschabel*, 1984], diffusion plays a minor role in the water saturated soil zone. On the other hand, methane diffuses relatively fast through the unsaturated soil zone, but there it is also exposed to oxygen and hence methane consumption.

Ebullition: In the water saturated soil layers methane is dissolved in water. Since the solubility of methane in water is fairly poor [e.g. *Pauss et al.*, 1990], saturation is reached at relatively low methane concentrations, usually around a concentration of 1875 µM at 10 °C [*Kaltofen et al.*, 1975]. In the case that there are several gases dissolved in the pore water, gas bubbles are formed as soon as the sum of the partial pressures of all gases exceeds a threshold value which is the sum of the hydrostatic and the atmospheric pressures plus the pressure required to move the soil particles [*Rothfuss and Conrad*, 1994]. The abundance of gases other than methane, such as nitrogen (N_2), which is a poorly soluble gas as well, depends on the occurrence of vegetation. In vegetated soils the concentration of N_2 was reported to be higher than in unvegetated soils [*Chanton and Dacey*, 1991]. Therefore, in vegetated soils bubble formation generally occurs at lower methane concentrations than in unvegetated soils. Bubbles formed in the pore water rise up to the water table. The velocity of bubbles ascending in pure water lies in the order of 1-10 cm/s [*Shafer and Zare*, 1991]. Since wetland soils are generally very porous, the relative pore volume being often greater than 90% [*Scheffer and Schachtschabel*, 1982], it is likely that the velocity of bubbles rising in a water saturated wetland soil is of similar magnitude. This means, that the occurrence of ebullition accelerates the transport of methane through the water saturated soil zone enormously.

Plant-mediated Transport: Several vascular plants are known to be capable of transporting gases through their stems [e.g. *Chanton et al.*, 1992a; *Schimel*, 1995; *Shannon et al.*, 1996]. Under water logged conditions, this mechanism is necessary to supply the roots with oxygen. Gas transport through plants is known to operate by molecular diffusion, effusion or active transport due to pressure differences [*Schütz et al.*, 1991; *Whiting and Chanton*, 1992]. Along the same pathway by which oxygen is transported down to the roots, methane can be transported up to the atmosphere. This transport mechanism can alter methane emissions from soils dramatically, since the oxic soil zone, where methane is consumed, is bypassed. On the other hand, the atmospheric oxygen transported down to the roots establishes a small aerobic region in the rhizosphere [*Gerard and Chanton*, 1993; *Holzapfel-Pschorn et al.*, 1986; *Schipper and Reddy*, 1996; *Schütz et al.*, 1989]. Therefore, even in the water saturated soil zone methane oxidation occurs in a small zone around the roots. This means, that a certain fraction of methane entering the root zone in the water saturated soil region is oxidized in the rhizosphere due to the presence of oxygen in this region. Nevertheless, in many studies, plant-

mediated transport has been shown to be the main emission pathway and thus enhancing methane emissions significantly (see Sect. 1).

2.2. Model Description

Since the processes leading to methane emission from wetlands occur in the soil we choose the following model structure (see Fig. 5): A 1-dimensional soil column is divided into 1 cm thick parallel layers. The position of the water table is assumed to be the boundary between the anoxic and the oxic soil zone. Methane is produced in the layers below the water table. The methane production rate is calculated as a function of the soil temperature and the Net Primary Productivity (NPP) which is assumed to be a measure for substrate availability. In the layers above the water table methane is consumed. The methane oxidation rate is calculated using the Michaelis-Menten equation. Besides, it is a function of the soil temperature. The three different transport mechanisms described above are modelled explicitly: (1) diffusion through the water or air filled soil pores, (2) the formation of gas bubbles in the water saturated soil layers and their ascent to the water table and (3) the transport of methane from layers above the rooting depth through the stems of plants up to the atmosphere.

The model forcing consists of daily values of the position of the water table, the soil temperature profile and the NPP. The model output are methane fluxes to the atmosphere and methane concentration profiles in the soil, both obtained on a daily basis by numerically solving the 1-dimensional continuity equation within the entire soil/water column:

$$\frac{\partial}{\partial t}C_{CH_4}(t,z) = -\frac{\partial}{\partial z}F_{diff}(t,z) + Q_{ebull}(t,z) + Q_{plant}(t,z) + R_{prod}(t,z) + R_{oxid}(t,z) \qquad (1)$$

where $C_{CH4}(t,z)$ is the methane concentration at time t and depth z, $F_{diff}(t,z)$ the diffusive flux of methane through the soil, $Q_{ebull}(t,z)$ and $Q_{plant}(t,z)$ represent sinks due to ebullition and plant-mediated transport, respectively. $R_{prod}(t,z)$ is the methane production rate, while $R_{oxid}(t,z)$ denotes the methane oxidation rate. In the following, each of the terms will be described in detail.

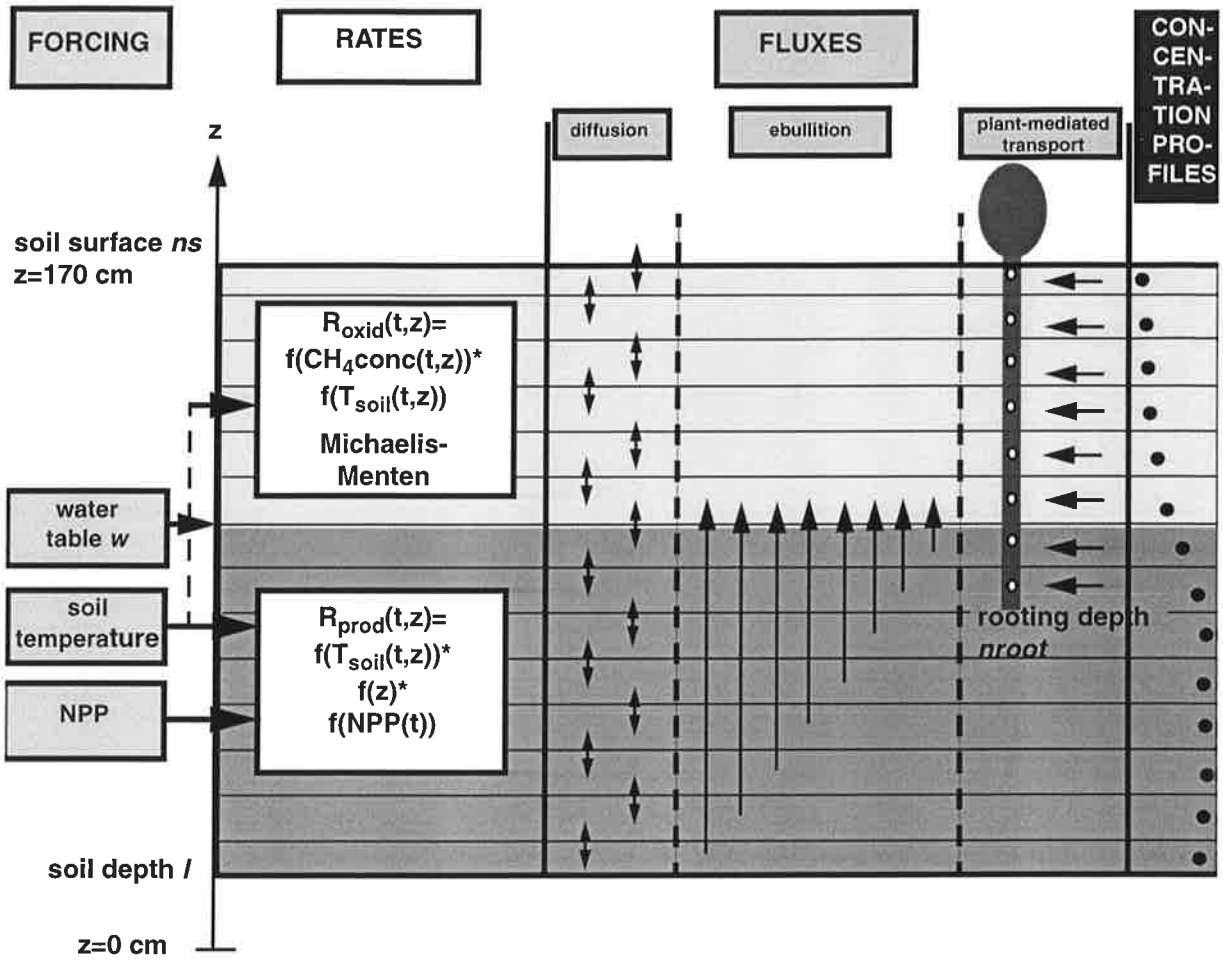

Fig. 5: Schematic representation of the model structure: the 1-dimensional soil column is divided into 1cm thick parallel layers. The forcing consists of daily records of the water table, the soil temperature and the NPP. Methane production occurs in the soil zone between the soil depth *l* and the water table *w*, which can be either below or above the soil surface *ns*. The methane production rate $R_{prod}(t,z)$ is a function of the soil temperature $T_{soil}(t,z)$ and the NPP, which is taken as a measure for substrate availability. In addition, it varies with depth taking into account that the availability of substrate decreases with increasing depth. Methane oxidation is confined to the soil layers between the water table and the soil surface. The methane oxidation rate $R_{oxid}(t,z)$ follows Michaelis-Menten kinetics, depends on the soil temperature $T_{soil}(t,z)$ and varies as a function of depth z. Transport proceeds by (1) molecular diffusion through the soil pores, (2) ebullition, which is the formation of gas bubbles in the water saturated layers and their ascent to the water table and (3) plant-mediated transport from layers above the rooting depth *nroot* to the atmosphere. The model calculates methane fluxes and methane concentration profiles in the soil on a daily basis

Methane Production Rate R_{prod}

As described above, there are two factors controlling the rate of methanogenesis: substrate availability and temperature. We consider only fresh organic matter produced by plants to be suitable substrate for methanogenesis. Therefore, the availability of substrate varies with time and soil depth. Its variation with time $f_{in}(t)$ has been parameterized in the following way: it is calculated as a function of the variation of the NPP with time, $f_{NPP}(t)$. Since part of the substrate is degraded from organic matter incorporated into the soil from dying plants in

autumn, we presume that in regions with a change between growing and non-growing season, i.e. where the growing season lasts for 3-9 months, the substrate availability increases again in autumn. We define the duration of the growing season as the time span when the soil temperature at 50 cm depth below ground is above 5 °C. The function $f_{in}(t)$ describes the variation of substrate availability with time t:

$$f_{in}(t) = 1 + \frac{1}{NPP_{max}} \cdot f_{NPP}(t) \tag{2}$$

where NPP_{max} denotes the annual maximum value of the NPP [gC*m^{-2}*mo^{-1}]. In regions where the growing season is shorter than 3 months or longer than 9 months $f_{NPP}(t)$ is:

$$f_{NPP}(t) = NPP(t) \qquad \text{at any time} \tag{3}$$

whereas in regions with a growing season lasting 3 to 9 months $f_{NPP}(t)$ is obtained from:

$$f_{NPP}(t) = \begin{cases} NPP(t) & \text{growing season} \\ NPP_{last} + \dfrac{NPP_{max} - NPP_{last}}{0.5 \cdot t_{nongrow}} \cdot t & \text{1. half non-growing season} \\ NPP_{max} - \left(\dfrac{NPP_{max} - NPP_{first}}{0.5 \cdot t_{nongrow}} \cdot t \right) & \text{2. half non-growing season} \end{cases} \tag{4}$$

Here, $t_{nongrow}$ means the duration of the non-growing season in days, and NPP_{last} and NPP_{first} denote the $NPP(t)$ values of the last and first day of the growing season, respectively. In addition, the availability of potential substrate for methanogenesis decreases with increasing soil depth z, because the sources of fresh organic material are located either at the soil surface or in the upper soil layers. Since root exudates represent a major source of substrate, it is assumed that in vegetated soils the availability of substrate is constant throughout the rooting zone and then decreases exponentially with depth. The substrate availability $f_{org}(z)$ is then given by:

$$f_{org}(z) = \begin{cases} 1 & \text{nroot} \le z \le \text{ns} \\ e^{(-|z - nroot|)/(10cm)} & 1 \le z < \text{nroot} \end{cases} \tag{5}$$

where *nroot* denotes the rooting depth, *ns* the soil surface and *l* is the soil depth, i.e. the lower boundary of the active layer. In unvegetated soils the vertical distribution of substrate $f_{org}(z)$ is

assumed to decrease exponentially from the soil surface to the lowest soil layer:

$$f_{org}(z) = 0.857 \cdot e^{(-|z-ns|)/(20cm)} \qquad 1 \le z \le ns \tag{6}$$

The variation of the methane production rate with temperature is formulated in the following way. We choose a Q_{10} dependence with a Q_{10} value of 6 lying within the range of observed Q_{10} values ranging from 1.7 to 16 [*Dunfield et al.*, 1993; *Valentine et al.*, 1994; *Westermann*, 1993]. We assume that this temperature function includes both, the temperature dependence of the production of substrate for methanogenesis and that of methane production. The temperature function describes the response to the seasonal variation of the soil temperature $T(t, z)$ at time t and depth z relative to the annual mean soil temperature T_{mean} at the site. Consequently, the methane production rate $R_{prod}(t, z)$ at time t and depth z is described as:

$$R_{prod}(t, z) = R_0 \cdot f_{org}(z) \cdot f_{in}(t) \cdot f(T) \cdot Q_{10}^{\frac{T(t,z)-T_{mean}}{10}} \tag{7}$$

R_0 is a constant rate factor expressed in units of µM/h (1M=1mol/l). It is a measure for the ‚absolute' substrate availability and quality (since $f_{in}(t)$ and $f_{org}(z)$ describe only relative changes of the substrate availability with time and depth). Because in the model those quantities are not simulated explicitly, the parameter R_0 is a tuning parameter which has to be adjusted to each data set. As shown in Sect. 3, it only changes the amplitude but not the pattern of the modelled methane emissions.

The function $f(T)$ is a step function being 1, if $T(t, z)$ is above 0 °C, and 0 else. This is equivalent to the assumption that there is no considerable methane production at sub-zero temperatures. There are a few studies that report winter methane emissions [*Dise*, 1992; *Melloh and Crill*, 1996] and at least one that reports methane production at temperatures down to -5°C [*Clein and Schimel*, 1995], but it does not seem that methane production at sub-zero temperatures is significant on a global scale. In some of those studies it is also suggested that part of the methane emitted in the winter is methane which was produced already in the summer and was stored in the soil. Furthermore, there are several studies showing that methane emissions during the winter time are significantly lower than during the growing season [e.g. *Whalen and Reeburgh*, 1992; *Shannon and White*, 1994]. For those reasons we choose to set $R_{prod}(t, z)$ to zero at sub-zero temperatures.

As mentioned in Sect. 2.1 the chemical conditions in the soil can also affect methanogenesis. This effect is not taken into account in the model. The potential effect of a disadvantageous pH and the availability of nutrients on methane production rates is included in the parameter R_0.

Concerning the effect of competing electron acceptors and the redox potential on methane production, it is assumed in the model, that the time scale, on which such effects are inhibiting methane production, are small compared to the time scale of the model, being one day. It is possible that under certain conditions it might take a few days after flooding until the proper redox potential is reached and all the competing electron acceptors are reduced. In general this assumption seems appropriate, especially considering that electron acceptors like SO_4^{2-} or NO_3^- usually occur only in small numbers in wetlands [*Conrad*, 1989].

Methane Oxidation Rate R_{oxid}

The methane oxidation rate $R_{oxid}(t, z)$ at time t and depth z is assumed to follow Michaelis-Menten kinetics [*Bender and Conrad*, 1992]. In addition, it depends on the soil temperature with observed Q_{10} values lying in the range between 1.4 and 2.1 [*Dunfield et al.*, 1993; *Knoblauch*, 1994]. In the model, Q_{10} for oxidation has been chosen to be 2. Thus, $R_{oxid}(t,z)$ is calculated from:

$$R_{oxid}(t, z) = -\frac{V_{max} \cdot C_{CH4}(t, z)}{K_m + C_{CH4}(t, z)} \cdot Q_{10}^{\frac{T(t, z) - T_{mean}}{10}} \tag{8}$$

where K_m and V_{max} are the Michaelis-Menten coefficients. $C_{CH4}(t, z)$ denotes the methane concentration [µM] at time t and depth z, whereas T_{mean} is the annual mean soil temperature [°C]. The observed values for K_m lie between 1 and 5 µM [*Dunfield et al.*, 1993; *Knoblauch*, 1994], while V_{max} has been found to cover the range of about 5 to 50 µM/h [*Dunfield et al.*, 1993; *Knoblauch*, 1994; *Krumholz et al.*, 1995; *Moore and Dalva*, 1997; *Sundh et al.*, 1994; *Watson et al.*, 1997]. In the model K_m and V_{max} have been set to 5 µM and 20 µM/h, respectively. During the tests of the model against data sets from various wetlands it turned out that a V_{max} value of 20 µM/h cannot be used at all sites. Therefore, at sites where a value of 20 µM/h did not yield satisfactory results we choose another value for V_{max}, the resulting values lying in the range from 3 to 45 µM/h being in good agreement with the observations. However, for the global model runs we choose a globally constant value of 20 µM/h.

In the model, methane oxidation occurs only in the unsaturated soil layers. It has been observed, that in ecosystems with a water table being several decimeters above the soil surface there can be, due to turbulent diffusion, enough oxygen in the standing water column to make methane oxidation possible [*Valentine*, pers. comm.; *Reeburgh*, pers. comm.]. Since it is not known, if this effect is of general importance in different wetland types, it has not been incorporated into the model.

Diffusion F_{diff}

The diffusive flux $F_{diff}(t,z)$ is calculated using Fick's first law:

$$F_{diff}(t,z) = -D_{CH4}(z) \cdot \frac{\partial}{\partial z} C_{CH4}(t,z) \tag{9}$$

where $D_{CH4}(z)$ is the diffusion coefficient of methane at depth z and $C_{CH4}(t,z)$ the methane concentration at time t and depth z. Since in the soil diffusion occurs only through the soil pores, the diffusion coefficient is obtained from:

$$D_{CH4}(z) = D_i \cdot 0.66 \cdot f_{coarse} \tag{10}$$

which is the so-called Penman relation [*Hillel*, 1982] using a tortuosity coefficient, which has been set to 0.66, suggesting that the distance covered by diffusion is about two-thirds of the length of the real average path. In the unsaturated soil layers, D_i is the diffusion coefficient of methane in bulk air, which is 0.2 cm^2/s [*D'Ans and Lax*, 1967] while in the water saturated soil layers D_i=10^{-4}*0.2 cm^2/s [*Scheffer and Schachtschabel*, 1984]. The factor f_{coarse} denotes the relative volume of the coarse pores, i.e. we assume that diffusion proceeds mainly through the large pores because of the following reasons: even in the unsaturated soil layers, the soil contains a certain fraction of water which is held mainly in the small and medium pores, because the capillary forces are higher in smaller pores. Therefore, we can assume that it is mainly the large pores, that are air-filled and through which diffusion occurs. Also in the water saturated layers we assume that diffusion proceeds mainly through the coarse pores.

To solve the diffusion equation we use the Crank-Nicolson scheme [*Press et al.*, 1992]. The methane concentration values are defined in the middle of each layer, whereas the diffusion coefficients are defined at the layer boundaries.

We choose the following boundary conditions:

$$\frac{\partial}{\partial z} C_{CH4}(t, z = l) = 0 \tag{11}$$

at the lower boundary l and

$$C_{CH4}(t, z = u + 4cm) = C_{atm} \tag{12}$$

at the upper boundary u, which is either the water table $w(t)$ (if $w(t)>s$) or the soil surface s. C_{atm} is the atmospheric methane concentration of 0.076 µM.

At the water-air interface the methane concentrations in both phases are assumed to be in equilibrium. Hence their ratio is specified by the Bunsen solubility coefficient.

Ebullition Q_{ebull}

As soon as the methane concentration in a layer exceeds a certain threshold concentration C_{thresh}, methane bubbles are formed. Since there are usually enough condensation nuclei in the soil and due to the occurrence of other gases, C_{tresh} usually is significantly lower than the saturation concentration. According to *Chanton and Dacey* [1991], *Shannon et al.* [1996] and *Holzapfel-Pschorn* [1986] we assume that C_{tresh} is lower at vegetated sites than at unvegetated sites. In the model it is assumed that bubble formation occurs at methane concentrations between 500 µM and 1000 µM at totally vegetated and unvegetated soils, respectively, being equivalent to a mixing ratio of (26.5-53)% of methane in the bubble (at 10 °C). Thus, the threshold concentration for bubble formation is calculated from:

$$C_{thresh} = C_{min} \cdot \left(1 + \frac{P_{unveg}}{100}\right) \tag{13}$$

where C_{min} is the concentration at which bubble formation occurs, if the site is totally vegetated (500 µM) and P_{unveg} is the percentage of unvegetated, bare soil.

In order to determine the flux $F_{ebull}(t)$ of methane reaching the water table $w(t)$ at time t in the form of gas bubbles, we first calculate the rate $Q_{ebull}(t, z)$ at which methane in the form of bubbles is removed from depth z:

$$Q_{ebull}(t, z) = -k_e \cdot f(C_{CH4}) \cdot (C_{CH4}(t, z) - C_{thresh}) \tag{14}$$

where k_e is a rate constant of the unit 1/h and $f(C_{CH4})$ is a step function taking the value 1, if the methane concentration $C_{CH4}(t, z)$ is greater than C_{thresh}, and 0 otherwise.

Bubbles are assumed to reach the water table within one model timestep being 1 hour. This is equivalent to the assumption that the bubbles ascent with a velocity of at least 1m/h which is much smaller than the velocity of bubbles ascending in pure water of 1-10cm/s [*Shafer and Zare*, 1991]. Thus, the ebullitive flux $F_{ebull}(t)$ is obtained by integrating $Q_{ebull}(t,z)$ over the whole water saturated zone:

$$F_{ebull}(t) = \int_l^w Q_{ebull}(t, z)dz \tag{15}$$

where l is the lower boundary of the active layer and w the water table. If the water table is at or above the soil surface, $F_{ebull}(t)$ contributes directly to the methane flux into the atmosphere.

Otherwise, the amount of methane rising to the water table in the form of bubbles is added to the methane concentration in the lowest unsaturated soil layer.

Plant-Mediated Transport Q_{plant}

The occurrence of vascular plants provides an effective mechanism by which methane can be transported up to the atmosphere. Moreover, oxygen can be conducted down to the roots this way. The results from several studies of plant-mediated transport suggest that the main emission pathway is by molecular diffusion or effusion through the plant stems [*Chanton et al.*, 1992a; *Chanton et al.*, 1992b; *Happell et al.*, 1993; *Nouchi and Mariko*, 1993; *Shannon et al.*, 1996]. Consequently, the flux of methane through plants is assumed to be proportional to the concentration gradient between the soil and the atmosphere. Since the atmospheric methane concentration is very small compared to the methane concentration in the soil it can be considered to be constant. Therefore, the plant-mediated methane flux can be taken to be proportional to the methane concentration in the soil. This assumption corresponds well with observations by *Nouchi and Mariko* [1993] who found a linear relationship between methane emission rates through plants and pore water methane concentrations. On the other hand, methane entering the roots of plants has to pass through the small oxic zone around the root tips and a certain fraction P_{ox} of methane is oxidized. There are a few studies examinig rhizospheric oxidation: *Schipper and Reddy* [1996] determined the fraction of methane consumed by rhizospheric oxidation using two different methods and found values of 65±24 % and 79±20 %. *Schütz et al.* [1989] observed that about 90% of the methane produced was oxidized in case plant-mediated transport was the main (97%) emission pathway, while *Gerard and Chanton* [1993] obtained values for rhizospheric oxidation between 39% and 98%. Taking the high variability of observed values we set P_{ox} to 50%. Hence, the rate $Q_{plant}(t, z)$ at which methane is removed by plants from depth z at time t is calculated from:

$$Q_{plant}(t, z) = -k_p \cdot T_{veg} \cdot f_{root}(z) \cdot f_{grow}(t) \cdot C_{CH4}(t, z) \cdot (1 - P_{ox}) \qquad (16)$$

where k_p is a rate constant of the unit 0.01/h and T_{veg} a factor describing the ‚quality' of plant-mediated transport at a site, depending on the density of plant stands and the plant types and being in the range from 0 to 15. At sites where the predominant plant types and their capability of conducting gas are known, T_{veg} is derived from that knowledge. Otherwise, we consider shrubs not contributing to plant-mediated transport and trees being poor, grasses and sedges being good gas transporters. According to this classification we have developed a data set of T_{veg} by which T_{veg} can be derived as a function of the relative densities of shrubs, trees, grasses and sedges (see Sect. 4). The function $f_{root}(z)$ represents the vertical distribution of roots in the soil. It is assumed to decrease with depth and for the sake of simplicity we choose a linear relationship between root biomass and soil depth:

$$f_{root}(z) = 2 \cdot \frac{|z - nroot| + 1}{ns - nroot} \tag{17}$$

where *nroot* denotes the rooting depth and *ns* the soil surface.

The ability of plants to conduct gas is considered to vary with the growing state of the plants. This assumption agrees well with observations by *Schütz et al.* [1989], who found that the fraction of methane transported through rice plants increases with growing maturity of the plants. In the model we use the leaf area index (LAI) as a measure for the growing state of the plants. According to *Dickinson et al.* [1993] we define a mean LAI depending on the daily mean temperature at 50 cm depth below ground $T_{50}=T(t, z=120cm)$:

$$f_{grow}(t) = \begin{cases} \Lambda_{min} & T_{50} < \hat{T}_{grow} \\ \Lambda_{min} + \Lambda \cdot \left\{ 1 - \left[\frac{\hat{T}_{mat} - T_{50}}{\hat{T}_{mat} - \hat{T}_{grow}} \right]^2 \right\} & \hat{T}_{grow} \le T_{50} \le \hat{T}_{mat} \\ \Lambda_{max} & \hat{T}_{mat} < T_{50} \end{cases} \tag{18}$$

where Λ_{min} and Λ have been choosen to be 0 and 4, respectively, and $\Lambda_{max}=\Lambda_{min}+\Lambda$. T_{grow} is the temperature at which plants start to grow. In regions where the annual mean soil temperature is below 5 °C, T_{grow} has been set to 2°C, elsewhere to 7°C. This distinction has been made, because in cold regions plants start to grow at lower temperatures than in temperate and warm regions. The same is valid for the temperature at which they reach maturity, T_{mat}, which has been set to $T_{mat}=T_{grow}+10$°C.

Finally, the methane flux due to plant-mediated transport $F_{plant}(t,z)$ is calculated from:

$$F_{plant}(t) = \int_{nroot}^{ns} Q_{plant}(t) dz \tag{19}$$

where *ns* and *nroot* are the soil surface and the rooting depth, respectively.

Total Methane Emission F_{tot}

The total methane emission $F_{tot}(t)$ is calculated by adding all the fluxes from the different transport mechanisms. The diffusive flux $F_{diff}(t, z=u)$ at the soil/water-atmosphere boundary u, the flux due to plant-mediated transport $F_{plant}(t, z)$ and the ebullitive flux $F_{ebull}(t, z)$. The latter contributes only to the total flux $F_{tot}(t)$, if the water table is at or above the soil surface. Hence $F_{tot}(t)$ is obtained from:

$$F_{tot}(t) = F_{diff}(t, z = u) + F_{ebull}(t) + F_{plant}(t) \tag{20}$$

3. Results of the 1-Dimensional Model

3.1. Tests Against Data

Overview of Used Data Sets and Methodology

The methane model is tested against observations from 15 microsites within 6 wetlands located in North America, Europe and Central America. The observation periods of these data sets range from 1 season up to 3 years. Tab. 3 gives a summary of the data sets used in this study:

Table 3: Data Sets Used in this Study

No.	Site	Location	Stations	Reference
1	Michigan	42°N, 84°W	1	Shannon and White [1994]
2	Minnesota	47°N, 93°W	5	Dise [1993]
3	Finland	63°N, 31°E	4	Saarnio et al. [1997]
4	Alaska	65°N, 148°W	3	Whalen and Reeburgh [1992]
5	Canada	54°N, 105°W	1	Valentine (unpublished)
6	Panama	9°N, 80°W	1	Keller [1990]

Tab. 3: Number, site name, location, number of examined stations/microsites within one wetland and source of each data set used in this study

Methane emissions. At each site methane emissions were measured at a frequency of 2-4 observations per month.

Methane concentration profiles. At two sites (site 1 and 2) methane concentration profiles in the soil were obtained 1-2 times per month.

Forcing data. At all sites except site 6 the position of the water table and the soil temperature at different soil depths were observed at least at the same frequency as the methane emissions. Since at site 6 the forcing data were not observed we use the ECHAM4 model [*Roeckner et al.*, 1996] and the hydrological model (see Sect. 5) to run the methane model at this site. Because the model requires daily forcing data we interpolate the observed input data linearly to daily values. The NPP is obtained from the BETHY model [*Knorr*, 1997] for that $1^{o}*1^{o}$ grid box in which the wetland is located.

Parameters. The parameters soil depth (l), rooting depth (nroot) and the quality of plant-mediated transport (T_{veg}) are chosen based on informations about the specific wetland site. The parameter V_{max} is set to 20 µM/h in most cases, but is adjusted to the data set in situations where a value of 20 µM/h does not yield optimal results. The values of V_{max} used in this study range from 3 to 45 µM/h. The parameter R_0 is adjusted to the data set in each case. At most wetland sites we can use the same value for R_0 for all microsites within the same wetland. The values for R_0 obtained this way lie between 0.15 and 0.6 at the high latitude sites (1-5) and between 2.5 and 2.8 at the tropical site (6). In Sect. 3.2 we examine the sensitivity of modeled methane emissions to those parameters.

The results of the tests of the model against data sets from 15 stations are compiled in App. B. There we show for each station a plot containing the observed forcing data, a comparison of the modeled and the observed methane emissions and the simulated contribution of the three transport mechanisms diffusion, ebullition and plant-mediated transport. Each of these plots is briefly described. Furthermore, App. B contains descriptions of all six sites and tables summarizing the choice of the model parameters.

In the following, we show and discuss some of the results in more detail. We focus on examples demonstrating the influence of differences in the soil temperature, the position of the water table and the vegetation on simulated methane emissions.

1. Effects of Soil Temperature, Water Table and Vegetation on Methane Emissions

First we show the results of a comparison between modeled and observed methane emissions at two sites, namely site 1 (Michigan) and a station (JC6) from site 2 (Minnesota). Besides comparing the patterns of simulated and measured methane emissions we demonstrate how modeled and observed methane emissions respond to changes in the soil temperature and the position of the water table. Furthermore, using those examples we want to stress the influence of the three transport mechanisms under different conditions.

Description of Sites:

The Michigan-Site. This wetland is an open ombrotrophic peatland called Buck Hollow Bog, located at 42°N, 84°W [*Shannon and White*, 1994]. The vegetation consists of a wet lawn of *Sphagnum* mosses densely covered by *Scheuchzeria palustris*, an arrow grass which is known to emit significant amounts of methane [*Shannon et al.*, 1996]. The roots of these vascular plants penetrate about 50-80 cm below the soil surface [*Shannon*, pers. comm.]. The methane emissions were measured using 3 flux chambers grouped in a triangular pattern about 10 m apart from each other. The observation period was 3 years.

The Minnesota Site. This wetland is an open poor fen called Junction Fen (JC6), located at 47°N, 93°W. The vegetation is dominated by *Carex oligosperma* and some *Scheuchzeria palustris* over a lawn of *Sphagnum* mosses [*Dise*, 1993]. Most of the roots of the vascular plants are found in the upper 40 cm [*Verry*, pers.comm.]. The methane emissions were measured using 1 chamber and the observation period was 2 years. The chosen model parameters are compiled in Tab. 4:

Table 4: Parameters at the Two Test Sites

Parameter	Michigan	Minnesota
R_0	0.6	0.3
V_{max}	45µM/h	20µM/h
l	80cm	80cm
nroot	50cm	30cm
T_{veg}	15	4

Fig. 6 and Fig. 7 show the results of the tests at the Michigan and the Minnesota sites, respectively. The forcing data are plotted in the lower part: (c) shows the observed positions of the water table relative to the soil surface and (d) the observed soil temperatures at different depths. In (a) the comparison between modeled and observed methane emissions is shown. At both sites the seasonal pattern of observed methane emissions is reproduced quite well by the model. Especially at site 1 the simulation of the interannual as well as the seasonal variations of methane emissions compare well with the data. At the Junction Fen, simulated methane emissions decrease too early in 1989 following directly the decrease of the soil temperature, and both simulated and observed methane emissions are lower in 1990 than in 1989, but this difference is bigger in the observations than in the model results. In (b) we show the simulated relative contributions of the three different transport mechanisms diffusion, ebullition and plant-mediated transport.

The influence of the soil temperature on methane emissions. At both sites the patterns of modeled as well as observed methane emissions are dominated by changes in the soil temperature, when the water table is above the soil surface. This applies also to the interannual variations of methane emissions. Methane emissions from Buck Hollow Bog are higher in 1991 than in 1992 and 1993, because of the slightly higher soil temperatures in 1991. The same can be seen at the Junction Fen. Here, methane emissions are higher in 1989 than in 1990

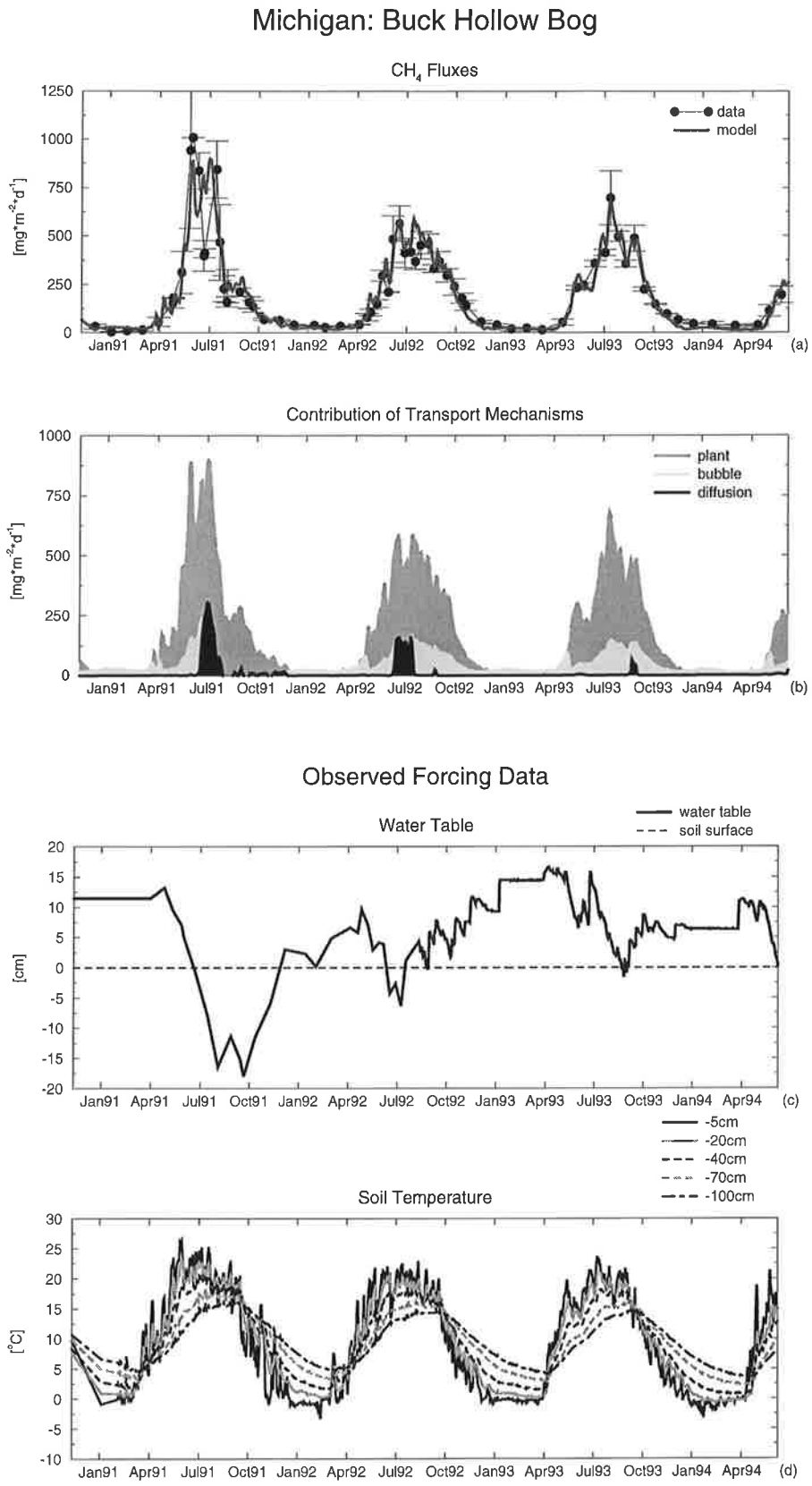

Fig. 6: (a): Comparison between modeled (thick line) and measured (dots with +/- 1SD error bars) methane emissions, (b): Modeled contributions of the three transport mechanisms to the total flux: Diffusion (black), ebullition (light grey), and plant-mediated transport (dark grey), (c): Forcing: Observed position of the water table, (d): Forcing: Observed soil temperatures at different soil depths

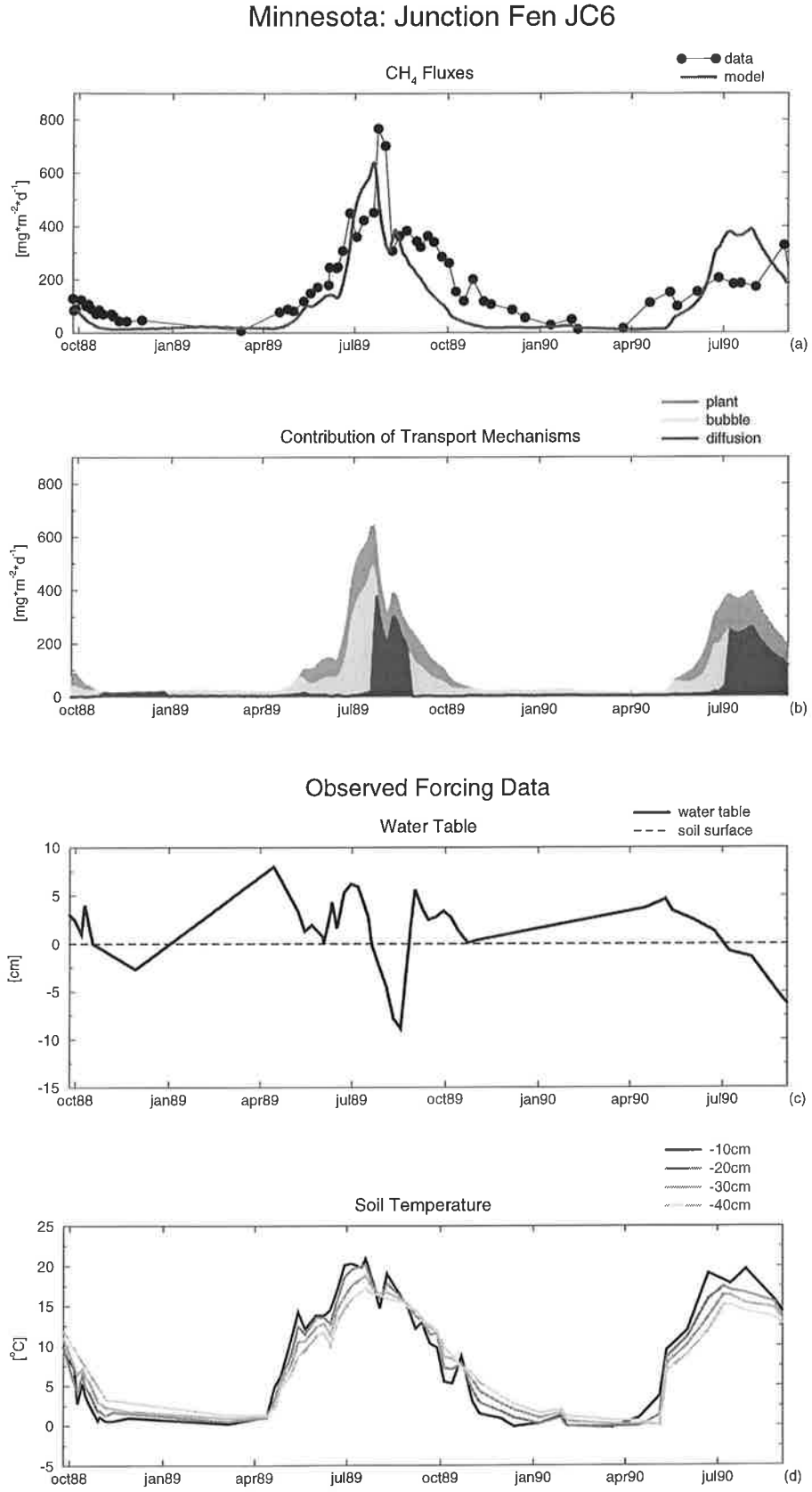

Fig. 7: (a): Comparison between modeled (thick line) and measured (dots) methane emissions, (b): Modeled contributions of the three transport mechanisms to the total flux: Diffusion (black), ebullition (light grey), and plant-mediated transport (dark grey), (c): Forcing: Observed position of the water table, (d): Forcing: Observed soil temperatures at different soil depths

again due to higher soil temperatures in the first year. Also day-to-day variations of methane emissions are caused by changes in the soil temperatures as long as the water table is above the soil surface. This effect is particulary clear at Buck Hollow Bog in 1993 and at the Junction Fen in 1990.

The influence of the position of the water table on methane emissions. As soon as the water table falls below the soil surface the observed connection between methane emission and soil temperature is no longer valid. In this situation methane diffuses through the soil pores and is partly oxidized in the unsaturated soil layers. Furthermore, rising bubbles cannot reach the soil surface anymore and only the deeper roots extend into the water saturated soil zone where high methane concentrations prevail. The consequence of a long period with the water table being below the soil surface can be seen at Buck Hollow Bog in 1991: There methane emissions drop to relatively small values of about 200 $mg*m^{-2}*d^{-1}$ already in August even though the soil temperature is still high at that time, because the water table stays at depths of about 15 cm below ground since July 1991. In 1992 and 1993 this drop of methane emissions occurs much later in the year, attributable to wetter conditions.

The influence of transport on methane emissions. At sites covered by vascular plants, as it is the case at Buck Hollow Bog and the Junction Fen, plant-mediated transport plays an important role during the growing season. At Buck Hollow Bog *Shannon et al.* [1996] observed in plant enclosure experiments that 64-90% of the net methane flux was emitted through *Scheuchzeria palustris*. The model results are in good agreement with this finding (see Fig. 6 (b)). Ebullition occurs only at times when the water table is above the soil surface. Diffusion plays only a role in case the water table is below the soil surface (see Fig. 6 (b) and Fig. 7 (b)).

Water table below the soil surface: As discussed above the presence of an unsaturated top soil layer reduces methane emissions and the way methane is transported into the atmosphere becomes crucial especially in this case. This can be demonstrated at Buck Hollow Bog. There the water table falls below the soil surface in June 1991. Immediately after this event emission by diffusion increases considerably. The same effect occurs at the Junction Fen in August 1989. The reasons for this behaviour lie in the diffusion coefficient which increases by a factor of 10^4 as soon as the soil becomes unsaturated, and in the high methane concentration in the uppermost soil layer shortly after the water table falls below the soil surface. After a period of about 15 days, emission by diffusion declines again due to oxidation in the unsaturated zone. *Moore and Roulet* [1993] observed a similar pattern: Increased fluxes with falling water table to 20 cm depth within 10 days, followed by decreased fluxes as the water table continues to fall further.

The amount of methane emitted through plants decreases in August 1991 at Buck Hollow Bog and in August 1989 at the Junction Fen, because less root extend into the water saturated zone due to the low water table. Ebullition of methane stops immediately when the water table declines below the soil surface. Now methane that is transported in the form of bubbles up to the water table is released into the unsaturated soil layer where it can be oxidized.

Water table above the soil surface: In case the water table is above the soil surface methane is transported mainly by ebullition and through plants. The relative contribution of these two transport mechanisms depends on the efficiency of vegetation to conduct methane (T_{veg}). This can be seen by comparing Fig. 6 (b) and Fig. 7 (b). The relative fraction of methane transported through plants is higher at Buck Hollow Bog than at the Junction Fen, since T_{veg} is higher there. In situations when the water table is above the soil surface a high contribution of plant-mediated transport reduces methane emissions, because part of the methane emitted through plants is oxidized in the rhizosphere. This effect was also observed by *Holzapfel-Pschorn et al.* [1986] who investigated methane emissions from vegetated and unvegetated sites. They found that there was more ebullition at unvegetated sites than at vegetated ones and that in case the water table was above the soil surface a larger fraction of produced methane was emitted from unvegetated soils.

2. Effect of Different Vegetation and Soil Moisture Within one Wetland

In this section we show and discuss the results of a comparison between modeled and observed methane emissions from 3 microsites of a Finnish wetland. We focus on intrasite variations within the same wetland, that is on differences in the position of the water table and the rooting depth and their influences on simulated methane emissions. The data set used here was obtained in the Salmisuo mire complex in eastern Finland, located at 63°N, 31°E [*Saarnio et al.*, 1997]. The study site consists of a minerogenic, oligotrophic low-sedge *Sphagnum* fen. The observation period was 1 season.

Descripiton of Microsites:

Flark. The dominant vegetation type is *Eriophorum vaginatum*. Its roots extend to a depth of about 30 cm [*Saarnio*, pers. comm.]. The methane emissions were measured using 4 collars.

Low Hummock. The dominant vegetation type is *Eriophorum vaginatum* with roots extending to a depth of about 30 cm. The methane emissions were measured using 2 collars.

Carex Lawn. The dominant vegetation type is *Carex rostrata* of which the roots are much deeper than those of *Eriophorum vaginatum* penetrating about 2 m below the soil surface

[*Saarinen*, 1995]. Therefore, we set the rooting depth equal to the soil depth. The methane emissions were measured using 4 collars.

Remarkable methane production was observed down to 40-50 cm below the water table [*Saarnio et al.*, 1997]. Therefore, we set the soil depth l to 70 cm at all microsites. In Tab. 5 the chosen parameters are compiled:

Table 5: Parameters at the Three Finnish Microsites

Parameter	Flark	Low Hummock	Carex Lawn
R_0	0.34	0.34	0.34
V_{max}	20μM/h	20μM/h	20μM/h
l	70cm	70cm	70cm
nroot	30cm	30cm	70cm
T_{veg}	12	12	12

As it can be seen from Tab. 5 we use the same values for R_0, V_{max}, l and T_{veg} at all microsites. In addition, the soil temperature is the same at all 3 microsites. Hence the differences in simulated methane emissions between those microsites are attributed either to differences in the positions of the water table or to the difference in the rooting depths between the Carex lawn on the one hand and the flark and the low hummock on the other hand.

Microsites with different water table levels. First we investigate methane emissions from the flark and the low hummock. The latter is elevated by about 15 cm relative to the wetland surface. In this case all model parameters are the same and the only difference lies in the water table levels. Fig. 8 (b) shows the positions of the water table at the low hummock and the flark. In Fig. 8 (a) the modeled and observed methane emissions from these 2 microsites are plotted (the grey areas were obtained by averaging the fluxes from all the collars of each microsite and adding/subtracting the standard deviation to/from that averages). The methane emissions from the flark are considerably higher than those from the low hummock due to the higher water table at the flark site. This effect agrees qualitatively and quantitatively well with the observations.

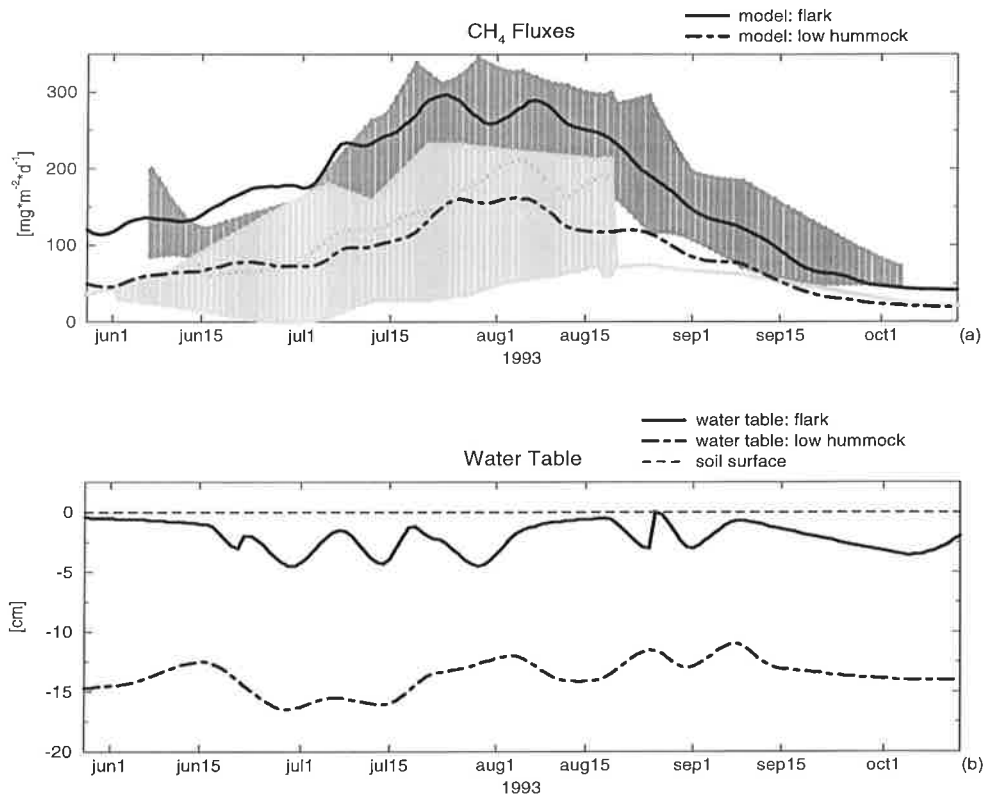

Fig. 8: Comparison of methane emissions from two microsites. (a): Modeled fluxes from the flark (solid line) and the low hummock (dot-dashed line); the shaded areas are the areas between the average of all measurements from the respective microsite +/- 1 SD: flark (dark grey) and low hummock (light grey); (b): observed positions of the water table at the flark (solid line) and the low hummock (dot-dashed line) relative to the soil surface (dashed line)

Microsites with different vegetation (rooting depths). Here we discuss methane emissions from the flark and the Carex lawn. At both microsites the position of the water table varies between the soil surface and 5 or 7.5 cm below ground for the flark and the Carex lawn, respectively. The main difference between the sites is that the roots penetrate down to 70 cm below ground at the Carex lawn as opposed to 30 cm below ground at the flark. In the model deeper roots affect methane emissions in various ways. The availability of substrate is highest in the rooting zone, plant-mediated transport operates from all layers of the rooting zone and rhizospheric oxidation occurs in all layers of the rooting zone. While the first two processes enhance methane emission if the roots are deeper, the latter reduces methane emission. Fig. 9 shows the modeled and observed methane emissions from those 2 microsites which compare quite well with the observations. At the Carex lawn plant-mediated transport is the main emission pathway, whereas at the flark the relative contributions of plant-mediated transport and diffusion are quite similar. The reason for this lies in the fact that at the Carex lawn methane is removed from all soil layers by plant-mediated transport in the model, while this occurs only in the upper 30 cm at the flark microsite. On the other hand, emission by diffusion is lower at the Carex lawn than at the flark for the same reason. The total emission from the

Carex lawn is higher than from the flark, with the maximum emission being 360mg*m^{-2}*d^{-1} at the Carex lawn as opposed to 300mg*m^{-2}*d^{-1}at the flark. Thus, plant-mediated transport enhances methane emissions at sites where the water table is below the soil surface. The magnitude of this plant induced enhancement is with 20% quite considerable taking into consideration that the position of the water table is not lower than 5 cm below ground at the flark microsite. This implies that a water table being only a few centimeters below the soil surface leads to significant amounts of methane being oxidized and hence to clearly decreased methane emissions.

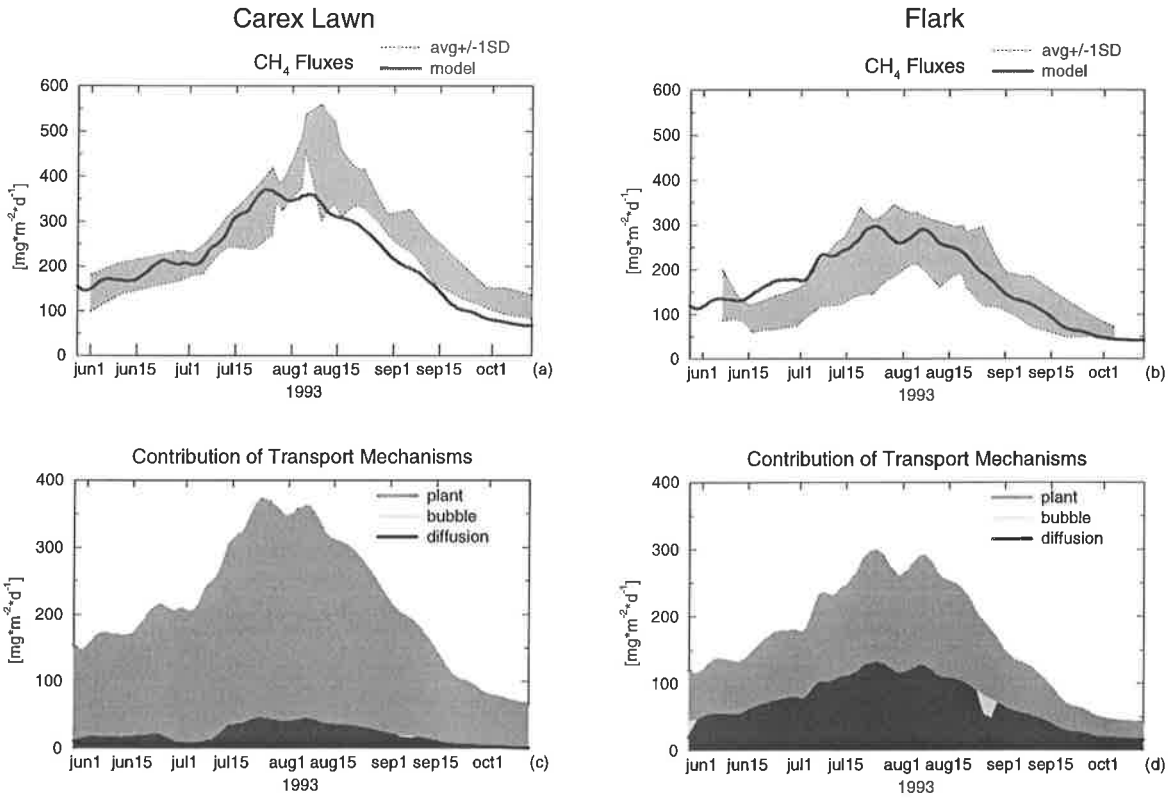

Fig. 9: Comparison of methane emissions from two microsites with different vegetation (rooting depths). Upper row: Comparison between modeled (thick line) and observed (grey area: average of all measurements at the respective microsite +/- 1 SD) methane emissions: Carex lawn (a) and flark (b); Lower row: Modeled contributions of the three transport mechanisms to methane emission: Carex lawn (c) and flark (d)

At the flark and the Carex lawn simulated methane emissions occur slightly too early (see Fig. 10). The modeled fluxes (Fig. 10 (a)) follow directly the changes in the soil temperature (Fig. 10 (b)) whereas in the observations there is a time lag between the soil temperature and methane emissions. The reason for this time lag could be that before methane production can start, appropriate soil conditions for methanogenesis must be established and suitable substrate for methanogenesis must be produced. This is not taken into account in the model. Another reason could be that at these microsites the deeper soil layers contribute more to methane

production than the upper ones, possibly due to better conditions (e.g. substrate availability and quality). This would cause modeled methane emissions to follow changes in the soil temperatures of the deeper soil layers of which the phase is delayed relative to the phase of the soil temperatures of the upper soil layers. However, this effect is only seen at that two microsites of the Finnish wetland and does not seem to be of general importance in other wetlands.

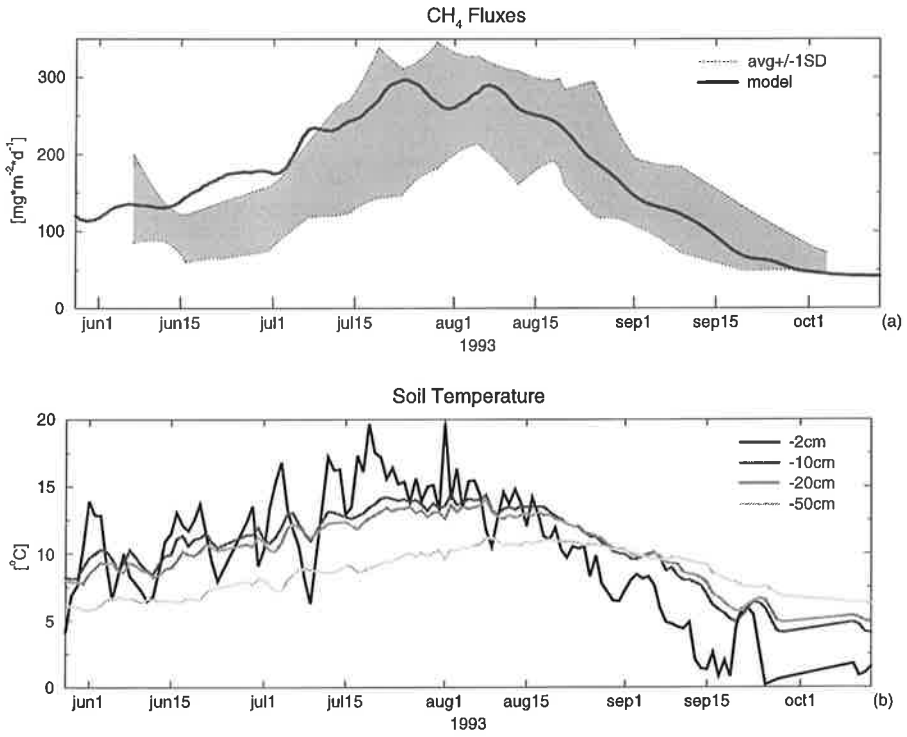

Fig. 10: Methane emissions from the flark microsite. (a): Comparison between modeled (thick line) and measured (grey area: average of all measurements at the flark microsite +/- 1SD), (b): Forcing: Observed soil temperatures at different soil depths

3. An Arctic Tundra Site in the Presence of Permafrost

We also test the model with data from an Alaskan Arctic tundra site which is underlain by permafrost, located at 65°N, 148°W [*Whalen and Reeburgh*, 1992]. During the summer the soil starts to thaw and the maximum thaw depth of about 70 cm below ground is attained in autumn. Here we want to discuss the results with measurements from the so called Black Hole site.

Black Hole. The vegetation consists of *Sphagnum* mosses and there are no vascular plants which means that plant-mediated transport does not occur. The organic horizon overlaying the

mineral soil is 12-50 cm thick. We choose to set the active layer depth equal to the thaw depth. Methane emissions were measured at three Black Hole stations called BH1, BH2 and BH3. The chosen model parameters are compiled in Tab. 6:

Table 6: Parameters at Black Hole

Parameter	Black Hole
R_0	0.3
V_{max}	3µM/h
l	thaw depth
nroot	0
T_{veg}	0

In Fig. 11 (a) modeled and observed methane emissions are plotted. Fig. 11 (c) and (d) show the averages of the observed forcing data soil temperature (d) as well as thaw depth and water table (c). In contrast to all other wetland sites used in this study the seasonal variation of the fluxes observed at the 3 stations BH1-3 differ considerably. Since the water table levels and the soil temperatures are quite similar at all BH sites (not shown) these differences in the measurements cannot be attributed to differences in the forcing. It is hard to guess what the cause for the high variation in the observed methane emissions might be. Therefore, we compare the modeled emissions to the observed fluxes from sites BH1-3 and to the average flux of the 3 sites. With the latter the simulated emissions compare quite well (see Fig. 11 (a)).

An increasing thaw depth means that the production zone is being enlarged with time. Therefore, simulated methane emissions are of the same magnitude in September as in August even though both the soil temperature and the water table levels are lower in September. In this context we want to point out that the chosen value of V_{max} describing the maximum methane oxidation rate in the unsaturated soil zone has been set to only 3µM/h as opposed to values of 20µM/h at most other sites. One could speculate what the reason for this might be (perhaps a lower oxidation potential of the methanotrophic bacteria at that site or a higher soil moisture content in the soil layers above the water table; the soil moisture in the unsaturated zone is not taken into account in the model), but we just want to leave it at the fact that V_{max} has a relatively low value at that site which is still close to observed values for V_{max} lying in the range between 5 and 50 µM/h [*Dunfield et al.*, 1993; *Knoblauch*, 1994; *Krumholz et al.*, 1995; *Moore and Dalva*, 1997; *Sundh et al.*, 1994; *Watson et al.*, 1997]. Because of the lower value of V_{max}, the effect of a declining water table on methane emission is smaller than at the Finnish wetland sites discussed in the previous paragraph.

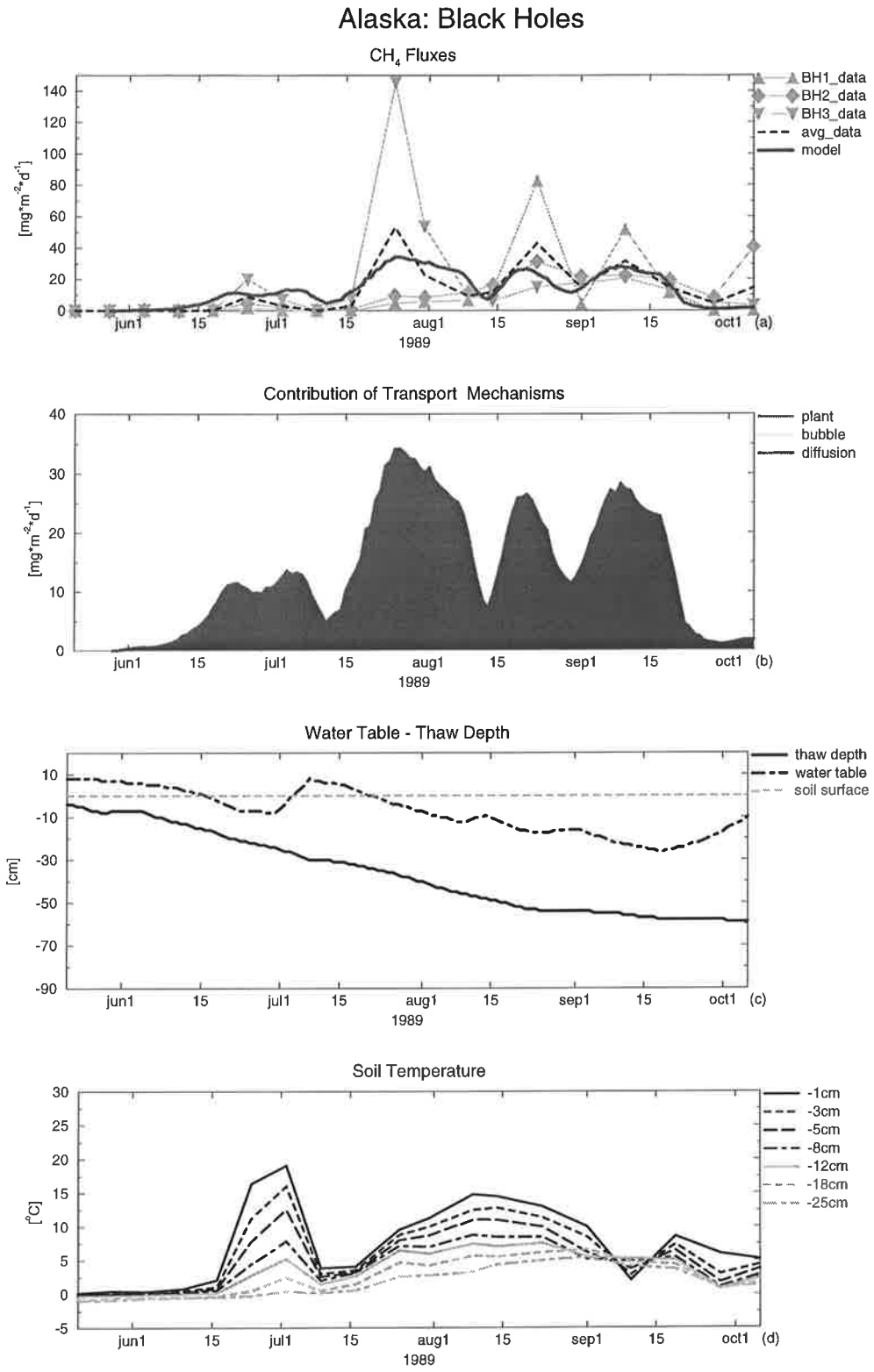

Fig. 11: (a): Comparison between modeled (thick line) and measured (the triangles and the square are observations from three stations within site „BH", the dashed line marks the average of those three measurements) methane emissions, (b): Modeled contributions of the three transport mechanisms to the total flux: Diffusion (black), ebullition (light grey), and plant-mediated transport (dark grey), (c): Forcing: Observed position of the water table (dot-dashed) and thaw depth (solid) relative to the soil surface (dashed), (d): Forcing: Observed soil temperatures at different soil depths

In Fig. 11 (b) we show the contributions of the 3 transport mechanisms to the total flux and it is clear that diffusion is the only emission pathway, because there are no vascular plants and the water table is below the soil surface at all times.

4. A Tropical Swamp Undergoing a Wet/Dry-Season Cycle

As a further example we discuss a simulation using a data set from a tropical wetland. We compare our model results with measurements from a wetland in Central Panama called Mojinga Swamp, located at 9°N, 80°W [*Keller*, 1990]. At this site methane emissions were observed over a period of 1 year, but neither the soil temperature nor the water table levels were observed. The information we have about the soil temperature is that it was nearly constant over the whole year. This site is characterized by a 4-month dry season between February and May. It is known that at the sites used in this study (MJ11-16 from *Keller*, [1990]) the water table rarely exceeded +30 cm during the wet season and was below 50 cm below ground, during the dry season [*Keller*, pers. comm.]. The input data of the methane model for this test were derived using the output of a climatological run of the ECHAM4 model [*Roeckner et al.*, 1996] in T106 ($1.1^{o}*1.1^{o}$). The soil temperature at different soil depths is calculated by the ECHAM4 model. To obtain the water table levels we use the hydrological model described in Sect.5 driven by climate data from the same run of the ECHAM4 model.

Mojinga Swamp. The vegetation of that swamp was dominated by the palm *Raphia taedigera*. Since we do not know much about the gas-conducting properties of this plant and do not have sufficient information to guess the soil and the rooting depths we use the parameters provided by the global data sets that were established for the global model runs (see Sect. 4). Since the global data sets do not provide values at that grid point where Mojinga Swamp is located (because the wetland coverage data set gives a value of 0% for the wetland coverage at that grid point) we use two neighbouring grid points (in the following denoted as p1 and p2) to derive the model forcing as well as all model parameters. The tuning parameter R_0 is adjusted to the data set in each case. In Tab. 7 the model parameters are compiled:

Table 7: Parameters at the Panama Site

Parameter	Mojinga Swamp p1	Mojinga Swamp p2
R_0	2.8	2.5
V_{max}	20µM/h	20µM/h
l	128cm	131cm
nroot	74cm	78cm
T_{veg}	9	4

Fig. 12 (d) shows the soil temperature at different soil depths as they are simulated by the ECHAM4 model for point p1 (those of point p2 are similar). They are consistent with the information that the soil temperature was almost constant throughout the year. In Fig. 12 (c) the water table calculated by the hydrological model forced by the ECHAM4 model is plotted. Again in this case the obtained values are consistent with the information that the water table was below 50 cm below ground during the dry season (February-May) and above the soil surface but below 30 cm above ground, during the wet season. Fig. 12 (a) shows the comparison between the simulated and the observed methane emissions. The latter are averages of 7 stations plotted with +/-1 standard deviation error bars. The most striking point is that the modeled as well as the observed methane emissions are zero or even negative during the dry season, attributable to the decline of the water table to depths of about 80 to 100 cm below ground, causing the development of a large oxic zone where methane is consumed. During the wet season the water is standing above the soil surface and ebullition is the dominant transport mechanism (see Fig. 12 (b)). Diffusion occurs only at times when the water table is below the soil surface and only if the oxic layer is small.

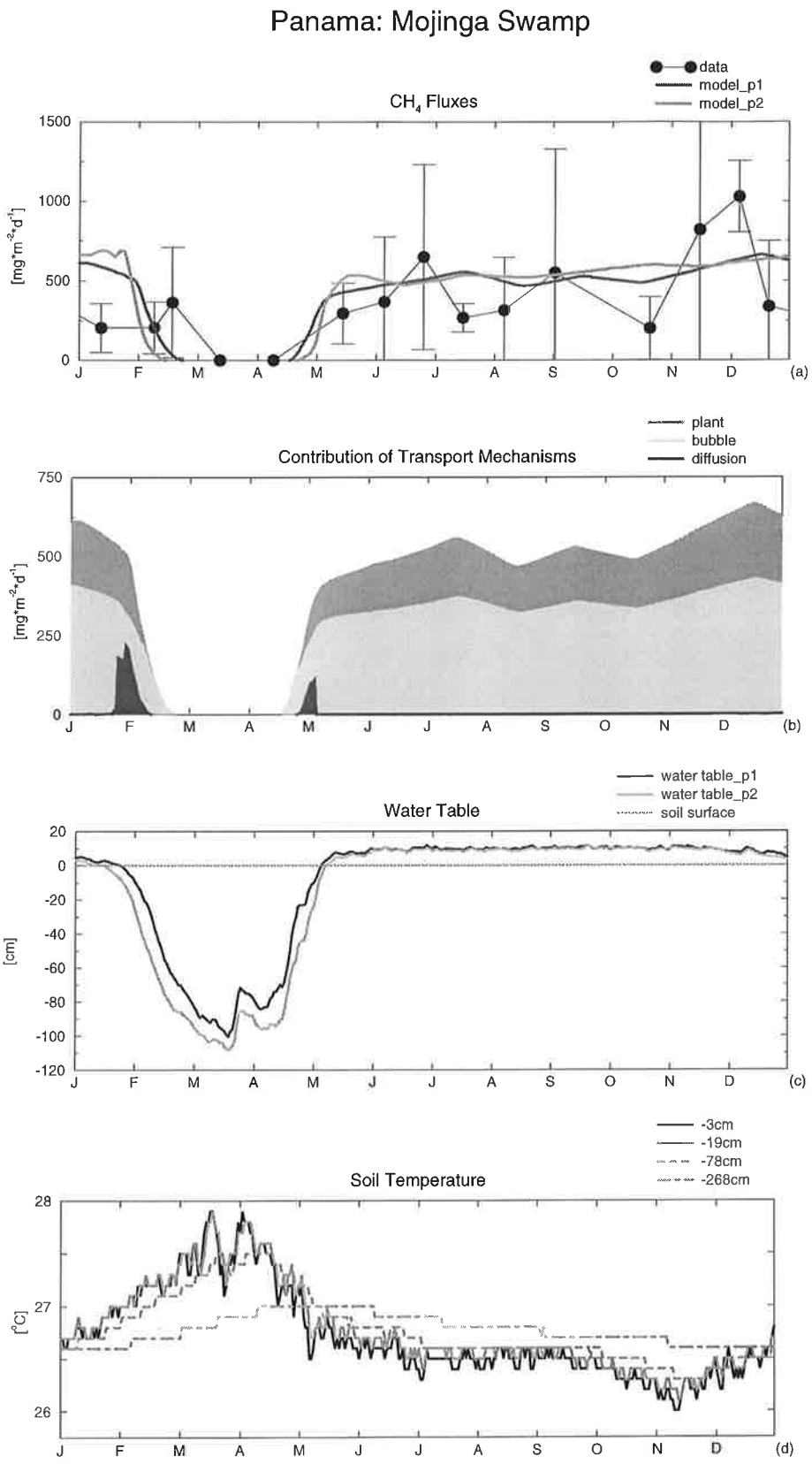

Fig. 12: (a): Comparison between modeled (thick lines: points p1 and p2 (see text)) and measured (dots with +/- 1SD error bars) methane emissions, (b): Modeled contributions of the three transport mechanisms (point p1): Diffusion (black), ebullition (light grey), and plant-mediated transport (dark grey), (c): Forcing: Position of the water table as calculated with the hydrological model forced by the ECHAM4 model, (d): Forcing: Soil temperature (point p1) at different soil depths as calculated by the ECHAM4 model

5. Comparison Between Modeled and Observed Concentration Profiles in the Soil

At site 1 (Michigan) methane concentration profiles were obtained 1-2 times per month. Fig. 13 shows a comparison between simulated and observed methane concentration profiles for the period between January 1992 and January 1993. It is clear that observed methane concentrations are smaller during the summer and the autumn (Jun 27 - Nov 14) than during the winter and the spring. This is due to plant-mediated transport. Even though methane production is much higher in the summer than in the winter, less methane is stored in the soil in the summer, because a large fraction is removed from the soil by plants. The same summer-winter pattern of methane concentrations in the soil is reproduced by the model. At many times modeled and observed concentration profiles compare well. However, in the model removal of methane from the soil by plants starts too early. On Apr 25 model results and observations agree well and on Jun 27 again, but in May the data still show high concentrations whereas in the model the concentrations are already decreasing. That means, that in the model the time the plants need to develop is underestimated. At the beginning of the winter the concentrations increase faster in the data than in the model as can be seen looking at the profiles of Nov 14, Dec 13 and Jan 9. However, these discrepancies occur only at times when the production rate is relatively low, and thus affect simulated methane emissions only slightly.

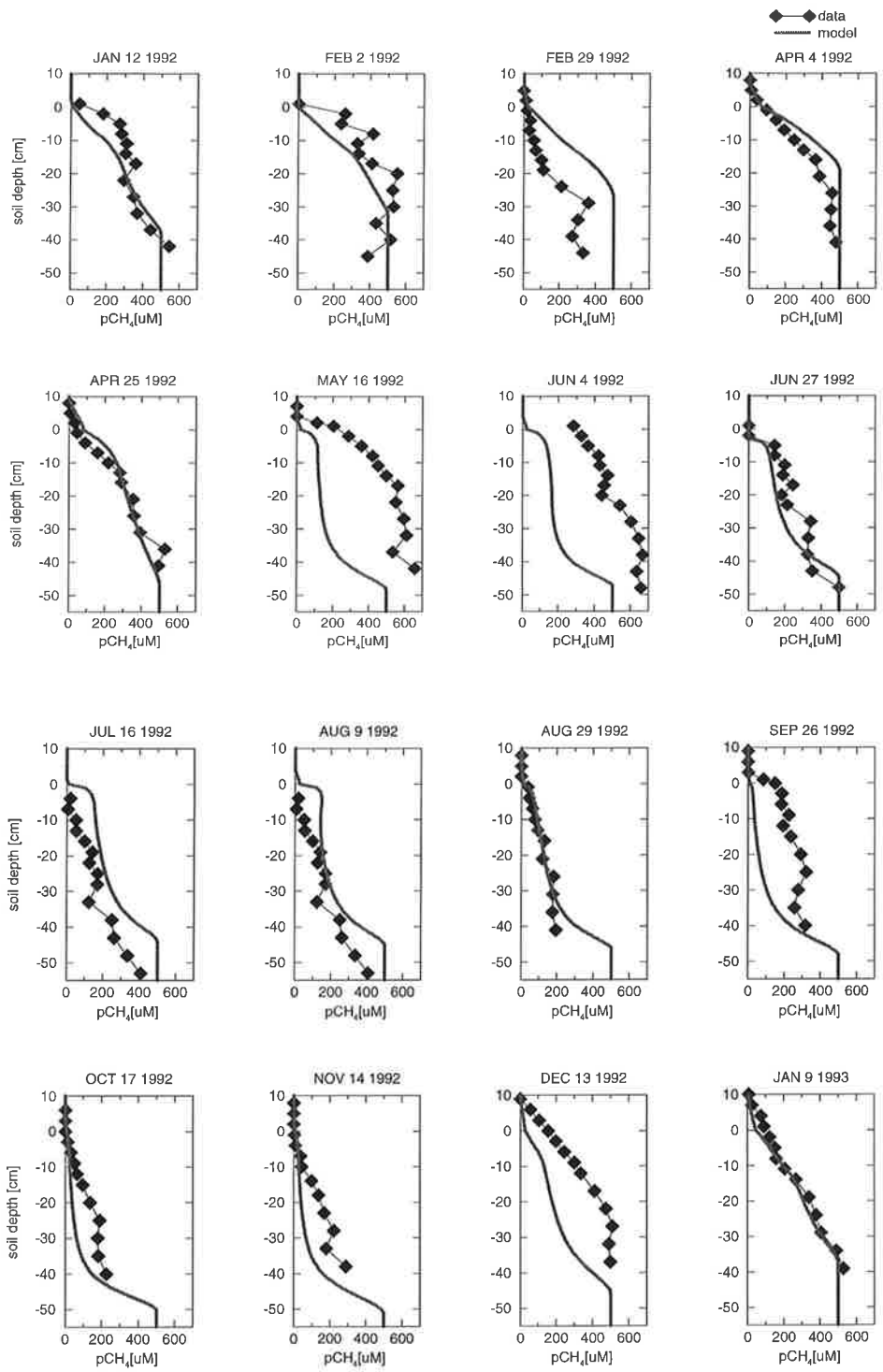

Fig. 13: Comparison between modeled (thick line) and observed (squares) methane concentrations in the soil

3.2. Sensitivity Tests

The sensitivity of the model to the choice of the model parameters R_0 (magnitude of the methane production rate), V_{max} (maximum methane oxidation rate), T_{veg} (quality of plant-mediated transport), l (soil depth) and nroot (rooting depth) is tested using data set 1 (Michigan). In addition, it is examined how the modeled methane emissions are affected by changes in the input data, i.e. by changes in the position of the water table and the soil temperature.

In the following we discuss the results of sensitivity tests with R_0, V_{max}, T_{veg} and the position of the water table. The results of the remaining sensitivity tests are compiled in App. C. In each case all model parameters except the one we are investigating are kept at the value of the control run, of which the parameters are compiled in Tab. 8:

Table 8: Parameters of the Control Run

R_0	V_{max}	l	nroot	T_{veg}
0.6	45µM/h	80cm	50cm	15

The simulated methane emissions obtained using different values of one of those parameters are always compared to the control run.

Sensitivity to R_0

Fig.14 shows how modeled methane emissions alter when R_0, i.e. the magnitude of the methane production rate, is modified. In (a) modeled methane emissions calculated with three different choices of R_0, namely 0.3, 0.6 (control) and 0.9 are plotted. It is clear that the amplitudes of modeled methane emissions change - higher emissions when the methane production rate is higher and vice versa - , but the pattern is the same in all three cases. In (b) and (c) we demonstrate how the contributions of the three different transport mechanisms react to a lower R_0 (b) and a higher R_0 (c). In case of a smaller R_0 the amounts of methane emitted by each of the transport mechanisms are smaller, and higher for a higher R_0, but the relative fractions are mainly unchanged. Only in July/August 1991 emission by diffusion stops earlier if R_0=0.3, and later, if R_0=0.9, because in case of a smaller R_0 the amount of methane entering the oxic soil zone is smaller and thus this methane is consumed sooner.

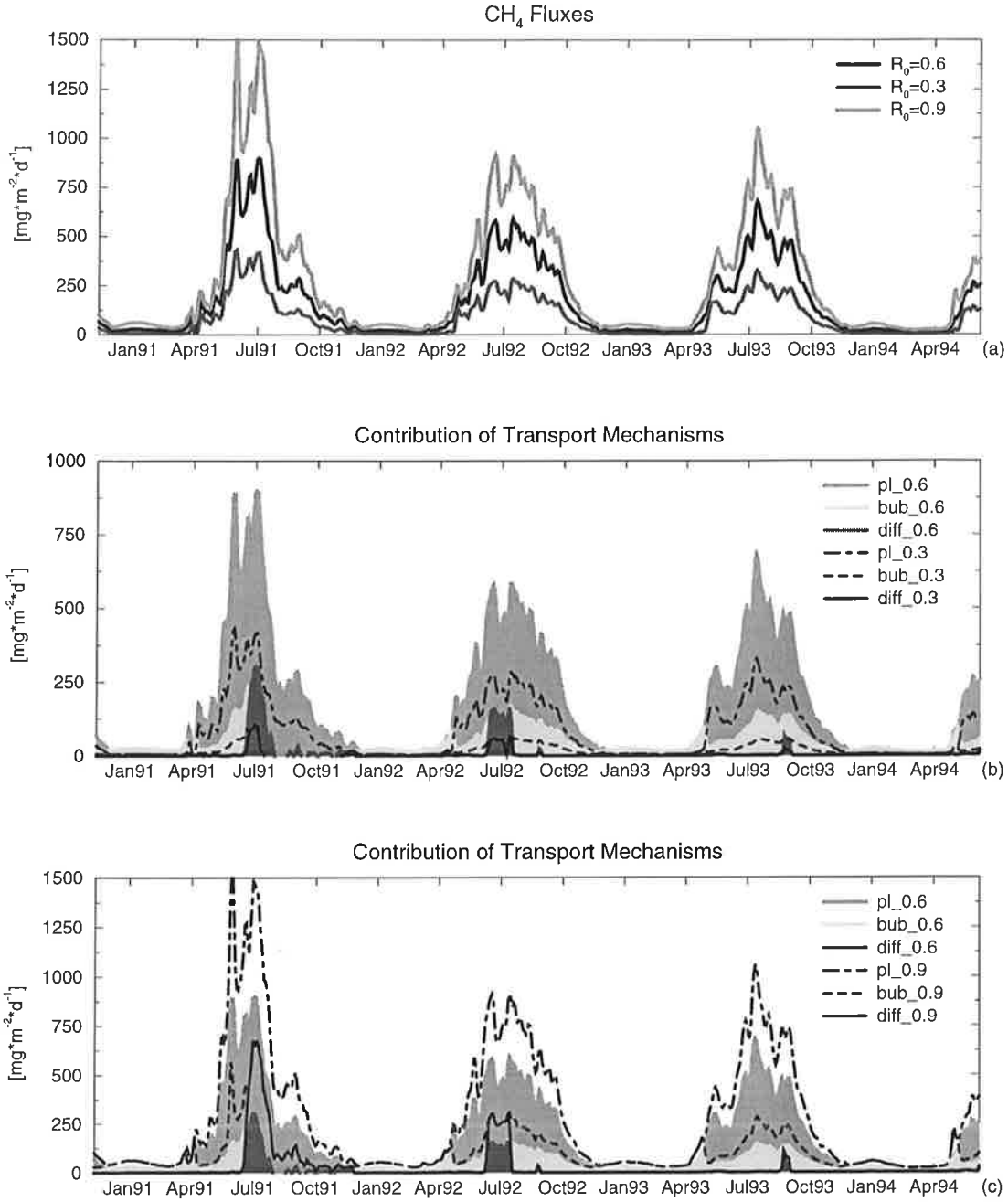

Fig. 14: Sensitivity to R_0: (a): Total modeled methane fluxes of the control run (R_0=0.6) (black) and two runs using R_0=0.3 (dark grey) and R_0=0.9 (light grey); (b): Comparison between the contributions of the three different transport mechanisms of the control run and the run with R_0=0.3: the shaded areas show the results of the control run: Diffusion (black), ebullition (light grey) and plant-mediated transport (dark grey), whereas the thick lines show the results of the R_0=0.3 run: Diffusion (solid), ebullition (dashed) and plant-mediated transport (dot-dashed); (c) Comparison between the contributions of the three different transport mechanisms of the control run and the run with R_0=0.9: Here we use the same nomenclature as in (b)

Sensitivity to V_{max}

The parameter V_{max} determines the maximum oxidation rate of methane in the unsaturated soil zone, i.e. in the soil layers above the water table. Therefore, it affects modeled methane

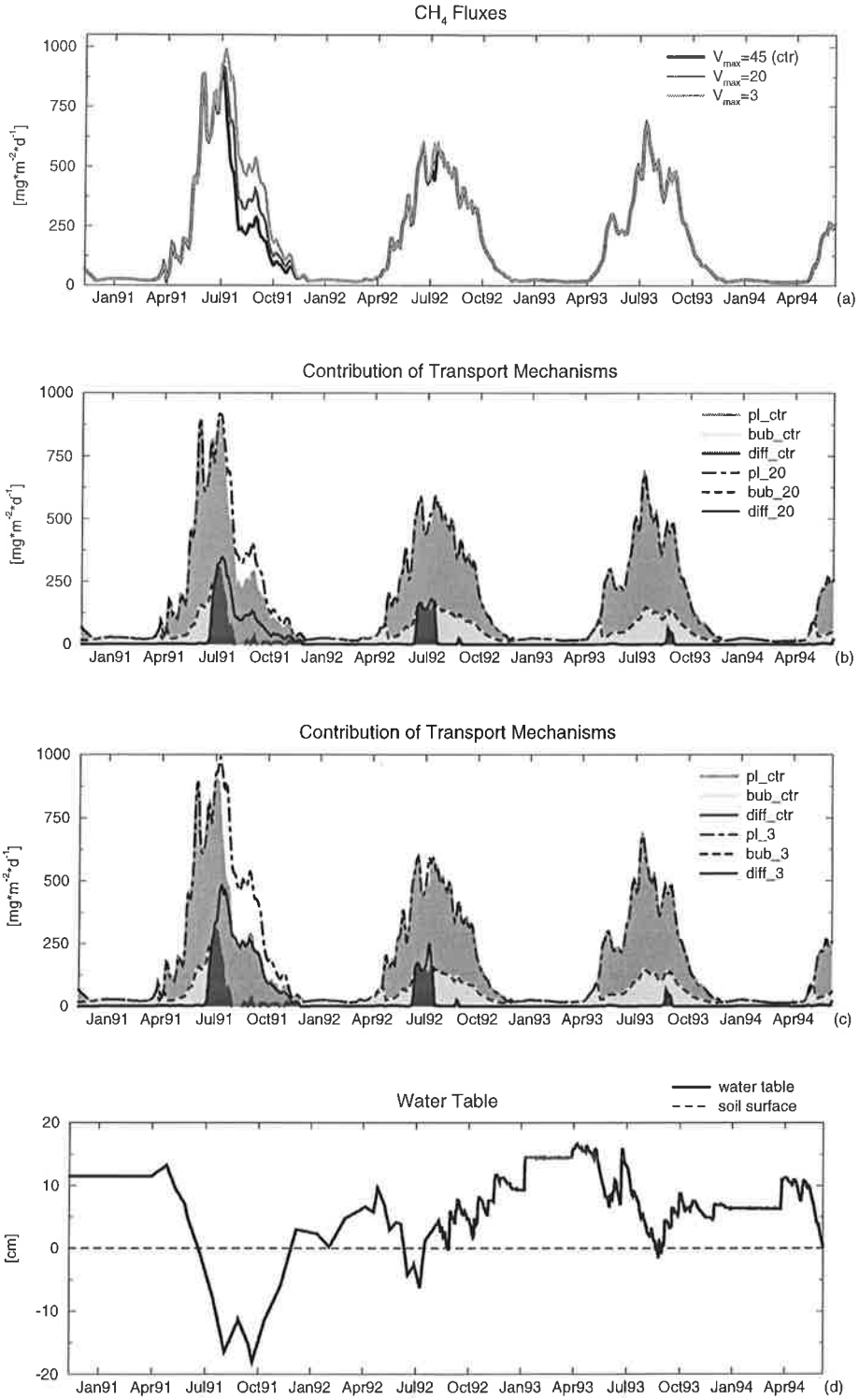

Fig. 15: Sensitivity to V_{max}: (a): Comparison between modeled methane fluxes of the control run (V_{max}=45µM/h) and two runs using V_{max}=20µM/h (dark grey) and V_{max}=3µM/h (light grey); (b) Contributions of the three different transport mechanisms to the total methane flux: the shaded areas show results of the control run: Diffusion (black), ebullition (light grey) and plant-mediated transport (dark grey), whereas the thick lines show the results of the run using V_{max}=20µM/h: Diffusion (solid), ebullition (dashed) and plant-mediated transport (dot-dashed); (c) Contributions of the three different transport mechanisms to the total methane flux: Comparison between the control run and the run using V_{max}=3µM/h: Here we use the same nomenclature as in (b); (d): Observed position of the water table

emissions only in situations when the water table is below the soil surface. This can be seen looking at Fig. 15: In (a) we plot modeled methane emissions obtained with V_{max} being 45µM/h (control), 20µM/h and 3µM/h. In July-October 1991, when the water table is below the soil surface for a longer period, a lower V_{max} value leads to higher methane emissions, because in this case less methane is oxidized in the oxic soil layers. Looking at Fig. (b) and (c) we see that in this situation the amount of methane emitted by diffusion increases, while the amount emitted through plants stays the same in all cases.

Sensitivity to T_{veg}

In the following we investigate how different T_{veg} values affect modeled methane emissions and concentration profiles in the soil. A higher value for T_{veg} means that a larger portion of methane is transported into the atmosphere by plants. That is, a higher amount of methane is removed from soil layers above the rooting depth and is directly added to the methane flux into the atmosphere, whereby a fraction of 50% is oxidized in the rhizosphere.

Effect on modeled concentration profiles in the soil. A lower T_{veg} value leads to less methane being removed from the soil layers above the rooting depth during the growing season. Therefore, the methane concentration stays high at that time (Jun 27 - Nov 14) which is clearly in contrary to the observations at that site (see Fig. 16).

Effect on modeled methane fluxes, if the water table is above the soil surface. In this situation a lower T_{veg} value decreases the portion of methane emitted through plants and hence increases the portion of methane emitted by ebullition. Since a fraction of 50% of methane emitted by plant-mediated transport is oxidized in the rhizosphere, the total flux to the atmosphere is higher, if T_{veg} is lower (see Fig. 17).

Effect on modeled methane fluxes, if the water table is below the soil surface. In this case a lower T_{veg} leads to a larger fraction of methane emitted by diffusion. This can be seen in Fig. 17 (b) and (c) in July 1991: A lower T_{veg} means that less methane is removed from the soil layers above the rooting depth by plants. Hence, before the decline of the water table below the soil surface, the methane concentration directly below the soil surface is higher if T_{veg} is lower. For that reason more methane is emitted by diffusion in the first 20 days after the drop of the water table below the soil surface if T_{veg} is lower. In all three runs (T_{veg}=1, 5, 15) diffusion decreases about 20 days after the decline of the water table below the soil surface.

In both cases (b) and (c) the modeled methane emission is higher if T_{veg} is lower, because the water table is above the soil surface most of the time. If methane is emitted by ebullition there is no oxidation, whereas methane diffusing through the oxic layer or emitted through plants is partly oxidized.

emissions only in situations when the water table is below the soil surface. This can be seen looking at Fig. 15: In (a) we plot modeled methane emissions obtained with V_{max} being 45µM/h (control), 20µM/h and 3µM/h. In July-October 1991, when the water table is below the soil surface for a longer period, a lower V_{max} value leads to higher methane emissions, because in this case less methane is oxidized in the oxic soil layers. Looking at Fig. (b) and (c) we see that in this situation the amount of methane emitted by diffusion increases, while the amount emitted through plants stays the same in all cases.

Sensitivity to T_{veg}

In the following we investigate how different T_{veg} values affect modeled methane emissions and concentration profiles in the soil. A higher value for T_{veg} means that a larger portion of methane is transported into the atmosphere by plants. That is, a higher amount of methane is removed from soil layers above the rooting depth and is directly added to the methane flux into the atmosphere, whereby a fraction of 50% is oxidized in the rhizosphere.

Effect on modeled concentration profiles in the soil. A lower T_{veg} value leads to less methane being removed from the soil layers above the rooting depth during the growing season. Therefore, the methane concentration stays high at that time (Jun 27 - Nov 14) which is clearly in contrary to the observations at that site (see Fig. 16).

Effect on modeled methane fluxes, if the water table is above the soil surface. In this situation a lower T_{veg} value decreases the portion of methane emitted through plants and hence increases the portion of methane emitted by ebullition. Since a fraction of 50% of methane emitted by plant-mediated transport is oxidized in the rhizosphere, the total flux to the atmosphere is higher, if T_{veg} is lower (see Fig. 17).

Effect on modeled methane fluxes, if the water table is below the soil surface. In this case a lower T_{veg} leads to a larger fraction of methane emitted by diffusion. This can be seen in Fig. 17 (b) and (c) in July 1991: A lower T_{veg} means that less methane is removed from the soil layers above the rooting depth by plants. Hence, before the decline of the water table below the soil surface, the methane concentration directly below the soil surface is higher if T_{veg} is lower. For that reason more methane is emitted by diffusion in the first 20 days after the drop of the water table below the soil surface if T_{veg} is lower. In all three runs (T_{veg}=1, 5, 15) diffusion decreases about 20 days after the decline of the water table below the soil surface.

In both cases (b) and (c) the modeled methane emission is higher if T_{veg} is lower, because the water table is above the soil surface most of the time. If methane is emitted by ebullition there is no oxidation, whereas methane diffusing through the oxic layer or emitted through plants is partly oxidized.

However, a higher T_{veg} value can also lead to higher methane emissions than a lower one. This happens in case the water table is below the soil surface for a period long enough to cause diffusive fluxes to become zero because of oxidation in the unsaturated soil layers. In this situation emission through plants becomes the only emission pathway and hence methane emissions are higher if T_{veg} is larger. In order to demonstrate this, we make a sensitivity test using the soil temperature data from the Michigan site (site 1) and an artificial water table, high in the winter and low in the summer, as shown in Fig. 18 (c) and (d). For that test a rooting depth of 20 cm is used, in order to examine what happens if the water table declines to the rooting depth. All parameters used in this run are compiled in Tab. 9:

Table 9: Parameters Used in the T_{veg} Test Run

R_0	V_{max}	l	nroot	T_{veg}
0.3	45µM/h	80cm	20cm	1 or 15

Fig. 18 (a) shows the modeled contributions of the different transport mechanisms to the total methane flux in case T_{veg} is 15, and (b) for T_{veg} being 1. Until the time the water table declines below the soil surface, methane emissions are dominated by ebullition in case ‚T_{veg}=1'. Therefore, the total flux is higher in that case (Fig. 18 (b)). In the first 20 days after the drop of the water table below the soil surface diffusion is the main emission pathway in (b), but then it decreases and becomes zero (and then negative) around June 20. From now on there is only methane emission in case ‚T_{veg}=15' (Fig. 18 (a)), because methane conducted through plants bypasses the oxic soil layer. As the water table keeps falling methane emission become zero also in case ‚T_{veg}=15', because now the roots do not extend any more into the water saturated soil, where high methane concentrations prevail.

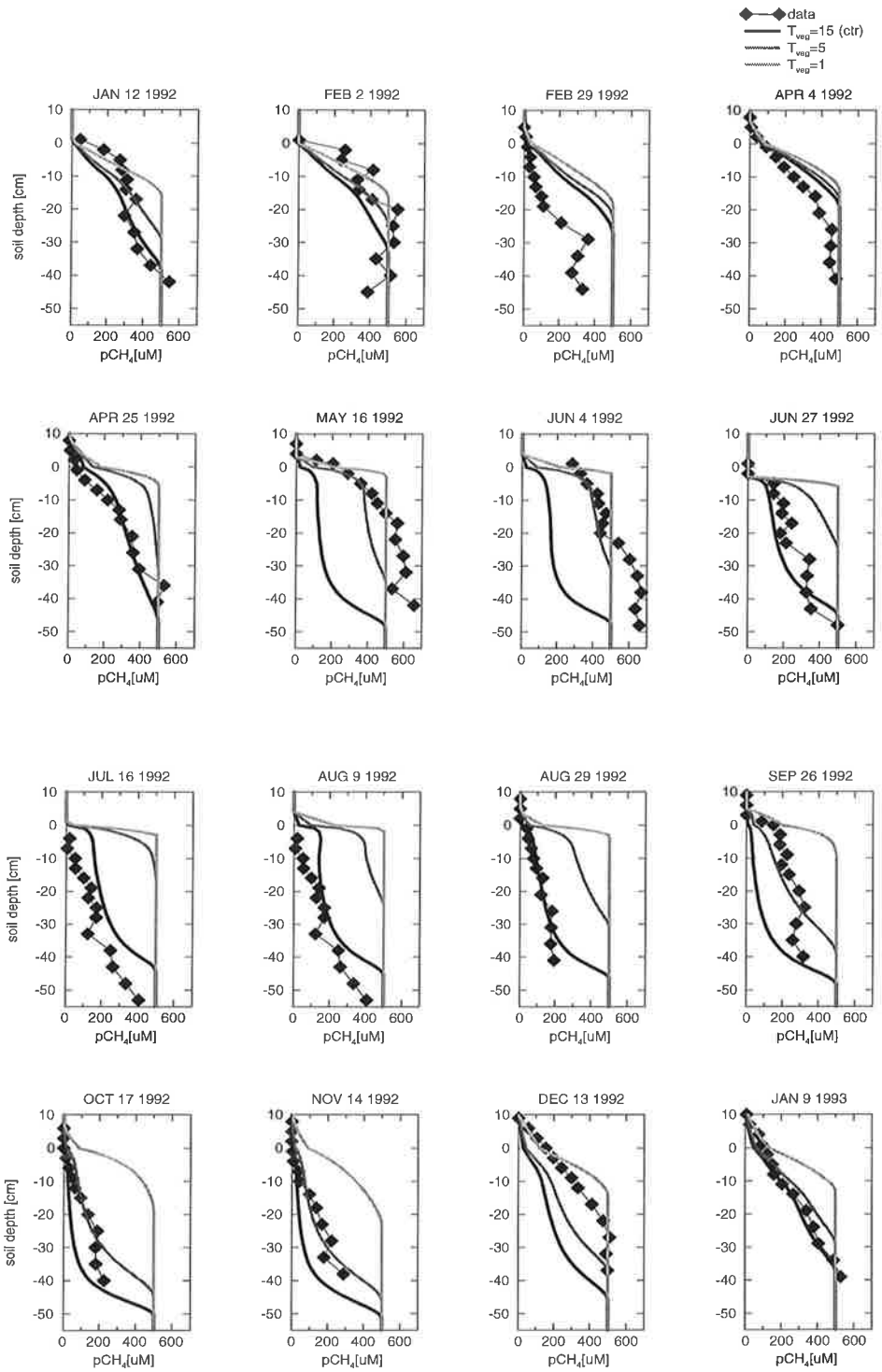

Fig. 16: Sensitivity to T_{veg}: Comparison between modeled (thick lines) and observed (squares) methane concentration profiles using three different values for T_{veg}: T_{veg}=15 (black line), T_{veg}=5 (dark grey line) and T_{veg}=1 (light grey line)

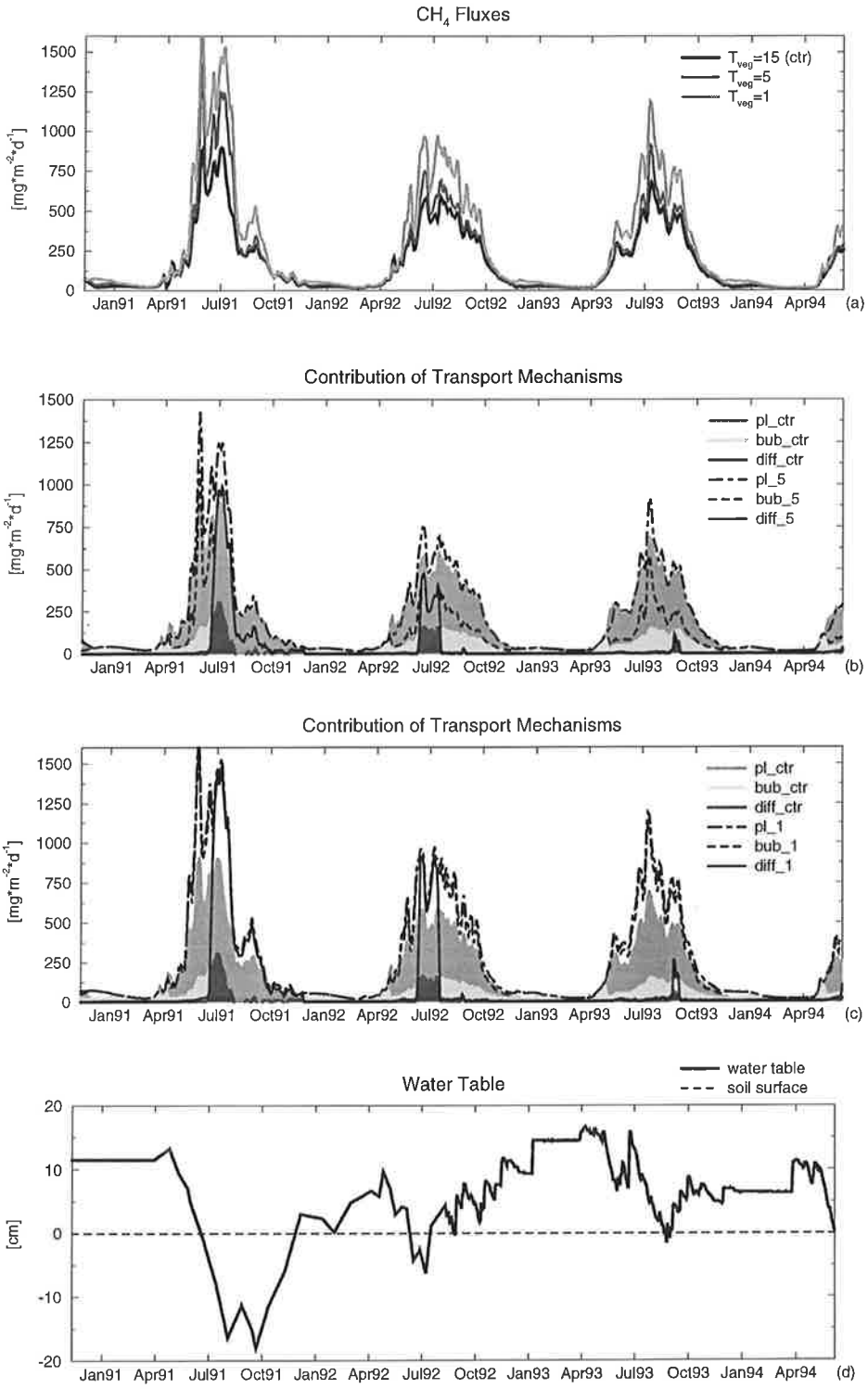

Fig. 17: Sensitivity to T_{veg}: (a): Comparison between modeled methane fluxes of the control run (T_{veg}=15) and two runs using T_{veg}=5 (dark grey) and T_{veg}=1 (light grey); (b) Contributions of the three different transport mechanisms to the total methane flux: the shaded areas show results of the control run: Diffusion (black), ebullition (light grey) and plant-mediated transport (dark grey), whereas the thick lines show the results of the run using T_{veg}=5: Diffusion (solid), ebullition (dashed) and plant-mediated transport (dot-dashed); (c) Contributions of the three different transport mechanisms to the total methane flux: Comparison between the control run and the run using T_{veg}=1: here we use the same nomenclature as in (b); (d): Observed position of the water table

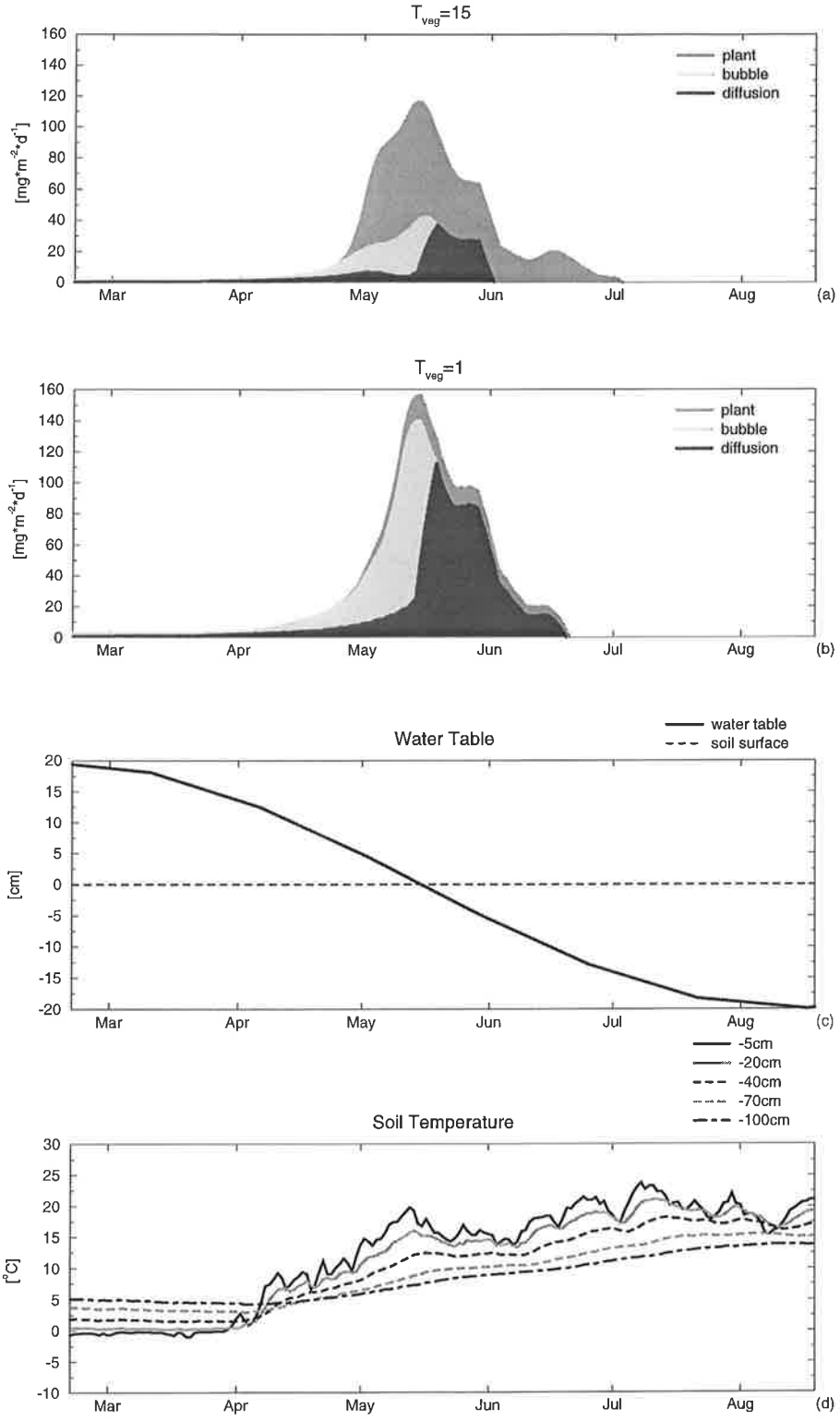

Fig. 18: Sensitivity to T_{veg}: Results of a test run using an artificial water table: (a): Run using T_{veg}=15; Contributions of the three different transport mechanisms to the total methane flux: diffusion (black), ebullition (light grey) and plant-mediated transport (dark grey); (b): Run using T_{veg}=1; Contributions of the three different transport mechanisms to the total methane flux: diffusion (black), ebullition (light grey) and plant-mediated transport (dark grey); (c) Artificial position of the water table used for this run; (d): Observed soil temperatures from site 1 (Michigan) at different soil depths

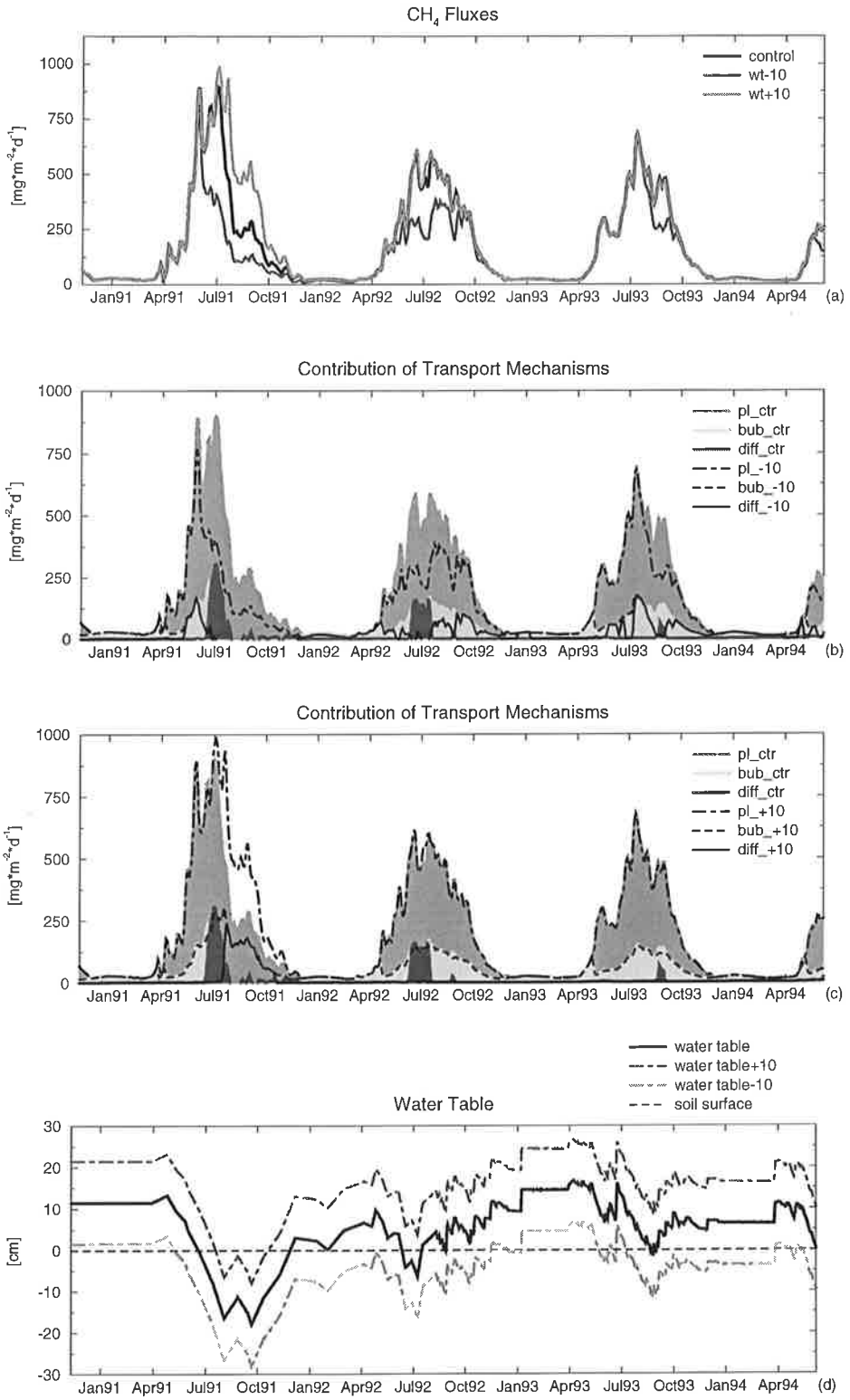

Fig. 19: Sensitivity to the position of the water table: (a): Comparison between modeled methane fluxes of the control run (black) and two runs using ‚water table -10cm' (dark grey) and ‚water table +10cm'(light grey) as input data; (b): Contributions of the three different transport mechanisms to the total methane flux: The shaded areas show results of the control run: Diffusion (black), ebullition (light grey) and plant-mediated transport (dark grey), whereas the thick lines show the results of the run using ‚water table -10cm': Diffusion (solid), ebullition (dashed) and plant-mediated transport (dot-dashed); (c) Contributions of the three different transport mechanisms to the total methane flux: Comparison between the control run and the run using ‚water table +10cm': Here we use the same nomenclature as in (b); (d): Positions of the water table (control and control +/- 10cm)

Sensitivity to Changes in the Water Table

Changes in the position of the water table can alter the relative extends of the saturated and the unsaturated soil zones and hence the sizes of the production and oxidation zones. Here, we run the model with a water table being 10 cm higher or lower than that of the control run (see Fig. 19 (d)). It is clear that at times when the water table is above the soil surface in all three cases (water table +/-10 cm and original water table) the total fluxes are the same (Fig. 19 (a)). In case ‚water table-10' the water table declines earlier below the soil surface, to a deeper soil depth and stays there longer. Therefore, there is less ebullition, diffusion decreases to or below zero 20 days after the decline of the water table below the soil surface and even plant-mediated transport becomes lower, because less roots extend into the water saturated soil zone (see Fig. 19 (b)). In case ‚water table+10' (Fig. 19 (c)) the modeled fluxes are unchanged at times the water table of the control run is above the soil surface as well. However, in July-October 1991 the methane emissions obtained by the control run decrease, because the water table falls below the soil surface. In the ‚water table+10' run simulated methane fluxes are considerably higher, because the time span when ebullition can occur is longer. Furthermore, plant-mediated transport is higher and diffusion is larger, because the water table is only a few centimeters below the soil surface and that for a shorter period of time than in the control run.

3.3. Conclusion

The methane model developed in this work resolves the processes leading to methane emission within a 1-dimensional soil column. Methane production occurs in the water saturated soil zone below the water table, while methane consumption is confined to the unsaturated soil region above the water table. Transport of methane from the soil to the atmosphere operates by molecular diffusion, ebullition and plant-mediated transport. The different emission pathways affect the fraction of produced methane that is emitted into the atmosphere and determines the velocity by which methane is transported to the atmosphere. The model forcing consists of daily values of the soil temperature at different soil depths, the position of the water table and the Net Primary Productivity. The model calculates methane fluxes into the atmosphere and methane concentration profiles in the soil on a daily basis.

The comparison between model results and observations from 15 field stations within 6 wetlands in Europe and North and Central America, showed good agreement for methane fluxes as well as methane concentration profiles in the soil. The tests revealed that the sensitivity of modeled methane fluxes to changes in the soil temperature and the water table as well as to differences in the vegetation is realistic. Since the testing of the model yields positive results under different conditions we conclude that this model can be applied globally.

Since until now there has been only one tropical data set available, it would be advantageous to test the model with further tropical data sets. For a more thorough testing of the model it would be desirable the have a comprehensive data set not only consisting of time series of the input and output data of the model (as it was the case in this study), but also of quantities calculated in the model such as production rate, oxidation rate and the fractions of methane transported by the different transport mechanisms. A next logical step would be to apply a modified version of the model to rice paddies, because the processes leading to methane emission from rice fields are the same as in wetlands. However, the cultivation practices affect methane emissions as well.

4. Determination of Global Data Sets

In order to apply the methane emission model described in Sect. 2 to the global scale, global input data consisting of daily values of soil temperature, water table and NPP are needed. Furthermore, all the model parameters have to be defined on the global scale. In App. A all model parameters are compiled most of which are assumed to be globally constant. Here, we describe the derivation of the spatially varying model parameters. As already mentioned in Sect. 1 the global distribution of natural wetlands is derived from a data sets by *Matthews and Fung* [1987] (see Fig. 3 of Sect. 1) that gives the percentage of wetlands within each 1^o*1^o grid cell. Therefore, for the global run a 1^o*1^o resolution was chosen. It is assumed that the wetland area given by this data set represents the maximum wetland area. The fact that in some regions the areal extent of a wetland varies seasonally is taken into account in the following way. The total area remains constant, but during the dry season the water table, computed by the hydrological model (see Sect. 5) becomes so low as to represent dry conditions. However, the interannual variation of the wetland areas is not taken into consideration in this study.

Global Forcing

As input for the global model runs we use ECMWF re-analyses [*Gibson et al.*, 1997] in a T106 resolution ($1.1^o*1.1^o$) which are interpolated to a 1^o*1^o grid. Soil temperatures at differing depths are calculated by the ECMWF model. The position of the water table at each grid point is calculated by a hydrological model (see Sect. 5) which is driven by precipitation, surface net radiation and the 2m-temperature, obtained from the ECMWF re-analyses. Monthly values of NPP are taken from the BETHY model [*Knorr*, 1997] and linearly interpolated to daily values.

Parameter R_0

The parameter R_0 is a measure for the amount and quality of available substrate for methanogenesis. It was adjusted to each data set in order to achieve a good agreement between the amplitude of the observed and the modeled methane emissions. To extrapolate this parameter to the global scale, it is important to understand which environmental factors affect R_0. Since large parts of the substrate originate from fresh, undecomposed organic matter, we take R_0 to be dependent on the annual productivity of the wetland. In addition, the productivity of methanogenic bacteria is assumed to be higher in regions with a higher annual mean temperature. Note that the equation of the methane production rate (see Eq. (7) of Sect. 2) accounts for the seasonal variations of the temperature relative to the annual mean temperature T_{mean}. Thus, $R_0(x,y)$ is considered to depend on the annual mean temperature $T_{mean}(x,y)$ and the total annual NPP $NPP_{tot}(x,y)$:

$$R_0(x, y) = f(T_{mean}(x, y), NPP_{tot}(x, y)) \quad (21)$$

The functional dependence of $R_0(x,y)$ is derived from the 6 sites assuming a linear relationship between R_0 and T_{mean} and NPP_{tot}. Note that we got 2 data points at the Panama site (see Sect. 3). The R_0, T_{mean} and NPP_{tot} values of the 7 data points are compiled in Tab. 10:

Table 10: Compilation of R_0, T_{mean} [°C] and NPP_{tot} [$gC*m^{-2}*yr^{-1}$] from all Sites

Site	R_0	T_{mean}	NPP_{tot}
Michigan	0.60	11.8	745
Minnesota	0.30	6.5	932
Finland	0.37	3.5	345
Alaska	0.23	0.0	273
Canada	0.15	6.0	730
Panama p1	2.80	27.5	575
Panama p2	2.50	26.8	726

A simple multiple linear regression yields the following relationship:

$$R_0(T_{mean}(x, y), NPP_{tot}(x, y)) = 0.45 + 0.1 \cdot \frac{T_{mean}(x, y)}{[^oC]} - 0.001 \cdot \frac{NPP_{tot}(x, y)}{[gC \cdot m^{-2} \cdot yr^{-1}]} \quad (22)$$

Since in the BETHY model the NPP is calculated as a function of the temperature, .i.e. $NPP_{tot}=f(T_{mean})$, R_0 is mainly a function of T_{mean}.

Global Datasets for the Model Parameters

All parameters used by the model are listed in App. A. Many parameters are globally constant, whereas a few parameters vary spatially. Those parameters are:

- The maximum NPP NPP_{max}, (Eq. (2), (4) of Sect. 2),
- The total annual NPP NPP_{tot} (Eq. (22) of Sect. 4),
- The rooting depth *nroot* (Eq. (5), (17), (19) of Sect. 2),

- The soil depth l (Eq. (15) of Sect. 2),
- The relative volume of coarse pores in the soil f_{coarse}, (Eq. (10) of Sect. 2),
- The fraction of unvegetated, bare soil P_{unveg} (Eq. (13) of Sect. 2),
- The ability of plants to conduct gas T_{veg} (Eq. (16) of Sect. 2).

In the following we will describe how these parameters are derived on a global scale.

NPP_{tot} and NPP_{max}. Mean monthly fields of the NPP are provided by the BETHY model [*Knorr*, 1997]. They are used to obtain the annual sum NPP_{tot} expressed in units of [$gC*m^{-2}*yr^{-1}$] (see Fig. 20) and the maximum value of the NPP NPP_{max} expressed in units of [$gC*m^{-2}*mo^{-1}$] (see Fig. 21) at all wetland grid points.

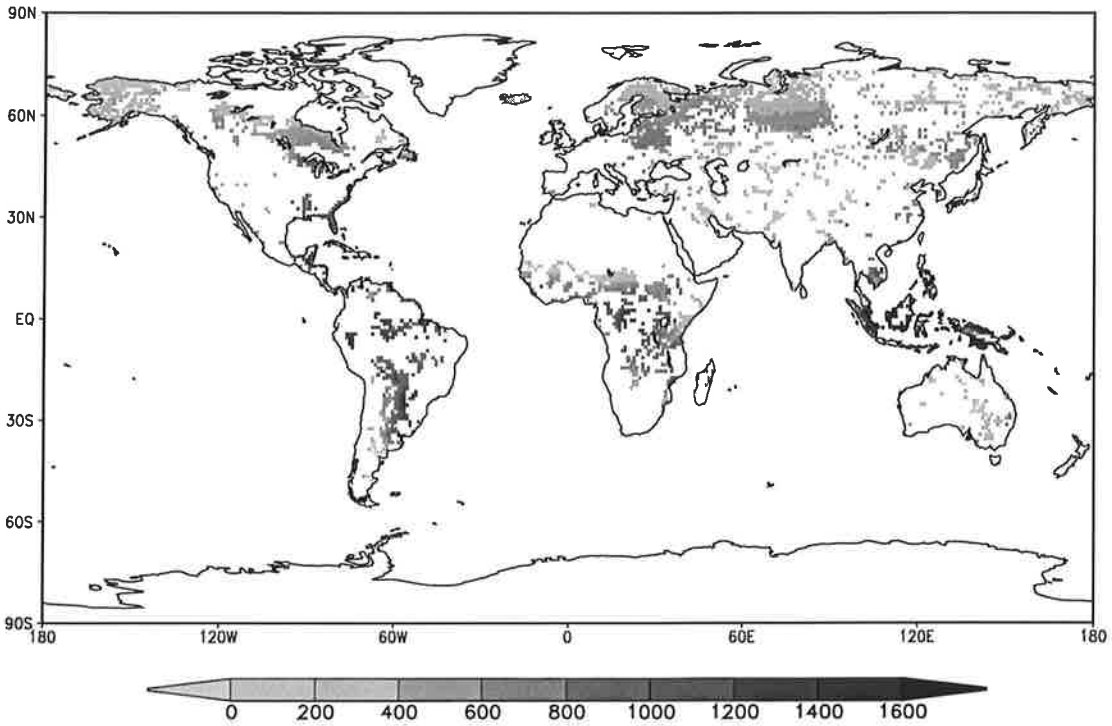

Fig. 20: Total annual NPP (NPP_{tot}) [$gC*m^{-2}*yr^{-1}$] as calculated by the BETHY model [*Knorr*, 1997]

Relative volume of coarse pores f_{coarse}. In order to determine the relative volume of coarse pores needed to calculated the diffusion coefficient (see Eq. (10) of Sect. 2) we use the global data set of soil profiles by *Dunne and Willmott* [1996]. This data set has a resolution of $0.5^{o}*0.5^{o}$. It is based on two soil data sets, namely the data sets by *Gildea and Moore* [1985] and by *Zobler* [1986], which are derived from the FAO/Unesco soil classification system [*FAO/ Unesco*, 1971-1981]. In the data set by *Dunne and Willmott* [1996] each soil profile is divided in up to 4 horizons which are characterized by soil texture and thickness. The soil texture is

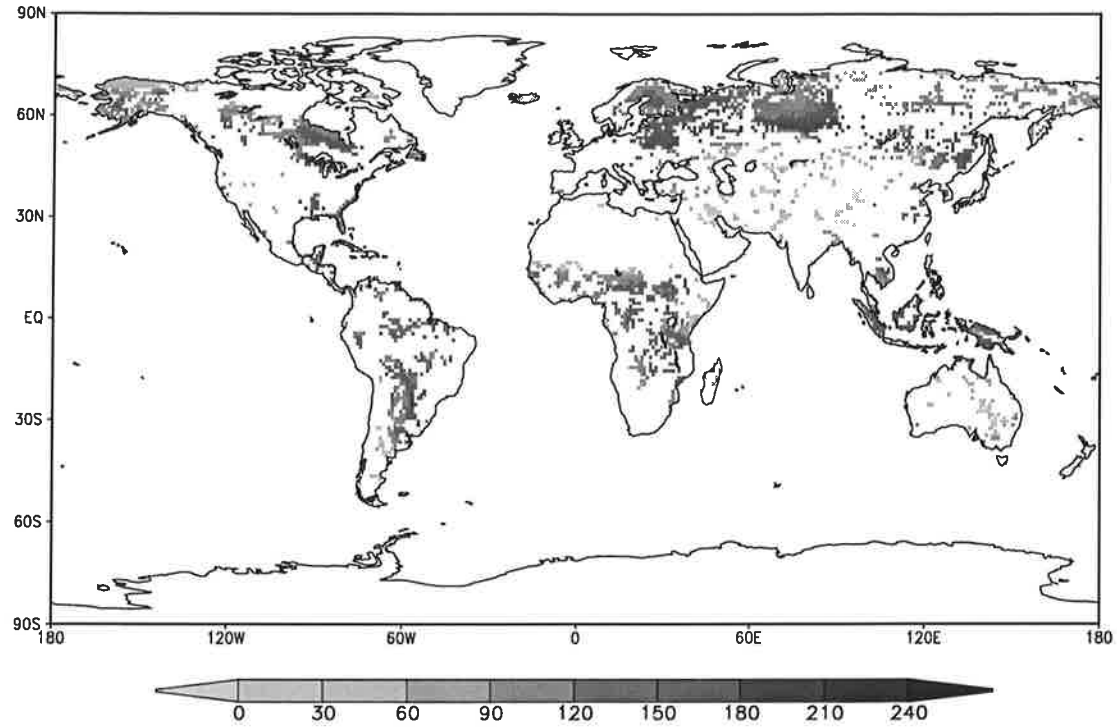

Fig. 21: Maximum NPP (NPP_{max}) [$gC*m^{-2}*mo^{-1}$] as calculated by the BETHY model [*Knorr*, 1997]

expressed in terms of sand, silt and clay content. Organic soils are also included.

The parameter f_{coarse} is obtained in the following way: for each horizon i the fraction of coarse pores $f_{coarse,i}$ is calculated using the following equation:

$$f_{coarse,i} = f_{sand,i} \cdot pv_{sand} + f_{silt,i} \cdot pv_{silt} + f_{clay,i} \cdot pv_{clay} + f_{org,i} \cdot pv_{org} \qquad (23)$$

where $f_{sand,i}$, $f_{silt,i}$, $f_{clay,i}$ and $f_{org,i}$ denote the relative contents of sand, silt, clay and organic material in each soil horizon i, respectively. The values pv_{sand}, pv_{silt}, pv_{clay} and pv_{org} indicate the relative volume of coarse pores in sandy, silty, clayic and organic soils, respectively. They were set to 0.45, 0.20, 0.14 and 0.45, respectively, according to *Hartge and Horn*[1991]. The parameter f_{coarse} is then obtained by calculating the average of the values of all soil horizons $f_{coarse,i}$. The obtained values are transformed from a $0.5^o*0.5^o$ grid to a 1^o*1^o grid by averaging. The obtained global distribution of f_{coarse} is depicted in Fig. 22 for all wetland grid points.

Global vegetation distribution. To derive the parameters P_{unveg} (percentage of unvegetated, bare soil), T_{veg} (quality of plant-mediated transport), *nroot* (rooting depth) and l (soil depth) the global 1^o*1^o land cover data set by *Wilson and Henderson-Sellers* [1985] is used. They defined

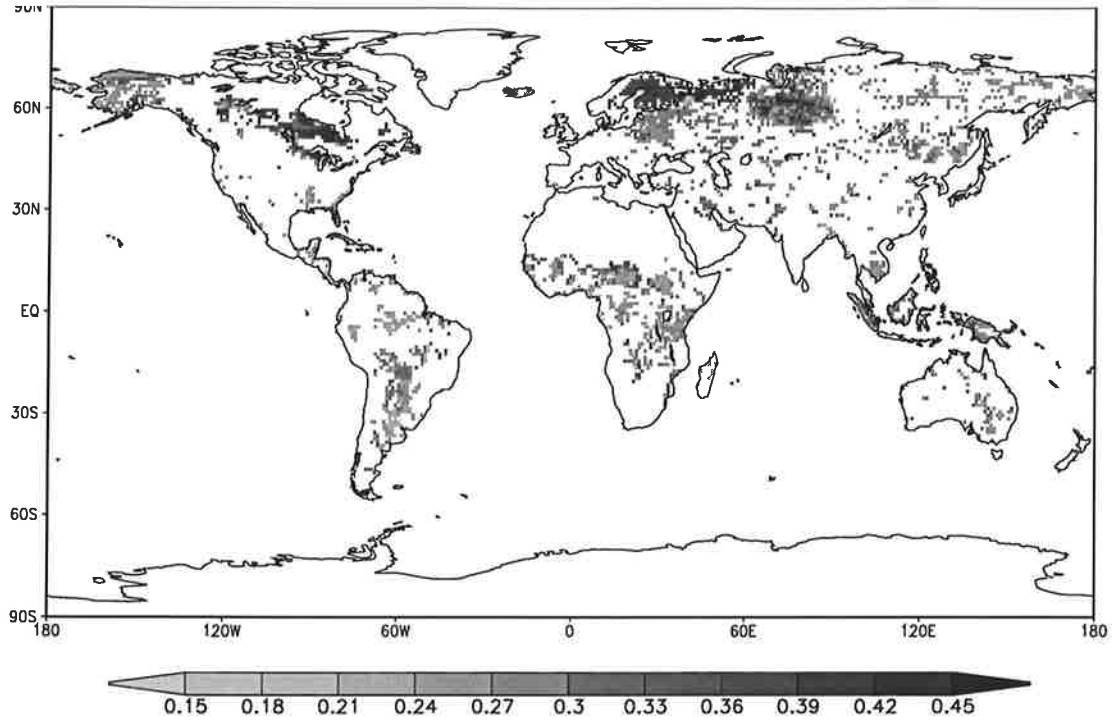

Fig. 22: Relative volume of coarse pores f_{coarse} as obtained using a data set by *Dunne and Willmott* [1996]

53 land cover types and assigned relative fractions of 24 possible vegetation types (in the following referred to as *WH-vegetation types*) to each of them. We reduce the number of vegetation types to 8 by combining the 24 WH-vegetation types as shown in Tab. 11. The WH-vegetation types are divided into the vegetation types tree, shrub, short grass, long grass, tundra, swamp and bare soil, because these types are appropriate classes for determining the parameters P_{unveg}, T_{veg}, *nroot* and *l*. Each 1^o*1^o grid cell can be covered by several vegetation types.

The fraction of unvegetated, bare soil P_{unveg}. The relative fraction of unvegetated soil in a grid cell is set to be equivalent to the fraction of vegetation type 7, bare soil.

The ability of plants to conduct gas T_{veg}. It is a quite difficult task to determine a global data set that gives information about the gas conducting properties of plants, because little is known about those properties for most plant types. There are some studies investigating the ability of certain plants to transport gas through their stems. Rice plants [*Schütz et al.*, 1989], *Eriophorum angustofolium* [*Schimel*, 1995; *Frenzel,* pers. comm.] or *Scheuchzeria palustris* [*Shannon et al.*, 1996] have been found to emit significant amounts of methane through their stems. That is, a small number of plants have been examined for their gas conducting properties, but in general little is known in this respect about most plants occurring in wetlands.

Table 11: Definition of Vegetation Types Used in This Work

Types used in This Work		Types by Wilson&Henderson-Sellers	
veg type	description	WH-veg type	description
0	other	1	water
		2	ice
		3	inland lake
		15	arable
		16	rice
		17	sugar
		18	maize
		19	cotton
		20	irrigated crop
		21	urban
1	tree	4	evergreen needleleaf tree
		5	evergreen broadleaf tree
		6	deciduous needleleaf tree
		7	deciduous broadleaf tree
		8	tropical broadleaf tree
		9	drought deciduous tree
2	shrub	10	evergreen broadleaf shrub
		11	deciduous shrub
		12	thorn shrub
3	short grass	13	short grass and forbs
4	long grass	14	long grass
5	tundra	22	tundra
6	swamp	23	swamp
7	bare soil	24	soil

Therefore, we make some simplifying assumptions and categorize the different vegetation types concerning plant-mediated transport the following way [*Frenzel*, pers. comm.]:

- Grasses are considered to be good gas conductors,
- Trees are assumed to be poor ones,
- Shrubs are assumed not to be able of transporting gas through their stems,
- Plants occurring in regions of the vegetation type tundra or swamp are considered as good gas conductors.

Thus, the following values to describe the quality of plant-mediated transport of each vegetation type are chosen (see Tab. 12):

Table 12: Ability of Vegetation Types to Conduct Gas $T_{veg,i}$

veg type	description	$T_{veg,i}$
0	other	0
1	tree	1
2	shrub	0
3	short grass	10
4	long grass	15
5	tundra	10
6	swamp	15
7	bare soil	0

In order to derive a global distribution of $T_{veg}(x,y)$, we multiply the relative coverage of each vegetation type $p_i(x,y)$ in each grid cell with the T_{veg} value of each vegetation type $T_{veg,i}$:

$$T_{veg}(x,y) = \frac{\sum_{i=1}^{7} p_i(x,y) \cdot T_{veg,i}}{\sum_{i=1}^{7} p_i(x,y)} \tag{24}$$

We sum only over vegetation types 1-7, because only those types are considered in a natural wetland. Fig. 23 shows the global distribution of the parameter T_{veg}.

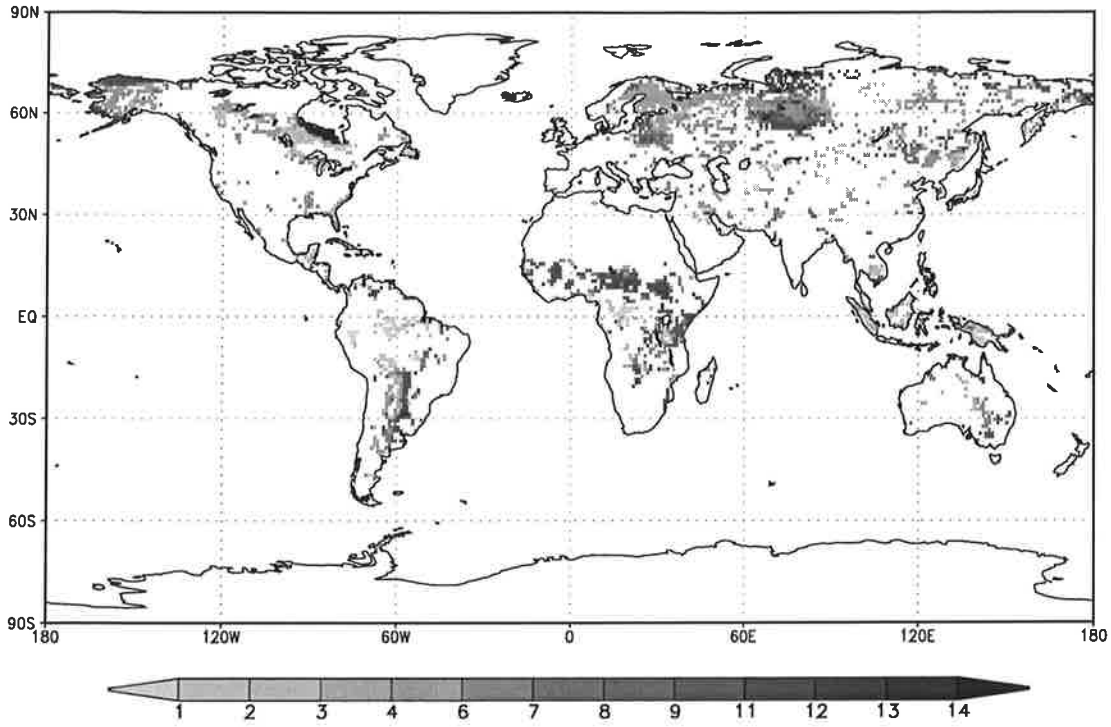

Fig. 23: Global distribution of the parameter T_{veg} which is derived by the method described here; high values mean good conduction and vice versa

Rooting depth nroot. In the model the parameter *nroot* is used in the context of plant-mediated transport (see Eq. (17) and (19) of Sect. 2). It is the depth until which methane can be extracted from the soil layers by those plants which are able to conduct gas through their stems. Here the rooting depth *nroot* is derived from the vertical distribution of the root biomass for different biome types given by *Jackson et al.* [1996]. An asymptotic, nonlinear equation is used, describing the cumulative root fraction *Y(z)* at depth z which is taken from a model of vertical root distribution by *Gale and Grigal* [1987]:

$$Y(z) = 1 - \beta^z \tag{25}$$

where β is the so-called extinction coefficient. β values are taken from *Jackson et al.*, [1996] who derived them from soil studies and biome analyses. The authors give β values for several biome types which were assigned to the vegetation types 1-6 the following way (see Tab. 13).

The rooting depths of the vegetation types 0 (other) and 7 (bare soil) are set to 0 cm. We assign the biome type temperate grassland to the vegetation type swamp, because most areas denoted as swamps by *Wilson and Henderson-Sellers* [1985] are located at higher latitudes, i.e. in non-

Table 13: Extinction Coefficient

veg type	description	biome	β
1	tree	boreal forest	0.943
		temperate coniferous forest	0.977
		temperate deciduous forest	0.966
		tropical deciduous forest	0.961
		tropical evergreen forest	0.962
2	shrub	sclerophyllous shrubs	0.964
3	short grass	temperate grassland	0.943
4	long grass	tropical grassland	0.972
5	tundra	tundra	0.914
6	swamp	temperate grassland	0.943

tropical regions. The rooting depth $nroot_i$ for each biome type i is derived by cutting off the cumulative root distribution $Y_i(z)$ in each biome type at 90%. Thus, $nroot_i$ is obtained by:

$$nroot_i = \frac{\ln(1 - Y_i(z))}{\ln \beta} \qquad Y_i(z) = 0.9 \tag{26}$$

The rooting depth for vegetation type 1 (tree) is obtained by averaging the 5 $nroot_i$ values obtained for the 5 forest biomes. Consequently, the resulting values for the rooting depths are (see Tab. 14):

Table 14: Rooting Depth nroot

veg type	description	nroot [cm]
1	tree	64
2	shrub	63
3	short grass	39
4	long grass	81
5	tundra	26
6	swamp	39

The rooting depth *nroot(x,y)* of a grid cell, which is in general covered by several vegetation types, is calculated the following way:

$$nroot(x, y) = \frac{\sum_{i=1}^{6} p_i(x, y) \cdot T_{veg,i} \cdot nroot_i}{\sum_{i=1}^{6} p_i(x, y) \cdot T_{veg,i}} \tag{27}$$

In Fig. 24 the global distribution of rooting depths obtained by this method is plotted. In this context it is interesting to note that the values for the rooting depth *nroot* obtained this way are comparable with values observed at the different field sites 1-6 (see Sect. 3 and App. B).

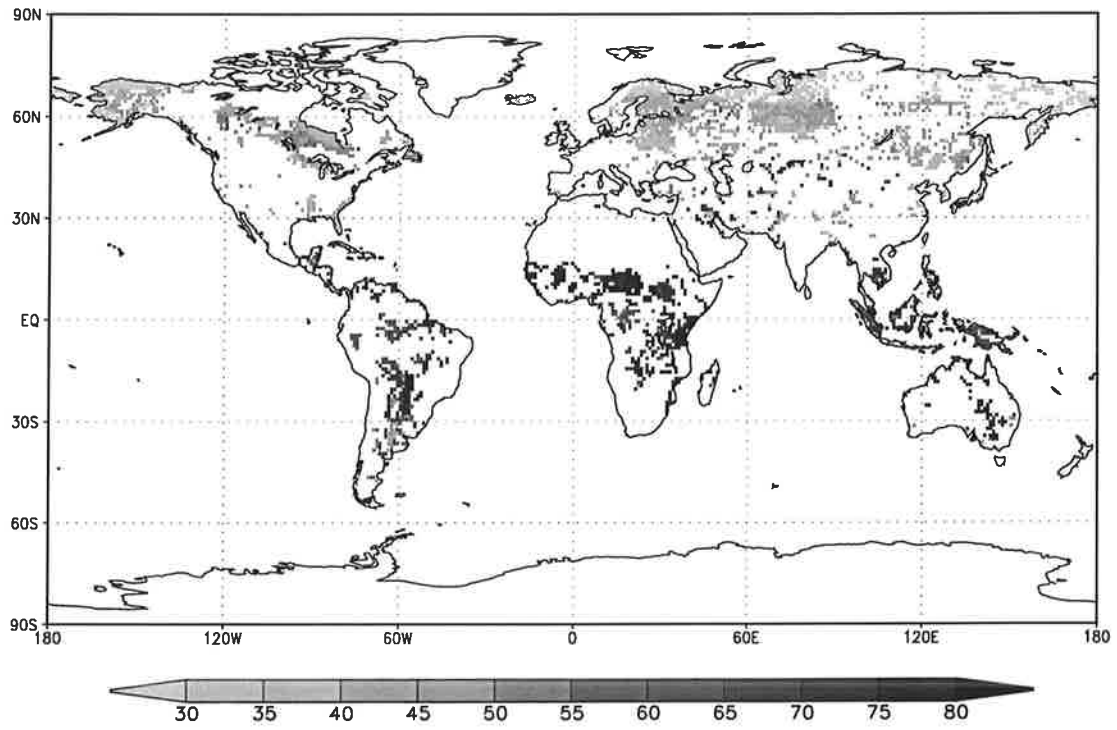

Fig. 24: Global distribution of the effective rooting depth [cm] as based on an equation by *Gale and Grigal* [1987] and a data set by *Wilson and Henderson-Sellers* [1985]

Soil depth l. The soil depth *l* is the lower boundary of the ‚active layer', that is, the soil zone where methane production can occur. Since we assume that methane is mainly produced from fresh organic material, the production zone is that soil region where the fresh organic fraction is available. Because the fresh organic matter is incorporated into the soil as root exudates, dead fine roots and litter, the depth of the ‚active layer' is connected with the vertical root distribution. Therefore, for calculating *l* the same approach is used which was used to derive *nroot*. The only difference is that the cutoff is at a value of 99%. The resulting values of the soil

depth l are compiled in Tab. 15:

Table 15: Soil Depth l

veg type	description	l [cm]
1	tree	129
2	shrub	126
3	short grass	79
4	long grass	162
5	tundra	51
6	swamp	79
7	bare soil	50

The soil depth of vegetation type 7 (bare soil) is set to 50 cm. The soil depth of a grid cell containing different vegetation types is derived using the following equation:

$$l(x, y) = \frac{\sum_{i=1}^{7} p_i(x, y) \cdot l_i}{\sum_{i=1}^{7} p_i(x, y)} \tag{28}$$

The resulting global distribution of the soil depth in wetlands is plotted in Fig. 25. Estimates or measurements of the soil depth at which the methane production potential becomes zero lie in the same order of magnitude as the l values derived by this method (see Sect. 3 and App. B).

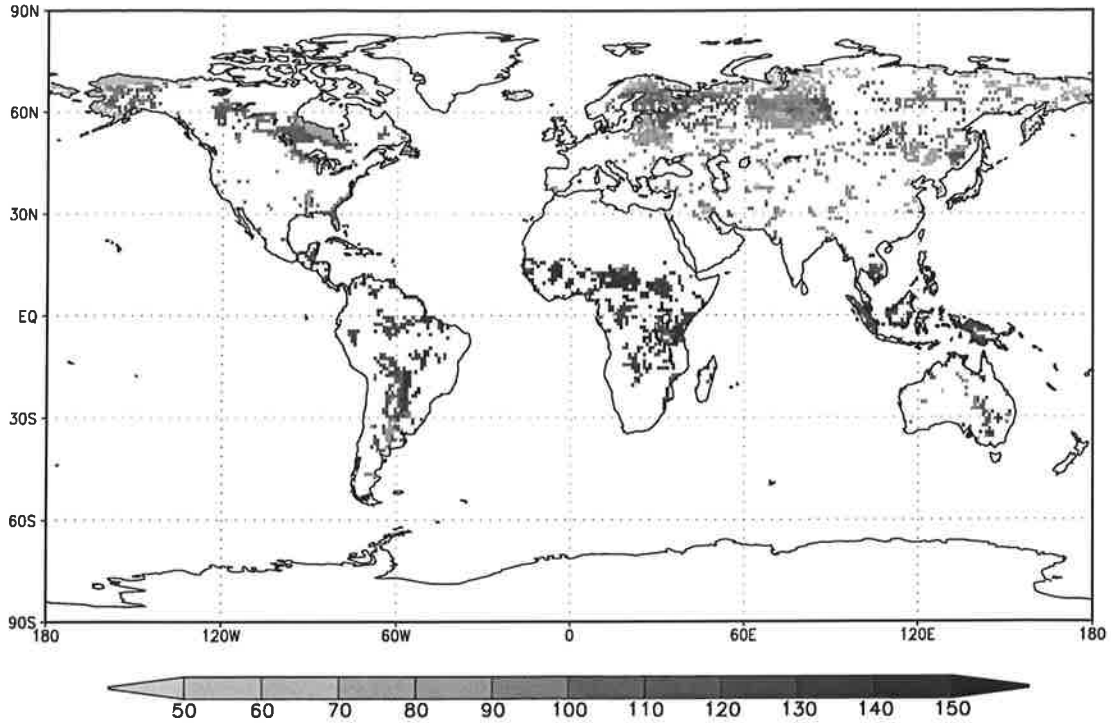

Fig. 25: Soil depth [cm] as obtained based on an equation by *Gale and Grigal* [1987] and a data set by *Wilson and Henderson-Sellers* [1985]

5. The Hydrological Model

5.1. Model Description

General Background

A wetland is characterized by the fact that the water table is at or near the soil surface for a significant part of the year. That means that inflow and outflow of water are balanced on an annual time scale. There can be strong seasonal or interannual variation in the hydroperiod of a wetland [*Mitsch and Gosselink*, 1993]. However, in general, compared to other ecosystems, the inflow of water is relatively high and/or the outflow is relatively low. The input includes precipitation, lateral surface or subsurface inflow, flooding rivers or tides. The outflow can be surface or subsurface outflow and evapotranspiration. This means that apart from the climate the topography plays a major role. Flat areas or areas located in depressions are favoured in this respect. The fact that wetland soils are very moist leads to slow decomposition rates and hence to the accumulation of large amounts of organic matter.

Hydrological Processes in Wetlands

The movement of water through a soil is affected by gravity and the capillary forces resulting from the soil matrix. Gravity causes the water to percolate downward while the soil matrix acts as a resistant against this flow.

There are two criterions that are important to describing the movement of water through a soil, namely the hydraulic conductivity and the water retention characteristics of a soil. The hydraulic conductivity depends on the size, form and continuity of pores in the soil [e.g. *Hartge and Horn*, 1991]. Generally, it is larger in soils with larger pores. Since water held in the soil changes the fraction of air-filled pores and their size, the hydraulic conductivity is a function of the water content of a soil as well. It increases with increasing soil moisture. Organic soils are very porous and at least the less decomposed organic soils contain many large pores. Therefore, because wetland soils contain a large fraction of organic matter and are very moist, their hydraulic conductivity is usually quite high.

The ability of a soil to retain water has been found to depend mainly on the pore size distribution [e.g. *Boelter*, 1968], which, in an organic soil, can be expressed by the decomposition stage of the soil. Normally, a wetland soil is layered. In the uppermost layer, the so-called fibric peat, the soil is only slightly decomposed, in the medium layer, the hemic peat, the peat is moderately decomposed, wheras in the deepest layer, the sapric peat, the soil is well decomposed [*Boelter*, 1968; *Mitsch and Gosselink*, 1993]. Hence, the ability to retain water

varies with depth. In general one can say that the fraction of coarse pores is larger in less decomposed soils which can therefore retain less water. In this context, the so-called water yield (*wy*) coefficient is a useful parameter [*Boelter*, 1968]. It is a measure of the quantity of water removed from a peat profile when the water table is lowered and has been found to vary between 0.08 and 0.85 for well decomposed and undecomposed soils, respectively [*Boelter*, 1968].

In summary, upon a simplified consideration, a wetland soil can be viewed as a medium with the following properties. It has a relatively high hydraulic conductivity. The amount of water removed from the soil, when the water table is lowered, decreases with increasing depth. The inflow of water is either precipitation or lateral inflow, whereas the outflow is either evapotranspiration or lateral outflow.

Definition of the Bucket

The purpose of the bucket model developed in this work is to simulate the position of the water table in wetlands as a function of the climate. On the basis of the physical properties of a wetland soil as they were described above, we consider the pore space of a wetland soil, through which the movement of water takes place, as a simple, modified bucket. This modified bucket differs from bucket models commonly used for mineral soils and has the following properties:

1. It has a lower boundary, across which no drainage of water occurs. In the case of a wetland, we assume that this lower boundary is the depth below that the soil is permanently water saturated. We assume, that water movement due to any kind of inflow or outflow happens only in the zone above that permanent reservoir. In the model this depth has been chosen to be equivalent to the soil depth l.

2. Only the region between field capacity and saturation is considered (see definition of the bucket size).

3. After a change of the water table the water distributes immediately in a way that the water surface in the bucket is horizontal, i.e. below the water table, the bucket is totally filled and above it, it is empty.

The Bucket Size

To define the total volume V_{tot} of the bucket, we take into account the fact that the soil is stratified as described above and consequently the water yield coefficient C_{wy} decreases with increasing depth. Based on values reported by *Boelter* [1968] the following values for C_{wy} were chosen (see Fig. 26). It is assumed to be 0.13 at -100 cm depth, 0.26 at -20 cm depth and

0.8 at the soil surface, and linearly increasing between those values. The qualitative behaviour of C_{wy} as a function of depth is considered to be the same at all grid points. However, it is assumed that the amount of water that is removed, when the water table is lowered, is smaller in less porous soils than in very porous ones. Therefore, the function $f_{wy}(z)$ describing the amount of water removed from depth z when the water table is lowered is defined by:

$$f_{wy}(z) = C_{wy}(z) \cdot \frac{f_{coarse}}{f_{coarse,max}} \tag{29}$$

where f_{coarse} is the relative volume of the coarse pores at a grid point as described in Sect. 2 and $f_{coarse,max}$ is the globally maximum occurring f_{coarse}. $C_{wy}(z)$ denotes the variation of C_{wy} as a function of depth z. Using $f_{wy}(z)$ we can calculate the maximum bucket size V_{tot} by integrating it over the whole soil depth:

$$V_{tot} = \int_{l}^{ns} f_{wy}(z)dz \tag{30}$$

where l is the lower boundary of the bucket (the highest level of permanent saturation) being equivalent to the soil depth l, while ns denotes the soil surface (see Fig. 26). The unit of V_{tot} is [cm], which has to be multiplied by the respective wetland area (or the surface area of the soil column considered in the model) to give a volume unit.

The Water Balance Equation

The volume of water V_{wat} that is stored in the bucket at time t is calculated on a daily basis using the following water balance equation:

$$\frac{d}{dt}Vwat = P - ET + L - R \tag{31}$$

where P denotes precipitation, ET evapotranspiration, L lateral inflow of water and R surface runoff. The units of the quantities P, ET, L and R are [cm/d] while the unit of V_{wat} is [cm].

Precipitation. For P we use the total daily precipitation taken either from a climatological run of the ECHAM4 GCM [*Roeckner et al.*, 1996] or 24-hourly forecasts of the ECMWF re-analyses [*Gibson et al.*, 1997] (see Sect. 6).

Evapotranspiration. Evapotranspiration includes evaporation from the soil surface and transpiration by plants. Evapotranspiration is calculated the following way:

$$ET = min(demand,supply) \tag{32}$$

where *demand* is the equilibrium evapotranspiration rate [*Jarvis and McNaughton*, 1986].

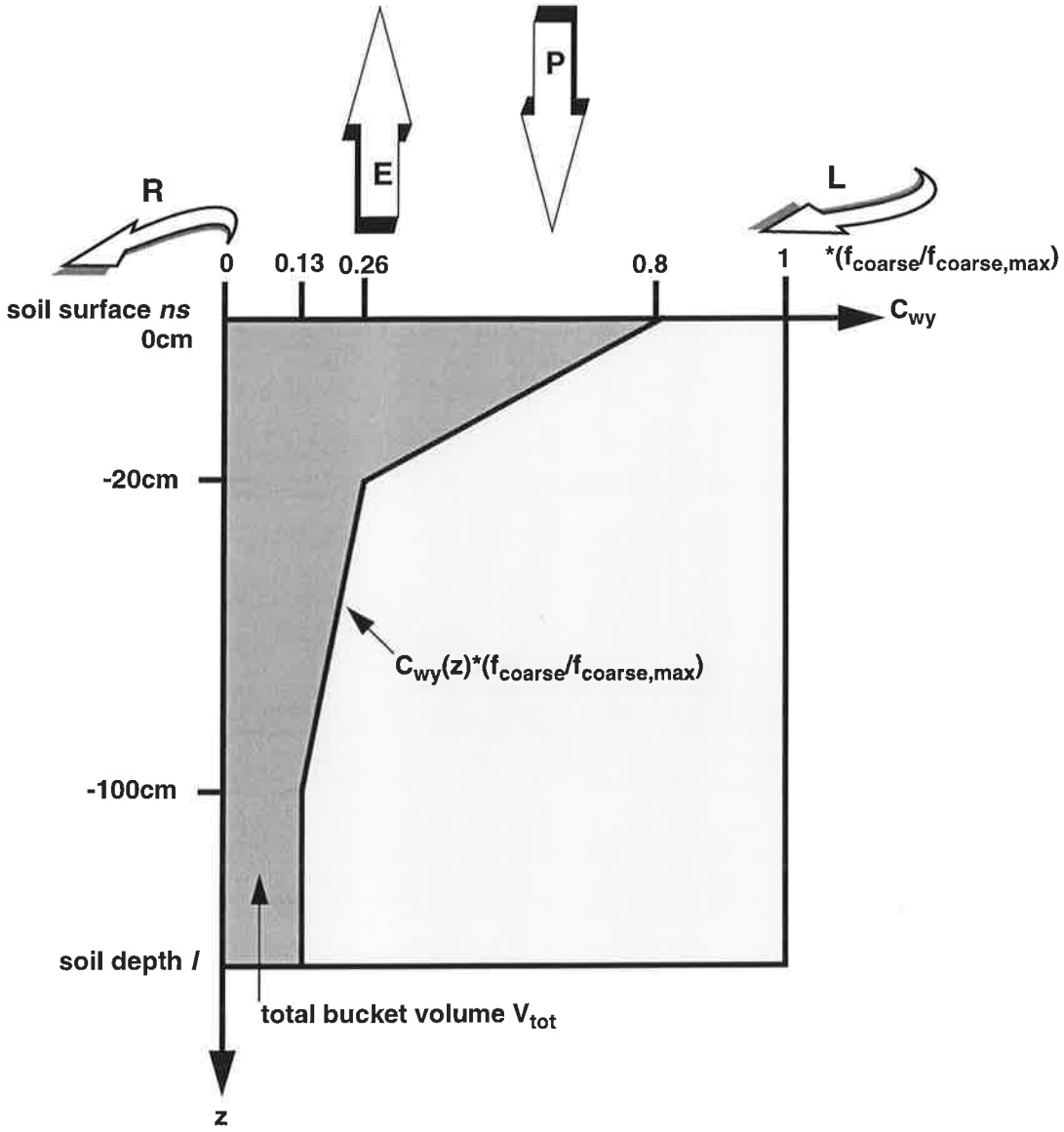

Fig. 26: Schematic diagram of the hydrological model: input of water by precipitation (P) and lateral inflow (L), output of water by evapotranspiration (E) and surface runoff (R); the dark grey area is the total volume of the bucket as defined in eq. (30)

supply denotes the limited evapotranspiration rate due to restricted availability of water in the soil. The demand is calculated using the equilibrium evapotranspiration rate, which is derived from the energy balance at the soil surface between the net radiation, the latent and sensible heat fluxes and the ground heat flux. Assuming that the ground heat flux is small compared to the latent and sensible heat fluxes, we calculate the demand after *Jarvis and McNaughton* [1986]:

$$demand = \frac{s_T}{s_T + \gamma} \cdot \frac{rad}{\lambda} \tag{33}$$

where λ is the latent evaporation heat of 2.45 MJ*kg^{-1} at 20°C and γ the psycrometric constant

of about 65 Pa/K. *rad(t)* denotes the net radiation at the soil surface calculated as the sum of the surface solar and thermal radiations (denoted as *srad(t)* and *trad(t)*, respectively). $s_T(t)$ denotes the temperature derivative of the saturation vapour pressure curve, de_s/dT, whereby the saturation vapour pressure e_s has been calculated after the Mangus formular [e.g. *Murray*, 1967]. Hence, $s_T(t)$ yields:

$$s_T = \lambda \cdot \frac{e^{\frac{l_1 \cdot T_{2m}}{l_2 + T_{2m}}}}{{l_2 + T_{2m}}^2} \tag{34}$$

where $T_{2m}(t)$ is the atmospheric temperature at 2m height and l_1 and l_2 are constants which are 17.269 and 237.3, respectively. The input data *srad(t)*, *trad(t)* and $T_{2m}(t)$ were taken from a climatological run of the ECHAM4 GCM or 6-hourly forecasts of the ECMWF re-analyses (see Sect. 6).

Supply. In case the soil does not contain enough water to evaporate with the equilibrium evapotranspiration rate, the evapotranspiration rate is calculated after *Federer* [1982]:

$$supply = c \cdot \frac{V_{wat}}{V_{tot}} \tag{35}$$

where c is a factor in the unit [cm/d], depending on the actual amount of water in the bucket and the relative vegetation coverage of the soil:

$$c = \begin{cases} 1.5 & \text{if}(V_{wat} \geq V_{tot}) \\ 0.24 + 0.96 \cdot \dfrac{100 - p_{bare}}{100} & \text{else} \end{cases} \tag{36}$$

where p_{bare} denotes the percentage of unvegetated, bare soil. We use maximum supply rates of 1.5 cm/d for grid points with standing water, and 0.24 cm/d for unvegetated and 1.2 cm/d for totally vegetated grid points according to *Kaduk* [1996].

Lateral Inflow. A certain fraction of wetlands lies in arid regions (see Fig. 3 of Sect.1), i.e. the total annual precipitation is less than the total annual evapotranspiration. According to this classification, there are regions, especially in Africa and South America, where wetlands are known to be located, but where the difference between the total annual precipitation and the total annual evapotranspiration (*PmE*) is negative. Therefore, those wetlands must be fed by lateral inflow originating from higher lands and/or rivers like the Niger or the Paraguay/Parana. Since on an annual basis, the inflow of water into a wetland must at least be balanced by its

outflow, the lateral inflow L of water into wetlands is calculated as follows:

$$L = \begin{cases} 0 & \text{if}(PmE > 0) \\ \dfrac{-PmE}{days} & \text{else} \end{cases} \tag{37}$$

where *days* denotes the number of days of the year. For the sake of simplicity we assume that L is constant throughout the year. Certainly, there are wetlands in regions where $PmE > 0$, which are fed by lateral inflow as well, but in those regions this would be balanced by higher run-off. Therefore, L is considered to be different from zero only in regions where $PmE \leq 0$, in order to close the water budget.

Runoff. Here only lateral surface outflow described by the expression runoff R is considered, assuming that the subsurface outflow is zero. In the model R occurs only, if $V_{wat} > V_{tot}$, i.e. in case of standing water. The amount of water flowing away as runoff is assumed to depend on the height of the standing water. In addition, it is considered to be a function of the terrain steepness. Hence, the runoff R is calculated from:

$$R = \begin{cases} 0 & \text{if } (V_{wat} < V_{tot}) \\ H_{wt} \cdot \left\{ \dfrac{H_{wt}^{\,2}}{k_1} + \dfrac{S}{k_2} \right\} & \text{else} \end{cases} \tag{38}$$

The surface outflow of water per unit area is assumed to depend on the curvature of the terrain. Thus, S is the Laplace operator of the terrain height, $S=|\Delta height|$. The values of S have been derived from the 5'x5' topographical data set ETOPO5 [*Edwards*, 1989] and been interpolated to each 1^o*1^o grid cell. H_{wt} is the height of the water table relative to the soil surface in cm and k_1 and k_2 are constants, which are set to 1500 d*cm^2 and 2000 d, respectively. The constants k_1 and k_2 are chosen in a way that the sum in the brackets normally yields values between 0.5 d^{-1} and 0.9 d^{-1} and that the influences of H_{wt} and S on R are balanced in situations with an average value for S and a value of about +10 cm for H_{wt}. In Sect. 5.4 we show that the modeled water table levels are not very sensitive to the choice of those values.

5.2. Tests Against Data

In order to test, if the hydrological model produces reasonable and representative seasonal simulations of the water table, we run the model forced by ECMWF re-analyses of the period from 1988 to 1993. As test data observed water table data from the sites, where the methane model was tested, were used. The modeled water table level of that 1^o*1^o grid cell, where the respective site is located, is compared to the observed water table level.

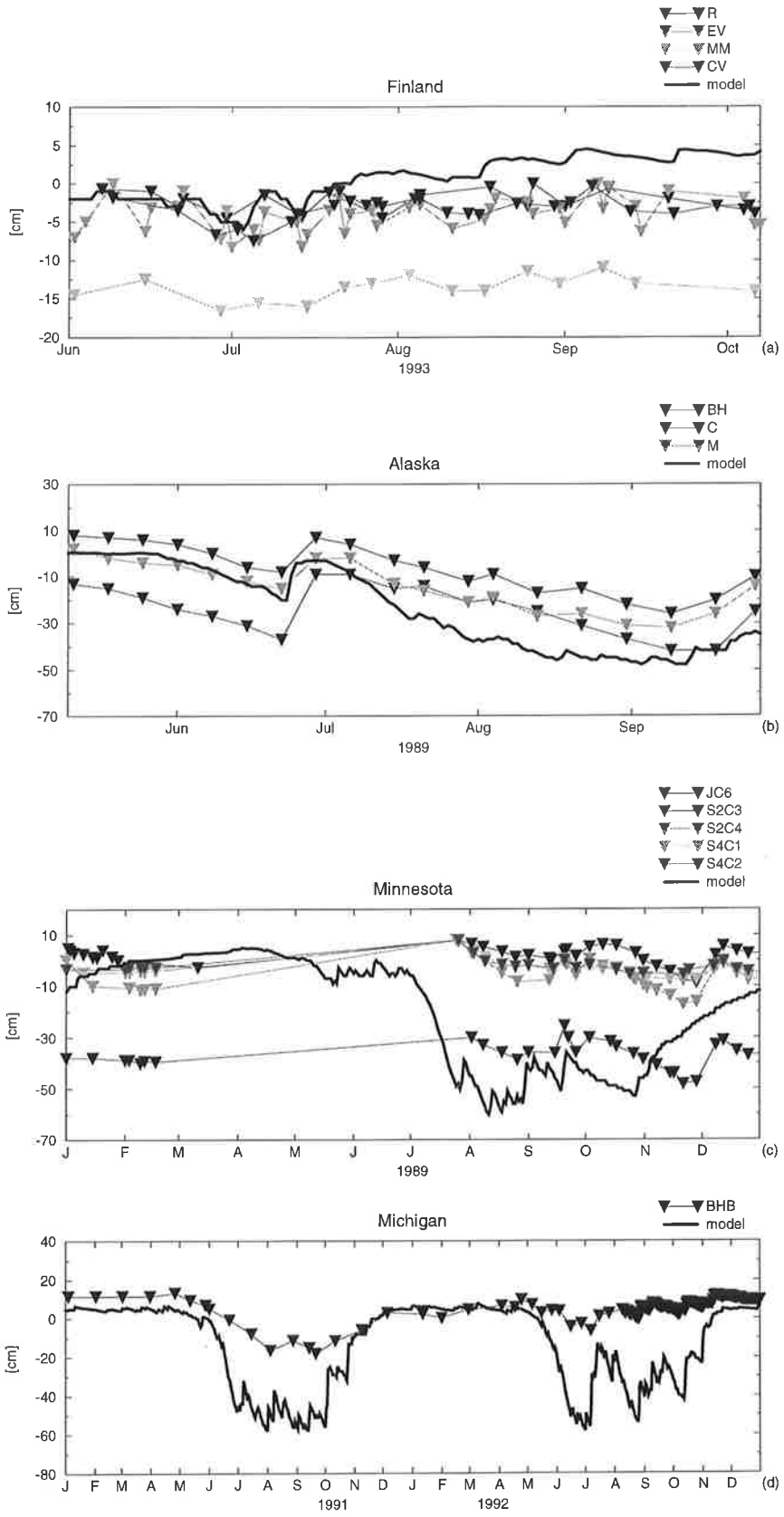

Fig. 27: Results of tests of the hydrological model against data from 4 sites: Model results (thick lines) and observations (triangles) from Finland (a), Alaska (b), Minnesota (c) and Michigan (d)

The results of the comparison (see Fig. 27) show that the seasonal patterns of the modeled water tables compare fairly well with the observations and that the magnitudes of modeled and measured water table levels are similar. In (a) the modeled water table is slightly higher than the observations, in (d) the opposite is the case. At the Alaskan site model results and the data from all three microsites (BH, C and M) compare well (see Fig. 27 (b)). At the Minnesota site both the modeled and the observed water tables decline in August, but the amplitude of the modeled one is larger. The same is valid for the Michigan site. There in July the water table goes down in the model outcome as well as in the observations, but again the amplitude of the modeled water table is larger.

5.3. Sensitivity Tests

Here the sensitivity of the hydrological model to variations of the two model parameters k_1 and k_2 is tested. In addition, it is examined how the model results change with increased or decreased precipitation. In each case we run the model forced with ECMWF re-analyses of the year 1988. In order to demonstrate the sensitivity of the model to changes in these values, six grid points located in the regions of the data sets we used to test the model were selected representing various soil and climatic conditions (see Fig. 28 to 30).

Fig. 28 shows the sensitivity of the model results to changes in k_1. We run the model using k_1 (control run) and either k_1*0.5 or k_1*2. It is clear that those changes do not affect the model results very much at any of these grid points. The same is valid for changes in k_2 (see Fig. 29). If k_1 or k_2 are higher, runoff is smaller. Since runoff occurs only at times when the water table is above the soil surface the water table is higher in case k_1 or k_2 are higher (see Fig. 28 Finland and Fig. 29 Alaska_I). Moreover, the decline of the water table below the soil surface occurs later in case k_1 or k_2 are higher (see Fig. 29 Alaska_II).

Changes in the precipitation affect modeled water table levels more strongly (see Fig. 30). Here we run the model using prec*100% (control) and either prec*80% or prec*120%. Higher precipitation leads to higher water table levels. Depending on the site those differences in precipitation can have a large effect (Alaska_II). Generally one can say that the effect of a 20% increase or decrease in precipitation has a larger effect at sites where the precipitation is low (Alaska_I/II, Finland).

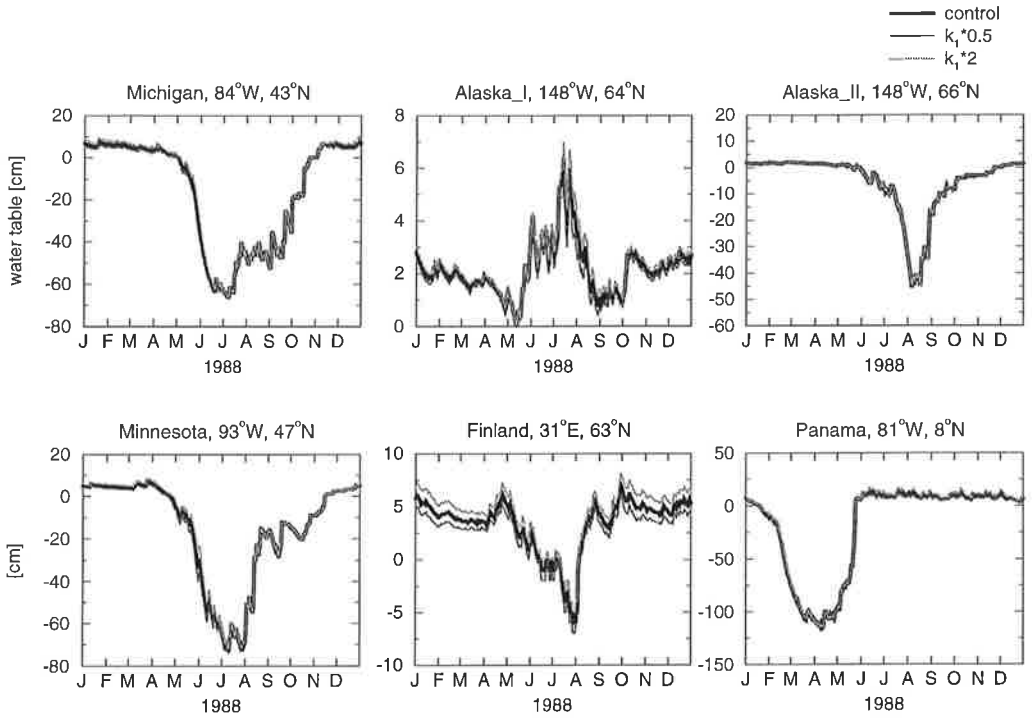

Fig. 28: Sensitivity test of the hydrological model to the parameter k_1: comparison of two runs using k_1*0.5 (dark grey) and k_1*2 (light grey) to the control run (black)

5.4. Conclusion

The hydrological model presented here is a relatively simple approach. However, the results of the comparison between modeled and observed water tables illustrate that the hydrological model yields realistic results. In the observational data there is reasonable variability of the water table level within one wetland due to the microtopography (hummock-hollow structure). Therefore, within site differences of the water table levels of 20-40 cm can easily occur (see Fig. 27 (a), (b) and (c)) and it is clear that we cannot expect the modeled water table to be equivalent to the observations in each case. Furthermore, the variability of the input data within one grid cell is quite high, i.e. the used input data (ECMWF re-analyses) differ most likely from the actual input data (precipitation, surface solar net radiation and 2m-temperature) at the respective sites. Hence, a true test of the model would include observational input data.

There are three factors that are not considered in this approach, namely (1) the occurrence of permafrost, (2) snow and (3) the microtopography of a wetland. (1) The occurrence of permafrost in some high-latitude wetlands leads to the fact that water is stored in the form of ice. Furthermore, water cannot infiltrate into a frozen soil. However, at the Alaskan site, which is underlain by permafrost, the modeled water table compares well with the observation (see Fig. 27 (b)) leading to the assumption that the consideration of permafrost is not of particular

importance. (2) Water is also stored in the form of snow and released in spring when the snow melts. Since our model results do not differ systematically from the observations in spring, this effect seems to be of minor importance at the test sites which represent a large variety of high latitude wetlands. (3) Since the methane model is rather sensitive to the position of the water table, the neglect of the microtopography of a wetland can affect modeled methane emissions. Usually, the surface of a wetland is not homogeneous. Some parts of a wetland are elevated by several decimeters relative to the wetland surface (hummocks), while a certain fraction consists of (generally water-filled) depressions (hollows). Especially the occurrence of hollows which can be water-filled even in relatively dry years can have a large effect on simulated methane emissions and hence microtopography should be included into an advanced version of the hydrological model.

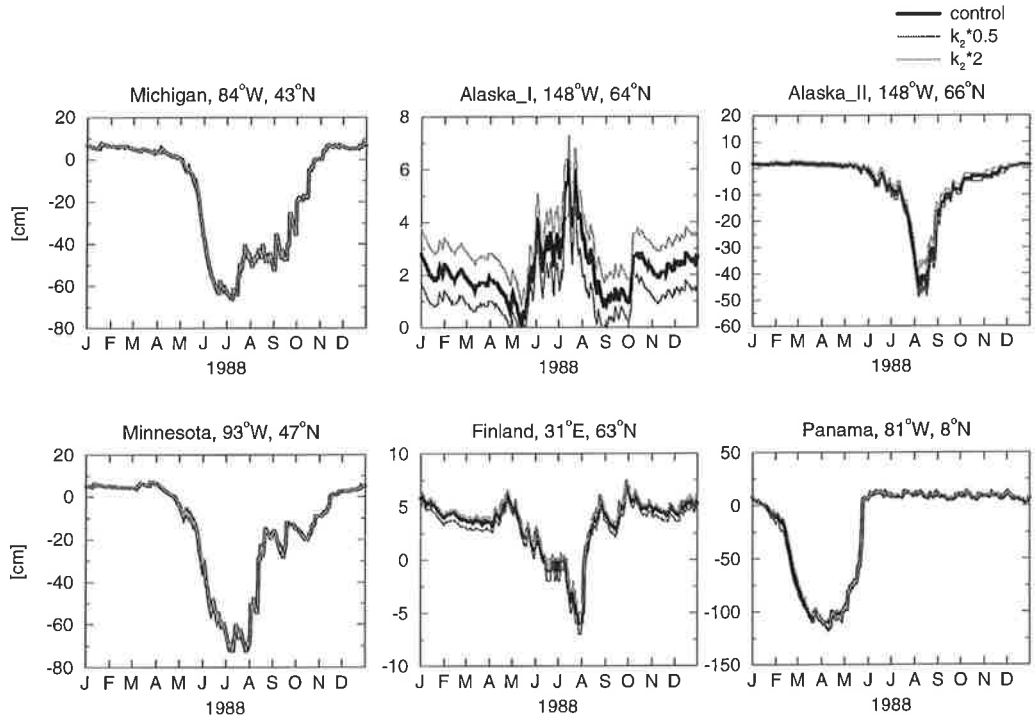

Fig. 29: Sensitivity test of the hydrological model to the parameter k_2: comparison of two runs using k_2*0.5 (dark grey) and k_2*2 (light grey) to the control run (black)

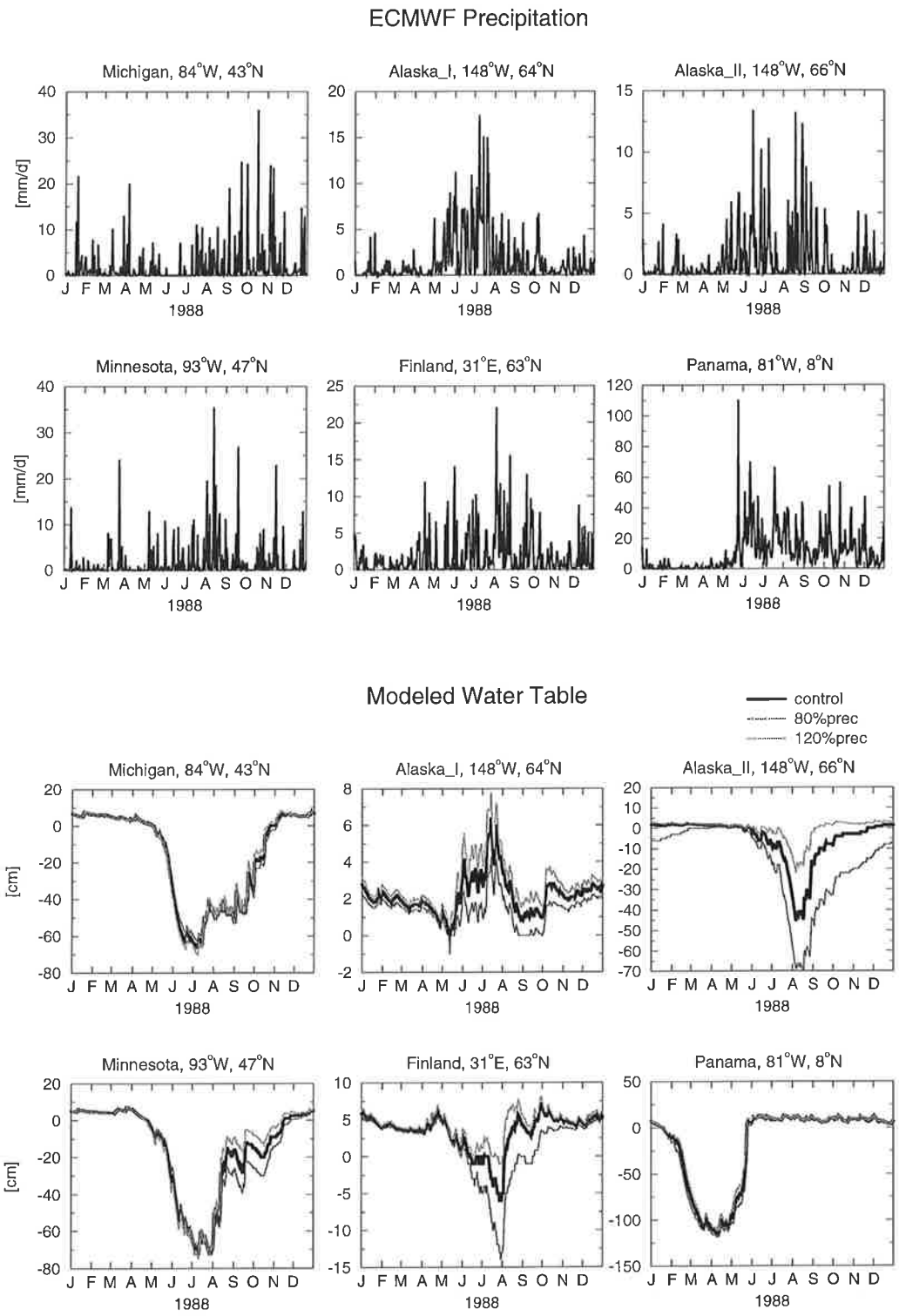

Fig. 30: Sensitivity test to precipitation: the upper two rows show the precipitation at the six test sites as obtained from the ECMWF re-analyses for the year 1988; the lower two rows show the modeled water table levels for the six test sites using 80%*precipitation (dark grey) and 120%*precipitation (light grey) in comparison to the control run (black) (note: y-axis units differ)

6. Results of Global Model Runs

In this section we present the results of global runs of the methane model using ECMWF re-analyses of the period from 1988 to 1993 as input. The seasonal and interannual variability of simulated methane emissions is investigated and the model results are compared to results obtained by an inverse modeling approach and with observations of the atmospheric methane growth rate. Moreover, sensitivity tests of the global methane model are performed.

6.1. Global Runs with the Methane Model

Setup

As forcing for the global model run we use ECMWF re-analyses of the period from 1988 to 1993 in T106 resolution ($1.1^{o}*1.1^{o}$), interpolated to a $1^{o}*1^{o}$ grid. The input for the hydrological model consists of:

- 24-hourly forecasts of the total precipitation,
- 6-hourly forecasts of the 2m-temperature,
- 6-hourly forecasts of the surface solar and thermal radiation.

For the precipitation 24-hourly forecasts are used, because they yield better results than forecasts over shorter periods [*Stendel*, pers. comm.]. For the other quantities we use 6-hourly forecasts, which are available 4 times a day, because here we needed diurnal cycles in order to calculate the evapotranspiration (Eq. (33) and (34) of Sect. 5). As forcing for the methane model we use:

- 24-hourly forecasts of the soil temperature at different soil depths (levels 1-4).

Global Distribution of Simulated Emissions

Fig. 31 shows the simulated annual mean methane emissions of the period 1988-1993. The methane fluxes are smaller in the higher latitudes than in the subtropics and the tropics which can be attributed to two effects: (1) the length of the period of time in which methane production can occur and (2) the annual mean temperature T_{mean} which increases the magnitude of the methane production rate. In the higher latitudes the length of the methane production period is determined by the seasonal cycle of the temperature, whereas in the subtropics and the tropics it is controlled by the hydrological cycle. This aspect will be further discussed in the next paragraph. In general, the length of the methane production period is shorter in the higher latitudes than in the subtropics and the tropics. Furthermore, the annual mean temperature T_{mean} is lower in the higher latitudes.

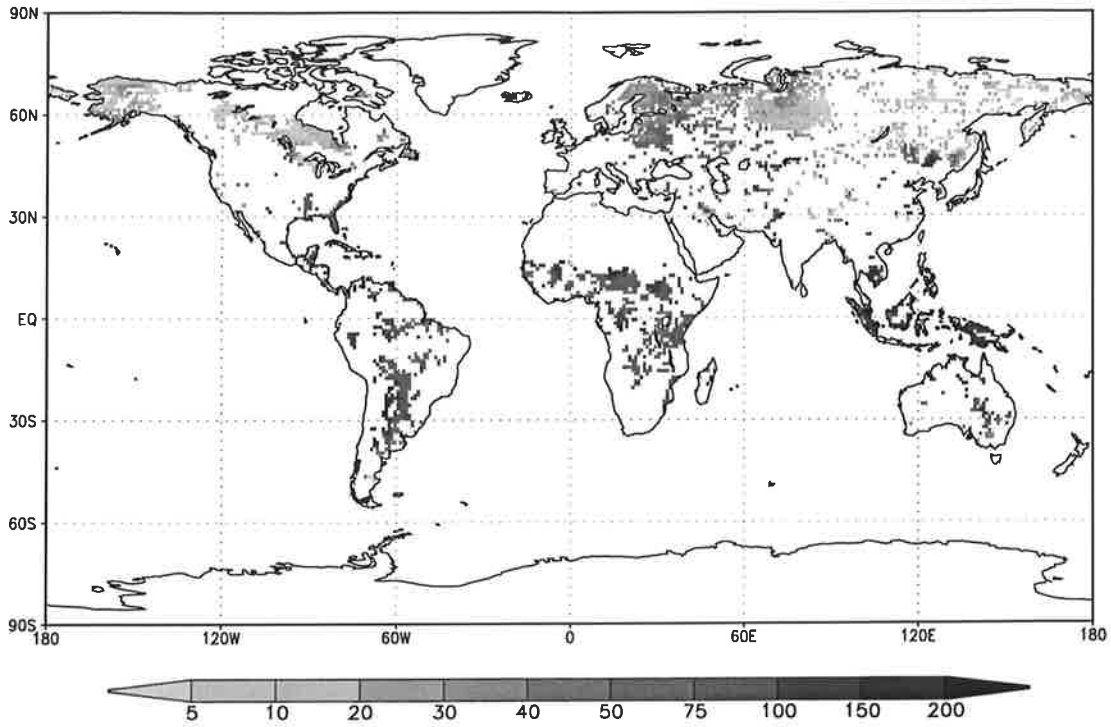

Fig. 31: Mean annual methane emissions in [$gCH_4*m^{-2}*yr^{-1}$] as simulated by the global model version using the ECMWF re-analyses of the period from 1988 to 1993 as forcing data

In Fig. 32 the zonally integrated methane emissions obtained by the methane model are compared to those derived from an inverse modeling approach by *Hein et al.* [1997]. *Hein et al.* calculated the global annual methane emission to be 232±27 Tg/yr, whereas we obtain a value of 263 Tg/yr. Fig. 32 (c) shows the zonally integrated wetland areas derived from a data set by *Matthews and Fung* [1987] which has been used in both studies. *Hein et al.* used a simple temperature dependence to obtain the temporal variation of methane emissions using a relatively low Q_{10} value of 1.5. The overall pattern of methane emissions is similar in (a) and (b). High emissions in the zone between 30°S and 15°N followed by low emissions from 15°N to 45°N and then relatively high emissions up to about 70°N. However, the amplitude of the meridional variation of methane emissions is higher in the methane model than in the inverse model. In our simulation methane emissions have a pronounced peak around the equator which is caused by the fact that the wetlands near the equator are flooded almost throughout the year, whereas the wetlands in the subtropical regions are dry for about 3-4 months. The meridional pattern of the simulated methane emissions from wetlands north of 60°N mainly follows the pattern of wetland areas leading to higher methane emissions than in *Hein et al.* [1997].

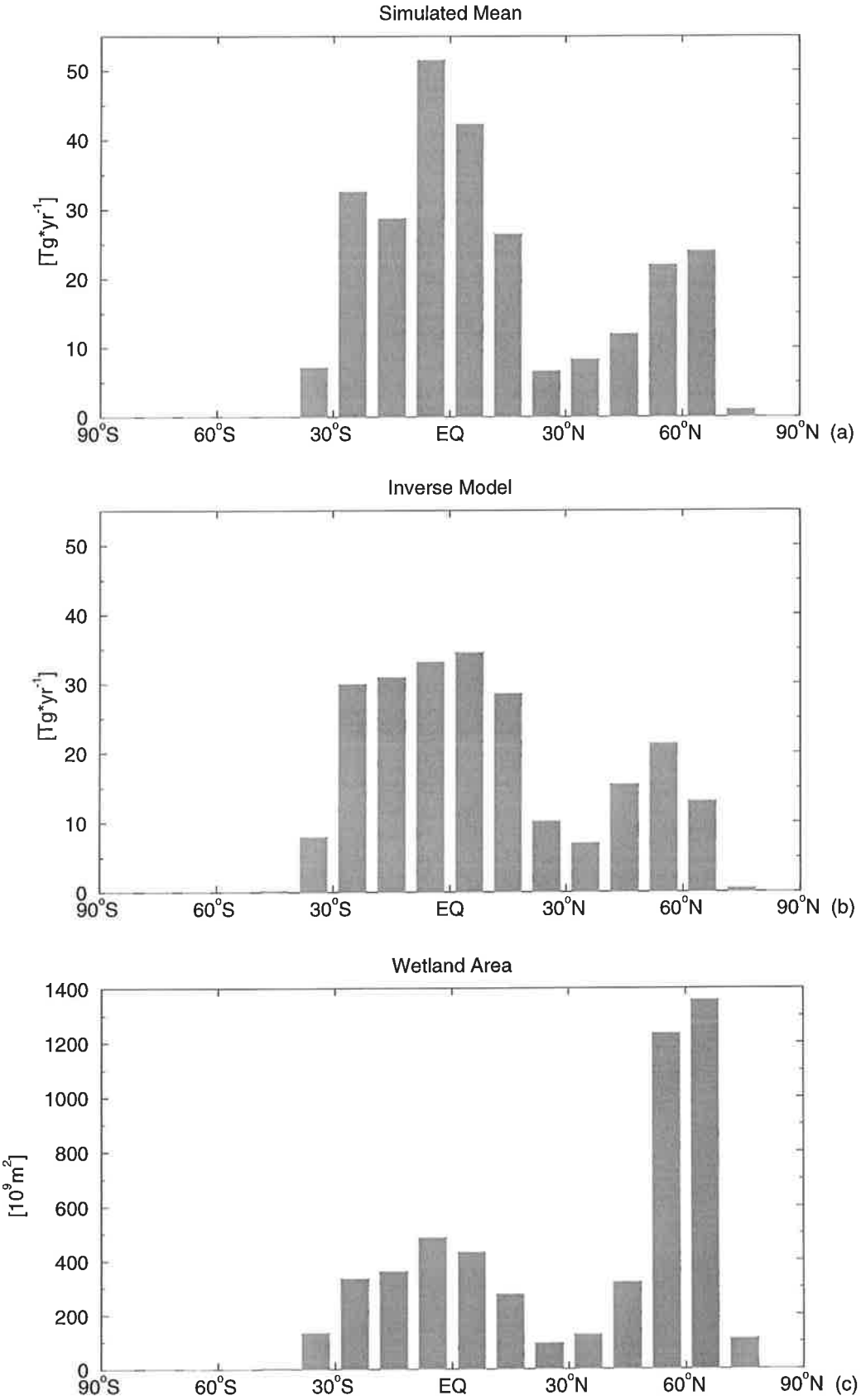

Fig. 32: Zonally integrated annual methane emissions [Tg*yr^{-1}]: (a): Mean of the results of a run of the methane model using ECMWF re-analyses of the period from 1988-1993 as forcing data; (b): Results from an inverse model [*Hein et al.*, 1997]; (c): Zonally integrated wetland area [*Matthews and Fung*, 1987]

6.2. Sensitivity Tests

In order to examine the response of simulated methane emissions to changes in the forcing (soil temperature, precipitation and water table) and to the choice of the most critical model parameter V_{max} (maximum oxidation rate) several sensitivity tests are performed. To test the model sensitivity to the input we use ECMWF re-analyses of the year 1988 as forcing and compare two runs using modified input to the control run obtained with the original forcing.

Sensitivity to the soil temperature T_{soil}. Two simulations are conducted, one with a uniform $+1^{o}C$ anomaly and one with a uniform $-1^{o}C$ anomaly. The results of these runs compared to the control run are shown in the upper row of Fig. 33. There are two processes in the model which are influenced by the soil temperature, namely methane production and methane oxidation. Since production has a larger Q_{10}, higher temperatures affect methane production rates more strongly than methane oxidation rates. Furthermore, plant-mediated transport is influenced by changes in the soil temperature, because the growing state $f_{grow}(t)$ of the vegetation is defined as a function of the soil temperature (see Eq. (18) of Sect. 2). Fig. 33 shows that higher temperatures lead to higher methane emissions and vice versa. A decrease of the soil temperature by $1^{o}C$ leads to a 17% reduction of methane emissions, while a temperature which is by $1^{o}C$ higher gives rise to an 20% increase in modeled methane emissions. The differences between the $\pm 1\ ^{o}C$ runs and the control run are higher in regions, where the total emissions are higher and vice versa.

Sensitivity to precipitation. We perform two simulations in which precipitation is changed uniformly by $\pm 20\ \%$. The water table levels obtained by these two runs of the hydrological model are used to force the methane model (Fig. 33, middle row). Lower precipitation leads to lower methane emissions almost everywhere and vice versa. A 20% reduction in precipitation leads globally to by 9% decreased methane emission, while 20% more precipitation increases global methane emissions by 8%. In the higher northern latitudes the effect of reduced precipitation is particulary pronounced, because here the water table fluctuates around the soil surface and thus less precipitation causes the water table to be above the soil surface for a shorter time or to be deeper below the soil surface. In the subtropics and the tropics changes in precipitation hardly affect the position of the water table and hence methane emissions, because during the wet season precipitation is sufficiently larger than the potential evapotranspiration rate (PET) and hence the soils are flooded throughout the wet season in all three cases of Fig. 33 (b) (see also Fig. 30 of Sect. 5, Panama). On the other hand, during the dry season, PET is cleary larger than precipitation so that the water table rapidly falls. There are two regions where increased precipitation does not enhance simulated methane emissions and vice versa: in the case of reduced precipitation, at $15^{o}S$ higher emissions are obtained, and in the case of increased precipitation, at $15^{o}N$ lower emissions are obtained. The reason for this

behaviour lies in the formulation of the lateral inflow L in the hydrological model (see Eq. (37) of Sect. 5). The more negative the difference between annual precipitation and annual PET is, the larger is L. Thus, L can increase in case of less precipitation and hence lead to slightly higher water table levels.

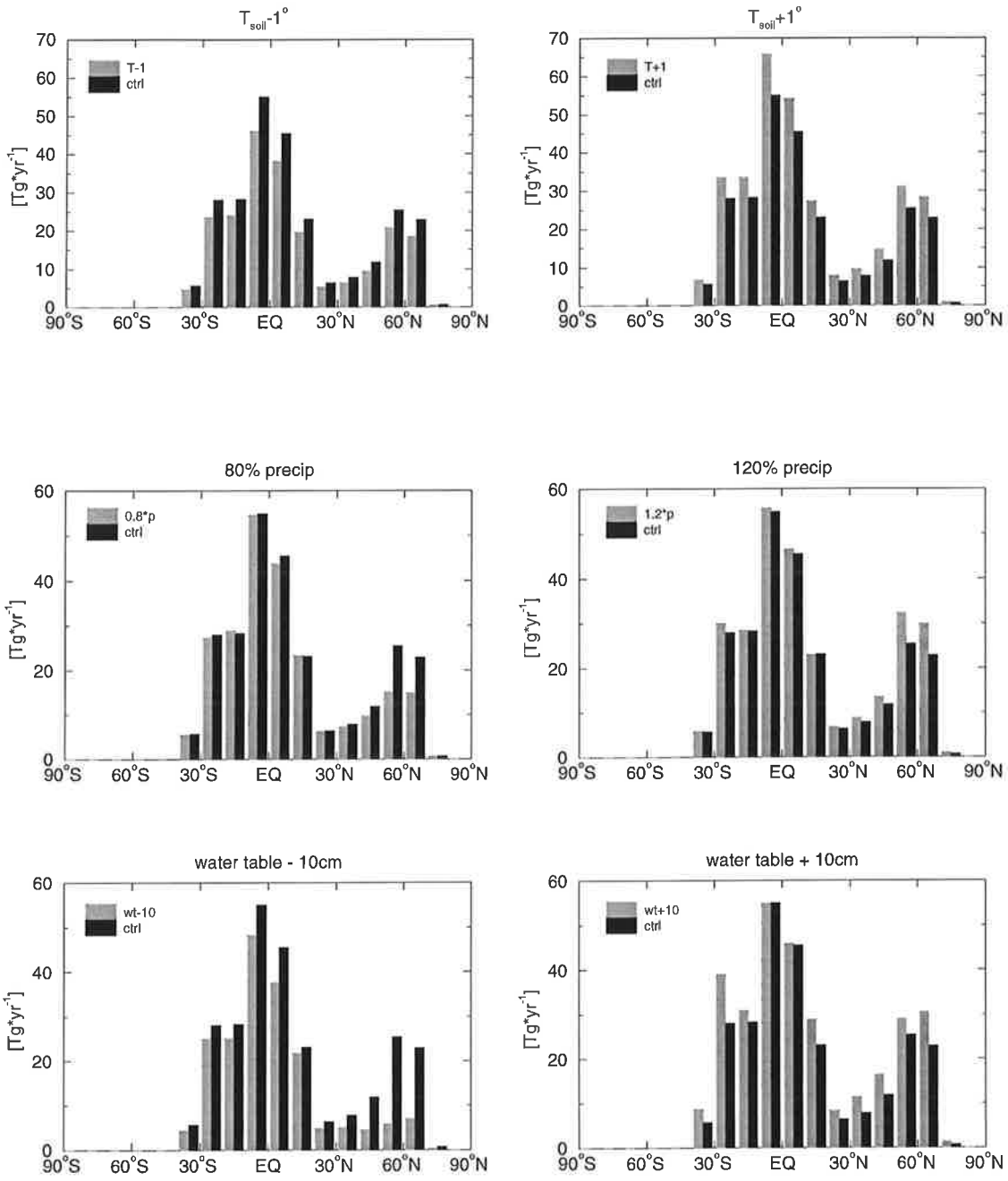

Fig. 33: Sensitivity tests: soil temperature (upper row), precipitation (middle row) and water table (lower row); plotted are the zonally integrated annual methane emissions; the control run is forced by the original ECMWF re-analyses of the year 1988; upper row: comparison between one run using the original soil temperature+1°C (left: grey) and one using the original soil temperature-1°C (right: grey) with the control run (black); middle row: comparison between one run using 80%precipitation (left: grey) and 120%precipitation (right: grey) and the control run (black); lower row: comparison between one run using the original water table-10cm (left: grey) and one using the original water table+10cm (right: grey) and the control run (black)

Sensitivity to the water table level. Since a uniform change in precipitation by ±20 % leads to different changes in the water table at different places and times, we carry out an experiment where the water table is changed uniformly by ±10 cm (see Fig. 33, lower row). Comparing the results of that experiment with the results of the ±20 % precipitation experiment (see Fig. 33, middle row) we see that a 20% change in the precipitation has a smaller effect than a 10 cm change in the water table almost everywhere. A water table that is lowered by 10 cm leads to by 27% reduced global methane emissions, whereas a water table that is 10 cm higher increases global methane emissions by 17%. Near the equator 20% less precipitation has hardly an effect on methane emissions, because there the water table is above the soil surface during the wet season in any case. However, a reduction of the water table by 10 cm shifts the water table below the soil surface even during the wet season and hence reduces the simulated methane emissions. These results are consistent with the findings of the sensitivity experiments at the Panama site (see Fig. 30 of Sect. 5). In the higher latitudes the effect of an increased water table is similar to the effect of increased precipitation. However, the effect of a by 10 cm decreased water table is significantly stronger than the effect of 80% precipitation. From Fig. 30 of Sect. 5 one can see that a by 20% reduced precipitation leads, in general, to smaller than 10 cm changes in the water table. At those sites where reduced precipitation decreases the water table by more than 10 cm, this occurs only during a few months of the year.

Sensitivity to V_{max}. The results of the 1-dimensional tests of the model against data (see Sect. 3) revealed that a V_{max} value of 20µM/h cannot be used everywhere. Since we could not find a connection between environmental parameters and V_{max} (as in the case of R_0) we set V_{max} to the globally constant value of 20µM/h. Therefore, we investigate the influences of different choices for V_{max} on the temporal and regional variation of simulated methane emissions. Here we run the model using V_{max} values of 2µM/h, 10µM/h, 20µM/h and 45µM/h. The results of these runs are compiled in Tab. 16:

Table 16: Simulated Annual Methane Emissions Using Different V_{max} Values

V_{max}=2µM/h	V_{max}=10µM/h	V_{max}=20µM/h	V_{max}=45µM/h
315 Tg/yr	282 Tg/yr	263 Tg/yr	238 Tg/yr

From Fig. 34 one can see that a higher value for V_{max} leads to lower methane emissions everywhere, because the higher V_{max} is, the more methane is oxidized in the unsaturated soil layers. This effect is less pronounced in the tropics and more pronounced in the northern latitudes due to the differences in the temporal variations of the water table between those regions. In the tropics the water table is above the soil surface most of the time, whereas in the

higher latitudes it fluctuates around the soil surface and can be below the soil surface for a considerable part of the year making methane oxidation possible.

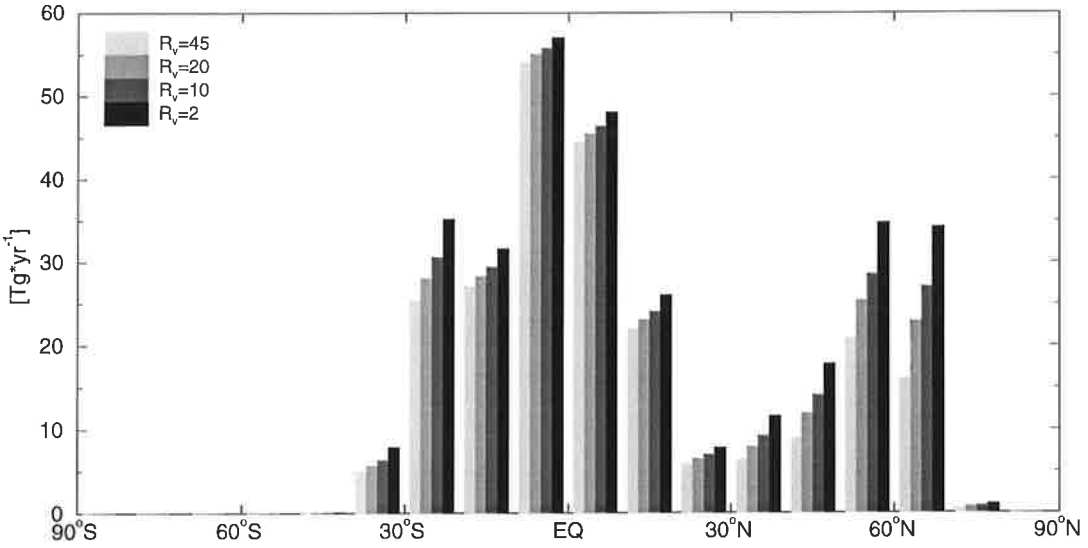

Fig. 34: Sensitivity test: Zonally integrated methane emissions of global runs of the methane model using different values for V_{max}: 2µM/h (black), 10µM/h (dark grey), 20µM/h (medium grey), 45µM/h (light grey); the model forcing consists of ECMWF re-analyses of the year 1988

The temporal variation of simulated methane emissions is not altered by the choice of V_{max}. In Fig. 35 we plot total annual methane emissions for the years 1988-1993. In (a) we show the results of a run using the original water tables and soil temperatures derived from the ECMWF re-analyses for that period, whereas in (b) and (c) we depict the results of the two factorial experiments exp_WT and exp_T (which are explained in the next paragraph), respectively, carried out with different V_{max} values. It can be seen that the interannual pattern of modeled methane emissions does not change in either case whatever V_{max} we use. Therefore, the results obtained in this section are qualitatively independent of V_{max}. However, a regionally varying V_{max} could alter those results.

The results of the sensitivity tests give us also an idea of how a changed climate might affect methane emissions from natural wetlands. The experiment with the by 1°C increased soil temperature results in by 20% increased global methane emissions. Changes in precipitation of 20% lead to 10% changes in methane emissions.The seasonal and regional patterns of climatic changes will differ from our sensitivity experiments, but our results give an idea about the order of magnitude of changes in methane emissions due to climate change.

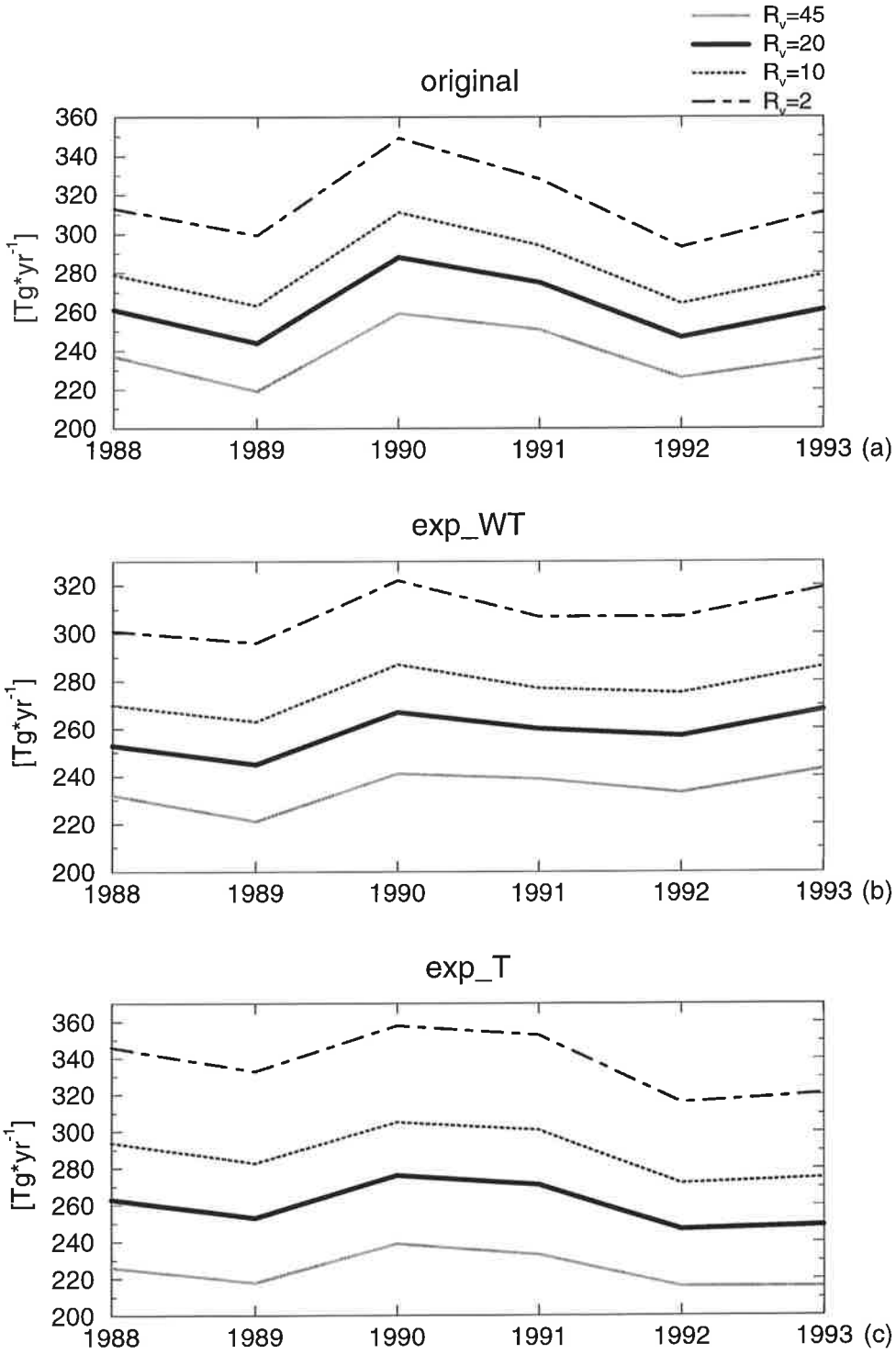

Fig. 35: Sensitivity test: annual methane emissions obtained by the methane model using different values for V_{max}: 2µM/h (dark grey dot-dashed), 10µM/h (dark grey dotted), 20µM/h (black solid) and 45µM/h (light grey solid); (a): Results from the control run using ECMWF re-analyses from the period of 1988-1993 as model forcing; (b): Results from the factorial experiment exp_WT (see text); (c): Results from the factorial experiment exp_T (see text)

6.3. Spatio-Temporal Variation of Simulated Methane Emissions

Fig. 36 shows the simulated mean seasonal cycle of the 6-year simulation period. The global seasonal cycle is determined by the seasonal cycle of the northern hemisphere (30°N-90°N) which has a much larger amplitude than the seasonal cycle of the tropics (30°S-30°N). The sensitivity test to the parameter V_{max} revealed that the effect of an altered V_{max} on modeled methane emissions is larger in the high northern hemisphere than in the tropics (see Fig. 34). Hence a different V_{max} alters the global seasonal cycle and the comparison between the observed and modeled seasonal cycles can be a constraint to the choice of V_{max}.

The spatio-temporal variation of simulated methane emissions is shown in Fig. 37. In the high northern latitudes there is a strong seasonal cycle with high emissions during the summer and low emissions during the winter. This is mainly attributable to the seasonal variation in temperature. Between 5°N and 15°N there is again a pronounced seasonal cycle, but here methane emissions are highest around September and lowest in the first 3-4 months of the year, reflecting the effect of the hydrological cycle. For example at the Panama site located at 9°N, there is a dry season between February and May during which the soil dries out and a wet season with a flooded soil during the rest of the year (site 6, see Fig. 12 of Sect. 3). In the zone of ±5° around the equator there is only a weak seasonal cycle, since there the wetlands are flooded almost throughout the year and the temperature does not vary much. Between 5°S and 30°S the temporal pattern of simulated methane emissions is similar as between 5°N and 15°N, but shifted in time. Here again the seasonal pattern is dominated by the hydrological cycle leading to maximum methane emissions at the beginning of the year.

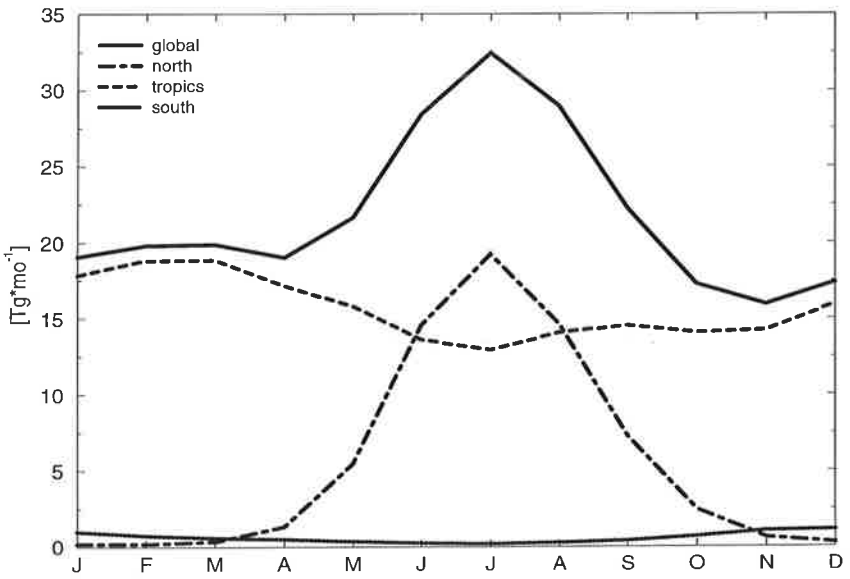

Fig. 36: Mean seasonal cycles of simulated methane emissions: global (black, solid), northern hemisphere (30°N-90°N) (dot-dashed), tropics (30°S-30°N) (dashed) and southern hemisphere (90°S-30°S) (dark grey, dotted)

Interannual Variation of Simulated Methane Emissions

Fig. 37 indicates significant interannual variation in the modeled methane emissions. In the northern hemisphere modeled methane emissions are highest in 1990 and 1991 and show a pronounced minimum in 1992. Modeled methane emission from the northern subtropics are also highest in 1990 and 1991. In the tropics there is an emissions minimum in 1989, while in the southern subtropics there is a maximum in 1992. In order to better understand what the causes of the interannual variation of modeled methane emissions from natural wetlands are, we make two factorial experiments to separate the influences of the changes in soil temperature and water table on the simulated methane emissions.

Factorial Experiments. In the first experiment (exp_T) we examine the influence of interannual variations of the soil temperature on modeled methane emissions. Here the model is forced with ECMWF re-analysis soil temperatures of the years 1988-1993 as in the control run, and the mean seasonal cycle of the water table is used for each year. In the second experiment (exp_WT) we investigate the influence of interannual variation of the water table on modeled methane emissions. Here we use the water table as in the control run, and the mean seasonal cycle of the soil temperature. The results of the factorial experiments are depicted in Fig. 38 which shows the anomalies of modeled methane emissions obtained by subtracting the mean seasonal cycle from the modeled methane emissions. Fig. 38 (a) shows the modeled global anomalous emissions, (b)-(d) show the modeled anomalous emissions integrated over 60^{o} latitudinal bands, i.e. from 30^{o}N to 90^{o}N (b), from 30^{o}S to 30^{o}N (c) and from 30^{o}S to 90^{o}S (d). The amplitude of the anomalies is largest in the northern hemisphere and smallest in the southern hemisphere (the unit of the y-axes in Fig. 38 differ). We compare the results of the control run to the results of the two experiments exp_T and exp_WT.

Fig. 38 (a) shows that in 1990 and 1991 modeled global methane emissions from natural wetlands are highest, while in 1989 and 1992 the emissions are lower than the average. The amplitude of the 1989 minimum is smaller than the amplitude of the 1992 minimum, but in 1989 there is a minimum in the spring (due to reduced methane emissions from the subtropics and the tropics) and one in the summer (due to reduced methane emissions from the high northern latitudes). In contrast to this, the 1992 minimum has its origin in lower methane emissions from the northern hemisphere only. In the northern hemisphere (see Fig. 38 (b)) the effect of changes in the water table and the soil temperature go into opposite directions in 1988 and 1989. In both years temperature alone causes higher emissions while the effect of the water table leads to reduced methane emissions. The 1992 emission minimum in the northern hemisphere is a response to lower temperatures and lower water table levels. In the model results about two thirds of the reduction of methane emissions in 1992 is due to decreased temperatures. In the tropics the 1989 minimum and the 1992 maximum are caused by variations in the soil temperature as well as the water table whereas the 1990 maximum is

mainly caused by increased temperatures. In the southern hemisphere the amplitudes of the modeled emission anomalies are significantly smaller. Both the 1989 emission minimum and the 1990 maximum are due to changes in the water table.

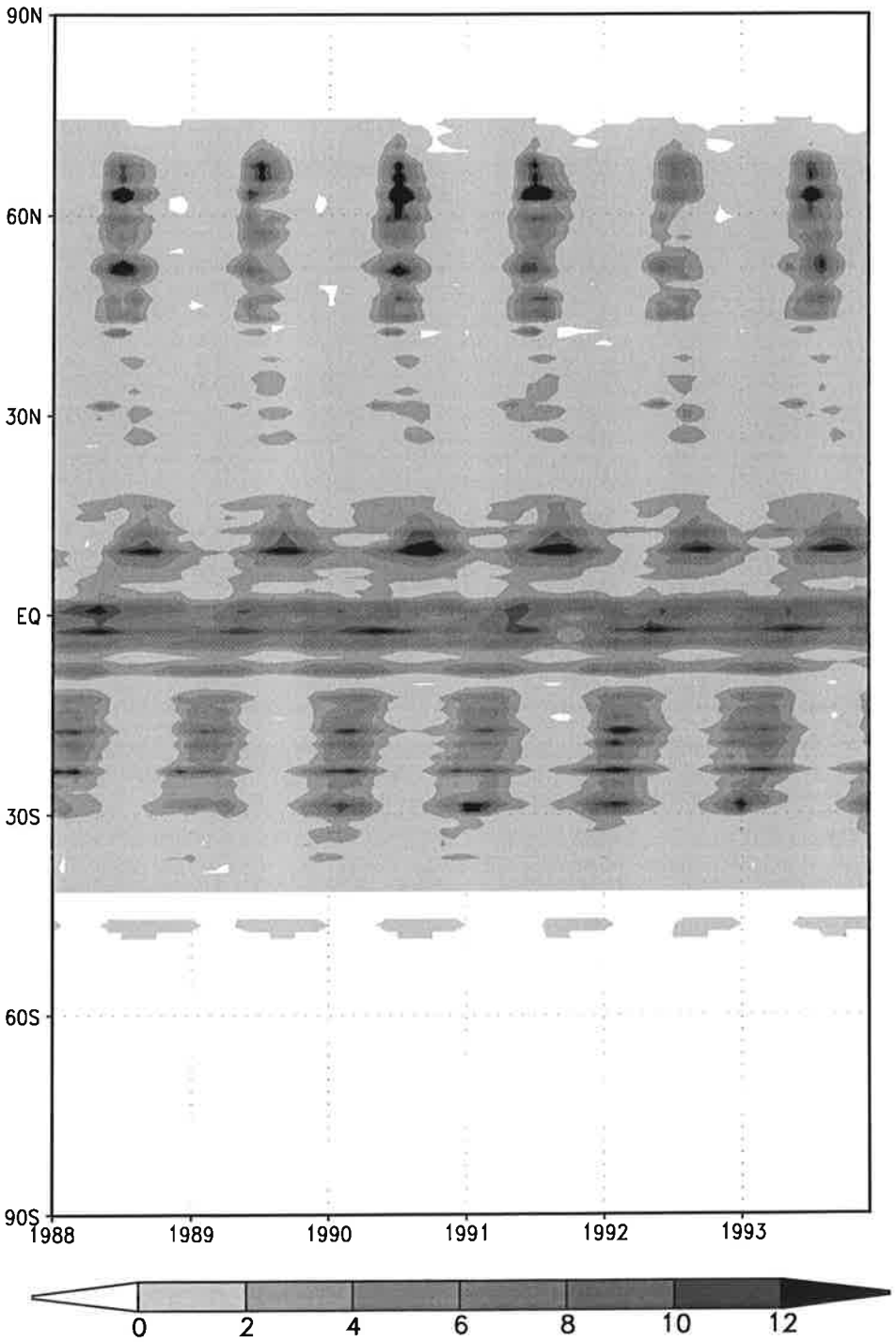

Fig. 37: Spatio-temporal variation of methane emissions [Tg*yr^{-1}]: methane emissions (zonally integrated over 1° latitudinal bands) from a run of the methane model using ECMWF re-analyses of the period from 1988 to 1993 as forcing data

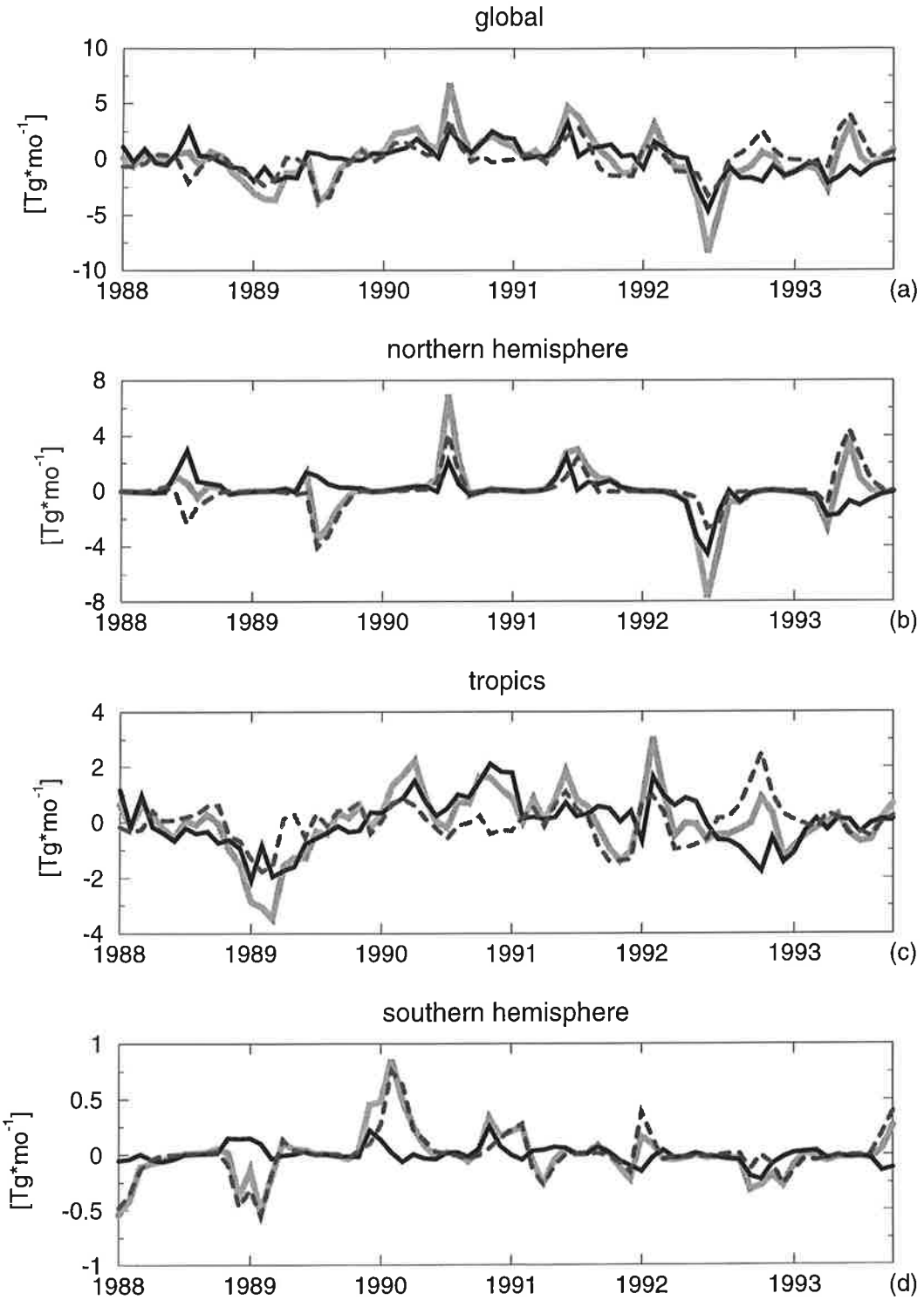

Fig. 38: Factorial experiments: anomalies of simulated methane emissions; control run (grey solid), exp_T (black solid) and exp_WT (black dashed) (see text); (a): global, (b): northern hemisphere (30°N-90°N), (c): tropics (30°S-30°N), (d): southern hemisphere (90°S-30°S)

In Tab. 17 the global annual methane emissions obtained from the control run and the two factorial experiments are listed. Again we see that the 1989 minimum of the original run originates mainly from low water table levels and the 1992 minimum mainly from low soil temperatures.

Table 17: Global Annual Methane Emissions [Tg/yr]

Year	**Original**	**exp_T**	**exp_WT**
1988	261	263	253
1989	244	253	245
1990	288	276	267
1991	275	271	260
1992	247	247	257
1993	261	249	268
Mean	263	260	258

Interannual Variations in the Forcing Data

In order to better understand the global model results we examine the regional patterns of anomalies in the model input (soil temperature and precipitation) and compare that to the simulated methane emissions. In Fig. 39 anomalies of the simulated annual methane emissions are plotted. Temperature anomalies are plotted in Fig. 40 (annual mean) and Fig. 41 (northern summer mean = mean of MJJASO). The precipitation anomalies are shown in Fig. 42 (annual mean) and Fig. 43 (northern summer mean = mean of MJJASO). The summer plots are relevant to interpret the emission anomalies from the high northern latitudes.

In the subtropics and the tropics the relative year-to-year changes in the simulated methane emissions are relatively small in Central and South America as well as in Africa and Asia. However, the forcing data show quite some interannual variability. Small variations in the soil temperature generally lead to slightly increased methane emissions, e.g. in 1990 and 1991 in Africa. However, the higher precipitation in central Africa in 1988, coinciding with average temperatures, does not lead to higher methane emissions. The reason for this behaviour lies in the fact that higher precipitation during the wet season, when the soils are flooded, does not lead to higher methane emissions in the model. Possibly the inundated area is larger in years with a higher precipitation. But this is not taken into account in the model, since we assume the global wetland distribution to be constant. The wetland area taken from the data set by

Matthews and Fung [1987] is considered to be the maximum wetland area. In the subtropics and the tropics the reduction of the wetland area during the dry season is taken into account by the decrease of the water table in the hydrological model. During the dry season the water table falls to the soil depth being equivalent to a dry soil. However, it would be desirable to have a global wetland distribution taking into consideration the interannual variations of the extent of subtropical and tropical wetlands.

In the higher latitudes the relative interannual changes in methane emissions are larger than in the subtropics and the tropics. Here more precipitation as e.g. in 1990 in Siberia, accompanied by average temperatures, leads to higher methane emissions, because in this region there is no pronounced dry or wet season. Therefore, more precipitation can lead to the fact that the water table is less deep below the soil surface causing higher methane emissions. In 1992 the soil temperature is below the average almost everywhere, whereas in other years there are quite some regional differences. Therefore, in 1992 modeled methane emissions are lower than the 1988-1993 mean in northern Europe, in most parts of northern Asia and North America. The relatively high temperatures in northern Europe and Asia in 1989 lead to high emissions in northern Europe, because there precipitation is high as well, but in northern Asia emissions are low nevertheless, since there precipitation is low during that year.

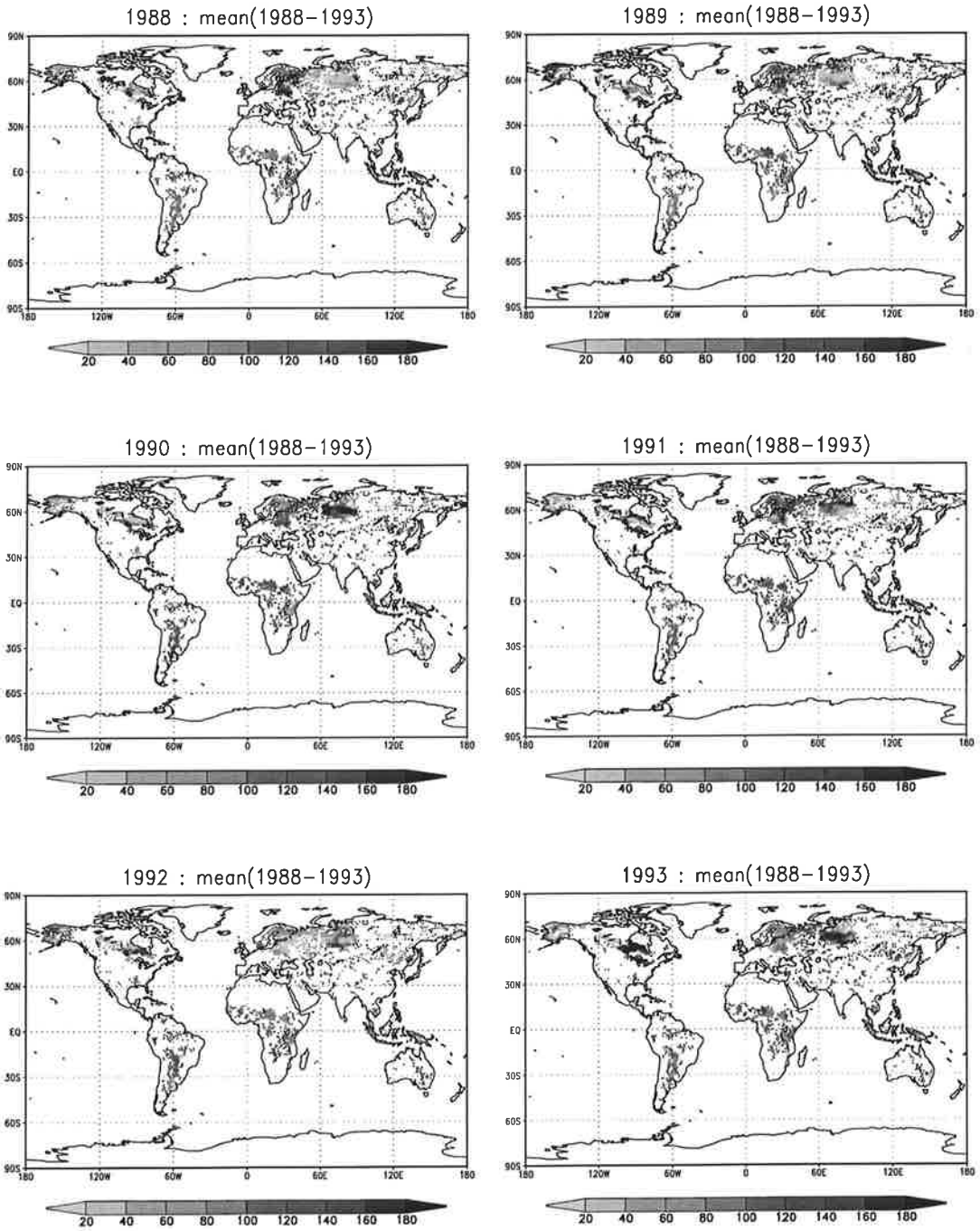

Fig. 39: Anomalies [%] of simulated annual methane emissions for the years 1988-1993; results from a run of the methane model using ECMWF re-analyses as forcing

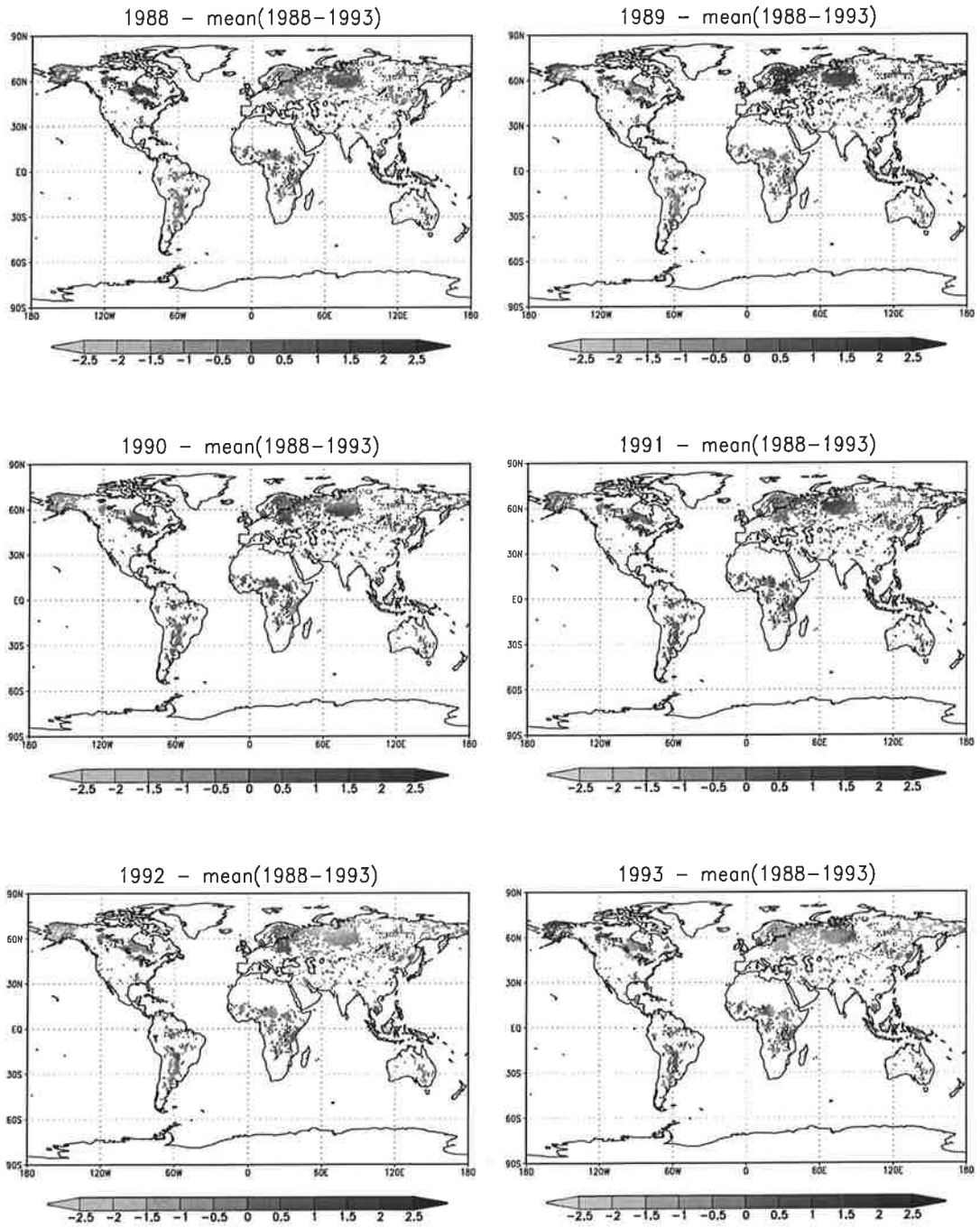

Fig. 40: Anomalies in the input data: Annual ECMWF soil temperature [°C] at all wetland grid points of the years 1988-1993 compared to the mean soil temperature of that period

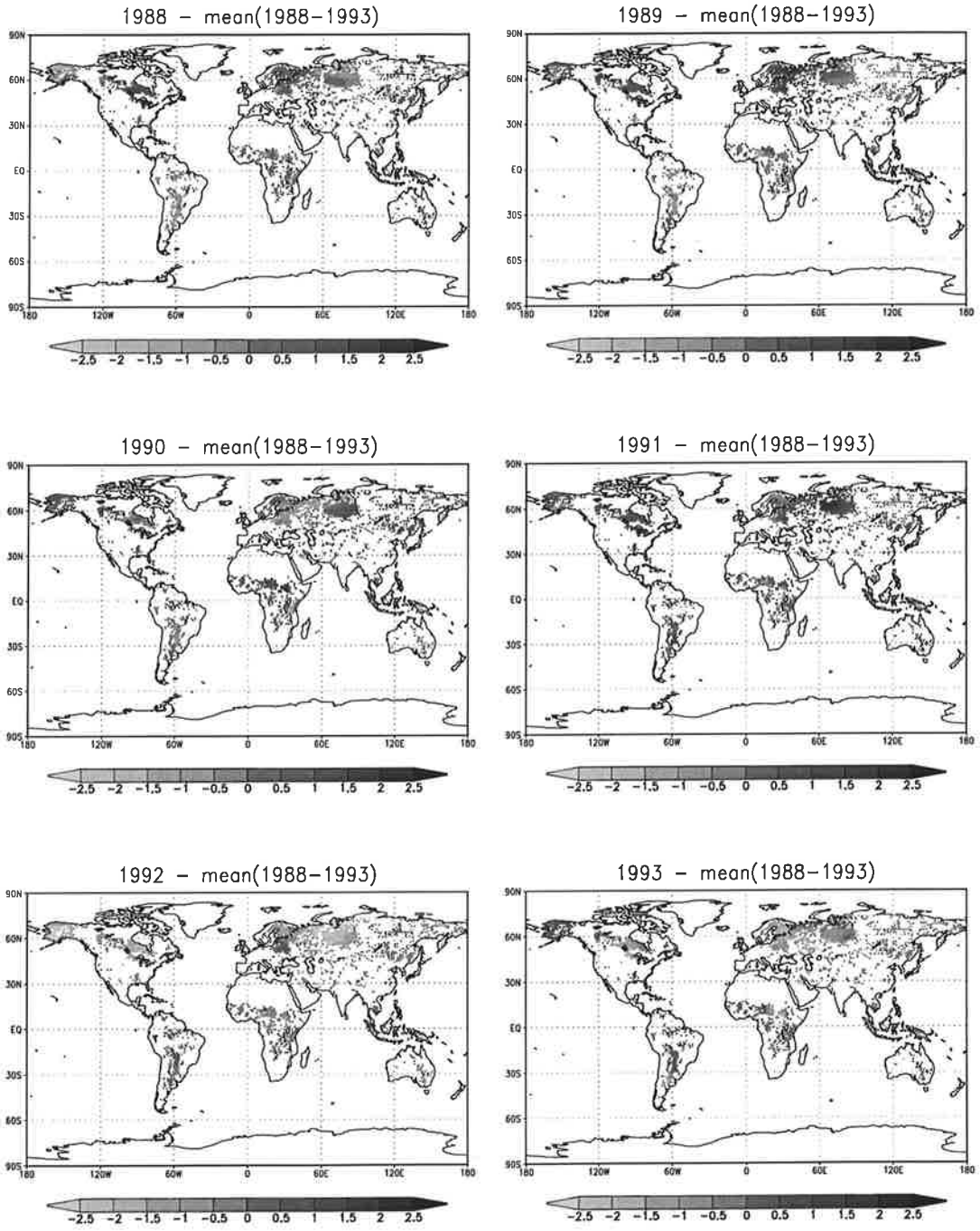

Fig. 41: Anomalies in the input data: ECMWF northern summer (MJJASO) soil temperature [°C] at all wetland grid points of the years 1988-1993 compared to the mean soil temperature of that period

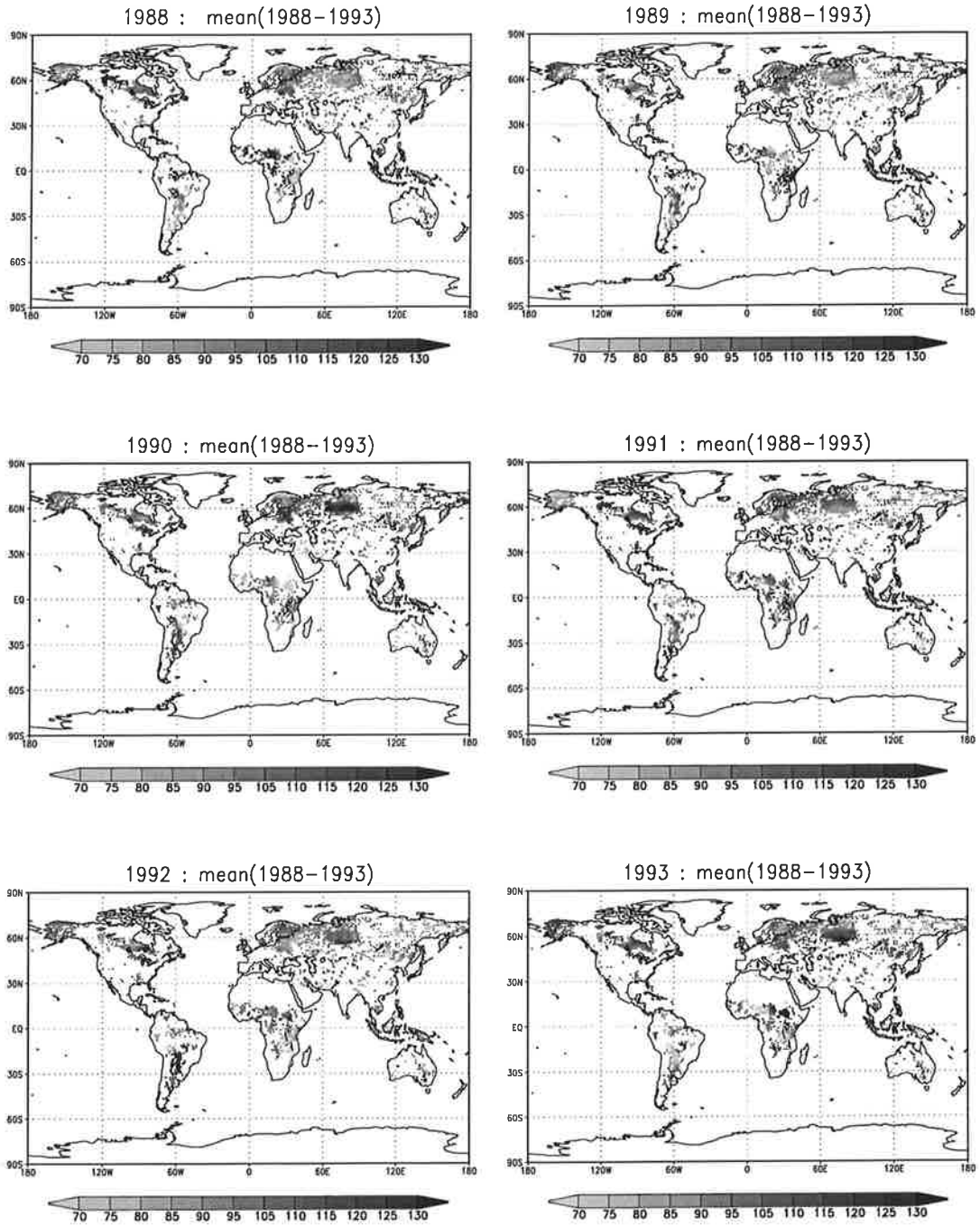

Fig. 42: Anomalies in the input data [%]: Annual ECMWF precipitation at all wetland grid points of the years 1988-1993 compared to the mean annual precipitation of that period

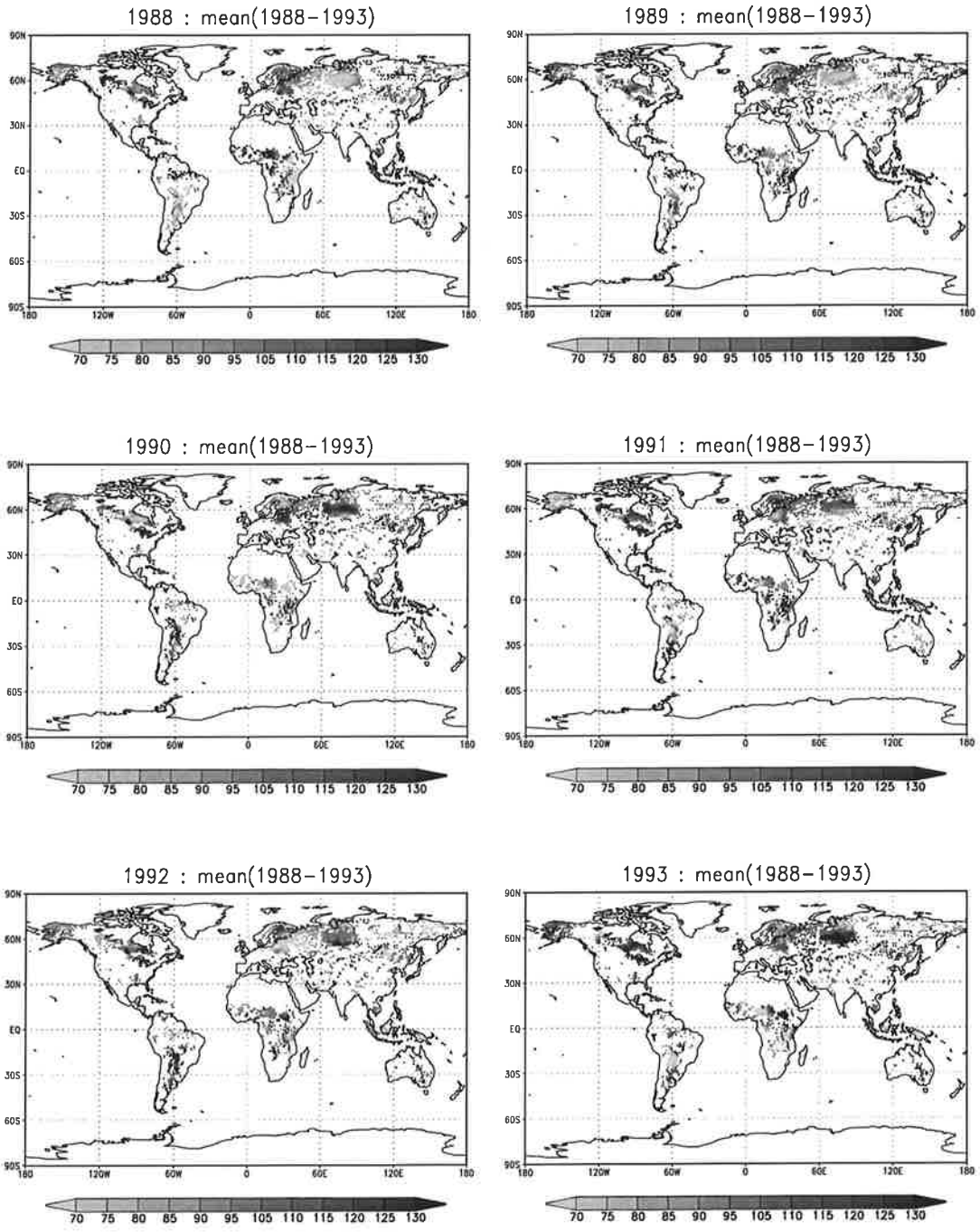

Fig. 43: Anomalies in the input data [%]: ECMWF northern summer (MJJASO) precipitation at all wetland grid points of the years 1988-1993 compared to the mean annual precipitation of that period

6.4. Comparison with Atmospheric Observations

As mentioned in Sect. 1 the recent (1983-present) changes in the global atmospheric methane concentration are observed by the NOAA/CMDL network consisting of about 30 stations worldwide. Here we compare the results of the global model forced by the ECMWF re-analyses of the years 1988-1993, to the observed atmospheric methane growth rate.

First we consider the global growth rate. We assume that the decreasing trend in the observed atmospheric methane growth rate (see Fig. 44 (top)) results from decreasing emissions from non-wetland methane sources and/or an increased sink. Therefore, the trend which was determined as a quadratic fit to the growth rate curve (see Fig. 44 (top)) is subtracted from the growth rate to obtain the observed anomalous methane growth rate (see Fig. 44 (bottom), dashed line). The anomalous methane growth rate resulting from simulated methane emissions from natural wetlands is obtained by subtracting the mean seasonal cycle of the 6-year simulation period from the modeled emissions and filtering it with a low-pass filter with a cutoff frequency of 1.5 years (see Fig. 44 (bottom), solid line). It is clear that the global anomalous methane growth rate due to emissions from natural wetlands as calculated by the methane model compares well with the observations in 1991-1993 (see Fig. 44 (bottom)). For the period from 1988 to 1990 this is not the case.

In Fig. 45 the spatio-temporal variation of the simulated anomalous methane emissions (top) is compared with the observed anomalous methane growth rate determined the same way as described above (bottom). The zonally integrated anomalies of modeled methane emissions are obtained from the simulated methane emissions by the method described above. We assume that the emitted methane accumulates within 15^{o} latitudinal bands. That means that meridional transport is not taken into account and the upper graph of Fig. 45 (top) shows merely the centers of action. Hence, in the upper graph the pattern is less smeared and the magnitudes are larger. Thus, the comparison between the two graphs of Fig. 45 is limited. A true comparison would include a 3-dimensional atmospheric transport model, but this is beyond the scope of this study. Furthermore, the lower graph is based on individual stations and does not reflect the true zonal average. Moreover, the upper graph shows only anomalies due to variations in the natural wetland source, whereas in the lower graph all methane sources and the methane sinks are included.

In the following we explain the structure of the model outcome in more detail and discuss the possible reasons for the agreements and the discrepancies between model results and observations. For this purpose we use Fig. 39-43 showing the global anomalies of the modeled methane emissions and the input data (soil temperature and precipitation).

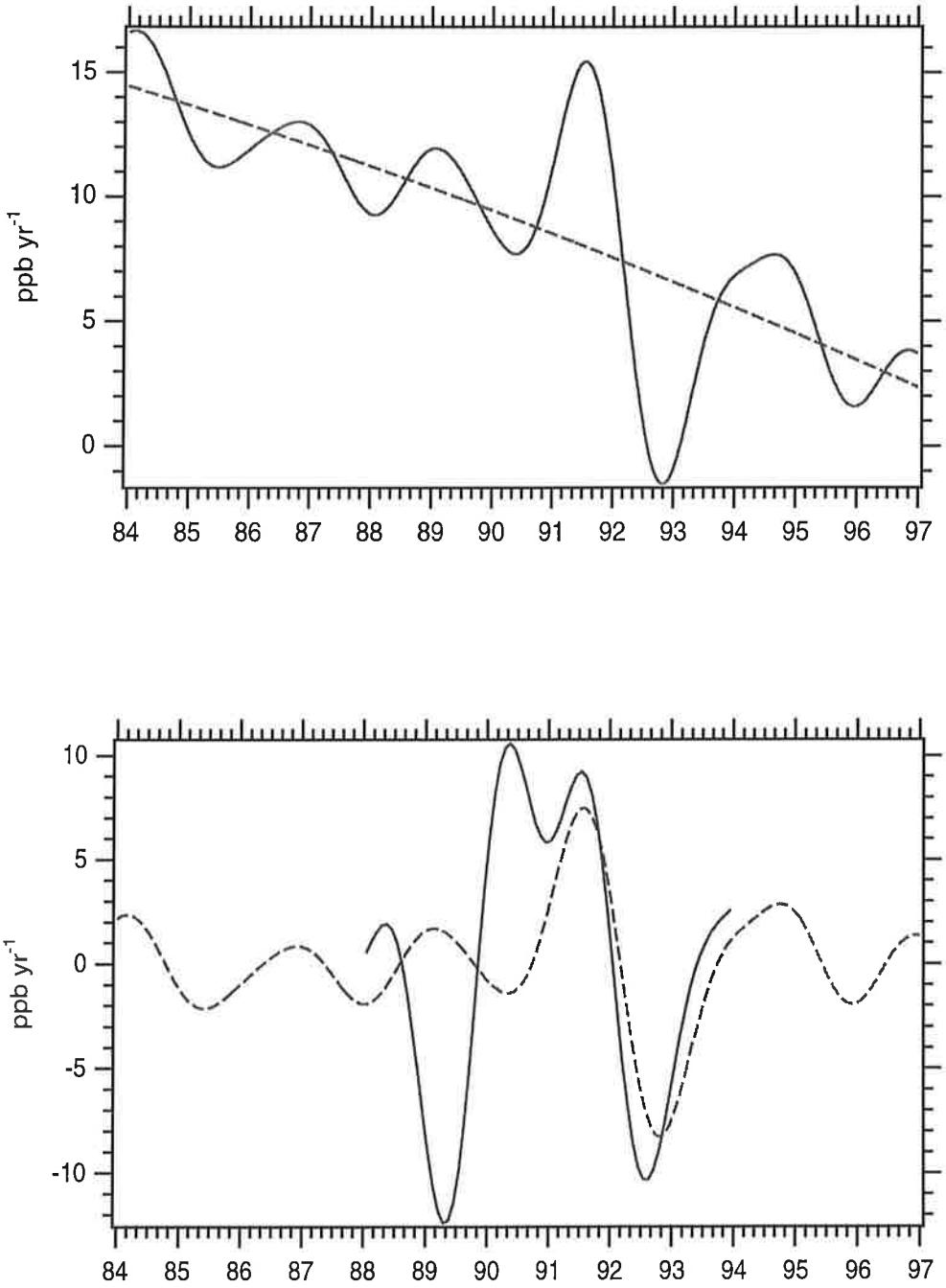

Fig. 44: Top: observed global atmospheric methane growth rate (solid) and fitted trend curve (dashed); bottom: observed anomalous methane growth rate (dashed) and simulated anomalous methane emissions from natural wetlands (solid)

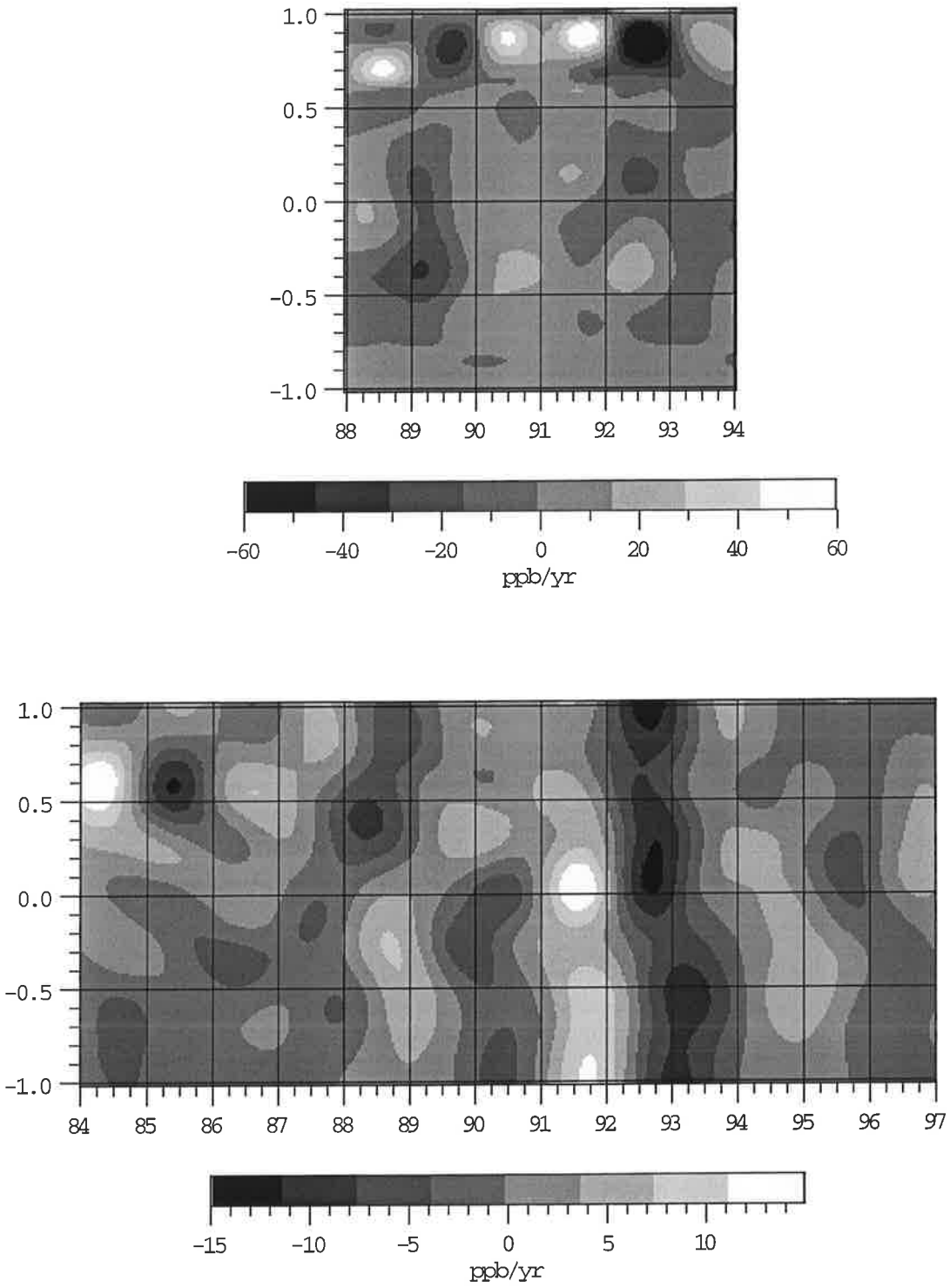

Fig. 45: Top: zonally integrated simulated anomalous methane emissions from natural wetlands as obtained by the method described in the text (without the consideration of atmospheric transport); bottom: zonally integrated observed anomalous methane growth rate derived from measurements from the NOAA/CMDL sampling network (x-axis: year, y-axis: sin(latitude))

1988: The simulated maximum in the high northern latitudes is due to higher methane emissions from eastern Europe caused by slightly higher temperatures and significantly higher

precipitation. The small modeled maximum south of the equator stems most likely from enhanced methane emissions from equatorial east Africa caused by slightly higher temperatures. The northern maximum is not seen in the observations, whereas there is a observed maximum south of the equator, but earlier and closer to the equator. The measured minimum in the middle northern latitudes (around 25°N) has most likely other sources than natural wetlands as its origin, because there are very few wetlands between 20°N and 30°N. It could be caused by reduced methane emissions from rice paddies which are located mainly in southeast Asia between 10°S and 30°N [*Hein*, 1994], where the temperatures were slightly lower than the average. In the observations it looks as if this minimum spreads northward.

1989: The modeled minimum in the high northern latitudes stems mainly from reduced methane emissions from Siberia due to slightly lower temperatures and significantly lower precipitation. In addition, methane emissions from the Hudson Bay lowlands and some parts of Europe show reduced methane emissions caused by lower precipitation even though the soil temperatures are clearly higher than the average. The modeled minimum in the southern hemisphere seems to have its origin in slightly lower temperatures in the southern tropics and subtropics. While the northern high latitude minimum cannot be found in the observations, there is a minimum in the southern tropics and subtropics in the data, but in the model outcome it is slightly earlier than in the observations.

1990: The modeled maximum in the high northern latitudes is due to enhanced methane emissions from Siberia, eastern Europe and Russia caused by considerably higher precipitation. The temperatures were slightly higher than the average in Siberia, but slightly lower in eastern Europe and Russia. The small maximum in the middle southern hemisphere is due to enhanced methane emissions from South America caused by slightly higher temperatures. The observations show a small enhancement in the growth rate in the high northern latitudes, but no pronounced maximum.

1991: The modeled maximum in the high northern latitudes is caused by higher methane emissions from different locations like the Great Lake and the northern Hudson Bay regions, Europe, Russia and parts of Siberia and is caused by slightly higher temperatures. There is no unique trend in the precipitation. The small modeled maximum in the low northern latitudes has its origin in slightly higher methane emissions from Africa due to slightly higher temperatures and precipitation. Like in 1990, the data show a small enhancement in the growth rate in the high northern latitudes, but no clear maximum. In the low northern latitudes there is a maximum in the model results as well as in the observations, but it is less pronounced in the simulations.

1992: The two pronounced minima in the northern hemisphere obtained by the model are

caused by reduced methane emission from all northern hemispheric wetlands due to significantly lower temperatures. The precipitation was lower in large parts of the northern hemisphere, but higher than the average in northern Finland, southern Siberia or the southern Hudson Bay region. The small minimum in the southern subtropics has its origin in reduced methane emissions from South American wetlands located south of 30°S, where the temperatures were below the average, but precipitation slightly above it. The small maximum in the southern tropics stems from enhanced methane emissions from South American wetlands located between 20°S and 30°S due to considerably higher precipitation. All three minima obtained by the model can be found in the observations.

1993: The two small maxima in the northern hemisphere are caused by higher methane emissions from the Hudson Bay and the Great Lake regions as well as from southern Siberia. In all these regions the precipitation was significantly higher than the average, but the temperatures were lower. In the observations the same structure can be found.

Discussion

The comparison between model results and observations - within the limitations explained above - shows in some instances good agreement, but also certain discrepancies. Here we discuss the differences between model results and observations explainable for example by variations in other methane sources, in methane sinks or shortcomings in the models used. In addition, we consider the 1992 anomaly.

Other methane sources. Very little is known about the interannual variation of other methane sources. Changes in the atmospheric methane growth rate in the northern hemisphere can be caused by changes in the fossil fuel emissions [e.g. *Dlugokencky et al.*, 1996]. Changes in the tropics can be related to changes in biomass burning [e.g. *Hein*, 1994; *Lowe et al.*, 1994]. Most of the rice paddies are located in south east Asia between 10°S and 30°N [e.g. *Hein*, 1994]. Methane emissions from rice paddies and natural wetlands are due to the same processes. However, since rice paddies are often irrigated artificially methane emissions from rice fields have no necessary connection to precipitation. Furthermore, the fertilization practices can affect emissions [e.g. *Neue and Sass*, 1994]. Although in most years the patterns of simulated methane emissions from the tropics compare fairly well with observations, the amplitude of the model results is too low. The simulated minima are mostly attributable to temperature changes. Hence temperature induced variations of methane emissions from rice paddies could be one reason why the amplitude of the observed temporal variations of methane emissions from the tropics is higher than in the simulations.

Changes in the sink(s). Here we consider only possible changes in the major sink, reaction with OH radicals. The tropospheric OH concentrations have not changed significantly over the

last 10 years [*Prinn et al.*, 1995]. However, the eruption of Mt. Pinatubo is believed to have affected the OH sink in two ways over roughly a one year period. (1) The attenuation of UV radiation of the wavelength region 290-330 nm (necessary for the formation of OH radicals) by SO_2 and sulfate aerosols resulted in decreased OH formation directly following the eruption (June 1991). This could account for the increased growth rate in 1991 [*Dlugokencky et al.*, 1996]. (2) It has been hypothesized that the enhanced stratospheric ozone loss in 1992 due to the eruption of Mt. Pinatubo led to increased OH formation in 1992. This effect could have enhanced the 1992 anomaly [e.g. *Bekki et al.*, 1994]. Since the reactions with CH_4 and CO constitute the major sink for OH [*Thompson et al.*, 1993] decreased concentrations of those trace gases would lead to an increased OH sink and are also named as one possible reason for the 1992 anomaly.

Sensitivity of the models. In the period from 1988 to 1989 the simulated methane emissions from the high latitudes show the opposite behaviour than the observations. In both cases the main reason for the modeled anomalies was precipitation. In 1989 the temperatures were even slightly higher than the average, but the modeled methane emissions show a minimum due to low water table levels. This finding suggests that the sensitivity of the hydrological model to changes in the precipitation might be too high in the high northern latitudes. However, in 1992 and 1993 the combined effects of temperature and precipitation on modeled methane emissions seem to be in the right order of magnitude. As discussed above, in the tropics the pattern of modeled methane emissions compares fairly well with observations, but the amplitude is too low. One reason for this behaviour could also be that the sensitivity of the methane model to changes in the temperature is too low in the tropics. Since we tested the model only with one tropical data set, we cannot exclude this possibility.

The 1992 anomaly. The possible causes for the observed minimum in the atmospheric methane growth rate in 1992 have been discussed widely (see Sect. 1) and *Lelieveld et al.* [1998] compile possible reasons, amongst them are reduced emissions from natural wetlands and rice paddies due to decreased temperatures caused by the eruption of Mt. Pinatubo in June 1991 [*Dutton and Christy*, 1992] and due to decreased precipitation. Both the amplitude and the pattern of our model results compare well with the observations, which suggests that reduced methane emissions from natural wetlands contribute significantly to the observed growth rate anomaly in 1992. As discussed above, it is possible that the hydrological model is too sensitive to changes in precipitation. This could have resulted in a too pronounced effect of the lower precipitation in 1992 on simulated methane emissions. However, the results of the factorial experiment show, that the decreased temperature alone causes a significant decrease of the modeled methane emissions in 1992, so that this effect would only reduce the amplitude of the model results.

6.5. Conclusion

The simulated methane emissions from natural wetlands obtained by a global run of the methane emission model using ECMWF re-analyses as forcing show considerable spatio-temporal variability.

The meridional pattern of simulated methane emissions compares surprisingly well with results obtained by an inverse modeling approach, considering the uncertainties of both methods. Therefore, we conclude that the extrapolation of the methane model to the global scale yields realistic results.

The global seasonal cycle of the simulated methane emissions is dominated by the seasonal cycle of methane emissions from the high northern latitudes. In the higher latitudes the seasonal cycle is mainly caused by the seasonal cycle of the soil temperature, whereas in the subtropics (and the tropics) it is mainly influenced by the hydrological cycle.

The interannual pattern of simulated methane emissions shows two emission maxima in 1990 and 1991 and two pronounced emission minima in 1989 and 1992. The comparison between anomalies of the simulated methane emissions and observed methane growth rate anomalies shows, within its limitations, good agreement in 1992 and 1993. Our results suggest that decreased methane emissions from natural wetlands contribute significantly to the observed 1992 growth rate anomaly. The discrepancies between model results and atmospheric observations could be explained by variations in other sources, in methane sinks or shortcomings in the used models.

7. Summary and Outlook

Methane emissions from natural wetlands, which constitute the biggest natural methane source at present, are highly climate-sensitive. Simulations of methane emissions from natural wetlands with a climate-sensitive model can help to better understand the observed spatio-temporal variations of the atmospheric methane growth rate. In this thesis, the following results were achieved:

- A process-based climate-sensitive model to derive methane emissions from natural wetlands was developed.
- The methane model was tested with observations, whereby the comparison between model results and data showed a good agreement.
- Global data sets of all parameters of the methane model were generated.
- A simple hydrological model to simulate the position of the water table in wetlands on a global scale was developed.
- Global model runs of the methane model were performed using ECMWF re-analyses of the period from 1988 to 1993 as forcing in order to simulate the interannual variation of methane emissions from natural wetlands.

Methane Model

The methane model developed in this work is the first approach to simulating the processes leading to methane emission within a 1-dimensional soil column. Furthermore, it differs from all other models in the literature in the way that transport is parameterized. Two opposing processes operate in soil, namely methane production in the anoxic soil zone and methane consumption in the oxic soil zone. Therefore transport, which occurs by diffusion, ebullition and through plants, plays an important role in determining the fraction of produced methane that is emitted into the atmosphere. Moreover, the different transport mechanisms influence the velocity at which methane is transported to the atmosphere.

The model was tested with observations consisting of time series of the input and output data of the model, carried out at 15 field stations within 6 different wetland sites. The test sites are located in northern Europe and North and Central America, representing a large variety of environmental conditions. One site is underlain by permafrost and undergoes a seasonal thaw-freeze cycle, while one site is located in the tropics where there is a dry/wet-season cycle. The response of simulated methane emissions to the temporal variation of the soil temperature and the water table, and also to the differences in the environmental parameters such as rooting

depth and type and density of vegetation, compares well with the observations. At two sites the simulated methane concentrations in the soil were compared with observed vertical concentration profiles which reflect the vertical distribution of methane production, methane oxidation and removal of methane by the different transport mechanisms. Hence, methane concentration profiles constitute an additional constraint to the model. In general the modeled methane concentration profiles agree well with the observations. From the results of the tests against data we conclude that this model can be applied to different wetlands under various conditions and hence be extrapolated to the global scale.

In the future the 1-dimensional methane model should be tested in particular with tropical data sets, since until now there has been only one tropical data set available. A next logical step would be to apply a modified version of the methane model to rice paddies, because the processes leading to methane emissions from rice fields are the same as in a natural wetland. However, the cultivation practices affect methane emissions as well. It would be advantageous to test the 1-dimensional model with a data set consisting not only of time series of the input and output data of the model (as it was the case in this study), but also of quantities calculated in the model such as the production rate, the oxidation rate and the fraction of methane transported by the different transport mechanisms. No such data is currently available and the development of such a data set is thus a priority to enable a more thorough testing of this model.

Hydrological Model

A simple hydrological model was developed in order to calculate the position of the water table in wetlands on a global scale. This model was tested against time series of observations of the position of the water table from different wetlands. For the model forcing high-frequency ECMWF re-analyses (precipitation, surface solar net radiation, 2m temperature) were used. The comparison between simulated and observed water table levels showed, in general, a good agreement. However, the observations of water table levels in wetlands reveal that the water table can vary by several decimeters within one site due to the wetland microtopography, i.e. the fact that the wetland surface is not homogenous, but consists of small elevations (hummocks) and, generally water-filled, depressions (hollows). In a hummock the water table can be several decimeters deeper below the soil surface than in a hollow. The results of the global runs of the methane modeled give rise to the suspicion that the sensitivity of the hydrological model to changes in the precipitation is too high at the high latitudes. We presume that this is due to the neglect of the microtopography in the hydrological model. Hence, in future studies the effects of microtopography should be included using a statistical approach. Because of the high spatial variability of precipitation, future pointwise tests of the 1-dimensional hydrological model should also include observational input data. In the present model version we have neglected the effect of permafrost on the hydrology of a wetland.

However, the comparison between a data sets from a wetland site underlain by permafrost shows a good agreement between model results and observations. Hence the results indicate that this is not a major limitation.

Global Data Sets

Global data sets for all model parameters were derived using a biosphere model and existing data sets of soil properties and vegetation and simple relationships between those quantities and the model parameters. The two most critical model parameters are V_{max} (the maximum methane oxidation rate) and R_0 (the constant rate factor of the methane production rate). Since there was no information available about the environmental factors controlling V_{max}, this parameter was set to a globally constant value. The rate factor R_0 is determined by a very simple procedure from the existing calibrating sites. It is assumed that it varies linearly with the local productivity and the local mean annual temperature. The extrapolation of R_0 is based on 7 data points only. Hence future work should include further tests of the 1-dimensional model with observational data, especially from tropical wetlands, in order to more accurately determine this central parameter.

The global wetland distribution is derived from a global data set giving the wetland fraction of each grid point. Thus, the wetland areas are assumed to be constant with time. However, especially in the subtropics and the tropics the areal extend of wetlands undergoes significant seasonal and interannual variations. Hence future studies should include the development of a method to calculate the temporal variation of wetland areas as a function of the site characteristics and the climate.

Further limitations are that the present model does not distinguish between different wetland types, such as bogs and fens (nutrient-poor and nutrient-rich wetlands), because the influence of nutrients on methane emission is not incorporated in the model (see Sect. 2). The distinction between forested and non-forested wetlands was also not made. However, the occurrence of trees is incorporated in the model, whereby the effects of trees on the soil depth, the rooting depth, plant-mediated transport and productivity are considered.

Global Model Runs

We carried out global model runs using high-frequency atmospheric forcing fields (precipitation, soil temperature, surface solar net radiation, 2m temperature) from the ECMWF re-analyses of the period from 1988 to 1993. The meridional pattern of modeled methane emissions compares well with results obtained by an inverse modeling approach. However, the amplitude of the meridional pattern of the model results obtained in this study is larger and the total annual emissions are by about 10% larger than those of the inverse model. Considering the uncertainties of the inverse model approach, and the limited number of calibrating sites on

which the global extrapolation of the 1-dimensional methane model is based on, this good agreement is quite surprising.

The modeled global methane emissions show high spatio-temporal variability. Simulated methane emissions from high northern latitudes are significantly lower than those from the subtropics and the tropics. The global seasonal cycle of simulated methane emissions is dominated by the seasonal cycle of methane emissions from the higher northern latitudes. There the simulated methane emissions are high in the summer and almost zero in the winter driven by the seasonal cycle of the temperature. On the other hand, in the subtropics and the tropics the amplitude of the seasonal cycle is small and the seasonal cycle of the simulated methane emissions is mostly determined by the hydrological cycle. The global model shows also reasonable interannual variability in the simulated methane emissions. The amplitude of the methane emission anomalies is highest in the northern hemisphere, slightly lower in the tropics and very small in the southern hemisphere. The simulated global methane emissions of the period from 1988 to 1993 show two maxima in 1990 and 1991 and two pronounced minima in 1989 and 1992.

The comparison of the simulated anomalous methane emission rate with the observed anomalous growth rate of atmospheric methane obtained from the global sampling network consisting of about 30 individual stations shows a good agreement at several times, but there are also some discrepancies. The comparison is limited, because we do not take atmospheric transport into account. A true comparison would include a 3-dimensional atmospheric transport model, but this is beyond the scope of this study. Moreover, the model results reflect only the natural wetland source, while all other sources and all the sinks are not included. Furthermore, the observed atmospheric methane growth rate does not reflect the true zonal average, because it is based on individual stations. The agreement between model results and observations is good in particular in 1992 and 1993. Our model results suggest that reduced methane emissions from northern wetlands in 1992 caused by decreased temperatures due to the eruption of Mt. Pinatubo in June 1991, contribute considerably to the observed growth rate minimum of atmospheric methane in 1992. Little is known about the interannual variations of the other methane sources and the methane sinks, which might be the cause for the discrepancies between model results and observations. However, if it is assumed that the interannual variations in the observed atmospheric methane growth rate are due to changes in methane emissions from natural wetlands, the discrepancies between model results and observations could be attributed to shortcomings in the used models: possibly the sensitivity of the hydrological model to changes in the precipitation is too high in the high latitudes and / or the sensitivity of the methane model to variations in the temperature is too low in the tropics.

Future Perspectives

The model developed in this work can be used to perform transient runs using atmospheric forcing fields from the ECMWF re-analyses covering the extended period from 1979 to 1996. It would be interesting to use the outcome of such an experiment as input for a 3-dimensional transport model in order to calculate the spatio-temporal pattern of the atmospheric methane growth rate resulting from methane emissions from natural wetlands. A next step would be to include also simulations of methane emissions from rice paddies which could be obtained using a modified version of the methane model developed in this work.

Another focus of future work using the global methane model could be to perform paleo experiments. Those experiments are motivated by ice core records which provide information about the methane concentration and the interhemispheric methane gradient at paleo time scales and which show that the changes in the methane concentration parallel changes in the temperature over the last 220,000 years.

Furthermore, considering that methane emissions from natural wetlands are highly climate-sensitive and that methane is an important greenhouse gas, it would be interesting to perform runs of the global methane model forced by future climate obtained from climate change scenario calculations of an atmospheric general circulation model.

Appendix A.

Tab. 18 lists all globally constant parameters of the methane model described in Sect. 2:

Table 18: List of Globally Constant Parameters

Parameter	Value	Equation
$Q_{10,\ prod}$	6	(7)
$Q_{10,\ oxid}$	2	(8)
V_{max}	20 $\mu M*h^{-1}$	(8)
K_m	5 μM	(8)
$D_{i,\ air}$	0.2 cm^2*s^{-1}	(10)
$D_{i,\ water}$	$10^{-4}*D_{i,\ air}$	(10)
C_{atm}	0.076 μM	(12)
C_{min}	500 μM	(13)
P_{ox}	50%	(16)
Λ_{min}	0	(18)
Λ_{max}	4	(18)
T_{grow}	2°C or 7°C	(18)
T_{mat}	T_{grow}+10°C	(18)

Tab. 19 lists all globally variable parameters of the methane model described in Sect. 2 and the model / data sets they are based on:

Table 19: List of Globally Variable Parameters

Parameter	Equation	Source
NPP_{max}	(2), (4); (Sect. 2)	calculated from NPP(t) from the BETHY model [*Knorr*, 1997]
NPP_{tot}	(21), (22); (Sect. 4)	calculated from NPP(t) from the BETHY model [*Knorr*, 1997]
R_0	(7); (Sect. 2)	calculated as a function of the annual mean soil temperature and the NPP, see Sect. 4
nroot	(5), (17), (19); (Sect. 2)	calculated after *Jackson et al.* [1996] using a data set by *Wilson and Henderson-Sellers* [1985], see Sect. 4
l	(5), (6), (11), (15); (Sect. 2)	calculated after *Jackson et al.* [1996] using a data set by *Wilson and Henderson-Sellers* [1985], see Sect. 4
f_{coarse}	(10); (Sect. 2)	calculated after *Hartge and Horn* [1991] using a data set by *Dunne and Wilmott* [1996], see Sect. 4
P_{unveg}	(13); (Sect. 2)	calculated using a data set by *Wilson and Henderson-Sellers* [1985], see Sect. 4
T_{veg}	(16); (Sect. 2)	calculated after *Frenzel* [pers. comm.] using a data set by *Wilson and Henderson-Sellers* [1985], see Sect. 4

Appendix B.

Here the results of the tests of the 1-dimensional methane emission model against data sets from 6 wetland sites in North America, Europe and Central America are compiled. After giving a short overview of the data sets used in this study we present the results obtained at each site. In this connection the characteristics of each site are described, the used model parameters are listed and the results are explained briefly.

1. Overview of the Used Data Sets

Table 20: Data Sets Used in this Study

No.	Site	Location	Stations	Reference
1	Michigan	42°N, 84°W	1	Shannon and White [1994]
2	Minnesota	47°N, 93°W	5	Dise [1993]
3	Finland	63°N, 31°E	4	Saarnio et al. [1997]
4	Alaska	65°N, 148°W	3	Whalen and Reeburgh [1992]
5	Canada	54°N, 105°W	1	Valentine (unpublished)
6	Panama	9°N, 80°W	1	Keller [1990]

1. Michigan

Period of observation: 3 years

Table 21: Characteristics of Site 1 - Michigan

Microsite 1	**Buck Hollow Bog**
No. of Chambers	3
Vegetation	*Sphagnum, Scheuchzeria palustris*

Table 22: Parameters at Site 1 - Michigan

Microsite	R_0	V_{max}	l	nroot	T_{veg}
Buck Hollow Bog	0.6	45µM/h	80cm	50cm	15

The parameters soil depth (l), rooting depth (nroot) were chosen according to informations given by the investigators [*Shannon*, pers. comm.]. The parameter T_{veg} was set to the maximum value of 15, because the dominant plant at that site *Scheuchzeria palustris* emits significant amounts of methane [*Shannon* et al., 1996].

Fig. 46 (c) and (d) show the observed forcing data which are the position of the water table and the soil temperature. In Fig. 46 (a) the observed (black dots: average of the three chamber measurements +/- 1 standard deviation error bars) compared to the modeled methane emissions (thick line) are plotted. In Fig. 46 (b) the modeled relative contributions of the three transport mechanisms diffusion, ebullition and plant-mediated transport are depicted.

Fig. 47 shows the comparison between modeled and observed methane concentration profiles in the soil. The observations as well as the model result show the same seasonal pattern. Higher methane concentrations in the winter and spring and decreased methane concentrations in the summer and autumn. The reason for this is that during the growing season a large fraction of methane is removed from the soil by plants. However, in the model removal of methane from the soil by plants seems to start too early (May 16 and Jun 4), but the general agreement is satisfactory.

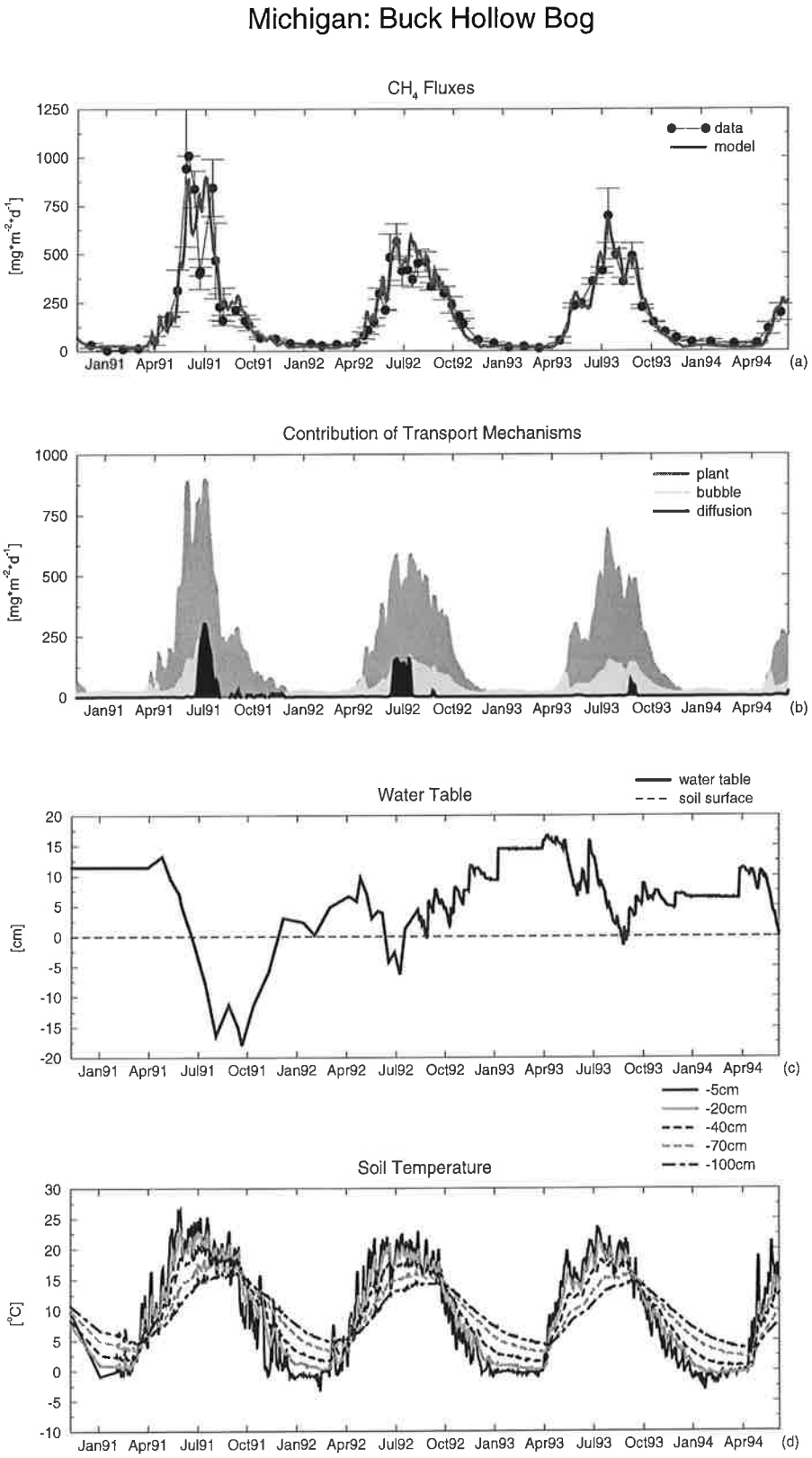

Fig. 46: (a): Comparison between modeled (thick line) and measured (dots with +/- 1SD error bars) methane emissions, (b): Modeled contributions of the three transport mechanisms: diffusion (black), ebullition (light grey), and plant-mediated transport (dark grey), (c): Forcing: Observed position of the water table, (d): Forcing: Observed soil temperature

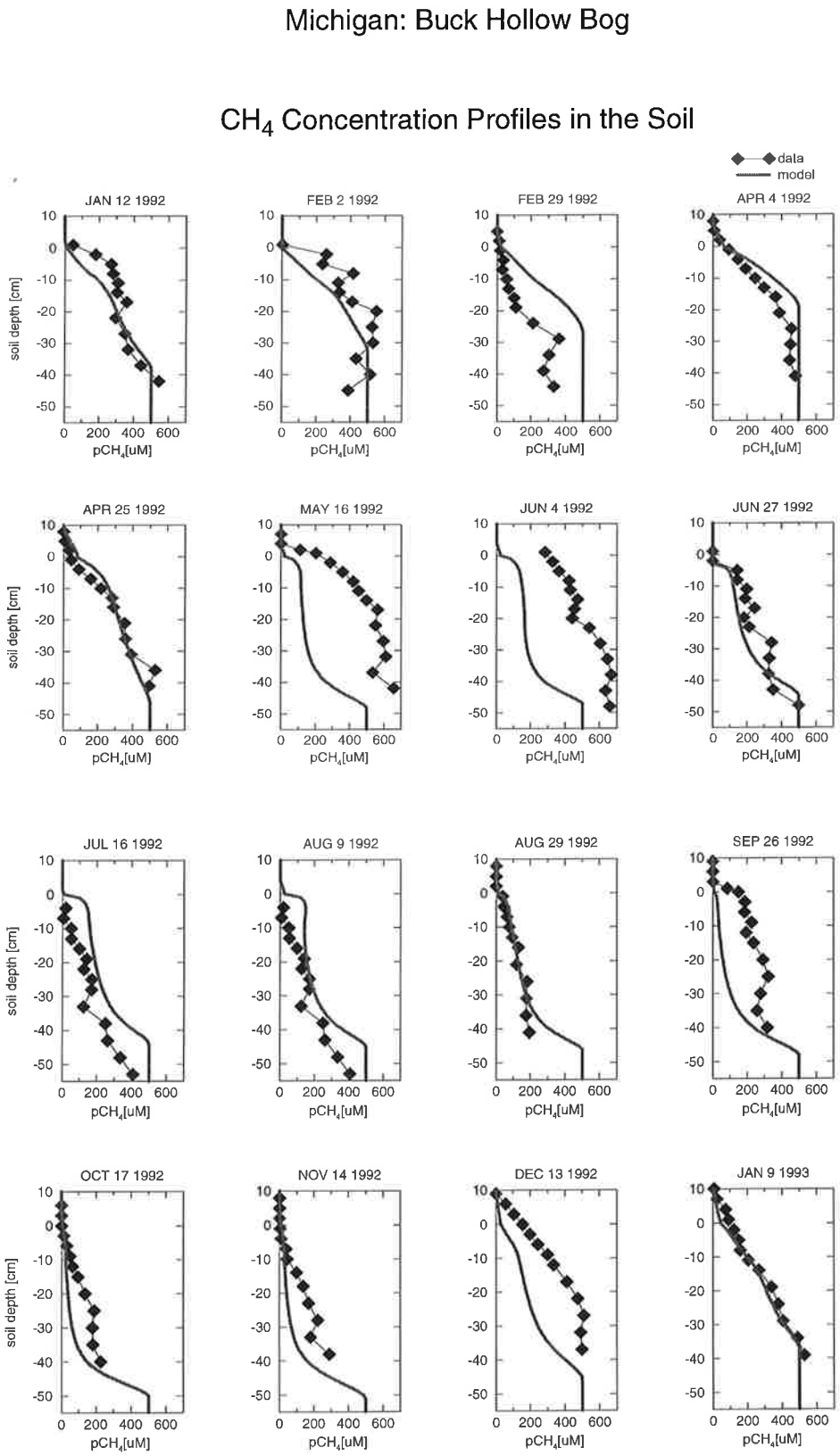

Fig. 47: (a): Comparison between modeled (thick line) and observed (squares) methane concentrations in the soil

2. Minnesota

Period of observation: 2 years

Table 23: Characteristics of Site 2 - Minnesota

Microsite 1	**Junction Fen (JC6)**
No. of Chambers	1
Vegetation	*Sphagnum*, *Carex*, *Scheuchzeria palustris*
Microsite 2	**Forested Bog (Hummock) (S2C3)**
No. of Chambers	1
Vegetation	*Black spruce*, *Sphagnum*, *Eriophorum*
Microsite 3	**Forested Bog (Hollow) (S2C4)**
No. of Chambers	1
Vegetation	*Black spruce*, *Sphagnum*, *Eriophorum*
Microsite 4	**Open Bog (S4C1)**
No. of Chambers	1
Vegetation	*Sphagnum*, *Carex*, *Eriophorum*
Microsite 5	**Open Bog (S4C2)**
No. of Chambers	1
Vegetation	*Sphagnum*, *Carex*, *Eriophorum*

Table 24: Parameters at Site 2 - Minnesota

Microsite	R_0	V_{max}	l	nroot	T_{veg}
Junction Fen (JC6)	0.3	20µM/h	80cm	30cm	4
Hummock (S2C3)	0.3	4µM/h	80cm	40cm	4
Hollow (S2C4)	0.3	20µM/h	80cm	30cm	4
Open Bog (S4C1)	0.3	20µM/h	80cm	30cm	4
Open Bog (S4C2)	0.3	20µM/h	80cm	30cm	4

The parameter rooting depth (nroot) was chosen according to the information that most roots were located in the upper 40 cm of the soil [*Verry*, pers. comm.]. Since the hummock is elevated relative to the wetland we chose a deeper rooting depth at that microsite. Because no information was available about the soil depth (l), it was set to 80 cm which seemed to be a reasonable guess. The density of vascular plants that are known to be good gas conducters is significantly lower here than at site 1. Therefore, we set T_{veg} to 4. At the hummock (S2C3), where the water table is at about 40 cm below ground all the time, the modeled methane emissions are relatively sensitive to the maximum oxidation rate V_{max} and we had to chose a small value for V_{max} to get positive methane emissions.

Fig. 48 and Fig. 50 to Fig. 53 show the results of the tests. In (c) and (d) we plot the observed forcing data, in (a) the comparisons between modeled and observed methane emissions and in (b) the relative contributions of the three transport mechanisms diffusion, ebullition and plant-mediated transport.

Fig. 49 shows the results of a comparison between modeled and observed methane concentration profiles in the soil. In the winter the methane concentration in the upper 20 cm of the soil decreases slightly, both in the model results and in the observations. When comparing these profiles with those of site 1 we see, that methane concentrations in the soil are higher at the Junction Fen, because less methane is removed from the soil by plants here (lower T_{veg}).

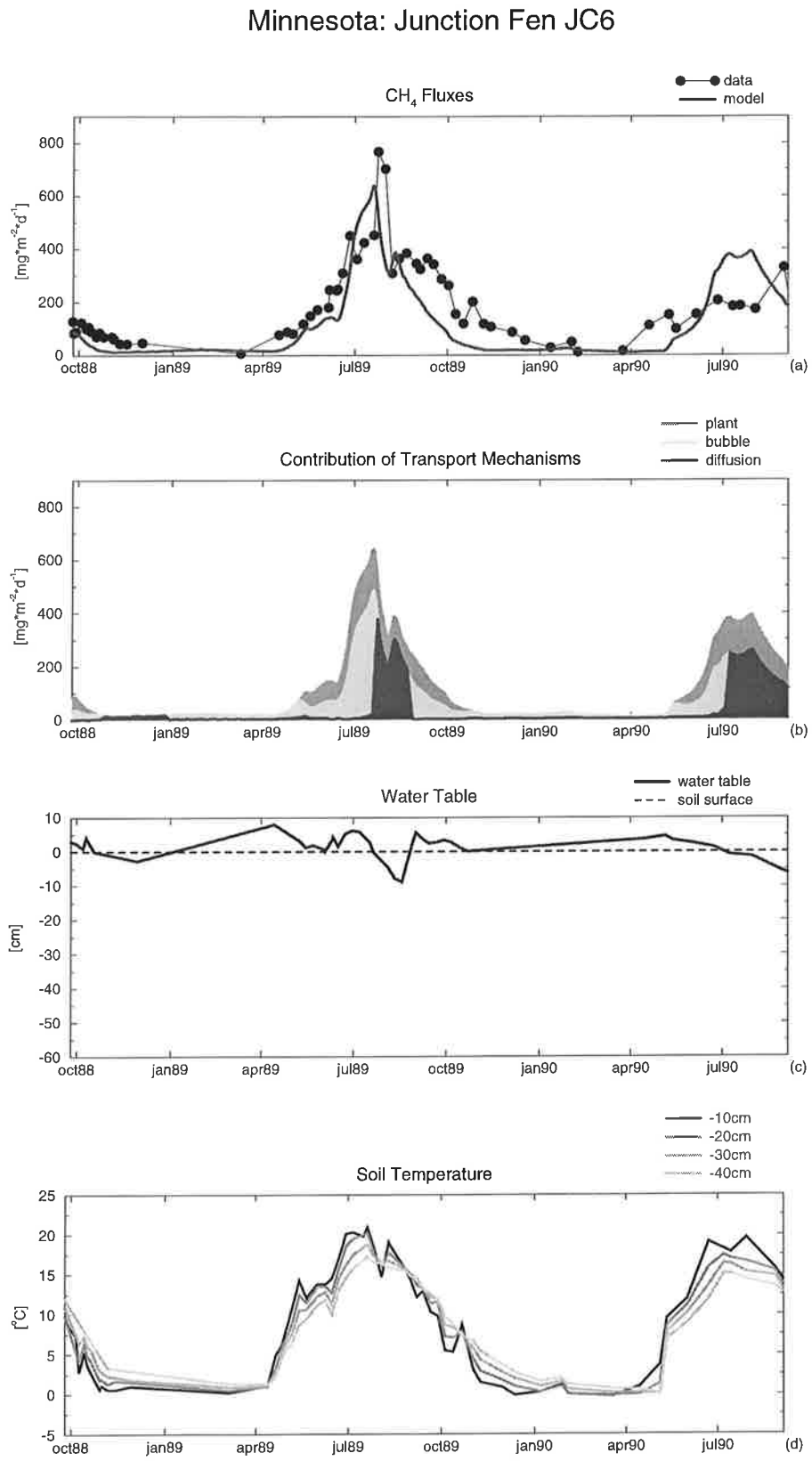

Fig. 48: (a): Comparison between modeled (thick line) and measured (dots) methane emissions, (b): Modeled contributions of the three transport mechanisms: diffusion (black), ebullition (light grey), and plant-mediated transport (dark grey), (c): Forcing: Observed position of the water table, (d): Forcing: Observed soil temperature

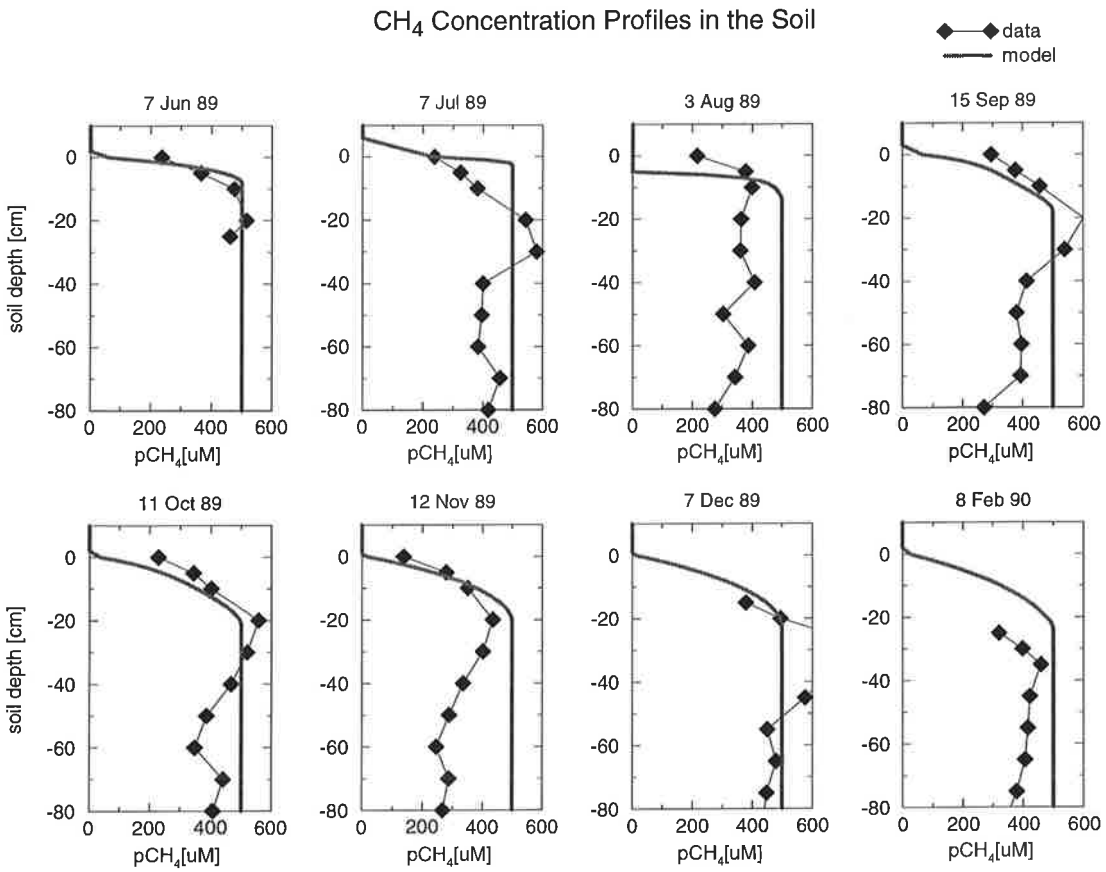

Fig. 49: (a): Comparison between modeled (thick line) and observed (squares) methane concentrations in the soil

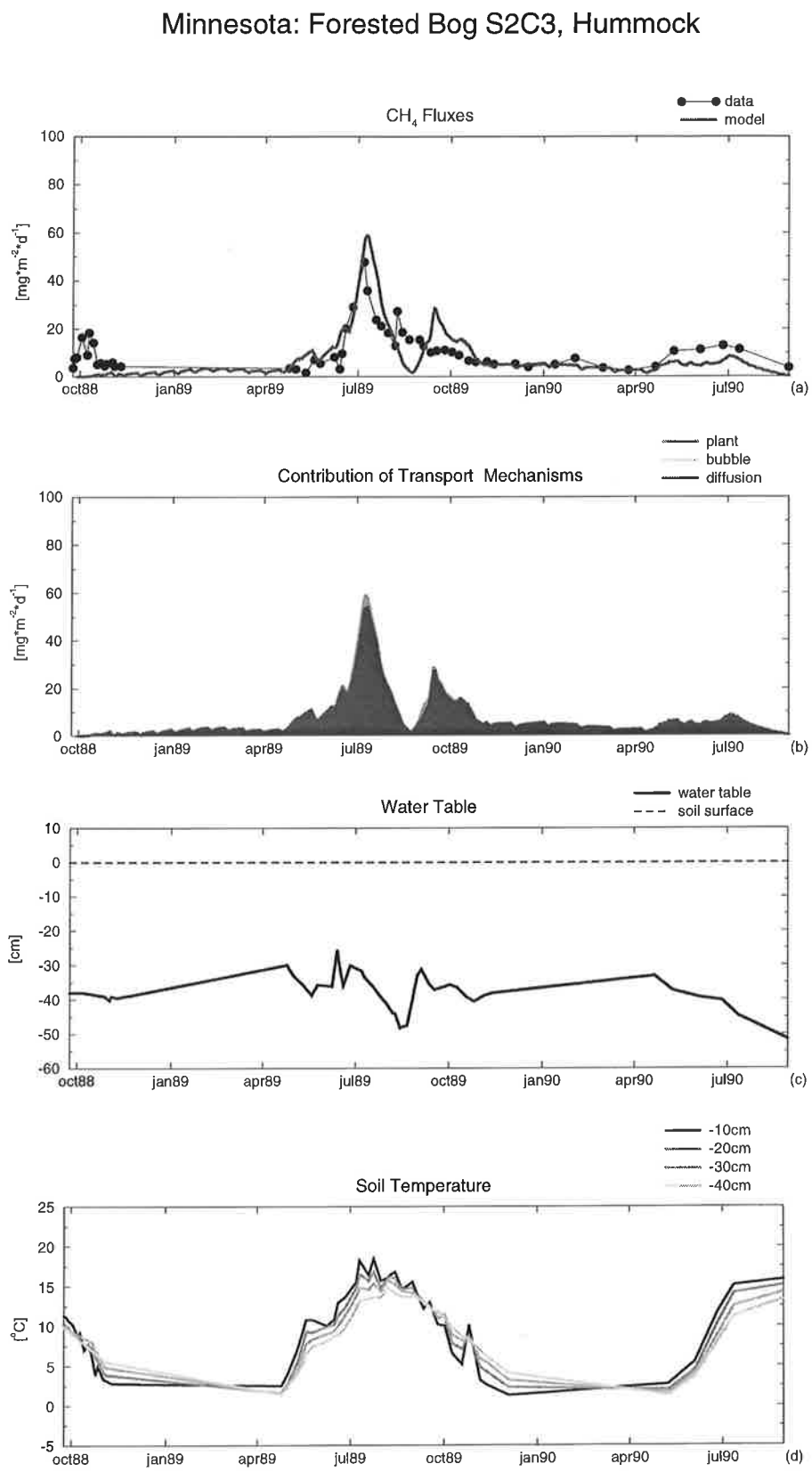

Fig. 50: (a): Comparison between modeled (thick line) and measured (dots) methane emissions, (b): Modeled contributions of the three transport mechanisms: diffusion (black), ebullition (light grey), and plant-mediated transport (dark grey), (c): Forcing: Observed position of the water table, (d): Forcing: Observed soil temperature

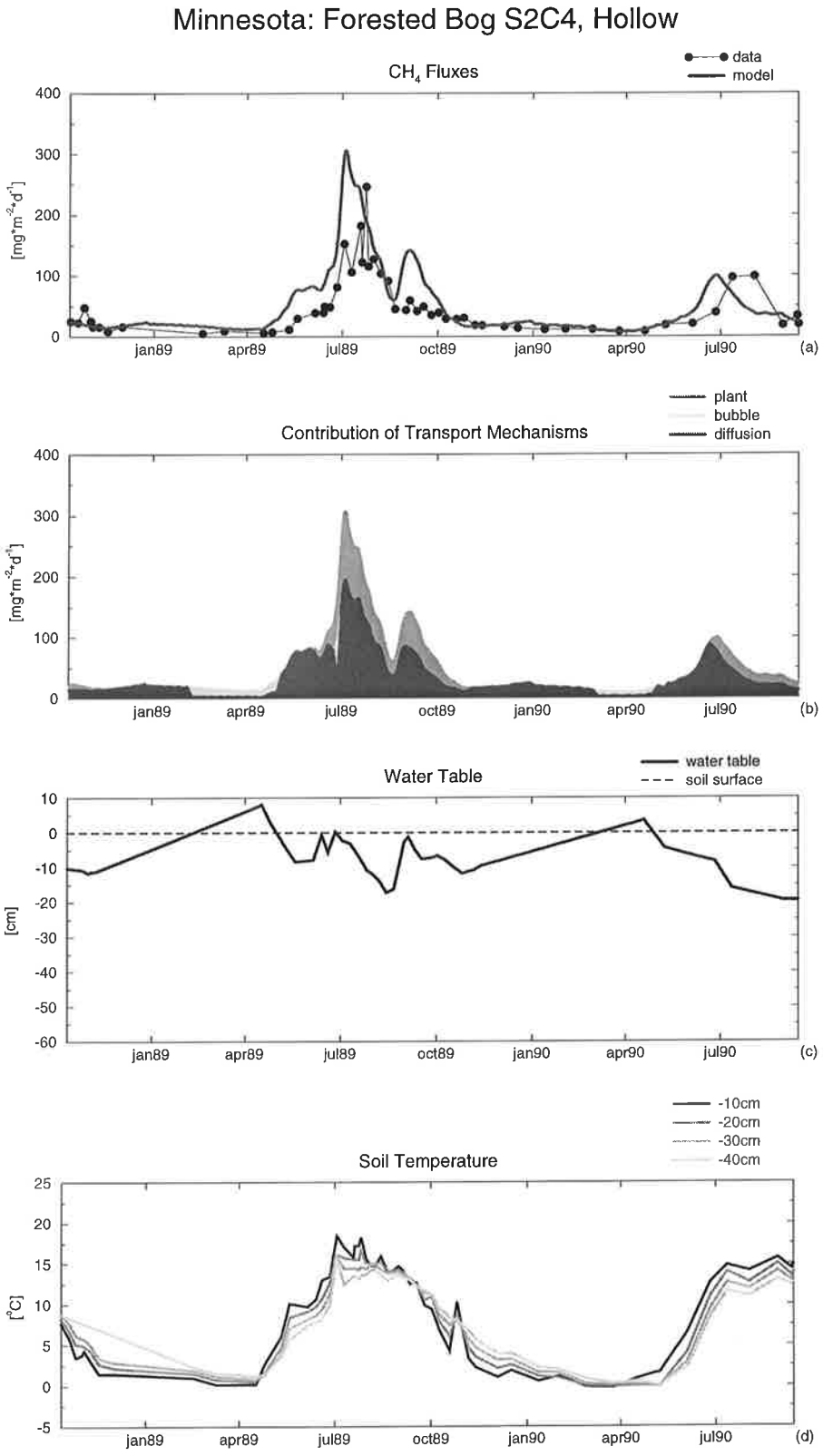

Fig. 51: (a): Comparison between modeled (thick line) and measured (dots) methane emissions, (b): Modeled contributions of the three transport mechanisms: diffusion (black), ebullition (light grey), and plant-mediated transport (dark grey), (c): Forcing: Observed position of the water table, (d): Forcing: Observed soil temperature

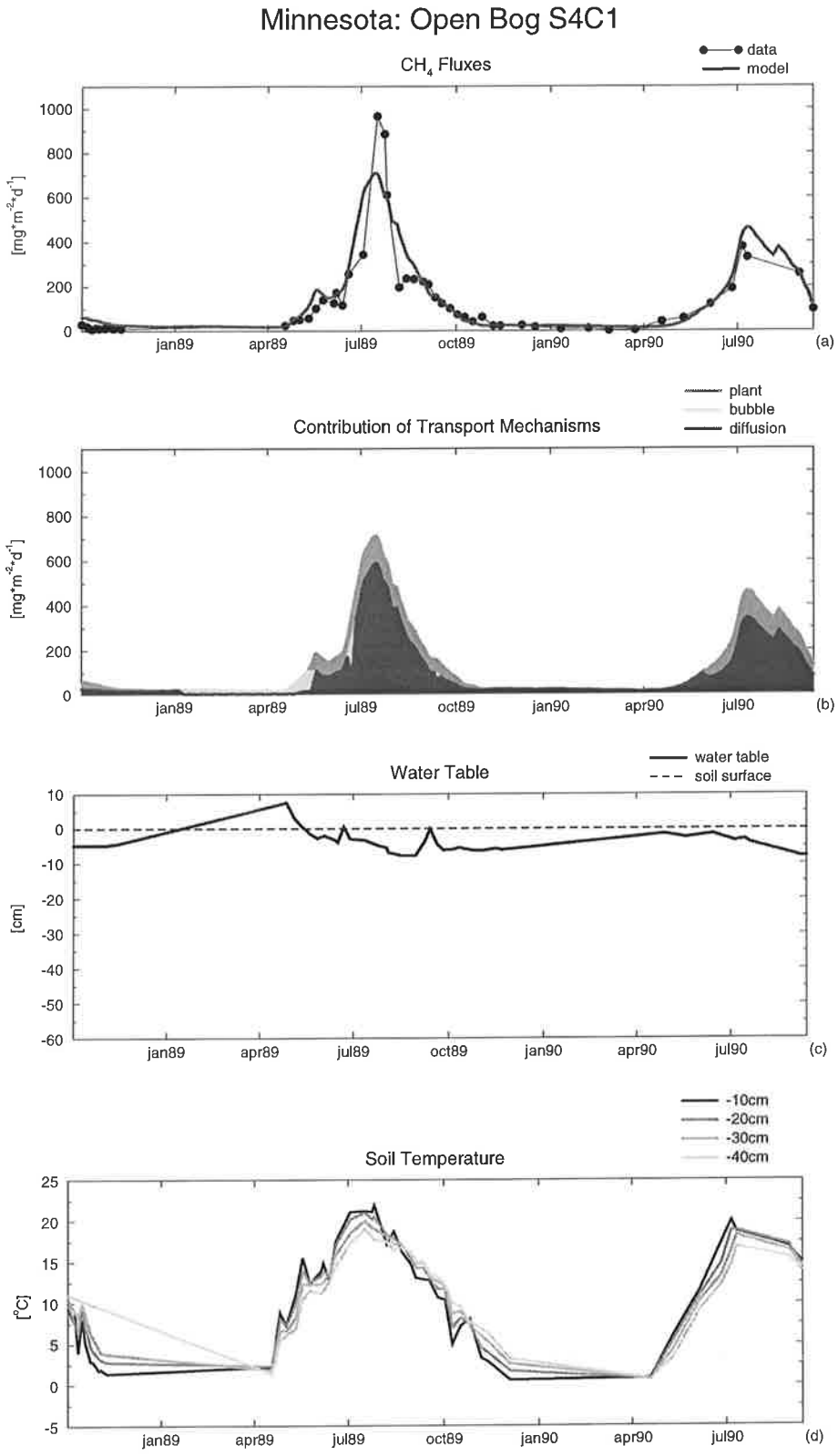

Fig. 52: (a): Comparison between modeled (thick line) and measured (dots) methane emissions, (b): Modeled contributions of the three transport mechanisms: diffusion (black), ebullition (light grey), and plant-mediated transport (dark grey), (c): Forcing: Observed position of the water table, (d): Forcing: Observed soil temperature

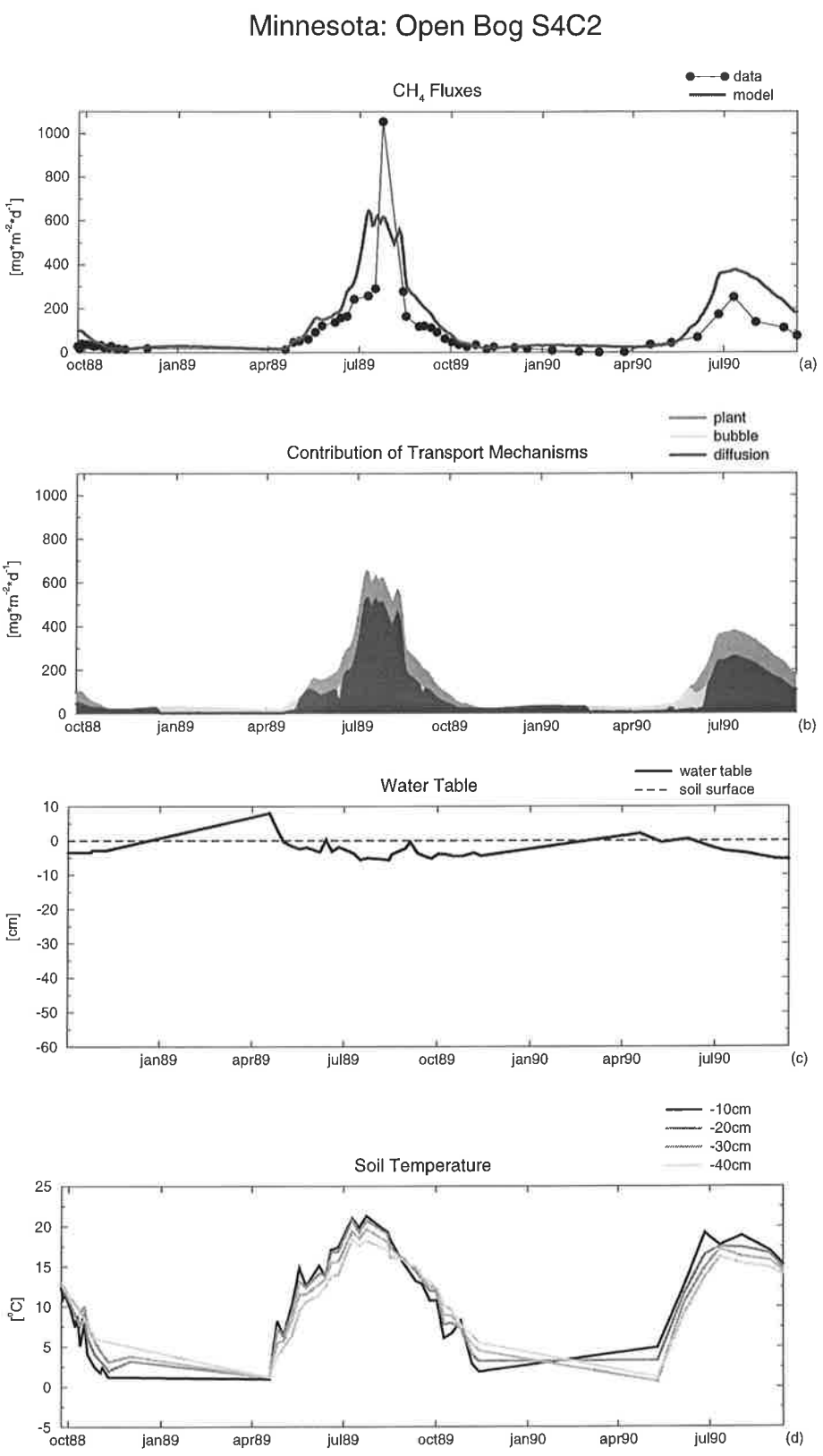

Fig. 53: (a): Comparison between modeled (thick line) and measured (dots) methane emissions, (b): Modeled contributions of the three transport mechanisms: diffusion (black), ebullition (light grey), and plant-mediated transport (dark grey), (c): Forcing: Observed position of the water table, (d): Forcing: Observed soil temperature

3. Finland

Period of observation: 1 season

Table 25: Characteristics of Site 3 - Finland

Microsite 1	**Carex Lawn**
No. of Chambers	4
Vegetation	*Sphagnum*, *Carex*
Microsite 2	**Eriophorum Lawn**
No. of Chambers	7
Vegetation	*Sphagnum*, *Eriophorum*
Microsite 3	**Low Hummock**
No. of Chambers	2
Vegetation	*Sphagnum*, *Eriophorum*
Microsite 4	**Flark**
No. of Chambers	4
Vegetation	*Sphagnum*, *Eriophorum*

Table 26: Parameters at Site 3 - Finland

Microsite	R_0	V_{max}	l	nroot	T_{veg}
Carex Lawn	0.34	20µM/h	70cm	70cm	12
Eriophorum Lawn	0.45	20µM/h	70cm	30cm	12
Low Hummock	0.34	20µM/h	70cm	30cm	12
Flark	0.34	20µM/h	70cm	30cm	12

The parameter rooting depth (nroot) was chosen according to the information that the roots of *Eriophorum vaginatum* penetrate 30 cm below the soil surface and those of *Carex rostrata* down to a depth of 2 m [*Saarnio*, pers. comm.]. Wet set the soil depth (l) to 70cm, because

investigations of the methane production potential revealed that methane production was significant down to a depth of about 40-50 cm below the water table [*Saarnio et al.*, 1997]. The parameter T_{veg} was set to a relatively high value of 12, because vascular plants known to emit methane were dominant at all sites.

In Fig. 54 to Fig. 57 we show the results of the comparison between modeled and measured methane emissions from that site, (c) and (d) are plots of the observed forcing data water table and soil temperature. The latter was the same at all microsites. In (a) we compare modeled (thick line) and observed methane emissions. The grey area is the area between the average of all chamber measurements +/- the standard deviation. In (b) the relative contributions of the three transport mechanims diffusion, ebullition and plant-mediated transport are depicted.

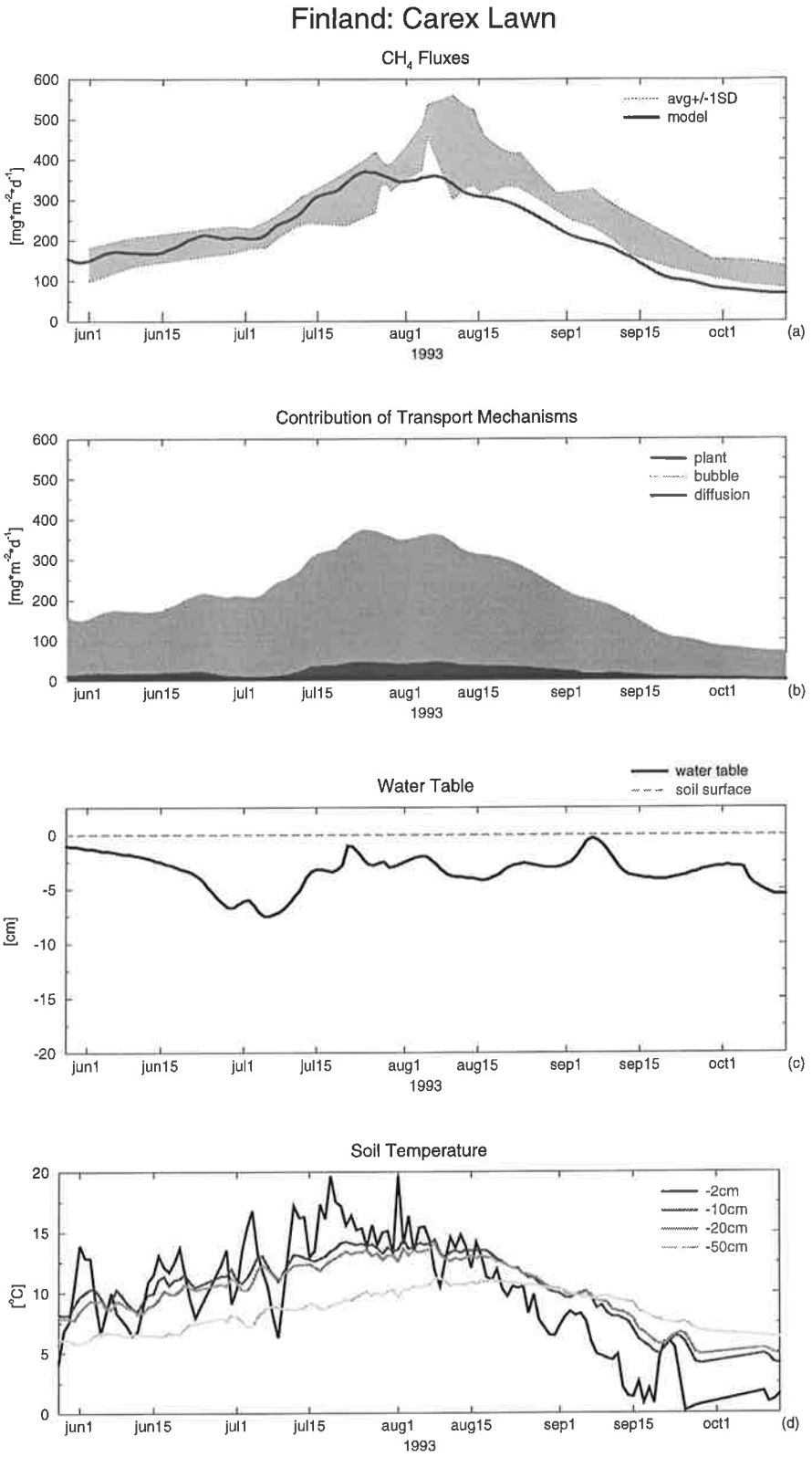

Fig. 54: (a): Comparison between modeled (thick line) and measured (grey area: average +/- 1SD) methane emissions, (b): Modeled contributions of the three transport mechanisms: diffusion (black), ebullition (light grey), and plant-mediated transport (dark grey), (c): Forcing: Observed position of the water table, (d): Forcing: Observed soil temperature

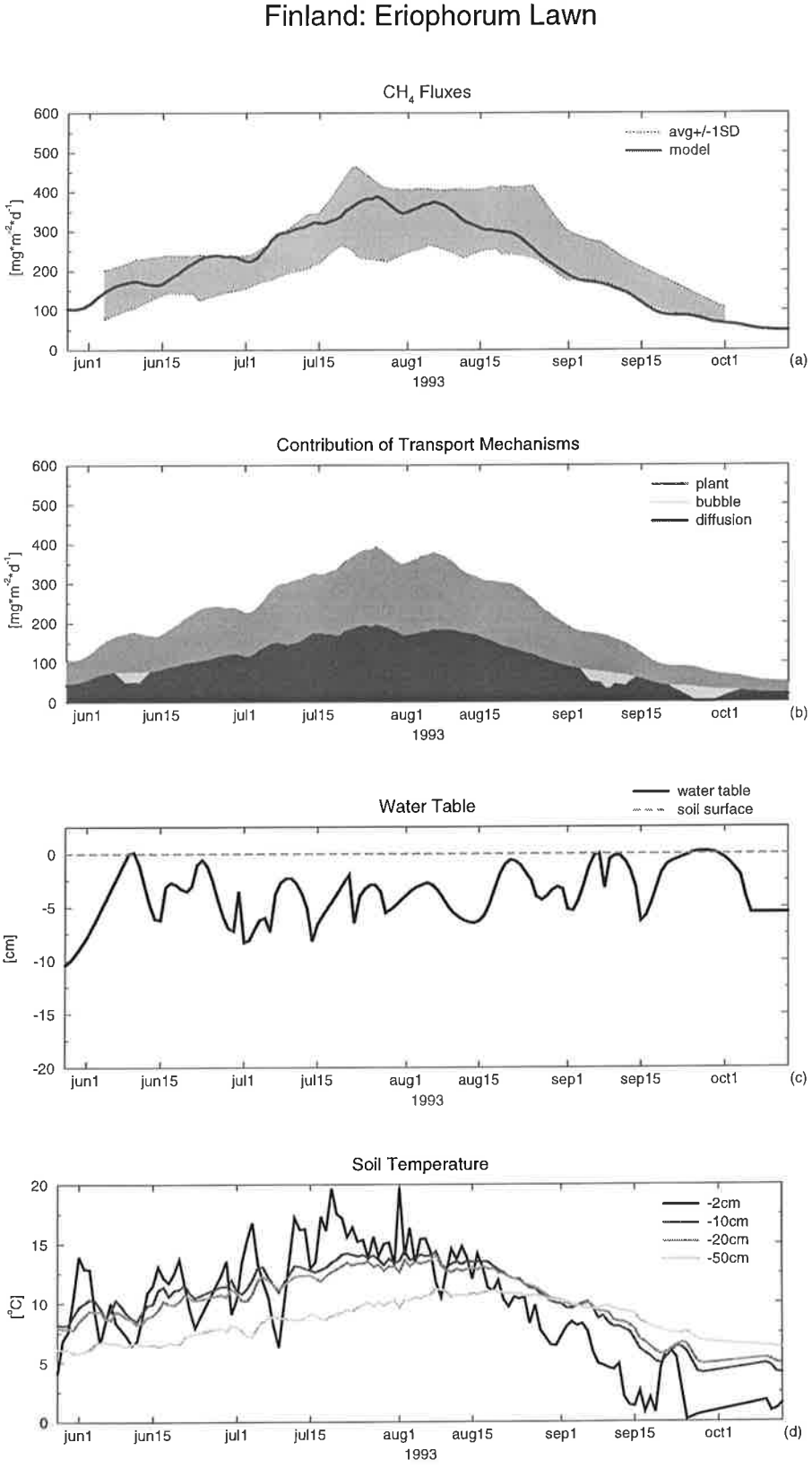

Fig. 55: (a): Comparison between modeled (thick line) and measured (grey area: average +/- 1SD) methane emissions, (b): Modeled contributions of the three transport mechanisms: diffusion (black), ebullition (light grey), and plant-mediated transport (dark grey), (c): Forcing: Observed position of the water table, (d): Forcing: Observed soil temperature

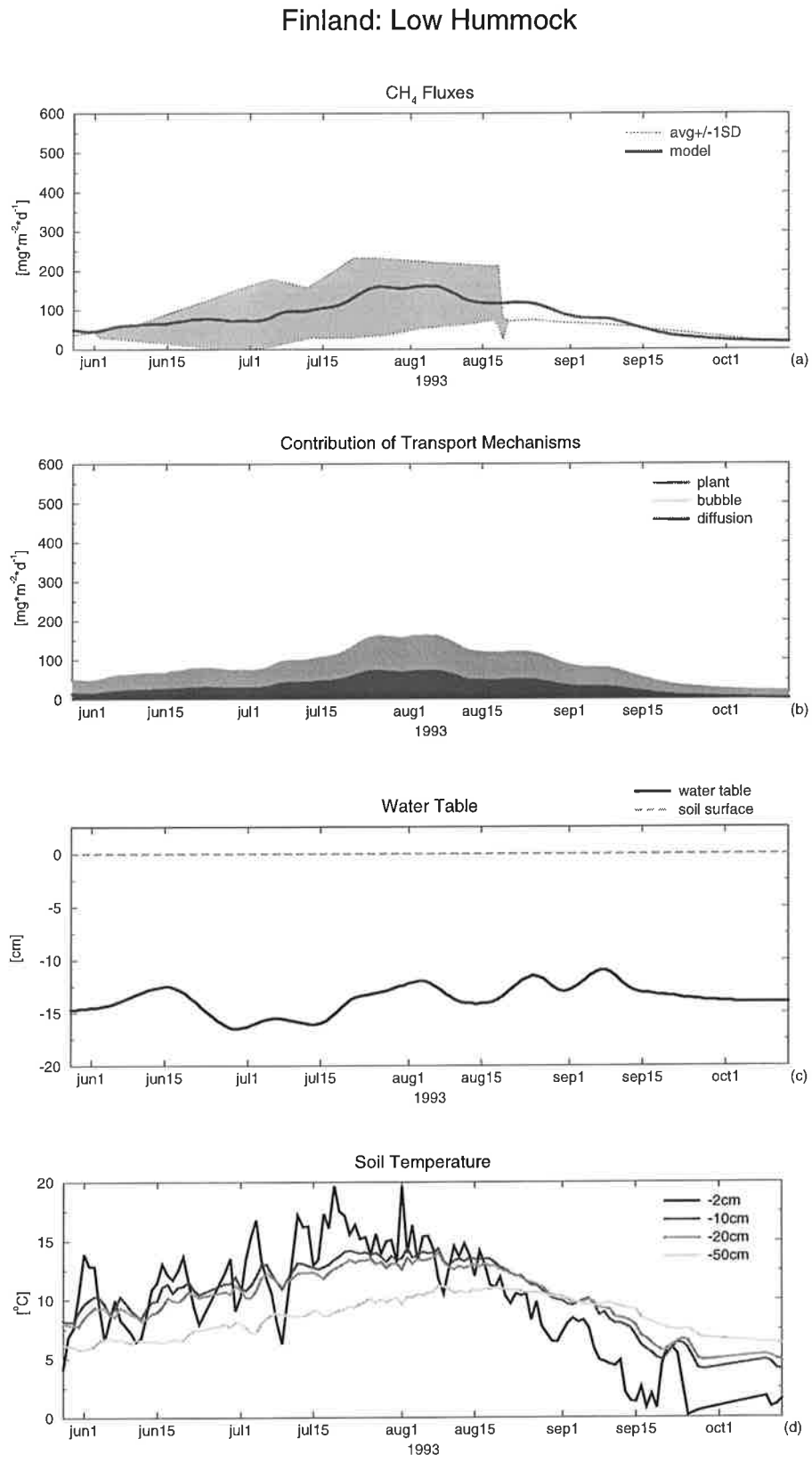

Fig. 56: (a): Comparison between modeled (thick line) and measured (grey area: average +/- 1SD) methane emissions, (b): Modeled contributions of the three transport mechanisms: diffusion (black), ebullition (light grey), and plant-mediated transport (dark grey), (c): Forcing: Observed position of the water table, (d): Forcing: Observed soil temperature

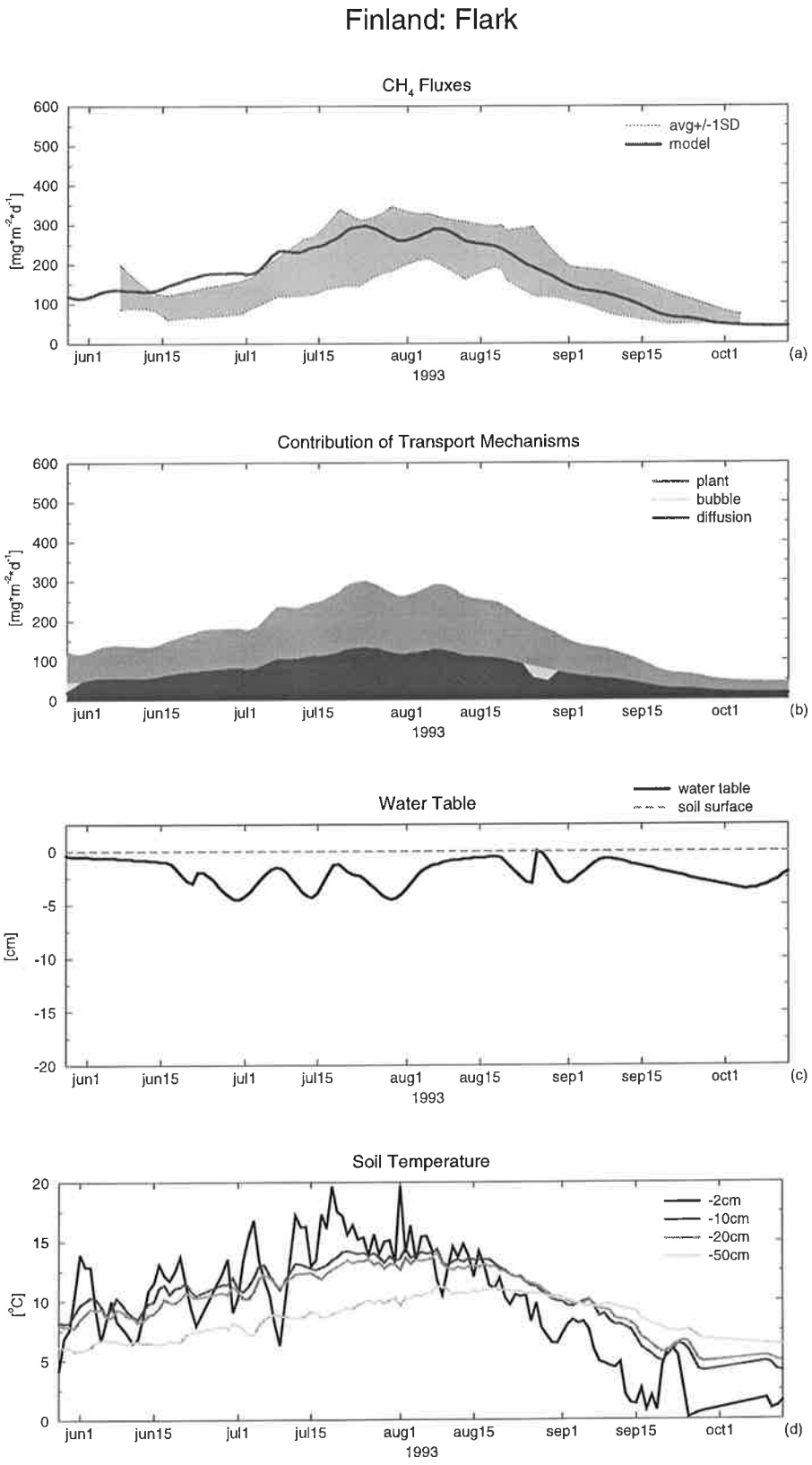

Fig. 57: (a): Comparison between modeled (thick line) and measured (grey area: average +/- 1SD) methane emissions, (b): Modeled contributions of the three transport mechanisms: diffusion (black), ebullition (light grey), and plant-mediated transport (dark grey), (c): Forcing: Observed position of the water table, (d): Forcing: Observed soil temperature

4. Alaska

Period of observation (used here): 1 season

Table 27: Characteristics of Site 4 - Alaska

Microsite 1	**Black Holes**
No. of Chambers	3
Vegetation	*Sphagnum*
Microsite 2	**Carex Stands**
No. of Chambers	3
Vegetation	*Carex*, *Eriophorum*, mosses
Microsite 3	**Mossy Area**
No. of Chambers	3
Vegetation	Mosses (no *Sphagnum*)

Table 28: Parameters at Site 4 - Alaska

Microsite	R_0	V_{max}	l	nroot	T_{veg}
Black Holes	0.3	3µM/h	thaw depth	0	0
Carex Stands	0.075	3µM/h	thaw depth	thaw depth	3
Mossy Area	0.3	3µM/h	thaw depth	0	0

Assuming that methane can be formed in the whole thawed soil zone we set the parameter soil depth (l) equal to the thaw depth. At the microsites ‚Black holes' and ‚Mossy area' there were no vascular plants and hence the rooting depth (nroot) as well as the parameter T_{veg} were set to 0 there. At the ‚Carex stands' microsite the rooting depth (nroot) was chosen to be as deep as the soil depth, because the roots of *Carex* can be relatively deep [e.g. *Saarinen*, 1995], and T_{veg} was set to 3, because the density of plants was presumed to be relatively low.

In Fig. 58 to Fig. 60 we show the results of the tests against this data set. (c) and (d) show the

observed forcing data water table and soil temperature. In (a) the modeled and observed methane emissions are compared. Since the seasonal cycles of the three chamber measurements differ much, we plot the obtained fluxes from each chamber as well as the average of those three measurements. At the ‚Black Hole' microsite the seasonal pattern of modeled methane emissions compares well with the average of the three chamber measurements. The agreement between modeled methane emissions and the average of the three chamber measurements is also quite good at the ‚Carex stands', whereas at the ‚Mossy area' this is not the case. There the model results compare rather well with the M2 and M3 data, but the high emissions at the beginning of August detected by chamber M1 are not reproduced by the model. In (b) the modeled contributions of the three different transport mechanisms are depicted. At the microsites ‚Black holes' and ‚Mossy area' diffusion is the only transport mechanism, whereas at the ‚Carex stands' plant-mediated transport is the dominant emission pathway.

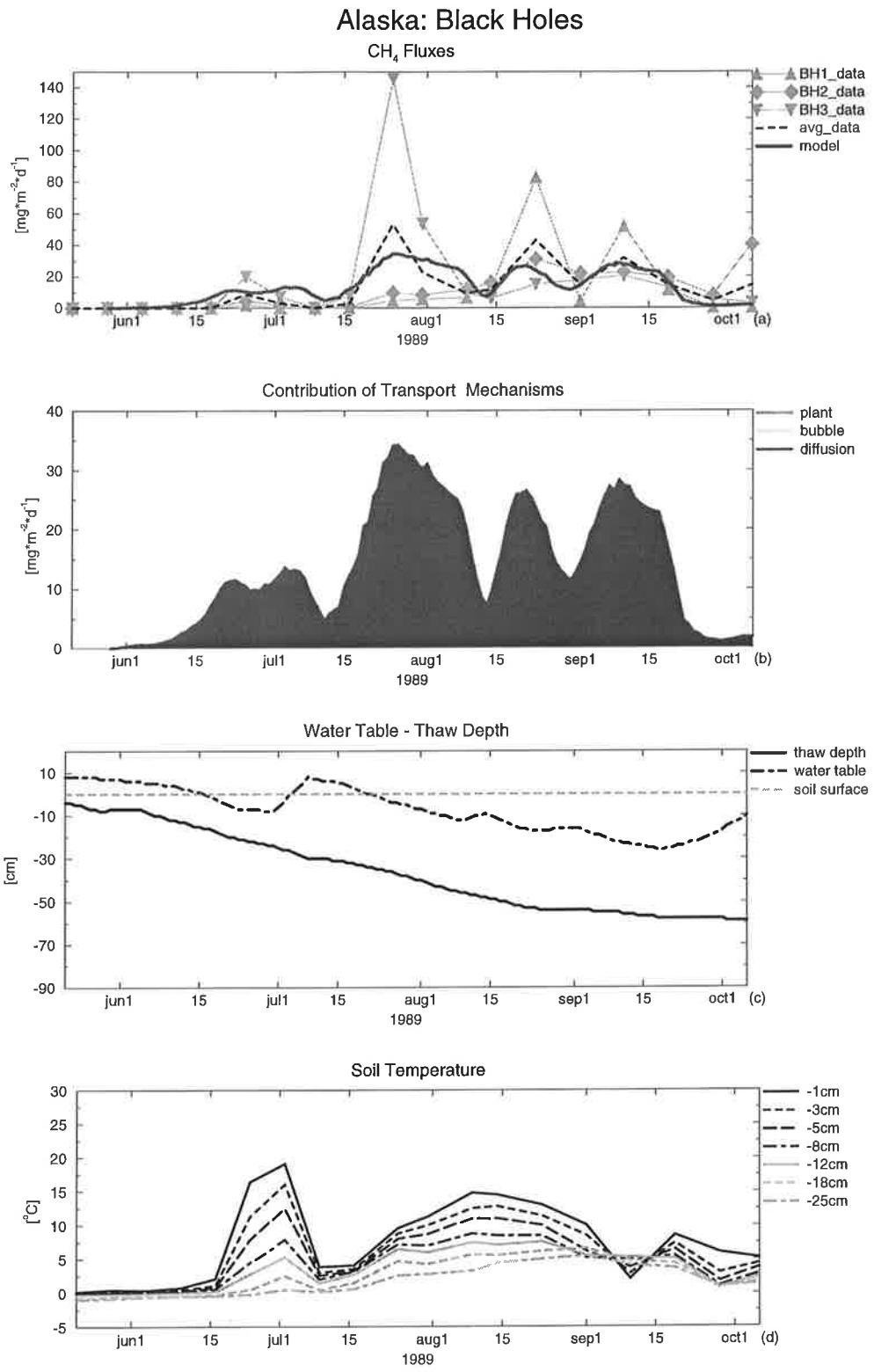

Fig. 58: Comparison between modeled (thick line) and measured (the triangles and the square are observations from three stations within site ‚Black Holes', the dashed line marks the average of those three measurements) methane emissions, (b): Modeled contributions of the three transport mechanisms: diffusion (black), ebullition (light grey), and plant-mediated transport (dark grey), (c):Forcing: Observed position of the water table, (d): Forcing: Observed soil temperature

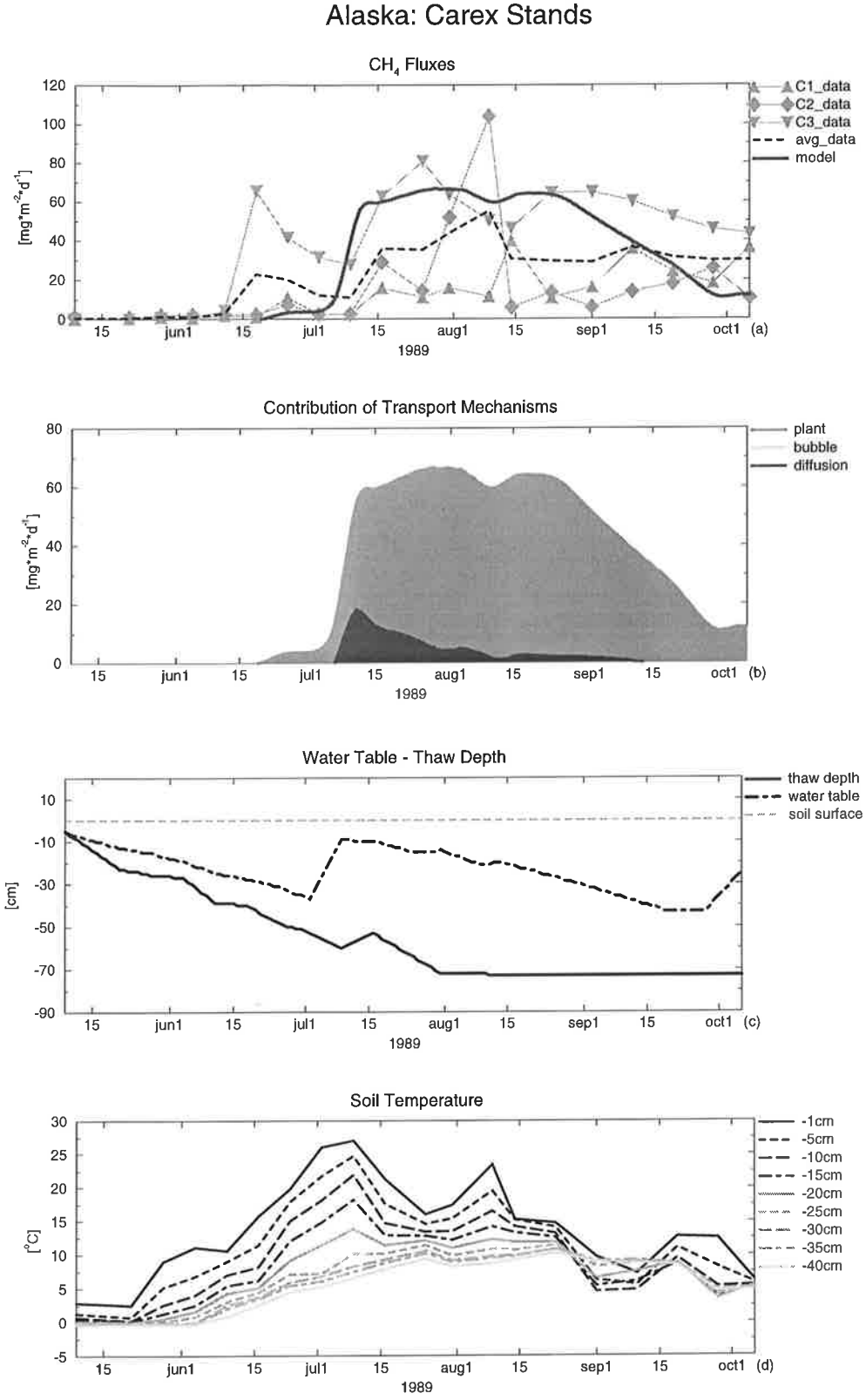

Fig. 59: Comparison between modeled (thick line) and measured (the triangles and the square are observations from three stations within site ‚Carex Stands', the dashed line marks the average of those three measurements) methane emissions, (b): Modeled contributions of the three transport mechanisms: diffusion (black), ebullition (light grey), and plant-mediated transport (dark grey), (c):Forcing: Observed position of the water table, (d): Forcing: Observed soil temperature

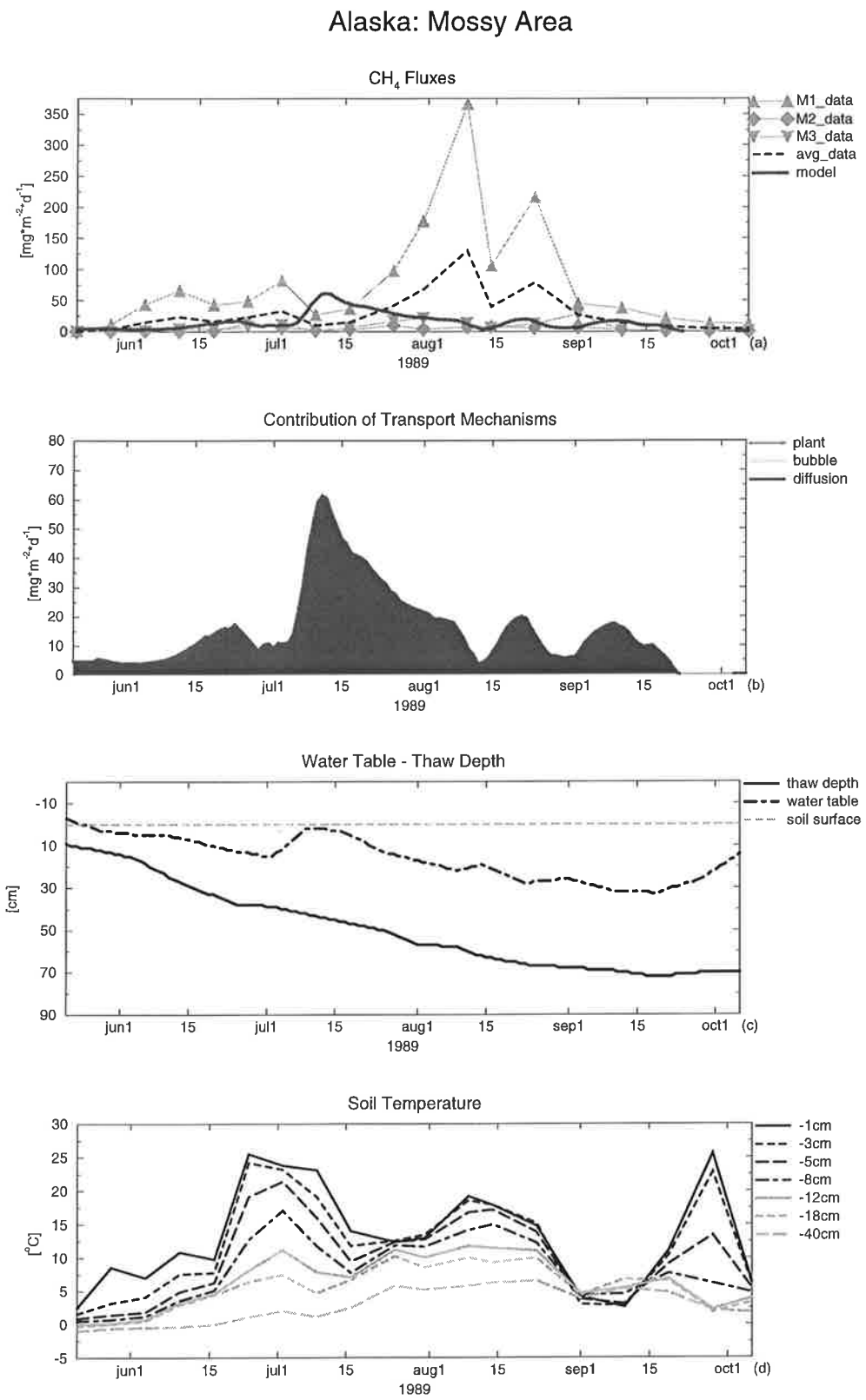

Fig. 60: Comparison between modeled (thick line) and measured (the triangles and the square are observations from three stations within site ‚Mossy Area', the dashed line marks the average of those three measurements) methane emissions, (b): Modeled contributions of the three transport mechanisms: diffusion (black), ebullition (light grey), and plant-mediated transport (dark grey), (c):Forcing: Observed position of the water table, (d): Forcing: Observed soil temperature

5. Canada

Period of observation: 1 season

Table 29: Characteristics of Site 5 - Canada

Microsite 1	**SSA-Fen**
No. of Chambers	8

Table 30: Parameters at Site 5 - Canada

Microsite	R_0	V_{max}	l	nroot	T_{veg}
SSA-Fen	0.15	20µM/h	80cm	50cm	1

Since the rooting depths (nroot) and the soil depths (l) were unknown at all chambers we chose similar values as at the other northern sites. Concerning the vegetation we know that there were some vascular plants that were likely to emit methane, but that they were not dominant in the chambers [*Valentine*, pers. comm.]. For that reason wet set T_{veg} to 1.

Fig. 61 shows the result of the test against this data set. In (c) and (d) the forcing data water table and soil temperature are plotted. Measurements were conducted at 8 microsites (4 hummocks and 4 hollows). The soil temperature is the same at all 8 microsites (d), whereas this is not the case for the water table levels (c). We ran the model driven by all 8 water table data sets. The modeled methane emissions from all microsites were similar, because at most microsites the water table was above the soil surface. The way ebullition and plant-mediated transport are parameterized in the model leads to the fact that - if the water table is above the soil surface - there is no difference in the ebullitive and the plant-mediated methane flux at differing water table levels. For that reason the 8 modeled methane fluxes (thick line) were averaged and compared to the average +/- 1 standard deviation (grey area) of the observations (Fig. 61 (a)). In (b) the relative contributions of the three different transport mechanisms is depicted.

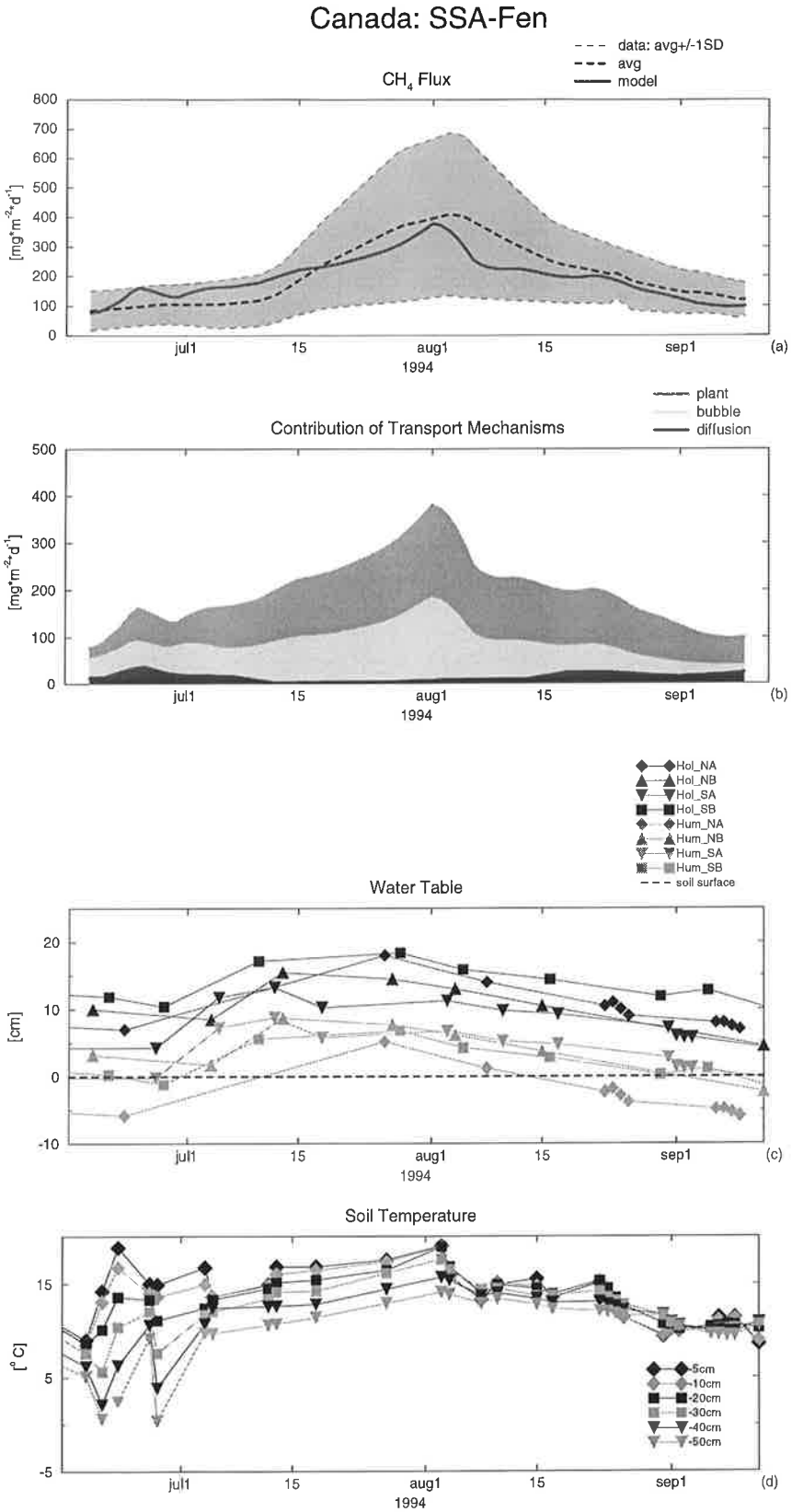

Fig. 61: (a): Comparison between modeled (thick line: average of modeled fluxes at all eight sites) and measured (grey area: average of measurements at eight sites +/- 1SD) methane emissions, (b): Modeled contributions of the three transport mechanisms: diffusion (black), ebullition (light grey), and plant-mediated transport (dark grey), (c): Forcing: Observed positions of the water table at all eight sites, (d): Forcing: Observed soil temperature (the same for all sites)

6. Panama

Period of observation: 1 year

Table 31: Characteristics of Site 6 - Panama

Microsite 1	**Mojinga Swamp**
No. of Chambers	7
Vegetation	*Raphia taedigera* (palm)

Table 32: Parameters at Site 6 - Panama

Microsite	R_0	V_{max}	l	nroot	T_{veg}
Mojinga Swamp p1	2.8	20µM/h	128cm	74cm	9
Mojinga Swamp p2	2.5	20µM/h	131cm	78cm	4

At that site the situation was different from the sites 1-5, because here only methane fluxes had been observed, but neither the position of the water table nor the soil temperature. Furthermore, there was no information about the soil depth (l) and the rooting depth (nroot). For that reason we used the output data of a climatological run of the ECHAM4 model in T106 (1.1^o*1.1^o) [*Roeckner et al.*, 1996] to derive the forcing data. The soil temperature at different soil depths is directly calculated by that model. The position of the water table was calculated using the hydrological model (see Sect. 5) driven by climate data of the same ECHAM4 model run. To derive the parameters for the methane model we used the global data sets. At the grid point were Mojinga Swamp is located the wetland data set gives a wetland coverage of 0%. Therefore, we used two neighboring grid points, referred to as p1 and p2 in the following.

Fig. 62 shows the results of that test. In (c) and (d) the obtained forcing data are plotted. The soil temperature is almost constant over the whole year. There is a pronounced wet/dry-season cycle. During the dry season the water table is at about 80-100 cm below ground while during the wet season it is always above the soil surface at about 10 cm above ground which is in good agreement with observations (below 50 cm below ground in the dry season and above the soil surface, but below 30 cm above ground in the wet season [*Keller*, pers. comm.]).

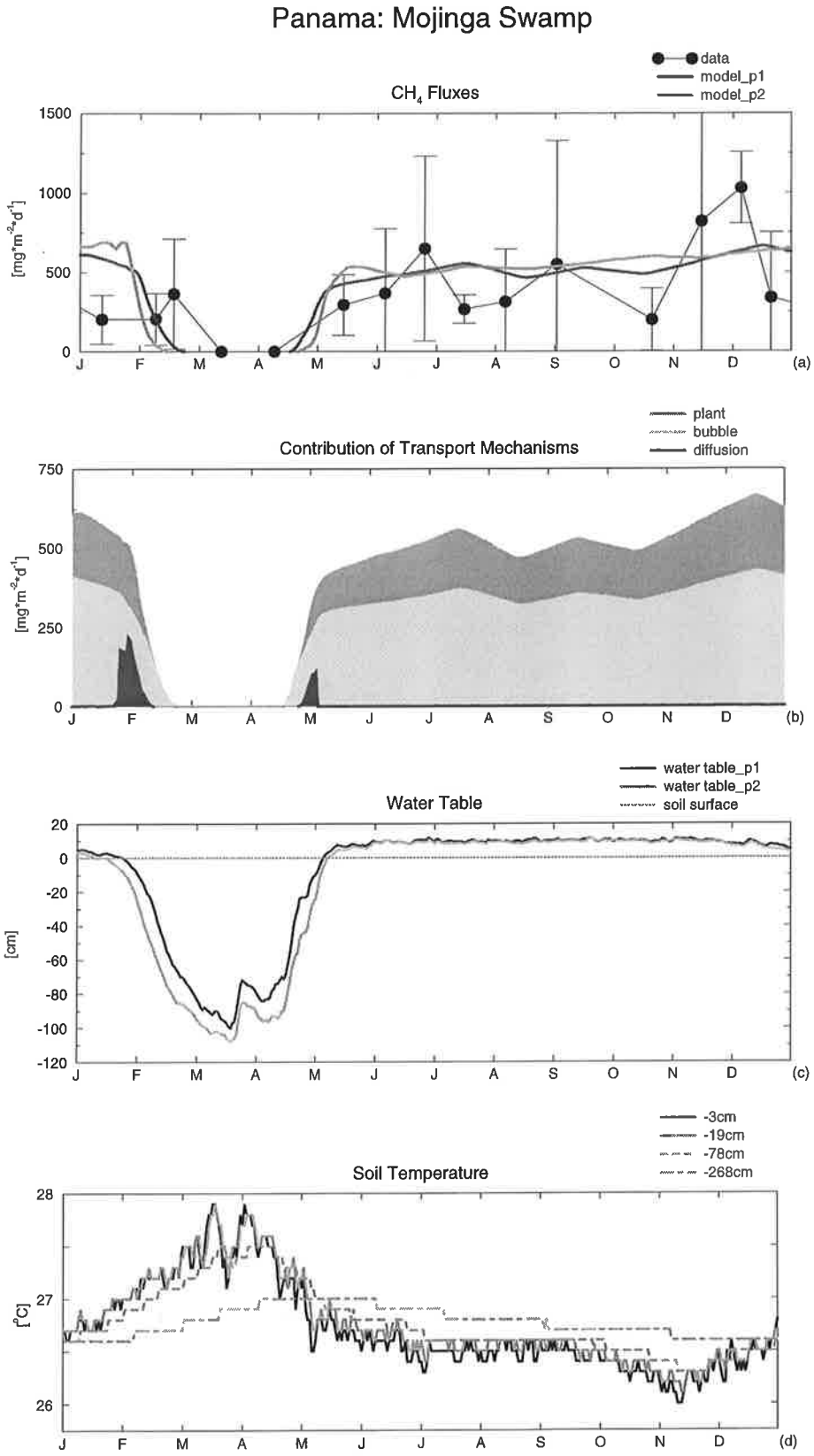

Fig. 62: Comparison between modeled (thick lines: points p1 and p2 (see text)) and measured (dots with +/- 1SD error bars) methane emissions, (b): Modeled contributions of the three transport mechanisms (point p1): diffusion (black), ebullition (light grey), and plant-mediated transport (dark grey), (c): Forcing: Position of the water table calculated with the hydrological model forced by the ECHAM4 model, (d): Forcing: Soil temperature (point p1) calculated with the ECHAM4 model

Appendix C.

Here we show the results of sensitivity tests of the 1-dimensional methane emission model to the parameters l (soil depth) and nroot (rooting depth) using the Michigan data set (site 1). Two further sensitivity tests with different values for V_{max} (the maximum methane oxidation rate) at one site in Alaska (site 4) and one in Panama (site 6) are conducted. Like in Sect. 3.2. we compare the results of the sensitivity tests with the control run, of which the parameters are compiled in Tab. 30:

Table 33: Parameters of the Control Run (Site 1)

R_0	V_{max}	l	nroot	T_{veg}
0.6	45µM/h	80cm	50cm	15

Sensitivity to the soil depth l

A larger value for l means that the zone were methane can be produced (if the soil is water saturated) extends deeper into the soil. Fig. 63 (a) shows the results of model runs using three different values for l, namely l=80 cm (control), l=100 cm and l=60 cm. All three values lie below the rooting depth, which is 50 cm deep. As one can see from Fig. 63 (a)-(c) those differences in the soil depth do rarely affect modeled methane emissions. The reason for this is that below the rooting depth the availability of substrate for methane production decreases exponentially (see Equ. (5) and (6) of Sect. 2). Therefore, at soil depths of more than 10 cm below the rooting depth the substrate availability is relatively small. Furthermore, the soil temperature decreases generally with depth leading to even smaller methane production rates at deep soil depths. Fig. 63 (c) shows that in case l=60 cm modeled methane emissions are slightly smaller than in the control run.

Sensitivity to the rooting depth

The rooting depth nroot is the depth of the lowest layer of the root zone. That means that from layers above that depth methane can be conducted by plants to the atmosphere. Apart from influencing plant-mediated transport they also affect the vertical distribution of substrate for methanogenesis (see Equ. (5) and (6) of Sect. 2). Throughout the root zone the substrate availability is constant, then it decreases exponentially. Therefore, the rooting depth

determines the extend of the zone with relatively high productivity. Fig. 64 (a) shows how the modeled total fluxes change depending on the rooting depth. The modeled methane emissions are higher, if the roots extend deeper into the soil. Fig. 64 (b) and (c) show that the fraction of methane emitted through plants is smaller when nroot is smaller (b) and vice versa (c).

Sensitivity to V_{max}

Sensitivity tests with V_{max} (the maximum methane oxidation rate) were performed at two further sites in order to demonstrate that depending on the moisture conditions of the specific site different values for V_{max} can either affect modeled methane emissions or do not have a large effect at all. At most sites and microsites used in this study different values for V_{max} did not have a large effect on modeled methane emissions (not shown) as it is the case at the Panama site (site 6) (see Fig. 65 (c) and (d)). But at the microsite ‚Black Holes' of the Alaskan site (site 4) the choice of V_{max} does affect modeled methane emissions significantly. If one chooses higher values for V_{max} the modeled methane emissions are clearly smaller than in the control run at times with a water table being below the soil surface due to a larger oxidation rate in the oxic soil zone. In this example high V_{max} values lead even to negative methane emissions which means uptake of atmospheric methane. The microsite ‚Black Holes' is that microsite where the effect of different V_{max} values is most pronounced. It is a site where methane fluxes are relatively low compared to the fluxes from other sites and where the water table is below the soil surface for a relatively long period. Furthermore, diffusion is the only transport mechanism at that site. Those conditions are responsible for the large effect that different V_{max} values have at that site.

Sensitivity to the soil temperature

Higher soil temperatures affect the rates of methane production (Q_{10}=6) as well as of methane oxidation (Q_{10}=2). Hence, higher soil temperatures lead to higher methane emissions and vice versa. Fig. 66 shows the results of two runs performed with the soil temperature of the control run +/- 1^{o}. It is clear that an increase in the soil temperature of 1^{o} leads to 10-20% higher methane emissions. If the soil temperature is by 1^{o} lower, simulated methane emissions are reduced by 10-20%.

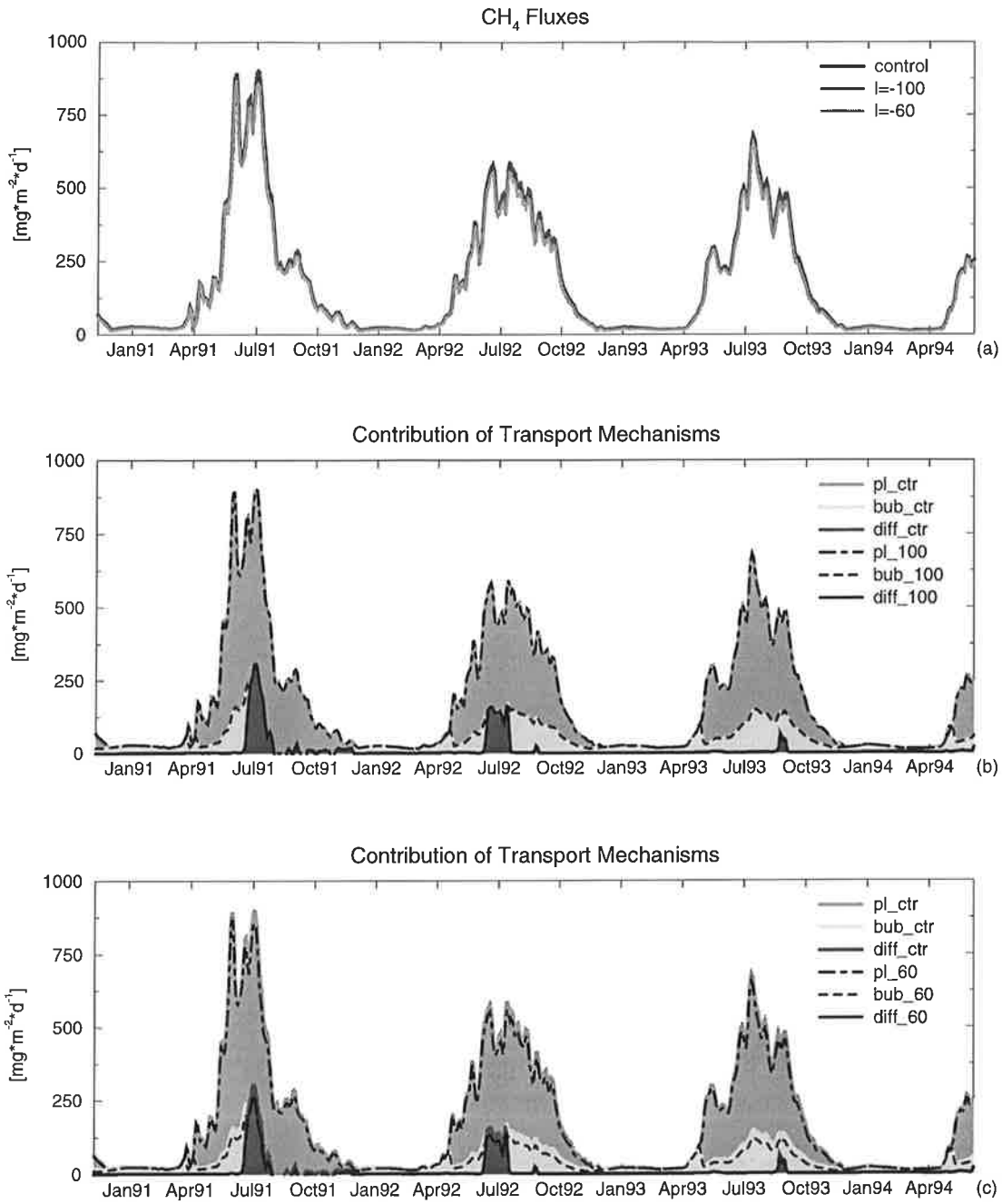

Fig. 63: Sensitivity to the soil depth l: (a): Comparison of the modeled total fluxes: Control run (black), run with l=-100cm (dark grey) and run with l=-60cm (light grey); (b): Contributions of the three different transport mechanisms : diffusion (black), ebullition (light grey) and plant-mediated transport (dark grey) and ‚l=-100cm' run: diffusion (solid), ebullition (dashed), and plant-mediated transport (dot-dashed); (c): Contribtutions of the three different transport mechanisms: Control run: diffusion (black), ebullition (light grey) and plant-mediated transport (dark grey) and ‚l=-60cm' run: diffusion (solid), ebullition (dashed), and plant-mediated transport (dot-dashed)

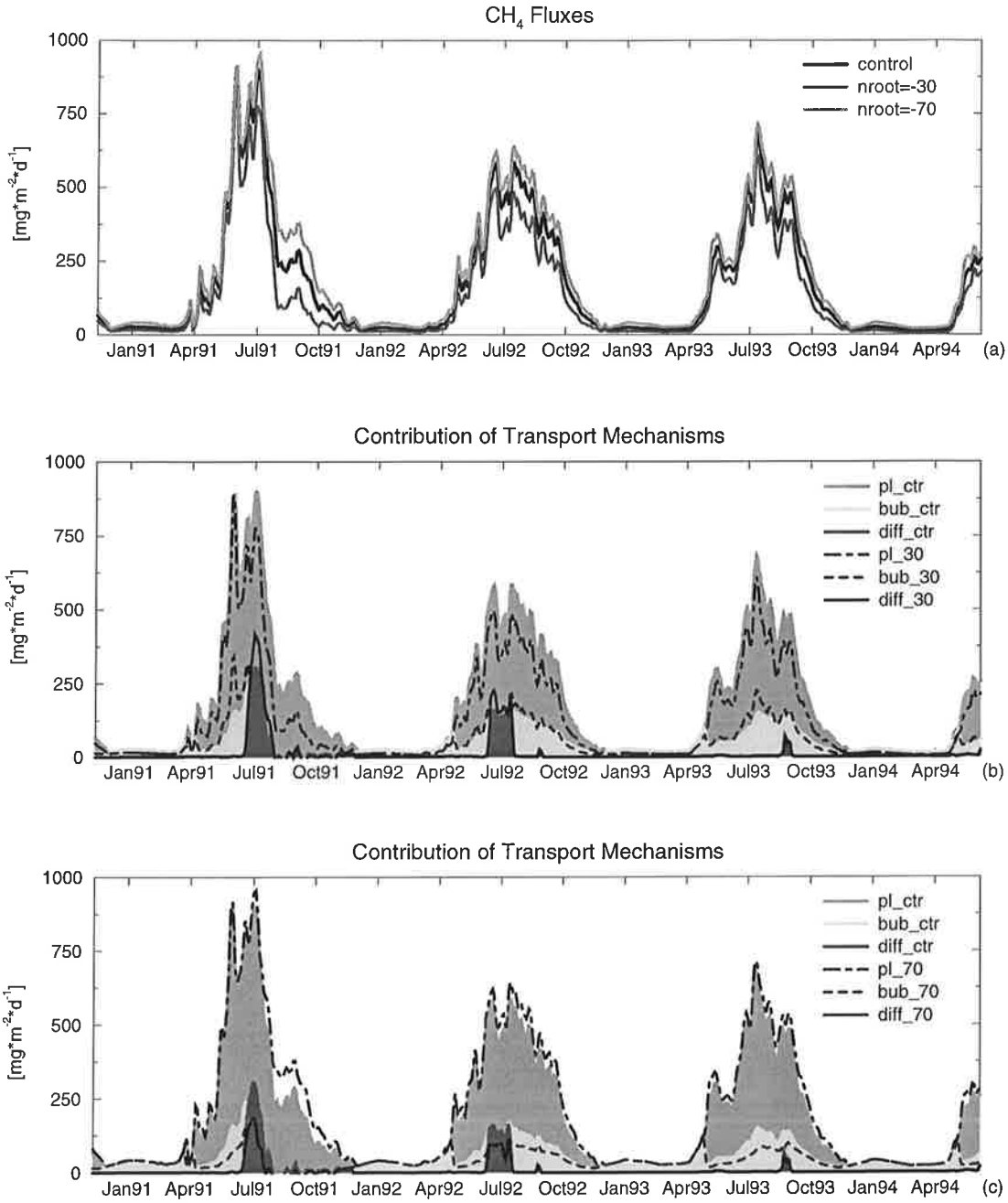

Fig. 64: Sensitivity to the rooting depth nroot: (a): Comparison of the modeled total fluxes: Control run (black), run with nroot=-30cm (dark grey) and run with nroot=-70cm (light grey); (b): Contributions of the three different transport mechanisms: Control run: diffusion (black), ebullition (light grey) and plant-mediated transport (dark grey) and ‚nroot=-30cm' run: diffusion (solid), ebullition (dashed), and plant-mediated transport (dot-dashed); (c): Contributions of the three different transport mechanisms: Control run: diffusion (black), ebullition (light grey) and plant-mediated transport (dark grey) and ‚nroot=-70cm' run: diffusion (solid), ebullition (dashed), and plant-mediated transport (dot-dashed)

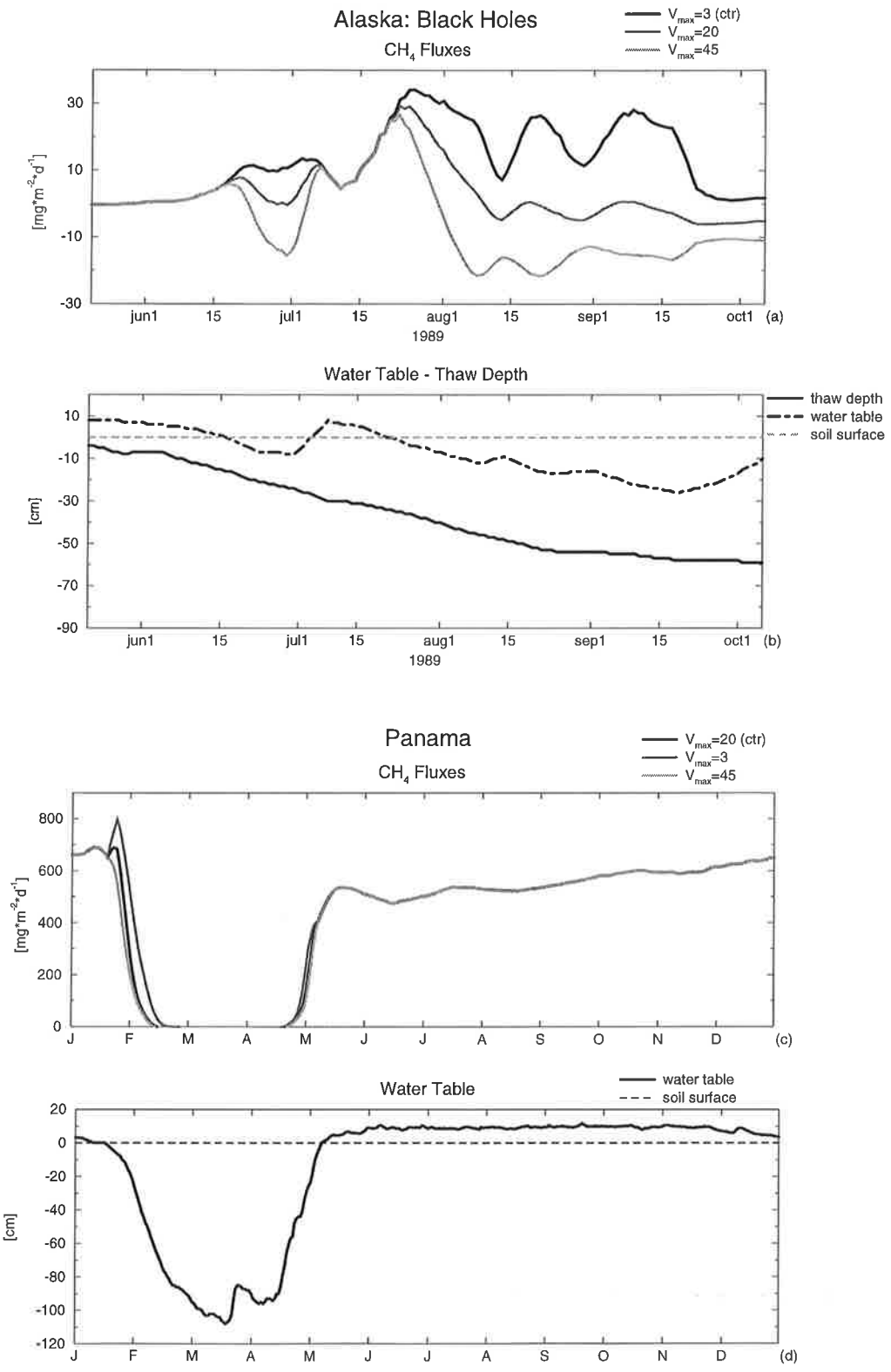

Fig. 65: Sensitivity to V_{max}: (a): Microsite ‚Black Holes' from site 4 (Alaska): Comparison between the control run (V_{max}=3µM/h) and two runs using higher values for V_{max} (20µM/h (dark grey) and 45µM/h (light grey)); (b): Position of the water table (dot-dashed) and thaw depth at the ‚Black Holes' microsite; (c): Site Panama: Comparison between the control run (V_{max}=20µM/h) and two runs using other values for V_{max} (3µM/h (dark grey) and 45µM/h (light grey)); (d): Position of the water table

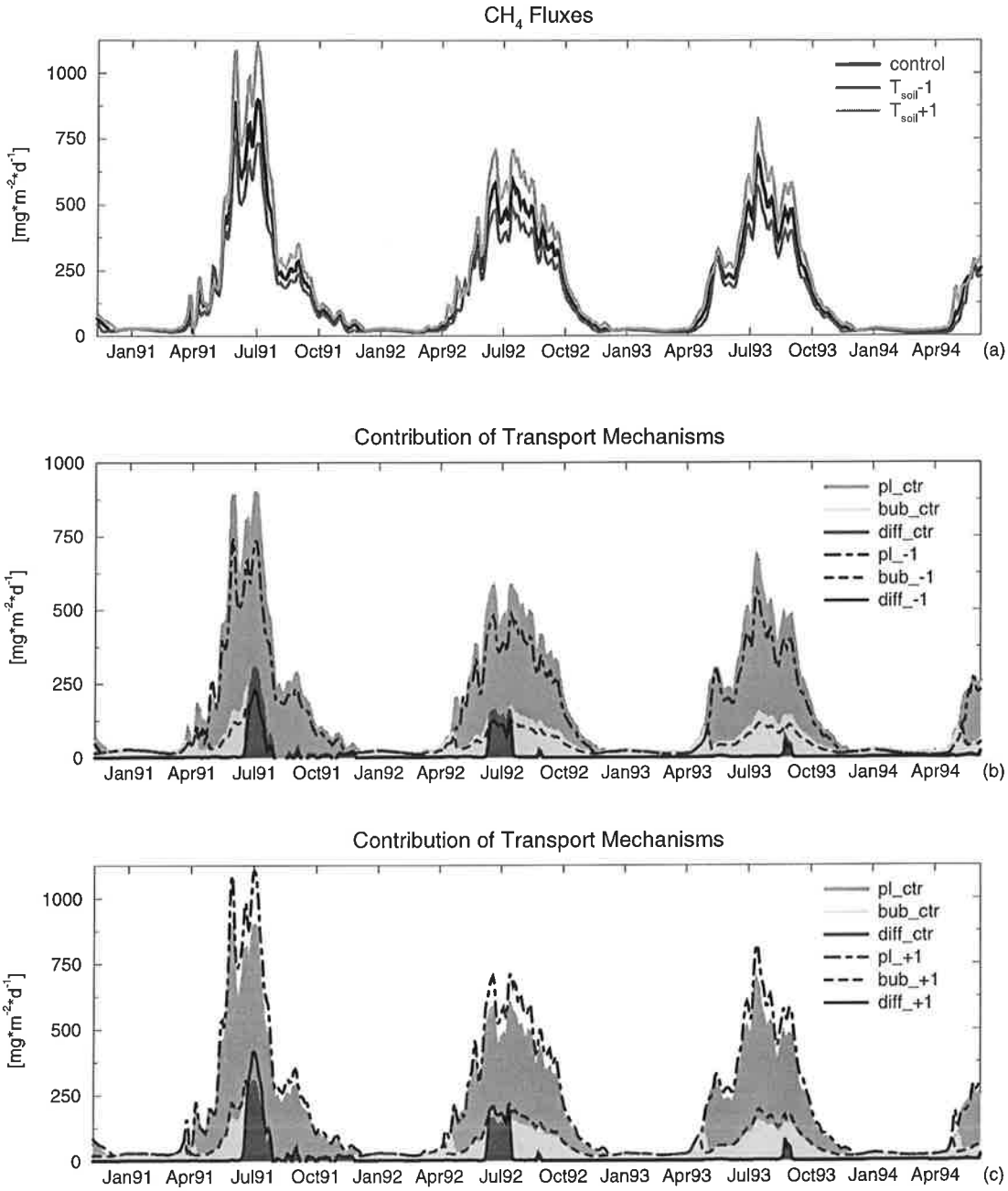

Fig. 66: Sensitivity to the soil temperature: (a): Comparison of the modeled total fluxes: Control run (black), run with soil temperature-1^{o} (dark grey) and run with soil temperature+1^{o} (light grey); (b): Contributions of the three different transport mechanisms. Control run: diffusion (black), ebullition (light grey) and plant-mediated transport (dark grey) and ,soil temperature-1^{o}' run: diffusion (solid), ebullition (dashed), and plant-mediated transport (dot-dashed); (c): Contribtutions of the three different transport mechanisms. Control run: diffusion (black), ebullition (light grey) and plant-mediated transport (dark grey) and ,soil temperature+1^{o}' run: diffusion (solid), ebullition (dashed), and plant-mediated transport (dot-dashed)

References

D'Ans, E. Lax, Taschenbuch für Chemiker und Physiker, Band I, *Springer-Verlag, Berlin, Heidelberg, New York*, 1967

Baker-Blocker, A., T. M. Donahue, K. H. Mancy, Methane flux from wetland areas, *Tellus, 29*, 245-250, 1977

Bartlett, K. B., P. M. Crill, R. L. Sass, R. C. Harriss, N. B. Dise, Methane emissions from tundra environments in the Yukon-Kuskokwim delta, Alaska, *Journal of Geophysical Research, 97, D15*, 16645-16660, 1992

Bartlett, K. B., P. M. Crill, J. A. Bonassi, J. E. Richey, R. C. Harriss, Methane flux from the Amazon floodplain: Emissions during rising water, *Journal of Geophysical Research,* 95, *D10*, 16773-16788, 1990

Bartlett, K. B., R. C. Harriss, Review and assessment of methane emissions from wetlands, *Chemosphere, 26*, 1-4, 261-320, 1993

Bekki, S., K. S. Law, J. A. Pyle, Effects of ozone depletion on atmospheric CH_4 and CO concentrations, *Nature, 371*, 595-597, 1994

Bender, M., R. Conrad, Kinetics of CH_4 oxidation in oxic soils exposed to ambient air or high CH_4 mixing ratios, *FEMS Microbiology Ecology, 101*, 261-270, 1992

Boelter, D. H., Important physical properties of peat materials, In: *Proceedings of the Third International Peat Congress, Quebec City, Quebec, Aug. 18-23, 1968, Department of Energy, Mines and Resources Canada. National Research Council of Canada*, 1968

Boon, P. I., B. K. Sorrell, Methane flux from an Australian floodplain wetland: the importance of emergent macrophytes, *Journal of the North American Benthological Society, 14, 4*, 582-598, 1995

Bridgham, S. D., C. J. Richardson, Mechanisms controlling soil respiration (CO_2 and CH_4) in southern peatlands, *Soil Biology and Biochemistry, 24, 11*, 1089-1099, 1992

Brook, E. J., T. Sowers, J. Orchardo, Rapid variations in atmospheric methane concentration during the past 110,000 years, *Science, 273*, 1087-1091, 1996

Brown, M., Deduction of emissions of source gases using an objective inversion algorithm and a chemical transport model, *Journal of Geophysical Research, D7*, 12639-12660, 1993

Brown, M., The singular value decomposition method applied to the deduction of the emissions and the isotopic composition of atmospheric methane, *Journal of Geophysical Research*, 100, 425-446, 1995

Bubier, J. L., The relationship of vegetation to methane emission and hydrochemical gradients in northern peatlands, *Journal of Ecology, 83*, 403-420, 1995

Bubier, J. L., T. R. Moore, L. Bellisario, N. T. Comer, P. M. Crill, Ecological controls on methane emissions from a northern peatland complex in the zone of discontinuous permafrost, Manitoba, Canada, *Global Biogeochemical Cycles, 9*, 455-470, 1995

Cao, M., S. Marshall, K. Gregson, Global carbon exchange and methane emission from natural wetlands: Application of a process-based model, *Journal of Geophysical Research, 101, D9*, 14399-14414, 1996

Chanton, J. P., J. E. Bauer, P. A. Glaser, D. E. Siegel, C. A. Kelley, S. C. Tyler, E. H. Romanowicz, A. Lazrus, Radiocarbon evidence for the substrates supporting methane formation within northern Minnesota peatlands, *Geochimica et Cosmochimica Acta 59, 17*, 3663-3668, 1995

Chanton, J. P. and J. W. H. Dacey, Effects of vegetation on methane flux, reservoirs, and carbon isotopic composition, in *Trace gas emissions by plants*, ed. by T. D. Sharkey, E. A. Holland, H. A. Mooney, *Academic Press, San Diego*, 65-92, 1991

Chanton, J. P., C. S. Martens, Seasonal variations in ebullitive flux and carbon isotopic composition of methane in a tidal freshwater estuary, *Global Biogeochemical Cycles, 2, 3*, 289-298, 1988

Chanton, J. P., C. S. Martens, C. A. Kelley, P. M. Crill, W. J. Showers, Methane transport mechanisms and isotopic fractionation in emergent macrophytes of an Alaskan tundra lake, *Journal of Geophysical Research, 95, D15*, 16681-16688, 1992a

Chanton, J. P., G. J. Whiting, W. J. Showers, P. M. Crill, Methane flux from Peltranda Virginica: Stable isotope tracing and chamber effects, *Global Biogeochemical Cycles,* 6, 15-31, 1992b

Christensen, T. R., S. Jonasson, T. V. Callaghan, M. Havström, Spatial variation in high-latitude methane flux along a transect across Siberian and European tundra environments, *Journal of Geophysical Research, 100*, 21035-21045, 1995

Clein, J. S., J. P. Schimel, Microbial activity of tundra and taiga soils at sub-zero temperatures, *Soil Biology Biochemistry, 27, 9*, 1231-1234, 1995

Conrad, R., Control of methane production in terrestrial ecosystems, in: *Exchange of trace gases between terrestrial ecosystems and the atmosphere*, ed. by M. O. Andreae and D. S. Schimel, *John Wiley & Sons*, 39-58, 1989

Crill, P. M., K. B. Bartlett, R. C. Harriss, E. Gorham, E. S. Verry, D. I. Sebacher, L. Madzar, W. Sanner, Methane flux from Minnesota peatlands, *Global Biogeochemical Cycles, 2, 4*, 371-384, 1988

Crill, P. M., R. C. Harriss, K. B. Bartlett, Methane fluxes from terrestrial wetland environments, in: *Microbial production and consumption of greenhouse gases, methane, nitrogen oxides, and halomethans*, J. E. Rogers, W. T. Whitman (eds), *American Society for Microbiology, Washington D.C.*, 1991

Dacey, J. W. H., M. J. Klug, Methane efflux from lake sediments through water lilies, *Science, 203,* 1253-1254, 1979

Devol, A. H., J. E. Richey, B. R. Forsberg, L. A. Martinelli, Seasonal dynamics in methane emissions from the Amazon river floodplain to the troposphere, *Journal of Geophysical Research, 95, D10*, 16417-16426, 1990

Dickinson, R. E., A. Henderson-Sellers, P. J. Kennedy, Biosphere-atmosphere transfer scheme (BATS) version 1e as coupled to the NCAR community climate model, *NCAR Technical Note NCAR/TN-387+STR, National Center for Atmospheric Research, Boulder, Colorado*, 1993

Dise, N. B., Methane emission from Minnesota peatlands: Spatial and Seasonal Variability, *Global Biogeochemical Cycles, 7, 1*, 123-142, 1993

Dise, N. B., Winter fluxes of methane from Minnesota peatlands, *Biogeochemistry, 17*, 71-83, 1992

Dise, N. B., E. Gorham, E. S. Verry, Environmental factors controlling methane emissions from peatlands in Northern Minnesota, *Journal of Geophysical Research, 98, D6*, 10583-10594, 1993

Dlugokencky, E. J., E. G. Dutton, P. C. Novelli, P. P. Tans, K. A. Masarie, K. O. Lantz, S. Madronich, Changes in CH_4 and CO growth rates after the eruption of Mt. Pinatubo and their link with changes in tropical tropospheric UV flux, *Geophysical Research Letters, 23,* 20, 2761-2764, 1996

Dlugokencky, E. J., K. A. Masarie, P. M. Lang, P. P. Tans, Continuing decline in the growth rate of atmospheric methane, *Nature, in press*, 1998

Dlugokencky, E. J., K. A. Masarie, P. M. Lang, P. P. Tans, L. P. Steele, E. G. Nisbet, A dramatic decrease in the growth rate of atmospheric methane in the northern hemispere during 1992, *Geophysical Research Letters, Vol. 21, No. 1*, 45-48, 1994

Dunfield P., R. Knowles, R. Dumont, T. R. Moore, Methane production and consumption in temperate and subarctic peat soils: Response to temperature and pH, *Soil Biol. Biochem., 25*, 321-326, 1993

Dunne, K. A., C. J. Willmott, Global distribution of plant-extractable water capacity of soil, *International Journal of Climatology, 16*, 16841-16859, 1996

Dutton, E. G., J. R. Christy, Solar radiative forcing at selected locations and evidence for global lower tropospheric cooling following the eruptions of El Chichón and Pinatubo, *Geophysical Research Letters, 19*, 2313-2316, 1992

Edwards, M. O., Global gridded elevation and bathymetry (ETOPO5). Digital raster data on a 5-minute geographic (lat/lon) 2160*4320 (centroid-registered) grid. *NOAA National Geophysical Data Center, Boulder, Colorado*, 1989

Enting, I. G., C. M. Trudinger, R. J. Francey, A synthesis inversion of the concentration and $\delta^{13}C$ of atmospheric CO_2, *Tellus, 47B*, 35-52, 1995

FAO/Unesco, 1971-1981: Soil map of the world, *Vols. 1-10, Unesco, Paris*

Federer, C. A., Transpirational supply and demand: Plant, soil, and atmospheric effects evaluated by simulation, *Water Resour. Res., 18, 355-362*, 1982

Fowler, D., K. J. Hargreaves, U. Skiba, R. Milne, M. S. Zahniser, J. B. Moncrieff, I. J. Beverland, M. W. Gallagher, Measurements of CH_4 and N_2O fluxes at the landscape scale using micrometeorological methods, *Philosophical Transactions of the Royal Society of London, A, 351, 1696*, 339-356, 1995

Frolking, S., P. Crill, Climate controls on temporal variability of methane flux from a poor fen in southeastern New Hampshire: Measurement and modeling, *Global Biogeochemical Cycles, 8, 4*, 1994

Funk, D. W., E. R. Pullman, K. M. Peterson, P. M. Crill, W. D. Billings, Influence of water table on carbon dioxide, carbon monoxide, and methane fluxes from taiga bog microcosms, *Global Biogeochemical Cycles, 8, 3*, 271-278, 1994

Gale, M. R., D. F. Grigal, Vertical root distributions of northern tree species in relation to successional status, *Canadian Journal of Forest Research, 17*, 829-834, 1987

Gerard, G., J. Chanton, Quantification of methane oxidation in the rhizosphere of emergent aquatic macrophytes: Defining upper limits, *Biogeochemistry, 23*, 79-97, 1993

Gibson, J. K., P. Källberg, S. Uppala, A. Hernandez, A. Nomura and E. Serrano, The ECMWF Re-Analysis (ERA). 1. ERA description, *ECMWF Re-Analysis Project Report Series No. 1, European Centre for Medium-Range Weather Forecasts, Reading, U.K.*, 71 pp, 1997

Gildea, M. P., B. Moore, FAOSOL - A global soil archive, *Complex systems research center, University of New Hampshire, Durham, New Hamsphire* (unpublished data tape and documentation), 1985

Granberg, G., C. Mikkelä, I. Sundh, B. H. Svensson, M. Nilsson, Sources of spatial variation in methane emission from mires in northern Sweden: A mechanistic approach in statistical modeling, *Global Biogeochemical Cycles,11, 2*, 135-150, 1997

Happell, J. D., J. P. Chanton, G. J. Whiting, W. J. Showers, Stable isotopes as tracers of methane dynamics in Everglades marshes with and without active populations of methane oxidizing bacteria, *Journal of Geophysical Research,* 98, *D8*, 14771-14782, 1993

Harriss, R. C., D. I. Sebacher, F. P. Day Jr, Methane flux in the Great Dismal Swamp, *Nature, 297*, 673-674, 1982

Hartge, K. H., R. Horn, Einführung in die Bodenphysik, *Ferdinand Enke Verlag, Stuttgart*, 1991

Hein, R., Inverse Modellierung des atmosphärischen Methan-Kreislaufs unter Verwendung eines drei-dimensionalen Modells des Transports und der Chemie der Troposphäre, *Dissertation, Max-Planck-Institut für Meteorologie, Examensarbeit Nr. 25*, 1994

Hein, R., P. J. Crutzen, M. Heimann, An inverse modeling approach to investigate the global

atmospheric methane cycle, *Global Biogeochemical Cycles, 11, 1*, 43-76, 1997

Hein, R., M. Heimann, Determination of global scale emissions of atmospheric methane using an inverse modelling method, in: *Non-CO_2 Greenhouse Gases*, ed. by J. van Ham et al., *Kluver*, 1994

Heyer, J., Der Kreislauf des Methans, *Akademie-Verlag Berlin*, 1990

Hillel, D., Introduction into soil physics, *Academic Press, New York*, 1982

Hogan, K., R. Harriss, Comment on „A dramatic increase in the growth rate of atmospheric methane in the northern hemisphere during 1992", by E. J. Dlugokencky et al., *Geophysical Research Letters, Vol. 21*, 2445-2446, 1994

Holzapfel-Pschorn, A., R. Conrad, W. Seiler, Effects of vegetation on the emission of methane from submerged paddy soils, *Plant and Soil, 92*, 223-233, 1986

IPPC, Climate Change 1995, The science of climate change, Contribution of workinggroup I to the second assessment report of the intergovernmental panel on climate change, *Cambridge University Press*, 1996

Jackson, R. B., J. Canadell, J. R. Ehleringer, H. A. Mooney, O. E. Sala, E. D. Schulze, A global analysis of root distributions for terrestrial biomes, *Oecologia, 108, 3*, 389-411, 1996

Jarvis, P. G., K. G. McNaughton, Stomatal control of transpiration: Scaling up from leaf to region, *Adv. Ecol. Res., 15, 1-49*, 1986

Jouzel, J., N. I. Barkov, J. M. Barnola, M. Bender, J. Chappellaz. C. Genthon, V. M. Kotlyakov, V. Lipenkov, C. Lorius, J. R. Petit, D. Raynaud, G. Raisbeck, C. Ritz, T. Sowers, M. Stievenard, F. Yiou, P. Yiou, Extending the Vostock ice-core record of paleoclimate to the penultimate glacial period, *Nature, 364*, 407-412, 1993

Kaduk, J., Simulation der Kohlenstoffdynamik der globalen Landbiosphäre mit SILVAN - Modellbeschreibung und Ergebnisse, *Dissertation, Max-Planck-Institut für Meteorologie, Examensarbeit Nr. 42*, 1996

Kaltofen, R., R. Opitz, K. Schuhmann, J. Ziemann, Tabellenbuch der Chemie, *VEB Deutscher Verlag für Grundstoffindustrie, Leipzig*, 1975

Keeling, C. D., T. P. Whorf, M. Whalen, J. van der Plicht, Interannual extremes in the rate of rise of atmospheric carbon dioxide since 1980, *Nature, 375*, 666-670, 1995

Keller, M., Biological sources and sinks of methane in tropical habitats and tropical atmospheric chemistry, *Dissertation, Cooperative Thesis No. 126, Princeton University and National Center for Atmospheric Research*, 1990

Kettunen, A., V. Kaitala, Modelling methane emissions from boreal peatlands, in: Laiho, R., J. Laine, H. Vasander (eds), *Northern peatlands in global climate change, Proceedings of the international workshop Acad. of Finland, Helsinki*, 277-281, 1996

Klinger, L. F., P. R. Zimmerman, J. P. Greenberg, L. E. Heidt, A. B. Guenther, Carbon trace gas fluxes along a successional gradient in the Hudson Bay lowland, *Journal of Geophysical Research, 99, D1*, 1469-1494, 1994

Knorr, W., Satellitengestützte Fernerkundung und Modellierung des globalen CO_2-Austauschs der Landvegetation: Eine Synthese, *Dissertation, Max-Planck-Institut für Meteorologie, Examensarbeit Nr. 49*, 1997

Knoblauch, C., Bodenkundlich-mikrobiologische Bestandsaufnahme zur Methanoxidation in einer Flußmarsch der Tide-Elbe, *Diploma thesis, Univ. of Hamburg*, Germany, 1994

Krumholz, L. R., J. L. Hollenback, S. J. Roskes, D. B. Ringelberg, Methanogenesis and methanotrophy within a Sphagnum peatland, *FEMS Microbiology Ecology, 18, 3*, 215-224, 1995

Lelieveld, J., P. J. Crutzen, F. J. Dentener, Changing concentration, lifetime and climate forcing of atmospheric methane, *Tellus, 50B*, 128-150, 1998

Lowe, D. C., C. A. M. Brenninkmeijer, G. W. Brailsford, K. R. Lassey, A. J. Gomez, Concentration and ^{13}C records of atmospheric methane in New Zealand and Antarctica: evidence for changes in methane sources, *Journal of Geophysical Research, 99*, 16913-16925, 1994

Matthews, E., I. Fung, Methane emission from natural wetlands: Global distribution, area, and environmental characteristics of sources, *Global Biogeochemical Cycles, Vol. 1, No. 1*, 1987

Melloh, R. A., P. M. Crill, Winter methane dynamics in a temperate peatland, *Global Biogeochemical Cycles, 10, 2*, 247-254, 1996

Mitsch, W. J., J. G. Gosselink, Wetlands, *Van Nostrand Reinhold, New York*, 1993

Moore, T. R., M. Dalva, Methane and carbon dioxide exchange potentials of peat soils in aerobic and anaerobic laboratory incubations, *Soil Biology Biochemistry, 29, 8*, 1157-1164, 1997

Moore, T. R., N. T. Roulet, Methane flux: Water table relations in northern wetlands, *Geophysical Research Letters, 20, 7*, 587-590, 1993

Moosavi, S. C., P. M. Crill, E. R. Pullman, D. W. Funk, K. M. Peterson, Controls on CH_4 flux from an Alaskan boreal wetland, *Global Biogeochemical Cycles, 10, 2*, 287-296, 1996

Morrissey, L. A., G. P. Livingston, Methane emissions from Alaska arctic tundra: An assessment of local spatial variability, *Journal of Geophysical Research, 97, D15*, 16661-16670, 1992

Murray, F. W., On the computation of saturation vapour pressure, *J. Appl. Meteorol., 6, 203-204*, 1967

Neue, H. U., R. L. Sass, Trace gas emissions from rice fields, in: *Global atmospheric-biospheric chemistry*, ed. by R. G. Prinn, *Plenum Press, New York*, 119-147, 1994

Nouchi, I., S. Mariko, Mechanism of methane transport by rice plants, in: *Biogeochemistry of Global Change*, ed. by R. S. Oremland, *Chapman & Hall, New York, London*, 336-352, 1993

Pauss, A., G. Andre, M. Perrier, S. R. Guiot, Liquid-to-gas mass transfer in anaerobic processes: Inevitable transfer limitations of methane and hydrogen in the biomethanation process, *Applied and Environmental Microbiology, 56, 6*, 1636-1644, 1990

Press, W. H., S. A. Teukolsky, W. T. Vetterling, B. P. Flannery, Numerical recipes in FORTRAN, The art of scientific computing, *Cambridge University Press*, 1992

Prinn, R., R. Weiss, J. Miller, J. Huang, F. Alyea, D. Cunnold, P. Fraser, D. Hartley, P. Simmonds, Atmospheric trends and lifetime of trichloroethane and global average hydroxyl radical concentrations based on 1978-1994 ALE/GAGE measurements, *Science, 269*, 187-192, 1995

Potter, C. S., An ecosystem simulation model for methane production and emission from wetlands, *Global Biogeochemical Cycles, 11, 4*, 495-506, 1997

Roeckner, E., K. Arpe, L. Bengtsson, M. Christoph, M. Claussen, L. Dümenil, M. Esch, M. Giorgetta, U. Schlese, U. Schulzweida, The atmospheric general circulation model ECHAM4: Model description and simulation of present-day climate, *Max-Planck-Institut für Meteorologie, Rep. 218, Hamburg*, 90 pp., 1996

Rothfuss, F., R. Conrad, Development of a gas diffusion probe for the determination of methane concentrations and diffusion characteristics in flooded paddy soils, *FEMS Microbiology Ecology, 14*, 307-318, 1994

Roulet, N. T., R. Ash, T. R. Moore, Low boreal wetlands as a source of atmospheric methane, *Journal of Geophysical Research, 97, D4*, 3739-3749, 1992

Saarinen, T., Biomass and production of two vascular plants in a boreal mesotrophic fen, *Canadian Journal of Botany, 74*, 934-938, 1995

Saarnio, S., J. Alm, J. Silvola, A. Lohila, H. Nykänen, P. J. Martikainen, Seasonal variation in CH_4 emissions and production and oxidation potentials at microsites of an oligotrophic pine fen, *Oecologia, 110*, 414-422, 1997

Schauffler, S. M., J. S. Daniel, On the effects of stratospheric circulation changes on circulation trends, *Journal of Geophysical Research, 99*, 25747-25754, 1994

Scheffer, F. and P. Schachtschabel, Lehrbuch der Bodenkunde, *Ferdinand EnkeVerlag, Stuttgart*, 1982

Schimel, J. P., Plant transport and methane production as controls on methane flux from arctic wet meadow tundra, *Biogeochemistry, 28*, 183-200, 1995

Schipper, L. A., K. R. Reddy, Determination of methane oxidation in the rhizosphere of *Sagittaria lancifolia* using methyl fluoride, *Soil Science Society of America Journal, 60*, 611-616, 1996

Schlesinger, W. H., Biogeochemistry, An Analysis of Global Change, *Academic Press, San Diego*, 1991

Schütz, H., P. Schröder, H. Rennenberg, Role of plants in regulating the methane flux to the at-

mosphere, in: *Trace gas emissions by plants*, ed. by T. D. Sharkey, E. A. Holland, H. A. Mooney, *Academic Press, San Diego*, 29-63, 1991

Schütz, H., W. Seiler, R. Conrad, Processes involved in formation and emission of methane in rice paddies, *Biogeochemistry, 27*, 35-60, 1989

Sebacher, D. I., R. C. Harriss, K. B. Bartlett, S. M. Sebacher, S. S. Grice, Atmospheric methane sources: Alaskan tundra bogs, an alpine fen, and a subarctic boreal marsh, *Tellus, 38B,* 1-10, 1986

Shafer, N. E., R. N. Zare, Through a beer glass darkly, *Physics Today, October*, 48-52, 1991

Shannon, R. D., J. R. White, A three-year study of controls on methane emissions from two Michigan peatlands, *Biogeochemistry, 27*, 35-60, 1994

Shannon, R. D., J. R. White, J. E. Lawson, B. S. Gilmour, Methane efflux from emergent vegetation in peatlands, *Journal of Ecology, 84, 2*, 239-246, 1996

Shurpali, N. J., S. B. Verma, R. J. Clement, D. P. Billesbach, Seasonal distribution of methane flux in a Minnesota peatland measured by eddy correlation, *Journal of Geophysical Research, 98*, 20649-20655, 1993

Sundh, I., M. Nilsson, G. Granberg, B. H. Svensson, Depth distribution of microbial production and oxidation of methane in northern boreal peatlands, *Microbial Ecology, 27*, 253-265, 1994

Tarantola, A., Inverse Problem Theory - Methods for Data Fitting and Model Parameter Estimation, *Elsevier, Amsterdam*, 1987

Thompson, A. M., J. A. Chappellaz, I. Y. Fung, T. L. Kucsera, The atmospheric CH_4 increase since the Last Glacial Maximum, *Tellus, 45B*, 242-257, 1993

Torn, M. S., F. S. Chapin, III, Environmental and biotic controls over methane flux from arctic tundra, *Chemosphere, 26*, 357-368, 1993

Valentine, D. W., E. A. Holland, D. S. Schimel, Ecosystem and physiological controls over methane production in northern wetlands, *Journal of Geophysical Research, 99, D1*, 1563-1571, 1994

Waddington, J. M., N. T. Roulet, R. V. Swanson, Water table control of CH_4 emission enhancement by vascular plants in boreal peatlands, *Journal of Geophysical Research, 101, D17*, 22775-22785, 1996

Walter, B. P., M. Heimann, R. D. Shannon, J. R. White, A process-based model to derive methane emissions from natural wetlands, *Geophysical Research Letters, 23, 25*, 3731-3734, 1996

Wassmann, R., U. G. Thein, M. J. Whiticar, H. Rennenberg, W. Seiler, W. J. Junk, Methane emissions from the Amazon floodplain: Characterization of production and transport, *Global Biogeochemical Cycles, 6, 1,* 3-13, 1992

Watson, A., K. D. Stephen, D. B. Nedwell, J. R. M. Arah, Oxidation of methane in peat - Ki-

netics of CH_4 and O_2 removal and the role of plant roots, *Soil Biology Biochemistry, 29, 8*, 1257-1267, 1997

Westermann, P., Temperature regulation of methanogenesis in wetlands, *Chemosphere, 26*, 321-328, 1993

Whalen, S. C., W. S. Reeburgh, Interannual variations in tundra methane emissions: A four-year time series at fixed sites, *Global Biogeochemical Cycles, 6*, 139-159, 1992

Whiting, G. J. and J. P. Chanton, Plant-dependant CH_4 emission in a subarctic Canadian fen, *Global Biogeochemical Cycles, 6*, 139-159, 1992

Whiting, G. J. and J. P. Chanton, Primary production control of methane emission from wetlands, *Nature, 364*, 794-795, 1993

Whiting, G. J., J. P. Chanton, D. S. Bartlett, J. D. Happell, Relationships between CH_4 emission, biomass, and CO_2 exchange in a subtropical grassland, *Journal of Geophysical Research, 96*, 13067-13071, 1991

Wilson, M. F., A. Henderson-Sellers, A global archive of land cover and soils data for use in general circulation models, *Journal of Climatology, 5*, 119-143, 1985

Yavitt, J. B., A. K. Knapp, Methane emission to the atmosphere through emergent cattail (*Typha latifolia* L.) plants, *Tellus, 47B*, 521-534, 1995

Zobler, L., A world soil file for global climate modeling, *National Aeronautics and Space Administration, Washington, DC, NASA, Technical Memorandum, 87802*, 1986

Danksagung

Ich danke allen, die zum Gelingen dieser Arbeit beigetragen haben:

Klaus Hasselmann für die Möglichkeit, die Arbeit am Max-Planck-Institut für Meteorologie zu erstellen. Es hat sehr viel Spaß gemacht, in dieser Atmosphäre zu arbeiten.

Martin Heimann für die Freiheit, die er mir gab, das Vertrauen, das er in mich setzte, für seinen Humor und die richtigen Fragen zum richtigen Zeitpunkt, die mir immer wieder neue Horizonte eröffneten.

Peter Frenzel, der mir in vielen anregenden Gesprächen ein ‚Gefühl' für das, was in einem Feuchtgebiet passiert, gab und mir auch bei der Erstellung eines Datensatzes half. Ebenso danke ich Eva-Maria Pfeiffer und Ingrid Brettar für ‚Nachhilfe' in Bodenkunde und Mikrobiologie.

Meinen Hamburger Kolleginnen und Kollegen: Denjenigen, die mir in der Anfangsphase beim Einarbeiten und Einleben geholfen haben. Allen, die mich mit ihrer ehrlichen Art, Wissenschaft zu betreiben, überzeugten, immer ein offenes Ohr für meine Fragen hatten und Zeit für gemeinsame wissenschaftliche Diskussionen. Den Korrekturlesern meiner Arbeit sei ebenfalls herzlich gedankt, ebensowie denjenigen, die mich bei technischen Problemen unterstützt haben. Besonderer Dank geht an alle, mit denen mich mehr als die gemeinsame Wissenschaft verbunden hat, für gute Gespräche, viel Spaß bei der Vorbereitung auf und Teilnahme an sportliche(n) Großereignisse(n), gemeinsames Musikmachen und lange Abende, an denen viel gelacht wurde.

Allen Kolleginnen und Kollegen weltweit, für die vielen anregenden Diskussionen bei Konferenzen und die Zusammenarbeit, die zum Teil daraus entstand.

David Valentine dafür, daß er mir seinen unveröffentlichten Datensatz zu Verfügung gestellt hat.

Meinen Freundinnen und Freunden hier in Hamburg und sonstwo, die daran ‚schuld' sind, daß diese Zeit einfach phantastisch war, für alles, was sie mir gegeben haben.

Meiner Familie für ihre Freundschaft und die moralische Unterstützung aus der ‚Ferne'.

Die verwendeten Reanalysedaten wurden von ECMWF und DWD in Zusammenarbeit mit dem DKRZ zur Verfügung gestellt.

Diese Arbeit wurde vom Bundesministerium für Bildung und Forschung (BMBF) als Teil des Klimaschwerpunktes ‚Spurenstoffkreisläufe' unterstützt.